# SYNTHESIS, CHARACTERIZATION, AND ANTICANCER ACTIVITY OF CHITOSAN THIOSEMICARBAZONES, AND THEIR COPPER(II) COMPLEXES

A THESIS SUBMITTED TO

**CENTRAL DEPARTMENT OF CHEMISTRY**

**INSTITUTE OF SCIENCE AND TECHNOLOGY**

**TRIBHUVAN UNIVERSITY**

**KIRTIPUR, KATHMANDU, NEPAL**

**FOR THE AWARD OF**

**THE DEGREE OF DOCTOR OF PHILOSOPHY**

**IN CHEMISTRY**

BY

**HARI SHARAN ADHIKARI**

**MARCH, 2021**

# RECOMMENDATION

This is to recommend that **Hari Sharan Adhikari** has carried out research entitled "**Synthesis, Characterization, and Anticancer Activity of Chitosan Thiosemicarbazones and their Copper(II) Complexes**" for the award of Doctor of Philosophy (Ph.D.) in **Chemistry** under our supervision. To our knowledge, this work has not been submitted for any other degree.

He has fulfilled all the requirements laid down by the Institute of Science and Technology (IOST), Tribhuvan University, Kirtipur for the submission of the thesis for the award of Ph.D. degree.

---

**Dr Paras Nath Yadav**
**Supervisor**
**(Professor)**
Central Department of Chemistry, Tribhuvan University,
Kirtipur, Kathmandu, Nepal

---

**Dr Rameshwar Adhikari**
**Co-Supervisor**
**(Professor)**
Central Department of Chemistry, Tribhuvan University
Kirtipur, Kathmandu, Nepal
**(March, 2021)**

# LETTER OF APPROVAL

On the recommendation of **Prof. Dr Paras Nath Yadav and Prof. Dr Rameshwar Adhikari**, this Ph. D. thesis submitted by **Hari Sharan Adhikari,** entitled "**Synthesis, Characterization, and Anticancer Activity of Chitosan Thiosemicarbazones and their Copper(II) Complexes**" is forwarded by Central Department Research Committee (CDRC) to the Dean, IOST, T.U..

**Dr Ram Chandra Basnyat**
**Professor,**
**Head,**
Central Department of Chemistry,
Tribhuvan University
Kirtipur, Kathmandu
Nepal

Date: 9th Sept. 2021

# DECLARATON

Thesis entitled "**Synthesis, Characterization, and Anticancer Activity of Chitosan Thiosemicarbazones and their Copper(II) Complexes**" which is being submitted to the Central Department of Chemistry, Institute of Science and Technology (IOST), Tribhuvan University, Nepal for the award of the degree of Doctor of Philosophy (Ph.D.), is a research work carried out by me under the supervision of Prof. Dr Paras Nath Yadav, Central Department of Chemistry, Tribhuvan University and co-supervision of Prof. Dr Rameshwar Adhikari, Central Department of Chemistry, Tribhuvan University.

This research is original and has not been submitted earlier in part or full in this or any other form to any university or institute, here or elsewhere, for the award of any degree.

Hari Sharan Adhikari

# ACKNOWLEDGEMENTS

I am gratefully thankful to my supervisor for his magnanimous superintendence, painstaking arrangement of works and inspirational teaching in materialization of this work. I am gratefully thankful to my co-supervisor for showing me the enlightening pathway of ingenuity to my research endeavour.

I owe my gratefulness to HOD and former HOD, Central Department of Chemistry, Kirtipur for their care and concern to my work. I am grateful to faculties, support services and friends in the department for cooperation and suggestions to my work. I acknowledge Tribhuvan university, Institute of Science and Technology (IOST), Dean's office for my research studies and Tribhuvan university, Institute of Engineering (IOE), Dean's office for providing three years' study leave for my research work. I am gratefully thankful to the Campus Chief, Assistant Campus Chiefs, HOD of the Department of Applied Sciences, colleagues and support services at IOE, Pashchimanchal Campus, Pokhara.

I would like to acknowledge Nepal Academy of Science and Technology (NAST) and Indian National Science Academy (INSA) for NAST-INSA fellowship to me at Indian Institute of Science (IISc), Bangalore, India. I am gratefully thankful to Professor A. R. Chakravarty and Dr Aditya Garai for their guidance and help to my work at Department of Inorganic and Physical Chemistry, IISc, Bangalore, India. In addition, I acknowledge NAST with thankfulness for supporting this research work with Ph. D. fellowship -2017.

I acknowledge Dr Yuba Raj Pokharel, South Asian University, New Delhi, India; Dr Agni Raj Koirala, Sogang University, Korea; Department of Plant Resources, Thapathali, Kathmandu and my friend Narendra Kumar Singh for their support to characterization part of my work. I gratefully acknowledge Head of the Department Prof. Krishna Das Manandhar and Chetana Khanal, Central Department of Biotechnology, IOST, TU, Nepal for the *in vitro* anticancer screening of the samples against the tumorigenic MDCK and MCF-7 cancer cell lines.

I am indebted to my parents for preparing me out of nothing except the struggle for my education. I am grateful to my spouse for all her woes and endurance to my studies. I am thankful to my beloved children and all members of my extended family for the moments of tear and laughter during my work and studies.

Hari Sharan Adhikari

(March, 2021)

# ABSTRACT

Chitosan and various chitosan derivatives have been found to lend themselves to selective permeation through the cancer cell membranes and exhibit remarkable anticancer activity *via* the immunoenhancement, enzymatic and antiangiogenic mechanism, antioxidant defence route and apoptotic pathways. They are sequestered from the normal cells and undergo permeation through the vascular micro environment to show the enhanced biodistribution level in cancer cells. They attract a great deal of research interest that is associated to more effective anticancer drug development strategy. In this juncture, the current studies were focussed at synthesis, characterization and anticancer activity assessment of low and high molecular weight chitosan functionalized thiosemicarbazones and their copper(II) complexes *in vitro*. The research work aimed to establish the pathway of chitosan tailoring in favour of structurally viable anticancer drug development strategy.

Chitin, obtained after demineralization and deproteinization of crab shells powder, was deacetylated into chitosan. Partial deacetylation was evident from Fourier Transform Infra - red (FT-IR) and solid state $^{13}C$ Nuclear Magnetic Resonance ($^{13}C$ NMR) spectra. The X ray diffraction (XRD) patterns with two characteristic crystalline peaks (2θ at 9.5° and 19.6°) and the elemental microanalysis corresponding to the monomer structure of chitosan (formula weight 161.15) were also in close agreement with the partial deacetylation of chitin to chitosan. The synthesized chitosan showed high thermal stability with a substantial mass of chitosan as residue at 1000 °C. The physicochemical properties *viz*. 71% degree of deacetylation (DDA) and 350 kDa of molecular weight ($M_w$) in average, 1.00% ash content and 7.40% moisture content with the chitosan yield of 31.4% revealed crab shells as a rich source of high molecular weight nanocrystalline chitosan and a biomaterial of multipurpose applications and futuristic potential.

Synthesis of chitosan thiosemicarbazone as a ligand *via* the key intermediate formation of one pot synthesized chitosan thiosemicarbazide, and copper(II) chitosan thiosemicarbazone complex in search of potential anticancer agent appeared significant with substantial inhibition of MDCK tumorigenic cell growth *in vitro*. Characterisation with FT-IR and solid state $^{13}C$ NMR spectroscopic techniques showed the involvement of C2 in pyranose ring of chitosan in the formation of chitosan thiosemicarbazones. Higher crystallinity phases in copper(II) chitosan thiosemicarbazone complexes than in the respective chitosan thiosemicarbazone ligands as shown by the respective X ray diffractograms are an indicative

of the coordination behaviour of thiosemicarbazones. Elemental analysis of chitosan thiosemicarbazone analogues showed the partial introduction of thiosemicarbazone group into amino group at C2 position of pyranose ring in chitosan. Further, the chelation of chitosan thiosemicarbazones with copper(II) was evident from correlative characterization by FT-IR spectra with decrease in the wave number of C=S and C=N bands from chitosan thiosemicarbazone ligands to the respective copper(II) complexes and the presence of an unpaired electron in copper(II) chitosan thiosemicarbazone complexes as shown by Electron Paramagnetic Resonance (EPR) spectra with $g > g_e$ (2.0023). The g value in EPR spectrum, estimated chlorine contents and elemental microanalyses supported a distortion in mononuclear square planar geometry of complexes. The thermal studies revealed enhanced stability and less thermal degradation behaviour of complexes than chitosan thiosemicarbazone ligands. More inhibition of tumorigenic Madin-Darby Canine Kidney (MDCK) and human breast cancer (MCF-7) cell growth *in vitro* by the complexes than chitosan thiosemicarbazone ligands is an indicative of anticancer enhancement or inhibition upon the process of complex formation.

**Keywords:** *Anticancer activity, Anticancer mechanism of action, Carboxaldehydes, Characterization, Chitosan, Chitosan thiosemicarbazones, Copper(II) chitosan thiosemicarbazone complexes*

# TABLE OF CONTENTS

# LIST OF TABLES

# LIST OF FIGURES

# LIST OF SCHEMES

# LIST OF SYMBOLS

| | |
|---|---|
| ° | Degree |
| °C | Degree Celsius |
| K | Kelvin |
| Da | Dalton |
| kDa | Kilo Dalton |
| μg | Microgram |
| mg | Milligram |
| h | hour |
| BM | Bohr Magneton |
| ν | (Vibrational) frequency |
| δ | Chemical shift |
| > | Greater than |
| < | Less than |
| GHz | Giga Hertz |
| MHz | Mega Hertz |
| Gs | Gauss |
| mT | Milli Tesla |
| $B_o$ | Magnetic field |
| h | Planck's constant |
| g | g tensor or Lande g factor in EPR spectrum |
| *et al*. | et alia (and others) |
| $\mu_{eff}$ | Effective magnetic moment |
| C | Concentration (in molarity) |
| $IC_{50}$ | Half inhibitory concentration |
| g | gram |
| $\chi_m$ | molar susceptibility |
| $\chi_g$ | gram susceptibility |

# LIST OF CODES OF THE SYNTHESIZED COMPOUNDS

| | |
|---|---|
| CCS: | Crab shell chitosan |
| CCSAPRTSC: | Crab shell chitosan 2-acetyl pyridine thiosemicarbazone |
| CCSAPTSC: | Crab shell chitosan 2-acetyl phenol thiosemicarbazone |
| CCSCLISTSC: | Crab chitosan 5-chloroisatin thiosemicarbazone |
| CCSIMTSC: | Crab shell chitosan imidazole-2-carboxaldehyde thiosemicarbazone |
| CCSISTSC: | Crab shell chitosan isatin thiosemicarbazone |
| CCSPCTSC: | Crab shell chitosan pyridine-2-carboxaldehyde thiosemicarbazone |
| CCSSTSC: | Crab shell chitosan salicylaldehyde thiosemicarbazone |
| CCSTHPTSC: | Crab shell chitosan thiophene-2-carboxaldehyde thiosemicarbazone |
| CSAPRTSC: | Oligo chitosan 2-acetyl pyridine thiosemicarbazone |
| CSAPTSC: | Oligo chitosan 2-acetyl phenol thiosemicarbazone |
| CSCLISTSC: | Oligo chitosan 5-chloroisatin thiosemicarbazone |
| CSIMTSC: | Oligo chitosan imidazole-2-carboxaldehyde thiosemicarbazone |
| CSISTSC: | Oligo chitosan isatin thiosemicarbazone |
| CSPCTSC: | Oligo chitosan pyridine-2-carboxaldehyde thiosemicarbazone |
| CSSTSC: | Oligo chitosan salicylaldehyde thiosemicarbazone |
| CSTHPTSC: | Oligo chitosan thiophene-2-carboxaldehyde thiosemicarbazone |
| Cu-CCSAPRTSC: | Copper(II) Crab shell chitosan 2-acetyl pyridine thiosemicarbazone |
| Cu-CCSAPTSC: | Copper(II) Crab shell chitosan 2-acetyl phenol thiosemicarbazone |
| Cu-CCSCLISTSC: | Copper(II) Crab shell chitosan 5-chloroisatin thiosemicarbazone |
| Cu-CCSIMTSC: | Copper(II) Crab shell chitosan imidazole-2-carboxaldehyde thiosemicarbazone |
| Cu-CCSISTSC: | Copper(II) Crab shell chitosan isatin thiosemicarbazone |
| Cu-CCSPCTSC: | Copper(II) Crab shell chitosan pyridine-2-carboxaldehyde thiosemicarbazone |
| Cu-CCSSTSC: | Copper(II) Crab shell chitosan salicylaldehyde thiosemicarbazone |
| Cu-CSAPRTSC: | Copper(II) oligo chitosan 2-acetyl pyridine thiosemicarbazone |
| Cu-CSAPTSC: | Copper(II) oligo chitosan 2-acetyl phenol thiosemicarbazone |
| Cu-CSCLISTSC: | Copper(II) oligo chitosan 5-chloroisatin thiosemicarbazone |
| Cu-CSIMTSC: | Copper(II) oligo chitosan imidazole-2-carboxaldehyde thiosemicarbazone |

| | |
|---|---|
| Cu-CSISTSC: | Copper(II) oligo chitosan isatin thiosemicarbazone |
| Cu-CSPCTSC: | Copper(II) oligo chitosan pyridine-2-carboxaldehyde thiosemicarbazone |
| Cu-CSSTSC: | Copper(II) oligo chitosan salicylaldehyde thiosemicarbazone |
| Cu-CSTHPTSC: | Copper(II) oligo chitosan thiophene-2-carboxaldehyde thiosemicarbazone |

# LIST OF ACRONYMS AND ABBREVIATIONS

| | |
|---|---|
| AGE: | Advanced Glycation End products |
| Ara-C: | 1-D-Arabinofuranosylcytosine |
| bFGF: | Basic Fibroblast Growth Factor |
| BM: | Basement membrane |
| C.I. | Crystallinity Index |
| CMCS: | Carboxymethyl chitosan |
| $^{13}$C- NMR: | $^{13}$Carbon Nuclear Magnetic Resonance |
| CNP: | Chitosan nanoparticles |
| COS: | Chitosan oligosaccharide |
| COX: | Cyclooxygenase |
| COX-2: | Cyclooxygenase-2 |
| CS: | Chitosan oligosaccharide |
| csf: | Cerebrospinal fluid |
| DDA: | Degree of deacetylation |
| DMSO: | Dimethyl sulfoxide |
| DNA: | Deoxyribonucleic acid |
| DS: | Degree of Substitution |
| EAC: | Erlich ascites carcinoma |
| EDC: | N-Ethyl-N′-(3-dimethylaminopropyl) carbodiimide hydrochloride |
| EAT: | Erlich ascites tumor |
| EPR: | Enhanced permeation and retention |
| EPR spectra: | Electron Paramagnetic Resonance spectra |
| ERK: | Extracellular Signal Regulated Kinase |
| FBS: | Fetal Bovine Serum |
| FT-IR: | Fourier Transform Infrared |
| FACS: | Fluorescent activated cell sorbent assay |
| FDA: | US Food and Drug Administration |
| FGF-2: | Fibroblast growth factor-2 |
| FGFR: | Fibroblast growth factor kinase receptor |
| 5-FU: | 5-Fluorouracil |
| FWHM: | Full Width at Half Maxima |
| G-Chi: | Glycol chitosan |
| GRAS: | Generally recognized as safe |
| GSH: | Glutathione |
| GST: | Glutathione S-transferase |
| HEPES: | 4-(2-hydroxyethyl)-1-piperazineethanesulfonic acid |
| HL: | Human Leukaemia |
| HMWC: | High molecular weight chitosan |
| HS: | Heparan sulfate |
| HUVECs: | Human umbilical vein endothelial cells |

| | |
|---|---|
| IELs: | Intraepithelial lymphocytes |
| IFN-$\alpha$: | Interferon cell signaling pathway-$\alpha$ |
| IFN-$\gamma$: | Interferon cell signaling pathway-$\gamma$ |
| IL: | Interleukin |
| IL-1: | Interleukin 1 |
| IL-2: | Interleukin 2 |
| IL-8: | Interleukin 8 |
| iNOS: | Inducible Nitric Oxide Synthase |
| LLC: | Lewis Lung Carcinoma |
| LMWC: | Low molecular weight chitosan |
| LPS: | Lipopolysaccharide |
| MCF-7 cell line: | Michigan Cancer Foundation-7, Human Breast Cancer cell line |
| MCNS: | Mifepristone loaded chitosan nanoparticles |
| MDCK cell line: | Madin Darby Canine Kidney cell line |
| MIF: | Mifepristone |
| MMC: | Mitomycin C |
| MMP9: | Matrix metalloproteinase 9 |
| MMPs: | Matrix metalloproteinases |
| MTT: | 3-(4,5-dimethylthiazol-2-yl)-2,5-diphenyltetrazolium bromide |
| mRNA: | Messenger ribonucleic acid |
| $M_w$: | Molecular weight |
| NaPaC: | Phenylacetate carboxymethyl benzylamide dextran |
| NHS: | N-Hydroxysuccinimide |
| NK: | Natural killer |
| NK-cells: | Natural killer cells |
| NO: | Nitric oxide |
| ODC: | Ornithine decarboxylase |
| PBS: | Phosphate Buffered Saline |
| PDGF: | Platelets derived growth factor |
| PHI: | Holmium-166 percutaneous (166Ho)/chitosan complex injection |
| PNA: | Peptide-nucleobase conjugate |
| PPC: | Polypyrrole chitosan |
| PXRD: | Powder X Ray Diffraction |
| QR: | Quinone/quinine reductase |
| RPMI media: | Roswell Park Memorial Institute media |
| RNA: | Ribonucleic acid |
| ROS: | Reactive oxygen species |
| RR: | Ribonucleotide reductase |
| SBCS: | Sulfated benzaldehyde chitosan |

| | |
|---|---|
| SCS: | Sulfated chitosan |
| SCC: | Squamous cell carcinoma |
| SCID: | Severe combined immune deficient |
| siRNA: | Short interfering RNA |
| Suc-Chi: | N-succinyl chitosan |
| TG/DTA: | Thermogravimetric/differential thermal analysis |
| TGF-$\beta$: | Transforming growth factor- $\beta$ |
| TIMP 1: | Tissue inhibitor of metalloproteinase 1 |
| TIMPs: | Tissue inhibitor of metalloproteinases |
| TNF -$\alpha$: | Tumor necrosis factor-$\alpha$ |
| TPA: | 12-O-tetradecanoylphorbol-13-acetate |
| TPP: | Tripolyphosphate |
| VEGF: | Vascular endothelial growth factor |
| VEGFR2: | Vascular endothelial growth factor receptor 2 |
| XRD: | X Ray Diffraction |

# CHAPTER 1

## 1. INTRODUCTION

## 1.1. Preface

### 1.1.1. Cancer Pathophysiology and Proliferation

Cancer often starts as a pathological entity because of genetic alteration in a single cell and it may take a few days to several years to become invasive and palpable. Cancer cells are malignant neoplasms that acquire invasive character owing to failure of normal immune mechanism or natural killer (NK) activity of the intraepithelial lymphocytes to promptly destroy them (Maeda & Kimura, 2004). They are transformed by genetic mutation of the cellular deoxyribonucleic acid (DNA) that acts as a selective template for the formation of transfer, messenger and ribosomal ribonucleic acid (RNA) (Karnofsky,1968). In a quantitatively altered metabolic pathway, such cells make their clones that abnormally proliferate irrespective of growth regulating signals in the environment through lymph and blood vessels. Despite the treatment of primary malignancy, this process of angiogenesis that governs normal embryonic development, tumour growth and metastasis (Karnofsky,1968; Miura, *et al.*, 2010; Nishida, *et al.*, 2006; Park, *et al.*, 2007) can lead to relapse and metastatic manifestations at the distant site of the system affected (Friedel, *et al.*, 2002). So, the inhibition of angiogenesis is critically important (Miura, *et al.*, 2010; Park, *et al.*, 2007) in cancer elimination and prevention.

Tumour metastasis, the pathological state of major complication in cancer, is a multi-step process that involves cell adhesion, invasion and migration (Yilmaz, *et al.*, 2007) and this process requires degradation of connective tissue and proteolysis of extracellular matrix (Stetler-Stevenson, *et al.*, 1993; Yilmaz, *et al.*, 2007; Yu, *et al.*, 1996). After an increase in size to a threshold of few millimetres, solid tumour requires new blood vessels to provide oxygen and nutrient and to take away the metabolic wastages (Folkman,1972). This process of formation of new capillaries called angiogenesis triggers under suitable pathological conditions as a result of angiogenic switch (Roskoski,2007) arising from the net balance between pro-angiogenic compounds like vascular endothelial growth factor(VEGF), basic fibroblast growth factor (bFGF), transforming growth factor –β ( TGF- β), platelet –derived growth factor(PDGF), matrix metalloproteinases (MMPs) and anti-angiogenesis factors like angiostatin, endostatin and tissue inhibitor of metalloproteinase (TIMPs) (Miura, *et al.*, 2010; Park, *et al.*, 2007; Roskoski,2007).The MMPs are the proteolytic enzymes that cause the

degradation of extracellular matrix (ECM) and play an important role towards regulation of vascular remodelling and angiogenesis (Benjamin, *et al.*, 2012) .

The pro angiogenic effects such as endothelial cell migration, proliferation and permeability through vascular membrane are most commonly stimulated and mediated by cell surface tyrosinase kinase receptor VEGFR2 (Shibuya and Claesson-Welsh, 2006) of VEGF. So, VEGF is a key regulator of tumour angiogenesis (Roskoski,2007). VEGF and VEGFR2 levels are unusually high in tumour cells and the overexpression of VEGF leads to clinically incurable increase in tumour growth and metastasis (Shweiki, *et al.*,1992; Zhang, *et al.*, 1995). Hence VEGF and VEGFR2 appear as potential molecular targets in cancer chemotherapy and VEGF-VEGFR2 signal blockers have been prepared for clinical use (Abou Alfa, *et al.*, 2006; Wilhelm, *et al.*, 2008; Witte, *et al.*, 1998).

Tumour angiogenesis that is essential for tumour growth and metabolism (Zong, *et al.*, 2013) is caused by proliferation and migration of endothelial cells (Wang, *et al.*, 2014). Newly formed capillaries take away the metabolic wastes and help metastasis (Wang, *et al.*, 2014). Chemo preventive agents can bring about better prognosis and intervention to neoplastic progression and metastasis by inhibition of angiogenesis and tumour growth before the occurrence of malignant invasion (Chen, *et al.*, 2005; Chen, Chu, *et al.*, 2006; Chen, Kuo, *et al.*, 2006; Muzzarelli,1997).

**1.1.2. Pathways of Anticancer Activity**

The general mechanism or pathway of anticancer drugs is associated with interference with the structure or function of DNA and deterioration in the synthetic processes of ribonucleic acid (RNA) templates and enzymes. Such disturbances in normal functioning of central dogma of molecular biology from DNA to RNA to protein or enzymatic synthesis (Karnofsky,1968) can bring about the desirable cytotoxic effects and the agents approved for anticancer use can damage DNA, block DNA synthesis by inhibition of nucleic acid synthesis, disrupt hormonal and enzymatic path to biosynthesis and inhibit the growth of cancer cells (Crick, 1970; Karnofsky,1968; Morgan, 1995).

Anticancer agents exert their cytotoxic action using their own specific pathways. For instance, antimetabollites inhibit DNA synthesis, alkylating agents disrupt DNA and intercalcating agents cause interference to DNA transcription or duplication (Karnofsky,1968). Ribonucleotide reductase (RR) plays a central role in the *de novo* synthesis of deoxyribonucleotides required for DNA replication and repair (Cory & Sato, 1983; Thelander & Reichard, 1979). As such, RR offers a particularly attractive target for neoplastic agents directed against rapidly growing tumors.

Anticancer pathways of various agents in clinical uses (scheme 1) include inhibition of synthesis of nucleic acid, disruption in hormonal and enzymatic path to growth of cancer cells and amplification of the signals to programmed cell death or apoptosis (Wimardhani, *et al.*, 2014) with activation of caspase-3 (Sugano, *et al.*, 1980) and also to extrinsic apoptosis with activation of caspase 8 (Takimoto, *et al.*, 2004). Necrosis can also be a cause of cell death (Qi, *et al.*, 2005). The checkpoint at S phase in the cell cycle (scheme 2) controls the progression of cell proliferation according to the signals from the cellular environment (Nurse, 2000; Zheng, *et al.*, 2006). Certain antimetabolites cause inhibition of biosynthesis of nucleic acids and vinca alkaloids produce metaphase arrest as a result of disorganization of mitotic spindle during cell division (Karnofsky,1968).

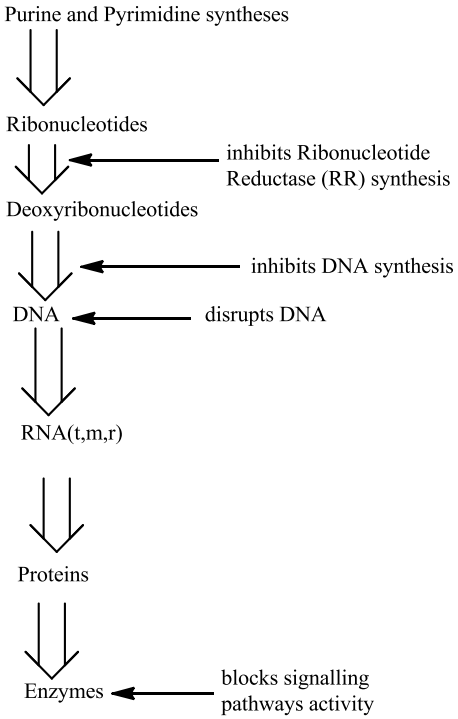


**Scheme 1:** General pathways of anticancer agents

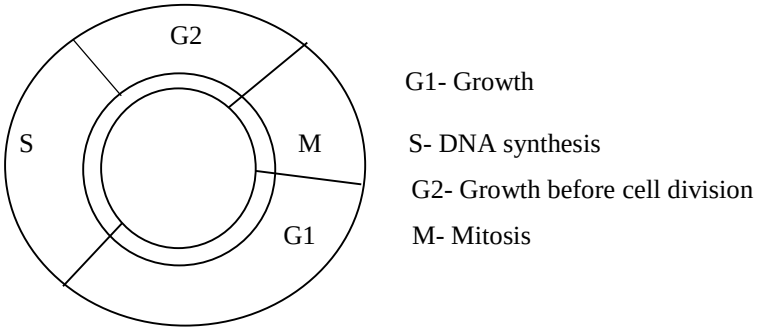


**Scheme 2:** Cell cycle

One of the mechanisms of action of chemopreventive drugs involves the induction of the detoxification enzymes such as quinone reductase (QR) and glutathione S-transferase (GST) (Talalay, *et al.*, 1995). QR acts with xenobiotic metabolism to protect the cells from the carcinogenesis and mutation (Nam, *et al.*, 2007a). GST detoxifies the exogenous and endogenous electrophiles by catalysing their conjugation with glutathione (GSH) and protects the cells from toxicity due to exposure in excessive amounts of these carcinogenic electrophiles (Nam, *et al.*, 2007a). GST performs this by interfering the formation of DNA adducts (Sheweita & Tilmisany, 2003).

The activity of enzyme ornithine decarboxylase (ODC) is more in tumour than in nontumour tissue (Rozhin, *et al.*, 1984). It is a rate limiting enzyme that acts on polyamine biosynthetic pathway (Lee, *et al.*, 2005) and its activity can be a useful biomarker of tumour growth and progression (Nam, *et al.*, 2007a).

Cyclooxygenase (COX) is an enzyme involved in biosynthesis of prostaglandin from arachidonic acid (Nam, *et al.*, 2007a) and secretion of its isoform COX-2 is induced by tumour promoters along with certain serum and growth factors and proinflammatory cytokines (Vane & Botting, 1998). COX-2 have been found to be more highly expressed in colon tumours (Eberhart, *et al.*, 1994).

Over expression of inducible nitric oxide synthase (iNOS) produced by proinflammatory cytokines (Marletta, 1993) is correlated to metastatic potential (Ambs, *et al.*, 1998; Lagares-Garcia, *et al.*, 2001; Nam, *et al.*, 2007b), and the regulation of blood vessel growth is affected by the unfavourable biological processes like angiogenic diseases and cancer (Folkman, 1995).

Antitumour effect is largely shown by enhanced cytotoxicity arising from increased natural killer (NK) activity of intestinal intraepithelial lymphocytes (IELs) and splenic lymphocytes through the activation of intestinal immune functions (Maeda & Kimura, 2004). Thus, antitumour effect is correlated with immune potentiating of tumoricidal immunocytes like T-lymphocytes (Truitt, *et al.*, 1979), macrophages (Nathan, *et al.*, 1979) and natural killer cells (Minato, *et al.*, 1980).

Cellular Invasion through a vascular basement membrane (BM) that lies as a barrier between malignant cells and bloodstream is critical step in metastasis (Liotta, *et al.*, 1980). This process involves degradation of interstitial connective tissue in BM before the approach of malignant cells in circulating blood (Stetler-Stevenson, *et al.*, 1993; Yu, *et al.*, 1996).

When antioxidant defense system is not effective, there is no proper scavenging of superoxide free radicals and the cellular oxidative damage *in vivo* can lead to diseases like cancer, arthritis, cataract, brain dysfunction, decline in immune system and heart disease (Gordon, 1996; Halliwell, *et al.*, 1995; Zhong, *et al.*, 2010). Natural antioxidants can show radical scavenging effect and retard the progress of these diseases (Kinsella, *et al.*, 1993).

### 1.1.3. Chitin and Chitosan

Chitin $(C_8H_{13}O_5N)_n$ (figure 1) is a naturally obtained biopolymer that shows most abundance in crustacean and mollusc shells, insect cuticles and cell walls of fungi. The crustacean shells, as the major source of chitin, consist of 15-40% chitin, 20-40% protein and 20-50% calcium carbonate and magnesium carbonate minerals in close association with minor constituents like lipids and pigments, astaxanthin, and other minerals (Khoushab & Yamabhai, 2010). Chitin is a homopolymer that consists of 2-acetamido-2-deoxy- β -D-glucose monomers (N-acetyl glucosamine units) linked through β (1→4) linkages (Percot, *et al.*, 2003; Ramya, *et al.*, 2012). It is the source of chitosan (figure 2), a polymer that is made of deacetyl α-(1, 4) glucosamine $(C_6H_{11}O_4N)_n$ monomers. Chitosan can be synthesized by alkaline deacetylation of chitin with sodium hydroxide (Sagheer, *et al.*, 2009; Zhang, *et al.*, 2002) (figure 3) after the finely powderd crustacen shells are demineralized with acid and deproteinized with alkali (scheme 3).

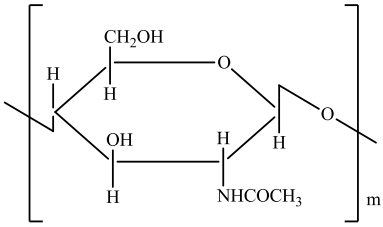


**Figure 1:** Structure of chitin

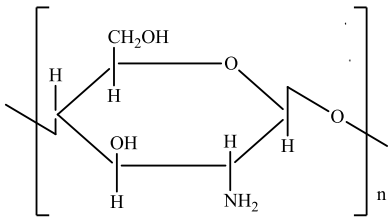


**Figure 2:** Structure of chitosan

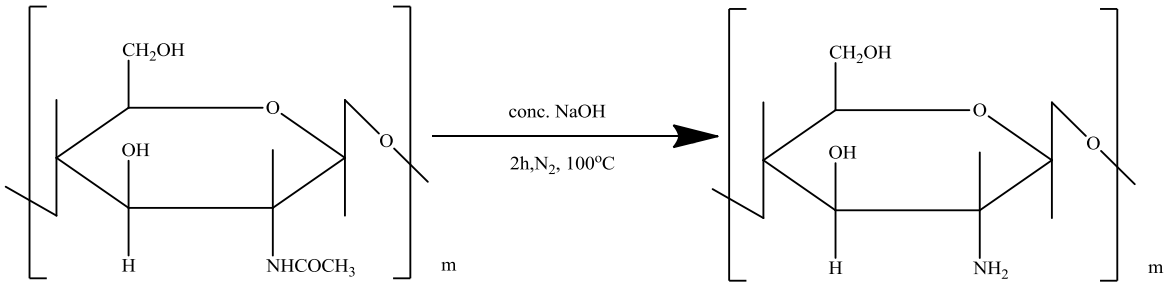


**Figure 3:** Deacetylation of chitin

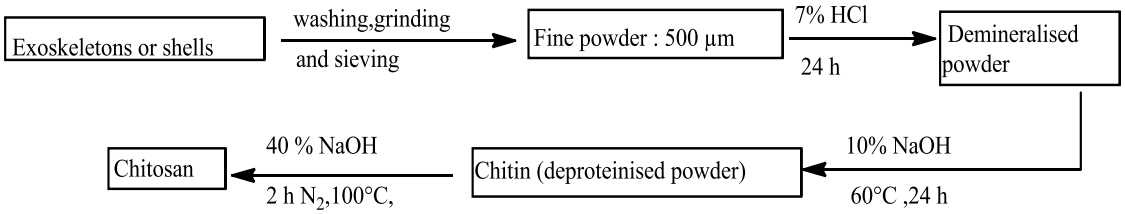


**Scheme 3:** Steps involved in the preparation of chitosan

It is a nontoxic, biocompatible and biodegradable material with adsorptive behaviour (Günbeyaz, *et al.*, 2010; Park, *et al.*, 2011; Wimardhani, *et al.*, 2012). It is a pharmaceutical excipient (Ray, 2011), permeation enhancer (Sadeghi, *et al.*, 2008) and hemostatic agent (Gu, *et al.*, 2010) used in targeted delivery of drugs (Park, *et al.*, 2010), wound healing and dressing (Burkatovskaya, *et al.*, 2006). It shows antimicrobial (Martins, *et al.*, 2014), anticancer (Wimardhani, *et al.*, 2014), antifungal (Lopez-Moya, *et al.*, 2015), antioxidant (Park, *et al.*, 2003) and anti-obesity (Han, *et al.*, 1999) activities. Owing to its non-toxicity, biodegradability, suitable physicochemical properties and thermal stability, chitosan has been found widely useful in the fields such as tissue engineering (Zhang & Zhang, 2002), gene therapy (Lavek & Singh, 2017), food preservation (No, *et al.*, 2007), dietary supplements (Muzzarelli, 1996), wastewater treatment (Onsosyen & Skaugrud, 1990) and pulp and paper industries (Habibie, *et al.*, 2016). The functional properties of chitosan such as film forming ability, chelation, adsorption, biocompatibility and bioactivity (Ravi Kumar, 2000) are greatly influenced by its physicochemical parameters, $M_w$ and viscosity (No & Lee, 1995). So, the standardisation of synthetic conditions and methods is very significant. High molecular weight chitosan (HMWC) has been found more effective as a food preservative (Lee, *et al.*, 2002), flocculating and chelating agent and heavy metal ions trapper (Dutta, *et al.*, 2004). The chitosan film or hydrogel can be used in burn dressing and fabrication of suturing threads (Harish Prashanth, *et al.*, 2007).

Nano chitosan, prepared as biocompatible polymeric nanoparticles, undergoes prolonged circulation in blood with more extravasation and passive targeting (Gaur, *et al.*, 2000). So, it is a suitable drug delivery candidate (Lee, *et al.*, 2008; Zhang, *et al.*, 2009), antimicrobial (Martins, *et al.*, 2014) and anticancer (Wimardhani, *et al.*, 2014) agent with a controlled delivery to the target cells in a sustained release manner by enhanced permeation and retention (EPR) effect (Maeda, 2001). The nanocrystalline chitosan, with a high hydrophilic and nanoparticulate creating behaviour, has a great potential towards the development of new complexes for regenerative medicine and tissue engineering (Pighinelli, *et al.*, 2016).

### 1.1.4. Thiosemicarbazones and Chitosan Thiosemicarbazones

Thiosemicarbazones are synthetic compounds obtained by the condensation of thiosemicarbazides with aldehydes or ketones. They are named by the class name thiosemicarbazone after the name of the aldehyde or ketone condensed (Casas, *et al.*, 2000). Upon the grafting of thiosemicarbazone with chitosan, there is an enhancement in antioxidant activity as a result of weakening of intermolecular and intramolecular linkages made by hydrogen bonds, and interaction of C=S and N-H groups with free radicals (Zhong, *et al.*, 2010). The antioxidant behavior is attributed to amino and hydroxyl groups attached to C-2, C-3 and C-6 positions of the pyranose ring that can introduce the abstraction of hydrogen easily from free radicals (Xie, *et al.*, 2001). Thiosemicarbazones have been shown to impart the potent anticancer effects (Beraldo & Gambinob, 2004; Zhong, *et al.*, 2011) and such effects are linked to scavenging of cancer-inducing free radicals and lowering of oxidative damage of cells (Zhong, *et al.*, 2010). Replication and repair of DNA require deoxyribonucleotides that are synthesized in *de novo* by the essential involvement of ribonucleotide reductase (RR) (Cory & Sato, 1983; Thelander & Reichard, 1979). Inhibition of RR activity by α-(N)-heterocyclic carboxaldehyde thiosemicarabazones (HCTs) has been found to trigger the antineoplasic activity (Moore & Sartorelli, 1989).

Synthetic modifications in the heterocyclic ring system or substituents and the side chain of thiosemicarbazone moiety can give the HCT derivatives with anticancer activity (Agrawal & Sartorelli, 1969; Brockman, *et al.*, 1956; French & Blantz Jr., 1966; French & Blantz Jr., 1971; Klayman, *et al.*, 1979). Antioxidant effects are introduced by scavenging of reactive oxygen species (ROS), preventing the generation of ROS and activating a battery of detoxifying proteins. Natural antioxidants are crucial to protect the human body from free radicals and retard the progress of many chronic diseases (Kinsella, *et al.*, 1993). Low molecular weight chitosan thiosemicarbazones have been reported to show better free radicals scavenging activity (Ji, *et al.*, 2007). The higher antioxidant behavior of chitosan thiosemicarbazones associated to better scavenging and curtailing of the free radicals (Zhong, *et al.*, 2010) is likely to bring about the cerebral dysfunction, immune system decline and cancer (Mc Cord, 2000; Rao, *et al.*, 2006). The cationic nature of chitosan with reactive functionalities can create some tight junctions in the cell membrane and biochemical modification of chitosan attributed to such behavior can give the derivatives of unique properties (Gavhane, *et al.*, 2013). The non-toxic behavior and higher abundance in nature can make chitosan an antioxidant of sustainable utility (Castagnino, *et al.*, 2008). On the basis

of antioxidant behavior and favorable structural molecular make-up of the chain, chitosan thiosemicarbazones are hypothesized to bring about the potent anticancer effects.

The better scavenging effect of chitosan thiosemicarbazone than chitosan has been revealed by the results of antioxidant activity with superoxide anion scavenging assay (Zhong, *et al.*, 2010). In this study, water soluble chitosan (Mw=8 k Da), high molecular weight chitosan (HMWC) ($M_w$ =200 k Da), hydrazine thiosemicarbazone chitosan (lower $M_w$) and 2-phenylhydrazine thiosemicarbazone- chitosan (higher $M_w$) were found to show the scavenging effects of 12.67, 0.4, 43.12 and 35.23 respectively (Zhong, *et al.*, 2010). The data revealed more scavenging activity of chitosan thiosemicarbazone than chitosan and a better scavenging effect with a decrease in $M_w$ of chitosan.

### 1.1.5. Chitosan – metal Complex

Chitosan is a multifunctional, cationic polymer that shows coordination behavior with several metal ions (Pestov & Bratskaya, 2016). Antitumor activity of chitosan-metal complex is favored by an appropriately fixed ratio of chitosan to metal ion (Zheng, *et al.*, 2006) and such ratio can be determined by cleavage of the chain at relatively weak points under the influence of coordinate covalent bonds. The cleavages at the weak points can give the coordination compounds of similar molecular weight, and such cleavages are brought about by the oxidative hydrolysis with the oxidants such as ozone, hydrogen peroxide and acetic acid under the controlled conditions of coordination like the rates of addition and stirring (Yin, *et al.*, 2004). Chitosan degradation by hydrogen peroxide has been found to cause a decrease in Mw in a manner that is dependent upon the increase in concentration of hydrogen peroxide, time and temperature. Chitosan was found to undergo a decrease in $M_w$ from 51 k Da to 1.2 k Da with the substantial structural changes attributed to the deamination, formation of 2.86 mmol/g of carboxyl group and loss of 40% amino groups in the products (Qin, Du, & Xiao, 2002). With an increase in pH, there was increase in the rate of chitosan degradation by the oxidative action of hydrogen peroxide, and this process was attributed to enhancement of degradation by hydroxy radicals. It showed that the controlled degradation could be carried out by maintaining the proper pH of the solution (Qin, Du, & Xiao, 2002).

Chitosan-copper complexes in copper(II) to chitosan ratio of 0.4:1 showed a selective inhibition of 293 cancer cell line ($IC_{50}$ 34 µmol/L) and HeLa tumor cell line ($IC_{50}$ 48 µmol/L) but no inhibitory effect was observed against the growth of HLF (Zheng, *et al.*, 2006). This was clearly an indicative of concentration dependent *in vitro* anticancer activity of chitosan-

copper complexes and their nontoxicity in normal cells. The synthetic reaction of 10 g of chitosan per litre of 1% acetic acid with copper(II) sulfate pentahydrate in a molar ratio of 1:0.4 has been found to give the chitosan -copper(II) complex of square planar geometry and conspicuous anticancer activity (Zheng, *et al.*, 2006) (figure 4).

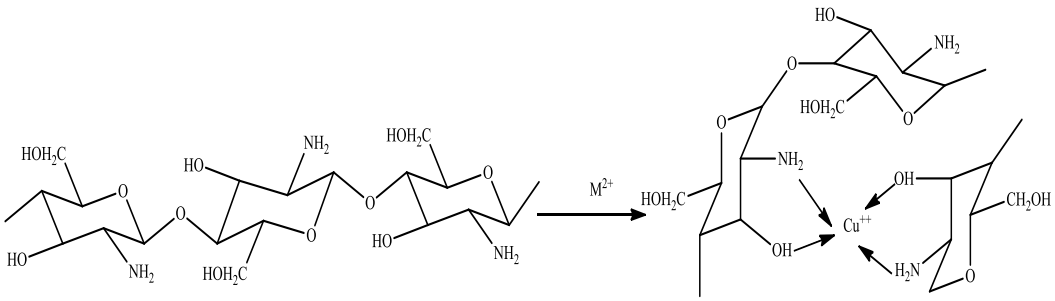


**Figure 4:** Structure of chitosan- metal complex

## 1.2. Rationale

The research provides a cutting-edge perspective towards development of the compounds with anticancer structural enhancement. Functionalization of chitosan as chitosan thiosemicarbazones is a novel approach of preparation of ligands, and the synthesis of copper(II) chitosan thiosemicarbazone complexes. Chitosan and chitosan derivatives show effective permeation through the negatively charged cancer cell surfaces so as to ensure the higher biodistribution of these materials in cancer cells. The study is expected to correlate the structural make-up of chitosan thiosemicarbazones and their copper(II) complexes with their tumor suppression and antimetastatic behavior in different cellular pathways, and leave a treasure of data for further mechanistic investigation. Synthetic preparation of chitosan, chemical modification of chitosan through functionalization, graft copolymerization and complex formation could open up an avenue towards the tailoring of biocompatible chitosan materials of anticancer applications.

## 1.3. Objectives of the Research Studies

The aim of this research is to bring about the synthesis and characterization of chitosan based thiosemicarbazones and their copper (II) complexes and study their cytotoxic activity on human cancer cell lines in search of potential anticancer drug formulae.

### 1.3.1. General Objectives

The general objectives of the studies are to synthesize oligo chitosan thiosemicarbazones and high molecular weight chitosan thiosemicarbazones with different carboxaldehydes,

synthesize and characterize their copper(II) complexes, and study the anticancer activity of both ligands and complexes *in vitro*. The research work aims to establish the pathway of chitosan tailoring through functionalization as chitosan thiosemicarbazones and their complex formation in favour of a viable anticancer drug development strategy.

### 1.3.2. Specific Objectives

- To prepare, characterize and investigate the physicochemical properties of chitosan from crab shells.
- To carry out the functionalization of both commercially available chitosan oligosaccharide and crab shell chitosan as chitosan-thiosemicarbazones.
- To characterize chitosan thiosemicarbazone ligands by FT-IR, $^{13}C$ NMR spectroscopic techniques, powder X ray diffraction, TG/DTA thermal studies and elemental microanalysis.
- To synthesize copper(II) chitosan thiosemicarbazone analogues and estimate their chlorine content.
- To characterize copper(II) chitosan thiosemicarbazone complexes by FT-IR, $^{13}C$ NMR, EPR spectroscopic methods, magnetic susceptibility measurement and the analytical ways of powder X ray diffraction, TG/DTA/DTG thermal studies and elemental microanalysis.
- To investigate the *in vitro* anticancer activity of chitosan thiosemicarbazones and their copper(II) complexes.
- To bring about the structure-activity relation, and recommend the compounds with anticancer activity against the prioritized cancer cell lines.

## 1.4. Scope of the Studies

Chitosan with higher reactivity under different chemical modifications (Kurita, *et al.*, 1993; Kurita, *et al.*, 1994) can give the derivatives that act as pharmaceutically active ingredient (Ray, 2011), permeation enhancer of cellular permeation (Sadeghi, *et al.*, 2008) and a hemostatic agent (Gu, *et al.*, 2010). It can be used in wound healing sheet, and dressing material (Burkatovskaya, *et al.*, 2006), weight loss and cholesterol management (Shields, *et al.*, 2003). Cancer cells have been found resistant to both the *in vitro* and *in vivo* use of chemotherapeutic drugs such as docetaxel, methotrexate, cisplatin, 5-fluorouracil (5-FU), and procarbazine (Andreadis, *et al.*, 2003). These compounds of the current chemotherapeutic applications have the adverse effects. They have been found to cause the acute, persistent,

and serious toxic effects on the lining of gastrointestinal tract, gonads, reticuloendothelial system and bone marrow (Remesh, 2012). Chitosan and chitosan derivatives, and their nanoformulations as the potential chitosan-drug candidates show non-toxicity to healthy cells, biocompatibility to cancer cells and biodegradability. These properties and in addition, the specificity of their anticancer effects can make these compounds stand as strategically favorable alternatives for the natural anticancer drug development.

## 1.5. Limitations of the Studies

Cancer appears as a major killer of human beings in the world and the comprehensive research works have been centred at the strategical focal point of anticancer drug development. It is critically worthwhile that chitosan and chitosan derivatives show marginal toxic effects in normal cells (Wimardhani, *et al.*, 2014), but the general therapeutic interventions of chitosan biomaterials are still limited by their low toxicity against many types of cancer cells (Kuppusami & Karuppaiah, 2013).

The US Food and Drug Administration (FDA) has labelled chitosan as a biocompatible and non-toxic polymer for dressing of wounds. Chitosan has been given the generally recognized as safe (GRAS) status, but it is likely to bring about the constipation and nausea as the adverse effects after a safe regular oral intake of 4.5 g/day for three months in humans (Baldrick, 2010). The alterations in pharmacokinetic behavior of nano particles upon the chemical modifications have been suspected to cause the *in vivo* toxicity (Kean & Thanou, 2010). This has necessitated the assessment of individual cytotoxicity profile of these chitosan biomaterials against the specific cancer cells. The biological activity and solubility of chitosan can be enhanced only through the repeated procedures of increasing the degree of deacetylation. Further, the synthetic routes and conditions of chemical modification have to be optimised to give the specific derivatives of chitosan (Gavhane, *et al.*, 2013).

Chitosan and chitosan-based biomaterials may show the accumulation in limited amount in the target cells and the conditions of arterio- venous shunting, necrosis, hypoxia, tumour perfusion and a high fluid pressure in interstitial spaces may arise as undesirable implications of the drug consumption. To get rid of such problems, the drug formulations should be prepared with specific moderations. The anticancer drug in nanoparticulated form shows better delivery and accumulation in cancer cells by EPR effect upon the encapsulation with chitosan. There is better delivery of doxorubicin to tumor cells when the doxorubicin-dextran conjugate is encapsulated with nano chitosan (Bisht & Maitra, 2009).

**CHAPTER 2**

# 2. LITERATURE REVIEW

## 2.1. Introduction

The semi synthetic natural product chitosan with multifaceted applications often exists as a cationic polysaccharide (Da Sacco & Masotti, 2010; Khoushab & Yamabhai, 2010; Percot, *et al.*, 2003; Yuan, *et al.*, 2011) The anticancer activity of chitosan against different cancer cell lines with marginal toxicity on healthy cells (Wimardhani, *et al.*, 2014) has been found to significantly depend upon $M_w$ and DDA (Park, *et al.*, 2011) and the pattern of distribution of D-glucosamine and β-(1,4)-linked- N-acetylglucosamine units in chitosan monomer determines $M_w$ and DDA (Vishu Kumar, *et al.*, 2007; Xia, *et al.*, 2008). Chitossan nanoparticles have been found to show antiangiogenic activity (Xu, Wen, & Xu, 2009) and chitosan nanoparticles with more DDA was found to undergo enhanced absorption by cultured fibroblasts (Huang, *et al.*, 2004). Chitosan oligosaccharide with low molecular weight is soluble in aqueous media and its conspicuous bioactivities with tumor growth suppression behavior have been reported in literatures (Harish Prashanth & Tharanathan, 2005; Maeda & Kimura, 2004; Park, *et al.*, 2011; Qin, Du, Xiao, Li, & Gao, 2002; Wang, *et al.*, 2008; Yamada, *et al.*, 2007).

An extensive survey of literatures shows that chemical modification of chitosan that involves amino group and acetamido residue can result in the tailoring of chitosan derivatives with augmented solubility and enhanced biological activity with a wide range of applications (Alves & Mano, 2008; Batista, *et al.*, 2006; Jayakumar, *et al.*, 2005; Jayakumar, *et al.*, 2007; Jayakumar, *et al.*, 2011; Jayakumar, Chennazhi, *et al.*, 2010; Jayakumar, Nagahama, *et al.*, 2008; Jayakumar, Prabaharan, *et al.*, 2010; Jayakumar, Tamura, *et al.*, 2008; Kumar, *et al.*, 2009; Kumar, *et al.*, 2011; Kumar, Dutta, *et al.*, 2010; Kumar, Nigam, *et al.*, 2010; Manna, *et al.*, 2009; Mourya & Inamdar, 2008; Rejinold, *et al.*, 2011). Anticancer activity of chitosan - metal complexes has been associated with their interaction with deoxyribonucleic acid (DNA) (Zheng, *et al.*, 2006) and free radicals scavenging behaviour (Wang, *et al.*, 2009; Yin, *et al.*, 2004; Zheng, *et al.*, 2006). Antitumor property of the derivatives carboxymethyl chitosan (CMCS) (Jiang, *et al.*, 2015), chitosan thymine conjugate (Kumar, *et al.*, 2012), sulfated chitosan (SCS) and sulfated benzaldehyde chitosan (SBCS) (Jiang, *et al.*, 2011), glycol-chitosan (GChi) and N-succinyl chitosan (Suc-Chi) conjugates (Kato, *et al.*, 2005), furanoallocolchicinoid-chitosan conjugate (Svirshchevskaya, *et al.*, 2016) and polypyrrole

chitosan (Salahuddin, *et al.*, 2017a; Salahuddin, *et al.*, 2017b) reported in literatures has been found to be attributed to different cellular apoptotic pathways.

## 2.2. Mechanism of Anticancer Activity of Chitosan

### 2.2.1. Permeation Enhancing Mechanism

Amino group in C2 position of ring chitosan is protonated in normal to acidic to medium, and this cationic polysaccharide (pKa ~6.5) becomes water soluble. It shows enhanced bio adhesivity and permeation through negatively charged surfaces of mucosal and basement membranes (Gavhane, *et al.*, 2013; Thonou, *et al.*, 2001). As a result, the polar drugs show higher bioavailability in oral route and a greater release through the epithelial cell surfaces. Since chitosan is biocompatible and nontoxic to healthy cells, it finds many applications in pharmaceutical and commercial fields, such as the preparation of binder in wet granulation, tablets with slow release of drugs, drug carrier in microparticle system, disintegrant, hydrogels, site specific drug delivery and carrier of vaccine delivery and gene therapy (Gavhane, *et al.*, 2013). Chitosan shows both *in vivo* and *in vitro* antimetastatic activity due to its permeation enhancing mechanism (Gavhane, *et al.*, 2013). Chitosan has been found to inhibit the migration of human breast carcinoma cells MDA-MB-231 through a matrigel coated membrane (Nam & Shon, 2009) as a result of the interacive effect of chitosan and carcinoma cell lines towards decreasing the activity and bulk of MMP9 protein, and this antimetastatic activity was found to increase in a dose dependent manner with the increase in concentration of native chitosan (Nam & Shon, 2009).

### 2.2.2. Antiangiogenic Mechanism

The antitumor effect of chitosan has been found to be associated with antiangiogenic mechanism in which there is interference to mutual regulation of anti-angiogenic and pro-angiogenic factors under the existing pathological conditions (Jiang, *et al.*, 2015). Growth inhibitory effect of chitosan nanoparticles (CNP) against the human hepatocellular carcinoma has been found to be attributed to CNP-mediated anti-angiogenic mechanism that involves a deterioration in the normal levels of vascular endothelial growth factor receptor 2 (VEGFR2) (Xu, Wen, & Xu, 2009).

### 2.2.3. Controlled Drug Delivery: A Sustained Release Mechanism

The anticancer functionality of chitosan is associated to its capacity to bring about an increased level of biodistribution and accumulation of drug in cancer cells. The mifepristone (MIF) loaded chitosan nanoparticles (MCNS) have been shown pharmacokinetically to cause

controlled drug delivery in a sustained release manner. Consequently, the anticancer activity increases with the increase in oral bioavailability of the drug *in vivo* (Zhang, *et al.*, 2016).

### 2.2.4. Immunoenhancement Mechanism

The mechanism of tumor growth inhibitiory effect of chitosan, as studied in sarcoma 180 bearing mice, has been found to be attributed to an enhancement in the immunological system that comprises the cytotoxic lymphocytes as natural killer tumoricidal immunocyte cells (Kuppusami & Karuppaiah, 2013; Maeda & Kimura, 2004). Chitosan oligosaccharide has been found to show anticancer activity *via* the invigoration of intestinal immune functions as a result of NK activity enhancement in splenic lymphocytes or intraepithelial lymphocytes (IELs) (Maeda & Kimura, 2004). Chitosan in microcrystalline state has been reported to cause the suppression of HepG2 tumor growth in the severe combined immune deficient (SCID) mice (Shen, *et al.*, 2009) and the growth inhibition of HT29 colon carcinoma cell line (Hosseinzadeh, *et al.*, 2012). The high molecular weight native chitosan has low solubility in aqueous and non-acidic media. So, it has to be depolymerized into low molecular weight COS (Qin, *et al.*, 2004). Water soluble chitosan oligosaccharide can be obtained by the treatment with cellulase that introduces enzymatic hydrolysis and chain degradation with no change in structural make-up of the residues (Qin, *et al.*, 2004). Such prepared water-soluble chitosan oligosaccharide product inhibits the growth of cancer cells (Seo, *et al.*, 2000; Suzuki, *et al.*, 1986; Tokoro, *et al.*, 1988). The tumor growth inhibitory activity of chitohexaose and hexa- N- acetylchitohexaose has been found to be associated with maturation of killer T- cells and splenic T- lymphocytes due to increase in interleukin (I and II) levels (Tokoro, *et al.*, 1988). The low molecular weight chitosan in the presence of IFN-γ was found to activate the murine peritoneal macrophases so as to kill the tumor cells (Seo, *et al.*, 2000).

The COS has been found to cause the direct killing of tumor cells, and this phenomenon is associated with the molecular mechanism of immunoenhancement that introduces an immune response or brings about an inhibition in the IL-1 and TNF-α cytokines mediated production of tumor cells by the activation of NK-cells and T-cells (Tokoro, *et al.*, 1989; Tsukada, *et al.*, 1990). The IL-1 and IL-2 mediated proliferation of Th1 cells is critically contributed by the synergistic effects shown by TNF-α *in vitro* (Tokoro, *et al.*, 1989) and the up-regulation of TNF-α, IL-1 and IFN-γ can make COS show the immune responses towards the increase in immunoefficiency of lymphocytes (Seo, *et al.*, 2000; Suzuki, *et al.*, 1986; Tokoro, *et al.*,

1989; Tsukada, *et al.*, 1990; Wang & He, 2001). Chitosan has also been shown to act *via* the antioxidant defence pathways to show the antitumor activity (Fernandes, *et al.*, 2012).

### 2.2.5. Cellular Apoptotic Mechanism

Cellular apoptosis has been found to be a critical mechanism of action of anticancer activity of chitosan (Park, *et al.*, 2011; Wimardhani, *et al.*, 2014; Xu, Jin, *et al.*, 2009) and this mechanism is associated with the activation of procaspase, breakage of the cascade due to signals triggered from outside, and amplification of the cellular death signals (Wimardhani, *et al.*, 2014).

Molecular weight ($M_w$) and degree of deacetylation (DDA) are the prominent factors that affect cytotoxicity of chitosan (Park, *et al.*, 2011). The *in vitro* cytotoxic activity of low molecular weight chitosan (LMWC) on the oral squamous cell carcinoma (SCC) Ca9-22 has been found to involve the extrinsic apoptotic pathways with activation of caspase-8 causing the arrest of cell cycle and caspase- 3 mediated induction of apoptosis by activation of caspase- 3 (Sugano, *et al.*, 1980; Takimoto, *et al.*, 2004; Wimardhani, *et al.*, 2014). The amino group in C2 position of the ring in LMWC undergoes a greater extent of protonation and gets easily attracted to more negatively charged cancer cell surfaces (Zhang, *et al.*, 2010). The anticancer activity of LMWC is attributed to introduction of electrostatic interaction with tumor cell surfaces or endocytosis from extracellular surfaces (Huang, *et al.*, 2004; Wimardhani, *et al.*, 2014). So, LMWC follows a different mechanism to show higher anticancer activity than high molecular weight chitosan.

A study by fluorescent activated cell sorbent assay (FACS) and DNA fragmentation assay has shown that the antiproliferative activity of chitosan on urinary bladder cancer cell line T24 was the consequence of cellular apoptosis (Kuppusami & Karuppaiah, 2013). The increase in the content of DNA up to G2 DNA level with the decrease in chitosan concentration was shown to proceed until the edge of the S phase. With the help of flow cytometry, this process was found to follow the mechanism of inhibition of T24 cell growth by chitosan. The arrest of tumor cell growth by chitosan by chitosan was shown by increase in duration of G1 phase with an increase in concentration, that ultimately caused the disruption of cell membrane and necrosis of cell lines *in vitro* (Hasegawa, *et al.*, 2001; Kuppusami & Karuppaiah, 2013).

The cancer cell cycle arrest at S phase has been found to be induced by LMWC (Wimardhani, *et al.*, 2014) and this process has been mechanistically attributed to cytokine

signaling from the environment and consequently a prolonged inhibition of DNA synthesis (Vermeulen, *et al.*, 2003). Cellular senescence followed by a permanent cell cycle arrest is a mechanism of anticancer activity and aging effects (Senturk, *et al.*, 2010). LMWC has been reported to cause cell senescence owing to cell cycle arrest at G1 and S- phase and this process, possibly associated to accumulated production of reactive oxygen species (ROS), is triggered by higher TGF-β expression. This causes an ultimate increase in ROS production *via* the progression in the activation of Smad 2/3, Smad 4, p15 and p21 (Senturk, *et al.*, 2010). Further research has been felt necessary to clarify the actual pathways of anticancer activity of chitosan (Wimardhani, *et al.*, 2014).

The cell cycle arrest at G1 phase by LMWC indicates the mechanistic pathway in which the cells donot enter the S phase irrespective of p53 expression due to alteration in protein expression (Vermeulen, *et al.*, 2003). The structural deterioration in DNA requires a rapid response with no translation or transcription, and this process introduces an increased rate of protein synthesis (Bartek & Lukas, 2001). The checkpoint at S or G1 phase makes TGF-β molecules induce the production of CKIp15 and p27, there is inhibition in the formation of Cdk-4/Cdk-6-cyclin complex, and there is no RB phosphorylation irrespective of p53 expression (Hannon & Beach, 1994; Reynisdottir, *et al.*, 1995). The checkpoint in mid to late G1 phase causes the cell cycle arrest with low activity of cyclin E-Cdk-2 in the late phase and absence of RB phosphorylation in the mid phase (Falck, *et al.*, 2001). The cell cycle arrest by LMWC at G1 phase possibly involves a lowering in Cdc25A concentration and cyclin E-Cdk2 inactivation as a result of ubiquitination of Cdc25A. The mammalian cells under the influence of UV radiation undergoes ubiquitination due to phosphorylation of Cdc25A through the acive mediation of ATM/ATR towards Chk1/Chk2 (Falck, *et al.*, 2001). Further investigation has been necessary to clarify and confirm this mechanism of anticancer activity of LMWC (Wimardhani, *et al.*, 2014).

Chitosan oligosaccharide (COS) has been reported to bring about an increase in p21 level and decrease in cyclin A and CDK-2 levels, and then a consequent inhibition of cell proliferation, decrease in number of cells involved in S phase and decrease in rate of DNA synthesis (Shen, *et al.*, 2009). COS has been reported to cause inhibition of tumorigenic MMP-9 factor in Lewis Lung Carcinoma (LLC) cells (Shen, *et al.*, 2009).

The nude mice taken as human pancreatic cancer xenografts were found to have a prolonged survival upon the treatment with porcine pancreatic enzyme (PPE) (Saruc, *et al.*, 2004) showing that the proteolytic enzymes act as defense against cancer. COS has been reported to

show chemo preventive activity in human colorectal adenocarcinoma cell line HT-29 due to an increase in activity of QR, GST and GSH enzymes (Nam, *et al.*, 2007a). COS was found to cause inhibition of pro-inflammatory cytokinin mediated nitric oxide (NO) and inducible NO synthase (iNOS) levels, and then a consequent decrease in proliferation of HT-29 (Nam, *et al.*, 2007b). The heparanase inhibition was found to be a possible cause of antiangiogenic activity of COS (Quan, *et al.*, 2009). COS was found to bring about a reduction in tumor size of colorectal adenocarcinoma HT-29 through the pathway of lowering the secretion of MMP-2, a zinc dependent proteolytic enzyme, in a concentration dependent manner (Nagaset & Woessner Jr., 1999) by cytokines IFN-γ, IL-1α and TNF-α (Nam, *et al.*, 2007b). The MMPs gelatinase and matrilysin types on HT-29 cells were found to be inhibited by COS (Brown, 1998). The activity of ODC induced by 12-O–tetradecanoylphorbol-13-acetate (TPA) and the expression of COX-2 induced by TPA in HT-29 cells were also found to be inhibited by COS (Nam, *et al.*, 2007a).

Metastasis *via* the tumor growth and vascular invasion are associated with the increase in iNOS expression (Lagares-Garcia, *et al.*, 2001; Yagihashi, *et al.*, 2000). COS can bring about the inhibition of platelet aggregation and angiogenic effect of NO (Folkman, 1997) by causing an inhibition of NO production *via* the reduction in iNOS expression (Nam, *et al.*, 2007b). COS has been shown to cause an inhibition of IL-8 expression induced by LPS in human umbilical vein endothelial cells (HUVECs), LPS-induced HUVECs migration and the adhesion of U937 monocyte to HUVECs (Liu, *et al.*, 2011). COS has been reported to bring about the apoptosis in HT-29, human colon adenocarcinoma (Hossain & Takahashi, 2008) and also in HL-60 cell lines (Dou, *et al.*, 2011). Chitosan in higher concentration was found to inhibit the mouse monocyte macrophage growth in RAW 264.7 cell lines (Hwang, *et al.*, 2000) and suppress the proliferation of gastric and colon cells (Hasegawa, *et al.*, 2001). The effect of chitosan on Erlich ascites tumor (EAT) cells *in vivo* with EAT bearing mice models showed a remarkable decrease in the volume of ascites (Harish Prashanth & Tharanathan, 2005) and Caco-2 cells showed 25% increase in the activity of caspase- 3 upon a 24 h incubation with chitosan in comparison to the control which was not treated with chitosan (Silano, *et al.*, 2004). Apoptosis induced by chitosan on EAT cells was monitored by nucleosomal DNA fragmentation study (Yamada & Clark, 2002).

Antitumor activity of chitosan against A549 (human lung), PC3 (human prostate) and HepG2 (human hepatoma) cancer cell lines was found to depend upon the molecular weight ($M_W$) and degree of deacetylation (DDA) of chitosan. The study on cytotoxic potentials of COS and

high molecular weight chitosan (HMWC) with different fractions of $M_W$ and DDA revealed that COS was more effective than HMWC against these cells (Park, *et al.*, 2011). The study shows that the antitumor activity is associated with chemical structure and polymeric size but the specific pathway of this activity of HMWC is still unclear.

## 2.3. Nano Chitosan and its Mechanism of Anticancer Activity

The solid particles or particulate dispersions at 10-1000 nm size have been referred to as nanoparticles (Koopaei, *et al.*, 2014). Nano chitosan with the particle size in this range can be obtained in a polymeric and biocompatible form. The prolonged circulation of nano chitosan in blood is associated with its behavior of showing hydrophilicity, extravasation and passive targeting (Gaur, *et al.*, 2000) and this makes nano chitosan a potential drug delivery candidate (Lee, *et al.*, 2008; Zhang, *et al.*, 2009).

Chitosan gel was obtained by dispersion of chitosan in a mixture of sodium chloride solution and 3% acetic acid solution on stirring for two hours. The gel was added in linseed oil with Span 80 as a surfactant on magnetic stirring for 30 min at room temperature, using an optimized spontaneous emulsification method. Then acetone and Glutaraldehyde-Saturated Toluene as a chemical cross-linking agent were further added to get nano chitosan. The nanoparticle size was found to depend upon the amounts of sodium chloride, surfactant, and chemical cross-linking agent, and in average, the particle size was found to range from 33.64 to 74.87 nm (Khanmohammadi, *et al.*, 2015). Another method of preparation of nano chitosan was the method of ionic gelation that involved tripolyphosphate (TPP) assisted gelation of chitosan solution. The nano chitosan particle sizes were optimized with different concentrations of TPP and chitosan. Nano chitosan with the particle size at 168-682 nm range was obtained with a concentration of chitosan up to 4 mg/mL and TPP up to 1.5 mg/mL (Agarwal, *et al.*, 2018). The biodegradable, mucoadhesive, cationic polysachharide chitosan finds its use in target delivery of therapeutics to cancer cells, and such formulations of therapeutic agent loaded with nano chitosan show more stability, permeability and bioactivity (Kamath & Sunil, 2017).

Inhibition of the proliferation of human hepatoma BEL7402 cells by chitosan nanoparticles has been attributed to cell necrosis owing to neutralization of negative charge on cell surfaces, permeation through the plasma membrane of the cells, decrease in MMP and the peroxidation of lipid *in vitro* (Lifeng, *et al.*, 2007). Chitosan nano particles have been found to lower the viability percentages of HT-29 colon carcinoma cells (Hosseinzadeh, *et al.*, 2012) and target the cancer cells owing to their selective accumulation in tumor cells by the mechanism of enhanced permeation and retention (EPR) followed by lowering of the p-

glycoprotein mediated multidrug resistance (Ai, *et al.*, 2017; Ramasamy, *et al.*,2017). Biocompatibility of copper nanoparticles loaded with chitosan favour the mechanism of enhanced permeation and retention (EPR) so that they undergo preferential accumulation in tumor cells. The destruction of cancer cells followed by apoptotic body formation has been marked towards the remarkable anticancer effect of chitosan (Ai, *et al.*, 2017).

The lower toxicity of chitosan to nan-cancer cells has been attributed to *in vivo* chitosan chain degradation by the kidney (Kean & Thanou, 2010). Nano chitosan lends itself to reciprocatory drug delivery trials as it is economical and biocompatible (Grenha, *et al.*, 2007). Cellular internalization of nano chitosan in an easier way (Malatesta, *et al.*, 2015) and the target specificity of nano chitosan to cancer cells have made it a potential anticancer candidate of therapeutic significance (Aruna, *et al.*, 2013; Qi, *et al.*, 2005; Xu, Wen, & Xu, 2009). The anti-angiogenic activity of nano chitosan in breast cancer mice model4 has been aattributed to RNA interference and immune enhancement (Xu, Wen, & Xu, 2009). Nano chitosan has been found to be released spontaneously towards the human gastric cancer cells *in vitro* in a controlled release manner (Qi, *et al.*, 2005).

The glycol chitosan nano particles (400 nm size) loaded with paclitaxel has been reported to show an inhibition of MCF-7 tumor growth with a sustained release of paclitaxel by EPR effect *in vitro* (Kim, *et al.*, 2006). Thymoquinone and paclitaxel encapsulated in nano chitosan has been detected to be effective against the breast cancer therapy (Soni, *et al.*, 2015). The study of binding of chitosan nano particles with protein is crucial to establish the target specificity of nano chitosan. For instance, the *in vivo* inhibition of ovarian cancer has been shown by binding of nano chitosan to αvβ3 integrin associated with the receptors for tumor cells (Han, *et al.*, 2010). The increase in immune response by nano chitosan has been found in murine model by elevation of IL-2, Il-4, IL-6 and IgG, IgA, IgM receptors (Li, Min, *et al.*, 2013). The protonation of amino group in C2 position of ring chitosan is favoured in the low vasculature acidic environment outside the tumor. It causes the swelling of nano particles and a consequent release of the drug in higher rate. The processes of protonation of amino group in ring chitosan and EPR effect owing to higher accumulation of nano chitosan in the micro environment of tumor cells (Maeda, 2001) are significant towards the anti-cancer usability of nano chitosan-drug formulations.

The *in vivo* anticancer activity of chitosan-curcumin nano formulation has been shown to follow the apoptotic pathways *via* the stages of structural deterioration of DNA, cell-cycle arrest and an increment in ROS levels (Yadav, *et al.*, 2018). The inhibition of the growth of human hepatocellular carcinoma (HCC) cells by nano chitosan has been attributed to cell

necrosis and restriction to tumor angiogenesis by lowering of VEGFR2 gene expression (Xu, Jin, *et al.*, 2009). The death of HCC cells by nano chitosan *in vitro* has been associated to disruption of cell membrane, reduction of negative charge on cell surfaces, reduction in mitochondrial membrane potential, on set of lipid peroxidation, fatty acid membranous layer disruption and DNA fragmentation (Lifeng, *et al.*, 2007). The *in vivo* inhibition of HCC cell growth by nano chitosan is owing to induction of apoptosis and reduction of tumor cells proliferation, in a manner to have no toxicity to healthy cells, but a specific and potent cytotoxicity to tumor cells (Xu, Wen, & Xu, 2009).

The nano particulate chitosan folate hesperetin has been observed to show apoptosis of HCT15 cells by the process of properly regulated proapoptotic gene expression in a more efficient way than hesperetin. This process follows a mechanism of passive targeting *via* the tumor micro environment of leaky vasculature. Consequently, the chitosan folate hesperetin nanoformulation is a suitable carrier of hesperetin to the cells of colorectal cancer *in vivo* (Mary Lazer, *et al.*, 2018).

Chitosan nanoparticle labelled with Arg-Gly-Asp (RGD) peptide (RGD-CH-NP) has been found to be a tumor targeted delivery formulation for short interfering RNA (siRNA). The siRNA loaded RGD-CH-NP was observed to bring about a significant increase in (i) selective delivery inside the tumors of orthotopic animal models with ovarian cancer, (ii) targeted silencing in different growth-promoting genes (POSTN, PLXDC1 and FAK), (iii) therapeutic efficacy in A2780, SKOV3ip1 and HeyA8 models, and (iv) the delivery of PLXDC1-targeted siRNA into the tumor endothelial cells (alphanubeta3 integrin-positive) in A2780 tumor-bearing mice *in vivo*, showing a remarkable tumor growth inhibition *in vivo* (Han, *et al.*, 2010).

## 2.4. Anticancer Derivatives Synthesized via Functionalization of Amino Group in Chitosan and their Anticancer Activity

### 2.4.1. Carboxymethyl Chitosan (CMCS) and CMCS Thiosemicarbazones

Carboxymethyl chitosan (CMCS) can be functionalized as carboxymethyl chitosan thiosemicarbazone that shows coordination behavior with metal ions (Nishat, *et al.*, 2008). CMCS is a water-soluble derivative of chitosan, with amphoteric behavior (Mohamed, *et al.*, 2014) and its synthesis involves a prolonged reaction of caustic soda alkalized chitosan with chloroacetic acid (Chen & Park, 2003).

Salicylaldehyde, p-chlorobenzaldehyde, and p-methoxybenzaldehyde analogues of CMCS thiosemicarbazones are synthesized by a one pot synthesis of thiosemicarbazide as a key

intermediate and its further reaction for 10 h with carboxaldehyde catalyzed by acetic acid and methanol under reflux at 65 °C (Mohamed, *et al.*, 2014) (figure 5a and 5b).

CMCS was found nontoxic to human umbilical vein endothelial cells (HUVECs) at 0.5- 1.5 mg/mL range, as the MTT assay showed only a marginal decrease in percentage viability of cells ($p>0.05$) after 24 h and 48 h of incubation. But, the trans well migration assay showed the *in vitro* inhibition of angiogenesis as there was a remarkable inhibition of two and three dimensional HUVECs migration upon the treatment with CMCS in a dose dependent manner ($p<0.05$) (Jiang, *et al.*, 2015). The treatment of CMCS on the mice model bearing the H22 tumor growth also showed a remarkable *in vivo* inhibition in tumor growth ($p<0.05$), and this inhibition was far more than the control group. The inhibitory rates were 32.63% at the dose of 75 mg/kg, 51.43% at the dose of 150 mg/kg, and 29.89% at the dose of 300 mg/kg (Jiang, *et al.*, 2015). Upon the examination with HE staining of paraffin parts, treatment of CMCS on hepatocarcinoma 22 (H22) cells demonstrated a histopathological state of necrosis and repression in most of the tumor cells treated with CMCS *in vivo*.

### 2.4.2. Chitosan-Thymine Conjugate

Potent anticancer effects of thymine derivatives have been revealed from the studies. The chitosan thymine conjugate nano particles (100-250 nm size) obtained by preferential binding with Poly(A) has been found to bring about an *in vitro* inhibition of the growth of colon cancer cells (Fangkangwanwong, *et al.*, 2016). Phosphonotripeptide thymine derivatives have been shown to inhibit the growth of human leukemia (HL-60) cells *in vitro* (Liu & Chen, 2001). Alpha-methylene-gamma-(4-substituted phenyl)-gamma-butyrolactone loaded with uracil, 5-bromouracil, and thymine have also been found to inhibit the leukemia cell lines *in vitro* (Kuan-Han, *et al.*, 1999). Ferrocenyl-thymine-3,6-dihydro-2H-thiopyrane derivatives can show the antiproliferative activity against human monocytic MonoMac6 cancer cells, estrogen-negative human breast adenocarcinoma MDA-MB-231, human colon carcinoma HT-29, estrogen receptor-responsive human breast adenocarcinoma MCF-7, and human promyelocytic leukemia HL-60 cell lines *in vitro* (Skiba, *et al.*, 2015). Hyaluronic acid and thymine are the compounds with which chitosan can be modified to get the derivatives of enhanced anticancer activity (Manna, *et al.*, 2009). One of the chitosan-thymine conjugates of important biomedical applications was synthesized by the reaction of thymine-1-yl-acetic acid with chitosan followed by successive acylation reaction (Kumar, *et al.*, 2012) (figure 6). The results of the assays for cellular cytotoxicity, viability and proliferation carried out with

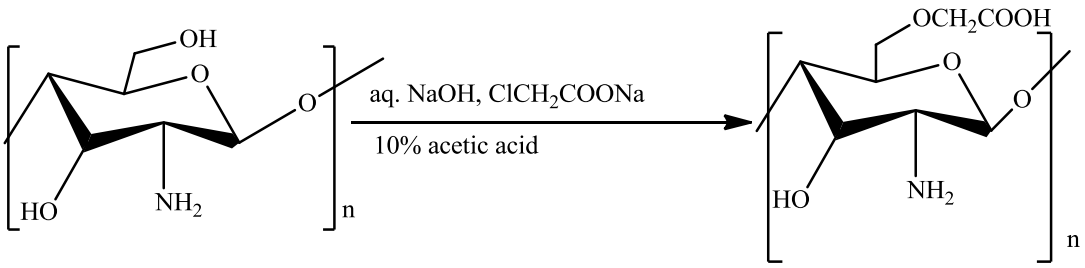


**Figure 5a:** Synthetic route of CMCS

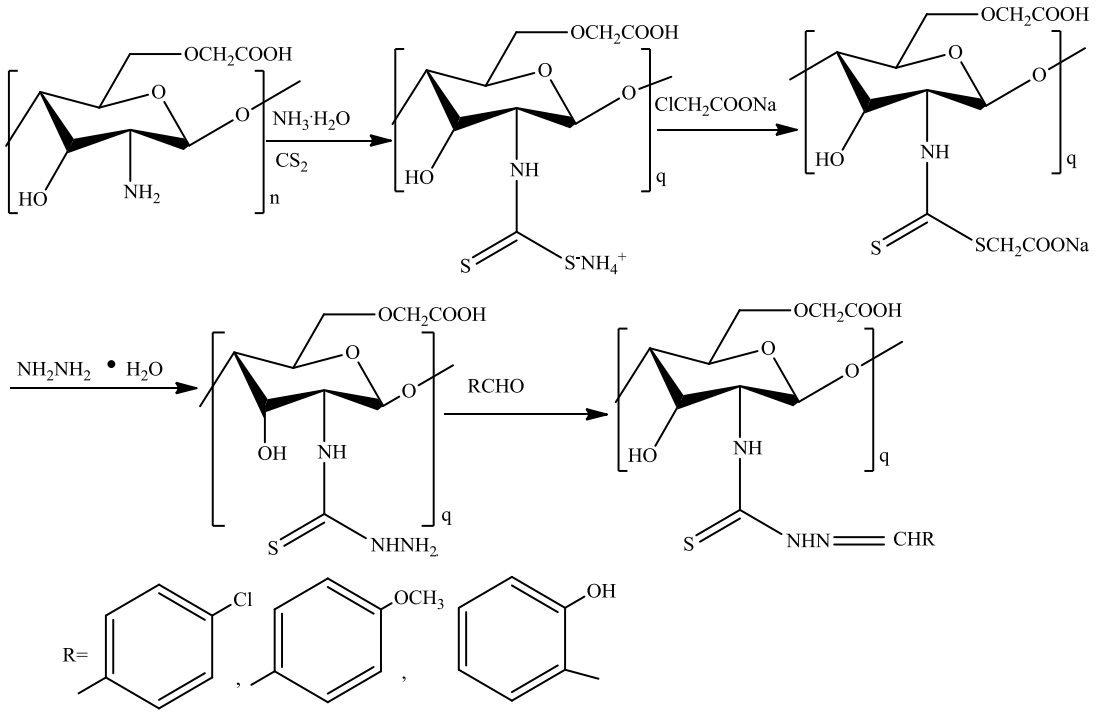


**Figure 5b:** Synthetic route of CMCS Thiosemicarbazones

human liver cancer cell line (HepG2) and mouse embryonic fibroblast cell line (NIH 3T3) have shown the significant dose-dependent inhibition ($p < 0.05$) of HepG2 proliferation, but no toxicity was found to noncancerous NIH 3T3 cell line (Kumar, *et al.*, 2012).

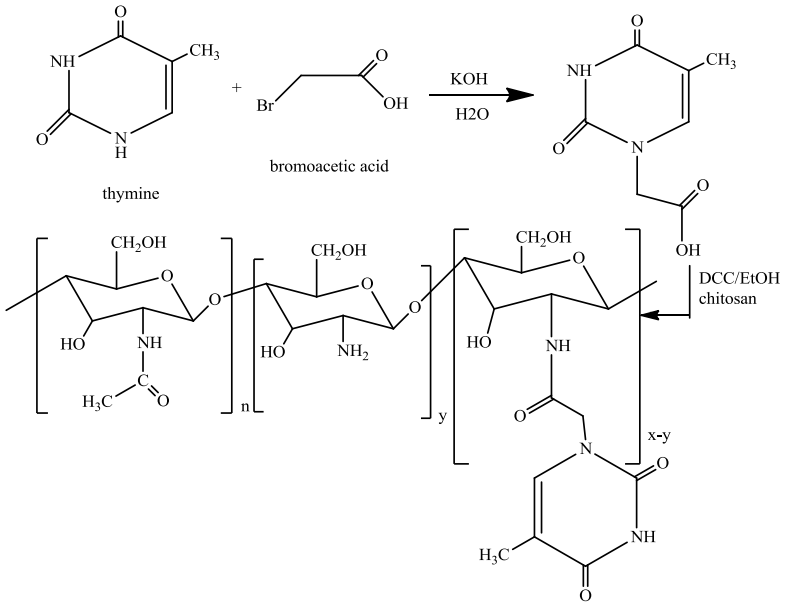


**Figure 6:** Synthetic route of chitosan–thymine conjugate

### 2.4.3. Sulfated Chitosan (SCS) and Sulfated Benzaldehyde Chitosan (SBCS)

Native chitosan of molecular weight of ~ 1000 k Da in average with one acetamido moiety from unreacted chitin and two hydroxyl groups in a monomeric unit (Singla & Chawla, 2001) was taken as a starting material to prepare a hybrid sulfated derivative, and the glycosyl unit of this derivative essentially possesses the sulfate group as an anticancer constituent (Pillai, *et al.*, 2009). So, the synthetic route of SCS follows the sulphonylation of chitosan and that of SBCS follows Schiff's addition with benzaldehyde and the consequent sulphonylation (Jiang, *et al.*, 2011) (figure 7). A remarkable inhibition of the proliferation and apoptosis of human breast cancer (MCF-7) cells by SCS and SBCS was shown by the studies comprising cells culture with DMEM media in heat-inactivated fetal bovine, determination of cellular inhibition, western blot analysis and monitoring of apoptosis by fluorescence-activated cell sorting (FACS) analysis (Jiang, *et al.*, 2011). The results showed higher inhibitory effects of SBCS derivative with lower $IC_{50}$ than SCS (Jiang, *et al.*, 2011).

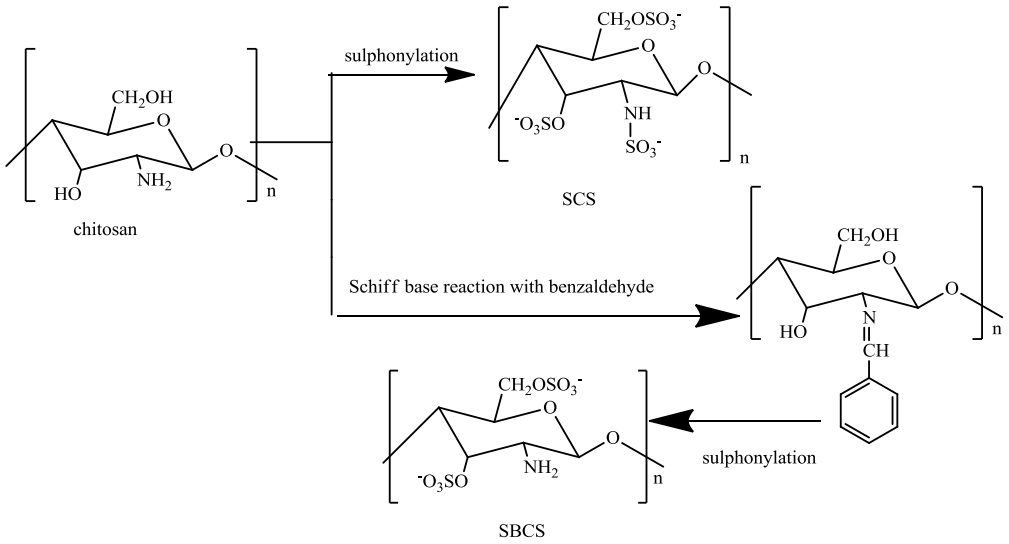


**Figure 7:** Synthetic route of sulfated Chitosan (SCS) and sulfated benzaldehyde chitosan (SBCS)

### 2.4.4. N-Succinyl chitosan (Suc-Chi) and Glycol Chitosan (GChi)

Chitosan with more inhibitory effects, minimal problems associated to cell viability, and more biocompatibility can be obtained by elimination of coexisting ions and increase in the degree of deacetylation and depolymerization (Carreno-Gomez & Duncan, 1997; Lee, *et al.*, 1995). Derivatization of hydroxy group in C6 position of chitosan ring like in GChi and Suc-Chi is essential to increase the enzymatic degradation of chitosan (Song, *et al.*, 1992; Song, *et al.*, 1993a; Song, *et al.*, 1993b; Kamiyama, *et al.*, 1999; Kato, *et al.*, 2000). The GChi and Suc-Chi are water-soluble chitosan derivatives that can effectively release the drugs to cancer cells both *in vivo* and *in vitro* (Hosoda, *et al.*, 1995; Nakanishi, *et al.*, 2001). The route of synthesis of N-succinyl chitosan is as shown in figure 8 (Yan, *et al.*, 2006). The single *in vivo* intraperitoneal administration of Suc-Chi-MMC conjugate in mice models at 24 hours after the inoculation of intraperitoneal L1210 tumor has been found to bring an increase in antitumor activity in a dose (equivalent MMC /kg) dependent manner. The Suc-Chi-MMC conjugate was found to have the ILS values of 45.3% and 65.3% at the doses of 5 mg equivalent MMC/kg and 20 mg equivalent MMC/kg respectively (Song, *et al.*, 1993c). Moreover, Suc-Chi-MMC conjugate has been observed to be more effective against the metastatic liver cancer and solid tumors (Kato, *et al.*, 2005).

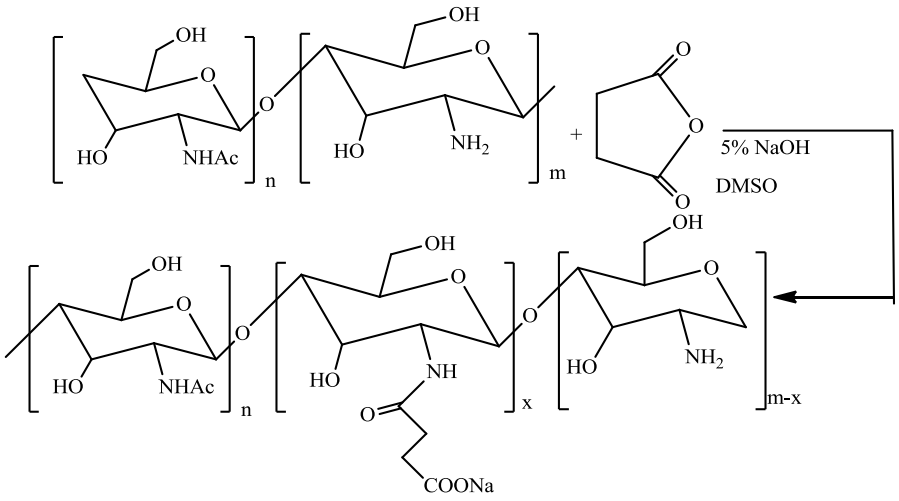


**Figure 8:** Synthetic route of N-succinyl chitosan

Glycol chitosan (G-Chi) can be synthesized by the reaction of chitosan with ethylene glycol (Muslim, *et al.*, 2001) (figure 9). G-Chi has been shown to have a prolonged localization in kidney and sustained retention in blood circulation by the *in vivo* intravenous study of fluorescein thiocarbamyl-G-Chi (G-Chi-FTC) that is obtained as a derivative of G-Chi with fluorescein isothiocyanate (FITC) labelled with fluorescein (Kato, *et al.*, 2005). The *in vivo* study *via* the intraperitoneal administration to P388 leukemic mice showed that the G-Chi-MMC conjugate had the decresed side effects, but the therapeutic effect of MMC was found better than this conjugate (Kato, *et al.*, 2005).

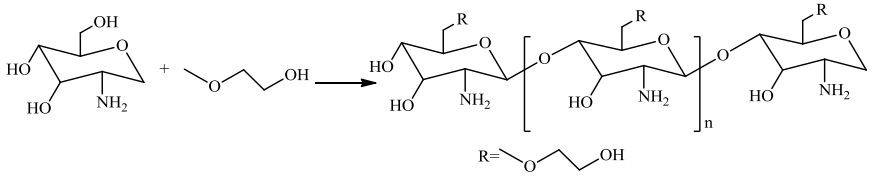


**Figure 9:** Synthetic route of glycol chitosan

### 2.4.5. Furanoallocolchicinoid-Chitosan

The low accumulation profile in tumor cells makes colchicine a less effective antitumor agent, but conjugation of colchicine with chitosan has been found to bring about a decrease in adverse effects, increment in $M_w$ to sequester it from healthy cells, and an enhancement in biodistribution level of colchicine in tumor cells (Crielaard, *et al.*, 2011).

Furanoallocolchicinoid–chitosan conjugate can be synthesized by the reaction of succinic anhydride in tetrahydrofuran with furanoallocolchicinoid under an inert atmosphere (Mathiyalagan, *et al.*, 2014; Voitovich, *et al.*, 2015) (figure10).

The investigation made upon the action of compound furanoallocolchicinoid chitosan in the mice model bearing the Wnt-1 breast tumor showed the association of actitumor activity with better accumulation in the tumour cells, reorganisation of tubulin and the arrest of cell cycle *in vivo* (Svirshchevskaya, *et al.*, 2016).

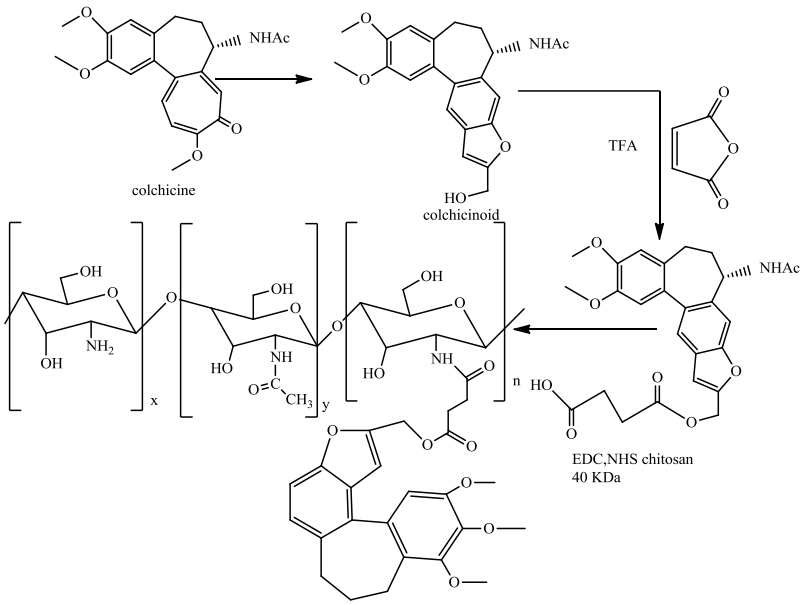


**Figure 10:** Synthetic route to furanoallocolchicinoid-chitosan

### 2.4.6. Polypyrrole-Chitosan (PPC): Graft Copolymerization

Polypyrrole chitosan (PPC) is a polyamine chitosan that is synthesized by graft copolymerization of pyrrole with chitosan (Salahuddin, *et al.*, 2017a) (figure 11). A significant enhancement in inhibitory activity against the proliferation of Erlich ascites carcinoma (EAC) cells was obtained after loading of the nanocomposite of silver chloride with 3-amino-2-phenyl-4(3H)-quinazolinone of polypyrrole-chitosan (PPC). In this investigation, the PPC nanoparticles were released into the EAC cells at pH 2 (Salahuddin, *et al.*, 2017a).

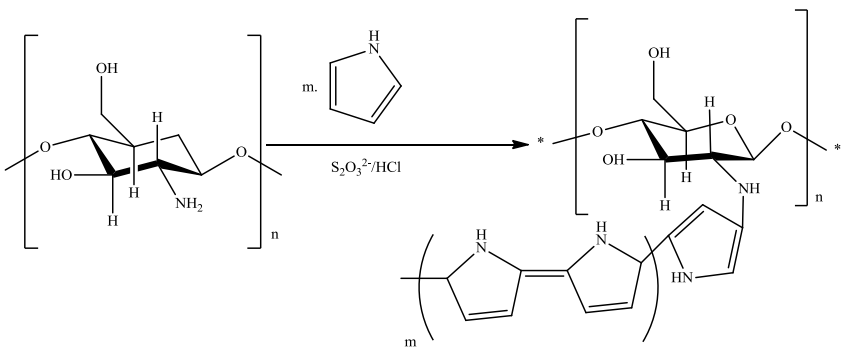


**Figure 11:** Graft copolymerization of polypyrrole-chitosan

## 2.5. Mechanism of Anticancer Activity of Chitosan Derivatives

### 2.5.1. Synergy of Cellular Oxidative Damage, DNA Fragmentation and Apoptotic Activity of Chitosan Matrix and Square Planar Complexes

The solid tumors are chemotherapeutically treated with the complex drugs that suffer from a limited spectrum of antineoplastic activity and several side effects that are ruined with severity in dose dependent manner (Astolfi, *et al.*, 2013; Fuertes, *et al.*, 2003). Complexes of both platinum and non-platinum metals with different ligands as carrier constituent have been synthesized in an attempt to tailor the compounds with a broad spectrum of antitumor activity and minimal side effects (Arkenau, *et al.*, 2008; Arnesano, *et al.*, 2008; Hannon, 2007; Kalinowska-Lis, *et al.*, 2008; Steinborn & Junicke, 2000). The chelation of chitosan with many metal ions is attributed to the presence of acetamido, amino and hydroxyl moieties as reactive functional groups in chitosan (Gritsch, *et al.*, 2018; Varma, *et al.*, 2004; Zheng, *et al.*, 2006). The *in vitro* investigation by sulforhodamine B assay of oligo chitosan salicylaldehyde Schiff-base and its zinc(II) complexes have shown the inhibitory effects against SMMC-7721 liver cancer growth owing to the synergistic effect of native chitosan matrix and planar make-up of the complexes (Wang, *et al.*, 2009).

The binding of zinc complexes to DNA, as observed by electrophoretic analysis, has been shown to be associated with electrostatic intercalation and interactions. The antitumor activity of chitosan has been found to get enhanced upon the complex formation, and moreover, oligo-chitosan zinc complex has been found to show more potent antitumor activity than high molecular weight chitosan analogue (Nam, *et al.*, 2007b). Chitosan-metal complex with the square planar geometry shows more scavenging of free radicals as such a geometry is sterically favorable towards the interaction of free radicals with metal ion (Yin, *et al.*, 2004). The antitumor activity of complexes is associated with the behavior of donor atoms in complexes to chemically induce the breakage of DNA (Zheng, *et al.*, 2006).

The anticancer activity of copper(II)-chitosan complex that depends upon the concentration of copper(II) ions is possibly associated with the strengthening of positive charge developed in amino group at C2 position of chitosan and the development of more interaction with negatively charged components of cell surfaces (Qi, *et al.*, 2004; Zheng, *et al.*, 2006). The key factors owing to which the copper(II)-chitosan nano particles show the antitumor activity are the oxidative stress, cellular apoptosis and inflammation of endothelial cells (Bondarenko, *et al.*, 2013; Niazi & Gu, 2009). In fact, the preferential accumulation and internalization of

copper(II)-chitosan nanoparticles (< 200 nm) on tumor cells has been a crucial pathway of their anticancer activity (Ai, *et al.*, 2017). The anticancer activity of copper(II)-chitosan nanoparticles has also been attributed to elevation of mitochondrial ROS level that leads to cellular oxidative damage, fragmentation of DNA and cellular apoptosis (Murphy, 2009). Increase in caspase 3 expression has been experimentally found to bring about an increase in caspase 3/7 activity and the elevated rate of apoptosis (Ai, *et al.*, 2017).

### 2.5.2. Antiangiogenic and Immunoenhancing Mechanism

CMCS can be used as a carrier of anticancer drug like curcumin, 5- fluorouracil and doxorubicin (Anitha, Chennazhi, *et al.*, 2012; Anitha, Maya, *et al.*, 2012; Jin, *et al.*, 2012; Wang, *et al.*, 2011) owing to its solubility in water (Kurniasih Purwati, *et al.*, 2014), biocompatibility, biodegradability and lower toxicity (Ji, *et al.*, 2012). Anticancer activity of CMCS both *in vitro* and *in vivo* has been found to follow the anti-angiogenic pathways (Jiang, *et al.*, 2015). The *in vitro* inhibition of the migration of HUVECs proceeds in time and concentration dependent manner, and a conspicuous decrease in the growth rate of hepatocarcinoma (H-22) in mice by CMCS is associated with cell necrosis *in vivo* (Jiang, *et al.*, 2015). The H-22 cells treated with CMCS were mostly found to get distorted in shape with the disintegration of nuclei (Jiang, *et al.*, 2015). The growth of HeLa, SGC-7901 and BEL-7402 cells has also been found to be inhibited by CMCS *in vitro* (Zheng, *et al.*, 2011).

CMCS has been found to bring about the stimulation of immune functions and suppression of angiogenesis (Jiang, *et al.*, 2015). The mechanism of its anti-angiogenic activity involves the physiological alterations in vascular endothelial cells to form the new blood vessels. In the mechanistic study of angiogenesis and immune histochemistry, these vascular endothelial cells from which the new blood vessels towards the tumor are developed are labelled as marker cells. The CD34 antigen cells are taken as such marker cells among many other endothelial cells to study the mechanism of angiogenesis in H-22 hepatic tumor cells (Folkman, 1996). The *in vivo* inhibition in CD34 expression ($p<0.05$) in H-22 tumor treated with CMCS (at a concentration of 150-300 mg/kg) has shown the dose dependent antiangiogenic activity of CMCS (Jiang, *et al.*, 2015).

The cellular antiangiogenic and proangiogenic factors act simultaneously to regulate the process of tumor angiogenesis. The antiangiogenic effect is associated to the inhibition of malignant cells transformation and degradation of extracellular matrix by TIMPs. Meanwhile, the proangiogenic effect is brought about by VEGF, a specific mitogen for endothelial vascular cells and its kinase receptors (Jiang, *et al.*, 2015). The tumor inhibitory effect of

CMCS was reflected by the simultaneous effect of these opposite factors upon the inhibition of angiogenesis in mouse serum on treatment with CMCS for 14 days. The result showed an increase in antiangiogenic TIMP1 level and decrease in proangiogenic VEGF level *in vivo* (Jiang, *et al.*, 2015). The antiangiogenic activity appears on effect by the stimulation of key cytokines that inhibits the activity of MMP and favors the inhibition of the degradation extracellular matrix and transformation of tumor cells (Jiang, *et al.*, 2015; Lifeng, *et al.*, 2007; Nam, *et al.*, 2007b; Shen, *et al.*, 2009).

The immune system in human body constitutes the thymus, spleen, lymph ducts and lymph nodes, and this system provides resistance to infection and cancer development (Effros, 2003). TNF-α and IFN-γ are the crucial immune- related cytokines that have been used in the clinical cancer chemotherapy for many years (Aulitzky, *et al.*, 1989; Eggermont, *et al.*, 1996). TNF- α brings about an enhancement in immune function (Ebert, *et al.*, 2006) and an increase in the rate of apoptosis of cancer cells (Chang, *et al.*, 2006; Hur, *et al.*, 2003). IFN- γ is an immunomodulatory and pleiotropic cytokine obtained as a product of NK cells and activated T cells. It causes the promotion of cellular apoptosis and death of tumor cells (Ahn, *et al.*, 2002; Trubiani, *et al.*, 1994). The treatment of CMCS in mouse serum was found to bring about an enhancement in the thymus index ($p<0.05$) and the ELISA assay detection showed an enhancement in IFN- γ and TNF- α levels in mouse serum upon the treatment with CMCS. These results were the clear indicatives of antitumor activity of CMCS that follows the mechanism of immune system improvement and regulation in the induction of immune-related cytokines (Jiang, *et al.*, 2015).

### 2.5.3. Nucleobase Conjugation and Interaction with Nucleic Acids

The derivatives of different synthetic and natural biopolymers with enhanced anticancer activity can be obtained by the conjugation with nucleobase. Some of such conjugates that block the transfer of genetic information from DNA to protein and cause the inhibition of a particular mRNA or DNA molecular expression are phenanthridinium–nucleobase conjugates (Tumir, *et al.*, 2010), symmetrical and unsymmetrical, ω-nucleobase mono- & bis-amide conjugates (Boncel, *et al.*, 2010), ferrocene–bis(nucleobase) conjugates (Kraatz, 2005; Wlassoff & King, 2002), metallocene–nucleobase conjugates (Pike, *et al.*, 2002), cyclodextrin–DNA conjugate (Ihara, *et al.*, 2009), DNA-peptide conjugates (Kubo, *et al.*, 2003), neamine–nucleoside conjugates (Xu, Jin, *et al.*, 2009), nucleobase PNA conjugates and peptide–nucleobase conjugates (Roviello, *et al.*, 2010). Mechanistically, the chitosan–nucleobase conjugate involves itself in DNA synthesis to get incorporated into the nuclear DNA, and then it gets further involved in transcription to get incorporated into mRNA. These

processes of incorporation of chitosan–nucleobase into DNA and mRNA result in the breakage of the strand and termination of the chain to cause the cell cycle arrest (Nelson & Cox, 2005). As a matter of fact, this mechanism is attributable to no more formation of additional nucleotides due to disappearance of 3OH group. Cancer cells undergo faster cell division and their cell cycle is short. These cells are highly affected by the nucleobase conjugate unlike the normal cells with slow pace of cell division (Hanahan & Weinberg, 2011). If a polynucleotide possesses a sequence complementary to that of mRNA product or oncogene, its conjugate with chitosan increases the selective activity against the cancer cells as a result of its interaction with the DNA or mRNA of a specific tumor cell. This interaction due to pairing of complementary bases (Cytosine with Guanine and Thymine or Uracil with Adenine) brings about the inhibition of DNA synthesis, transcription of mRNA and translation of gene with cancer-causing attributes (Kumar, *et al.*, 2012). Chitosan-thymine conjugate was found to cause *in vitro* inhibition of HepG2 proliferation in a manner that depends upon the concentration of the conjugate (Kumar, *et al.*, 2012).

### 2.5.4. Fibroblast Growth Factor Associated Inhibition of Cellular Proliferation

Metastatic breast carcinoma has been investigated to show endothelial cells proliferation and angiogenesis that is mediated by heparin-binding growth factor (Fernig, *et al.*, 1994; Mundhenke, *et al.*, 2002; Qiao, *et al.*, 2003). The fibroblast growth factor-2 (FGF-2) shows an interaction with heparan sulfate (HS) (figure 12a), a low affinity receptor, and this process subsequently introduces a conformational change and binding of FGF-2 to FGFR, a high-affinity tyrosine kinase receptor. It shows that HS is a significant receptor required for accumulation of FGF-2 and regulation in the release of FGF-2 and other HS-binding factors like vascular endothelial growth factor (VEGF) on the surface of the cells. Hence, the alterations in HS at the time of breast cancer progression may cause the change in the assembly of fibroblast growth factor–receptor (FGFR) ternary complex and FGF-2 binding (Jiang, *et al.*, 2011).

Some of the natural sulfated polysaccharides within the current search in literature that show binding with FGF-2 and block FGF-2 binding with HS (Marshall, *et al.*, 1997) introducing the inhibition of cell proliferation (Zaslau, *et al.*, 2004) and metastasis (Liu, *et al.*, 2005) are tecogalan (Yunmbam, *et al.*, 2001), fucoidan (Liu, *et al.*, 2005) and pentosan polysulphate (Marshall, *et al.*, 1997; McLeskey, *et al.*, 1996; Zaslau, *et al.*, 2004). Heparin like binding of carboxymethyl benzylamide dextrans (CMDB) (Bagheri-Yarmand, *et al.*, 1997; Bittoun, Avramoglou, *et al.*, 1999; Di Benedetto, *et al.*, 2003; Liu, *et al.*, 1997; Morere, *et al.*, 1992) and phenylacetate carboxymethyl benzylamide dextran (NaPaC) (Di Benedetto, *et al.*, 2001;

Di Benedetto, *et al.*, 2002; Garvelas, *et al.*, 2002; Malherbe, *et al.*, 2004) with FGF-2 has also been found to cause the alteration in cell growth. CMDB has been found to inhibit autocrine and paracrine growth of the breast tumor cells owing to formation of an equimolar stable complex FGFR (Bittoun, Bagheri-Yarmand, *et al.*, 1999) and NaPaC has been found to introduce antiproliferative activity, inhibition of VEGF binding to VEGFR2 and terminated activity of VEGFR2 (Di Benedetto, *et al.*, 2008). The anticancer functionalities are phenyl group in CMDB and NaPaC (Di Benedetto, *et al.*, 2003) and sulfate group in heparin, tecogalan (Song, *et al.*, 1993a). The sulfate group was brought at the end of the phenyl group in CMDB (figure 12b) to get both of these functional groups in carboxymethyl benzylamide sulfonate dextran as the hybrid compound (Logeart-Avramoglou & Jozefonvicz, 1999). This hybrid compound showed no antiproliferative behavior, but it was observed to have a strong interaction with FGF to initiate and propagate the FGF-induced mitogenic activity (Logeart-Avramoglou & Jozefonvicz, 1999). Starting from chitosan with an acetamido moiety and two hydroxyl groups in a monomeric unit, a hybrid compound containing the sulfate group on opposite sites of glycosyl unit was synthesized (Pillai, *et al.*, 2009).

Both SCS and SBCS were found to induce apoptosis and block the FGF-2-induced phosphorylation in extracellular signal-regulated kinases (ERK) in the human breast cancer (MCF-7) cells and show a remarkable *in vitro* inhibition of its cellular proliferation (Jiang, *et al.*, 2011).

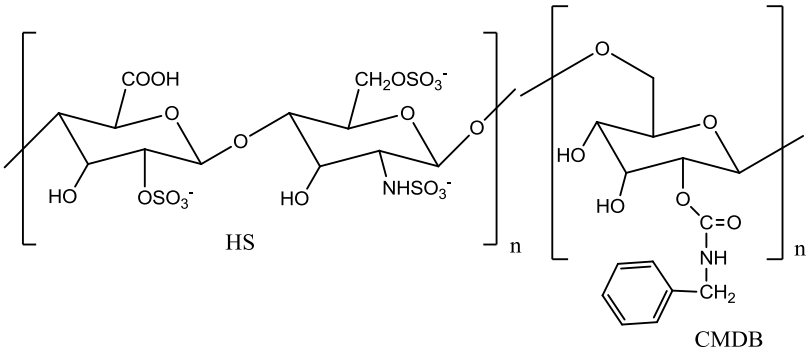


**Figure 12a:** Heparan sulfate (HS). **Figure12b:** Carboxymethyl Benzylamide Dextran (CMDB)

### 2.5.5. Bioavailability Enhancement through Sustained Release Mechanism

The conjugate derivatives of chitosan obtained as anticancer drug formulations have been reported to have minimal adverse effects due to a far more biodistribution in tumor cells. Because of this property of higher bioavailability in tumor cells, both the insoluble and soluble synthetic conjugates of glycol chitosan (G-Chi) and N-succinyl-chitosan (N-Suc-Chi) with MMC find their potential applications in cancer chemotherapy as polymeric drug

carriers (Kato, *et al.*, 2005). N-Suc-Chi has been found to have a prolonged biodistribution level in tumor cells and relatively a long systemic half-life (Kato, *et al.*, 2005). As a result of the i*n vivo* study of bioactivity of G-Chi employing its intravenous administration with fluorescein labelled derivative in normal mice, G-Chi was found to show more biodistribution level in blood and kidneys and a higher retention in kidneys (Kato, *et al.*, 2005).

A significant *in vivo* antitcancer activity against the P388- leukemia bearing mice has been shown by a conjugate of doxifluridine and 1-β-D-arabinofuranosylcytosine (Ara-C) obtained by using chitosan with glutaric spacer. A significant activity against the solid tumors, metastatic liver cancer and leukemia was shown by the conjugates of mitomycin C (MMC) with N-Suc-Chi and G-Chi (Song, *et al.*, 1992; Song, *et al.*, 1993a; Song, *et al.*, 1996) and the mechanism of this this *in vivo* and *in vitro* activity was found to be associated with a controlled release of the drug in free state from conjugates (Kato, *et al.*, 2005). The MMC – G-Chi conjugate was found to have lesss side effects than free MMC, and this may have been attributed to higher biodistribution of G-Chi in cancer cells (Kato, *et al.*, 2005).

### 2.5.6. Inhibition of Microtubule Formation and Cell Cycle Arrest

Tubulin in serum albumin lends itself to binding with small hydrophobic molecules of colchicine to make colchicine get accumulated in leukocytes (Chappey, *et al.*, 1993; Sabouraud, *et al.*, 1994). Such a binding of tubulin with colchicine has been found to prevent the formation of microtubule and inhibit the cell division (Cortes & Vidal, 2012; Katsetos & Dráber, 2012; Seligmann, *et al.*, 2012; Stec-Martyna, *et al.*, 2012). But still, the use of colchicine as an antitumor agent is limited by its low accumulation level in tumor cells. The conjugation of chitosan with colchicine has been found significant so as to get an increase in molecular weight and sequester the colchicine molecules from the normal cells to cancer cells. The increased accumulation of colchicine in cancer cells essentially causes the decrease in its biodistribution in normal cells and it decreases the adverse effects (Crielaard, *et al.*, 2011).

Furonoallocolchicinoid chitosan has been taken as a “smart” Ringsdorf’s drug conjugate with a potent antitumor activity (Ringsdorf, 1975). The antiproliferatory activity of furonoallocolchicinoid chitosan against the tumor cells in Wnt-1 breast tumor bearing mice model has been found to be linked with tubulin reorganization and the cell cycle arrest (Svirshchevskaya, *et al.*, 2016; Voitovich, *et al.*, 2015). Furanoallocolchicinoid chitosan

conjugate has been found to get more accumulated in tumor cells and it shows more inhibitory activity ($p < 0.05$) than chitosan towards tumor growth (Svirshchevskaya, *et al.*, 2016). But, the tumor growth inhibitory activity of chitosan has not been reported to comply with this specific mechanism of tubulin reorganization and the cell cycle arrest (Svirshchevskaya, *et al.*, 2016).

### 2.5.7. Target Delivery and Controlled Release Mechanism

An increase in bioaccumulation of chitosan in tumor cells has been obtained by loading of 3-amino-2-phenyl-4(3H)-quinazolinone on polypyrrole chitosan (PPC) – silver chloride nanocomposite *via* the mechanism of sequestering of conjugate molecules from normal cells and their sustained release to cancer cells (Salahuddin, *et al.*, 2017a; Salahuddin, *et al.*, 2017b). The 1,2,4- triazoles loaded with polypyrrole chitosan nanoparticles are stabilized by a high surface area to volume ratio (Salahuddin, Elbarbary, Salem, & Elksass, 2017; Zhang & Webster, 2009), and the *in vitro* study against Ehrlich ascites carcinoma (EAC) and breast cancer cell line (MCF-7) has shown that they exhibit higher anticancer activity than 1,2,4-triazole (Salahuddin, Elbarbary, Salem, & Elksass, 2017). The nanoparticles loaded with polypyrrole chitosan show biocompatibility to mammalian cells (Wong, *et al.*, 1994) and they lend themselves to easier target delivery in a controlled release manner (Li, *et al.*, 2005; Salahuddin, *et al.*, 2017a). Polypyrrole chitosan nanoparticles can not be easily removed by phagocytes and they undergo cellular permeation towards the target organs through the smallest blood capillaries (Salahuddin, *et al.*, 2017a).

The PPC nanoparticles have been found to get released in a sustained way *in vitro* to EAC and MCF-7 at pH 2 following the zero-order kinetics (Salahuddin, Elbarbary, Salem, & Elksass, 2017). The 1,2,4- triazoles have been found to be rapidly released from nanoparticulate chitosan at pH 2 owing to perpetual electrostatic repulsion between $NH_2^+$ and $NH_3^+$ groups developed in ring chitosan (Shivashankar, *et al.*, 2013). The decrease in percentage release of triazoles at basic medium (pH 7.4) has been attributed to strengthening of hydrogen bond between N-H fraction in chitosan and S-H in triazole (Salahuddin, Elbarbary, Salem, & Elksass, 2017).

## 2.6. Chitosan and Chitosan Derivatives on Anticancer Clinical Study and Trial

After two months of holmium-166 percutaneous (166Ho)/chitosan complex injection (PHI) therapy, 77.5% of patients with HCC lesions less than 3 cm in size and 91.7% of patients

with HCC lesions less than 2 cm size had complete tumor necrosis, according to the phase IIb clinical research. The survival rates were 87.2% for 1 year, 71.8% for 2 years, and 65.3% for 3 years, with cumulative local recurrences and transitory bone marrow depression interfering. As a result, PHI was demonstrated to be a safe and unique for the treatment of minor HCC that might be employed as a bridge to transplantation, and the need for a phase III randomized active control trial in a larger study population was emphasized (Kim, *et al.*, 2006).

The drug, device and implant interventions of chitosan and its derivatives being made under the clinical trials are as (i) Chitosan against the prostate cancer, title: Study of Chitosan for Pharmacologic Manipulation of AGE ( Advanced Glycation End products) Levels in Prostate Cancer Patients (Medical University of South Carolina, 2018); (ii) Chitosan, morphine, placebo, ketamine against the cancer pain, title: Comparison of Oral Morphine Versus Nasal Ketamine Spray With Chitosan in Cancer Pain Outpatients (University Hospital, Basel, Switzerland , 2015), (iii) Axillary dessecttion of breast cancer device adhesive barrier, title: Anti-adhesive Effect and Safety of a Mixed Solid of Poloxamer, Gelatin and Chitosan (Medichlore®) After Axillary Dissection for Breast Cancer (Seok Won Kim, Samsung Medical Center, 2016), (iv) Glycated chitosan (1%) and the photochemical laser device against the breast cancer stage IIIA, IIIB and IV, title: Randomized Clinical Trial Evaluating the Use of the Laser-assisted Immunotherapy (LIT/inCVAX) in Advanced Breast Cancer (Eske Corporation S.A.C., 2017) and (v) Implant: bilaminar chitosan scaffold against cerebrospinal fluid (csf) leakage, title: Chitosan Scaffold for Sellar Floor Repair in Endoscopic Endonasal Transsphenoidal Surgery (Ivan Segura Duran, University of Guadalajara, 2017).

**CHAPTER 3**

**3. MATERIALS AND METHODS**

## 3.1. Materials

Crab shells as fishery wastages were collected from the local market of Kathmandu, Nepal. Glacial acetic acid (Merck 99-100 %), hydrochloric acid (Merck 99 %), sodium hydroxide (Merck, 99%), sodium acetate (Merck), and ethanol (Sigma-Aldrich, 99.80 %). Chitosan oligosaccharide, $(C_{12}H_{24}N_2O_9)_n$ (87% DDA, $M_w$ < 3000 Da) Sisco Research Laboratories Pvt. Ltd., Maharashtra, India), salicylaldehyde, pyridine-2-carboxaldehyde, 2-acetyl pyridine, isatin, 5-chloroisatin, imidazole-2-carboxaldehyde, thiophene-2-carboxaldehyde and 2- acetyl phenol (Sigma-Aldrich), carbon disulphide (s d fine-chem limited), copper(II) chloride (Merck), hydrazine monohydrate (Thermo Fisher Scientific), sodium chloroacetate (Thermo Fisher Scientific), acetone (Thermo Fisher Scientific), ethanol, methanol, ammonium hydroxide, and all other chemical reagents were of analytical grade and used without further purification.

## 3.2. Measurements

The FT-IR spectra in powdered state were measured in the 4000-400 $cm^{-1}$ regions with ATR-GeXPm experimentation with BRUKER 1 003 3610 FT-IR spectrophotometer. Solid state $^{13}C$-NMR spectrum was measured in BRUKER AC-800 Delta 2 NMR spectrometer with cross polarization at a field strength 9.389766[T] (400[MHz]), scans 276 and contact time of 3.5 mins. Powder X Ray Diffraction (PXRD) measurements were performed at scanning scope of 2θ at 0 to 60 degrees with an exposure time of 400 S using a D8 advance BRUKER diffractometer with Cu target (λ= 0.1541 nm) at 40 KV. The elemental analysis was performed with a Thermo Finnigan FLASH EA 112CHNS microanalyzer with carrier gas He (140 ml/min) using CHNS/ NCS column PQS SS 2M 6X5 mm in oven at 75 °C. The TG/DTA was taken to reveal the thermal events, stability and degradation behaviour with DTA/TG Al crucible at the rate of temperature rise by 10 °C per minute. The effective magnetic moment $\mu_{eff}$ of the complexes were measured by magnetic susceptibility balance (Sherwood Scientific, Cambridge, UK) at $X_1$ range setting using a weighing tube of 0.8233 g with the powdered sample compactly filled in it up to height (L) of 1.5 cm. EPR spectra were taken at 9.8577-9.8630 GHz (X band frequency), Bruker biospin corp. (EMX series) Model: A 200-9.5/12B/S, 2000 Gs scan range, 3000 Gs field set.

The *Debye- Scherer formula:* $D = \frac{k\lambda}{\beta cos\,\theta}$ was used to find the particle size (D) from PXRD curves *w*here 'k' is shape factor (0.9), 'λ' is wavelength of X-ray (0.1541 nm), 'β' is full width at half maxima (FWHM)) (0.043 radian observed upon Gaussian peak fit after the baseline correction) and 'θ' is the Bragg angle (Dehaghi, *et al.*, 2014; Kucukgulmez, *et al.*, 2011). The crystallinity index was determined with the formula: $\text{crystallinity index} = \frac{I_{max}-I_{am}}{I_{max}} \times 100$ where $I_{max}$ (arbitrary unit) is the maximum intensity peak intensity and $I_{am}$ (arbitrary unit) is amorphous diffraction intensity (Kumirska, *et al.*, 2010; Lomadze *et al.*, 2005; Zhang, *et al.*, 2005). From the equation, $\hbar g = \frac{\text{e bal.L.(R}-\text{R0)}}{10^9.\text{m}}$ where m =$m_2$ –$m_1$, $e_{bal}$ is proportionality constant of unity, gram susceptibility ( $\hbar g$ ) was calculated. Molar susceptibility ($\hbar$m) was obtained from the equation $\hbar\text{m} = \hbar g.molecular\ weight$. The Curie equation, $\mu\text{eff} = \mu\text{B} = \frac{2.84\sqrt{\hbar\text{m.T}}}{1}$ BM was employed to find magnetic moment (μB) (T= 298 K, $R_0$ = -34, L= 1.5 cm) (Djord jevic, 1960; Syamal & Kale, 1975). The g values in EPR spectra were calculated from the equation: $g = \frac{h\nu}{\mu_0 B_0} = 71.45\,X\frac{\nu}{B_0}$ (Segal, *et al.*, 1965), (where h/ $\mu_o$ = 71.45, h = 6.626 x $10^{-34}$ JS, $\mu_o$= Bohr magneton value of 9.27 x $10^{-24}$ J/T = 9.27 x $10^{-27}$ J/ mT), $\nu$ is frequency and $B_0$ is magnetic field.

## 3.3. Crab Shells as a Source of Chitin and Chitosan

### 3.3.1. Isolation of Chitin from Crab Shells

The loose tissue of crab shells was washed away and the shells were dried in sun for several days. The dry shells were pulverized and sieved into a powder of ≥ 500 nm grain diameter size. Crab shell powder was demineralized by stirring with 4% HCl in the ratio of 1:14 (w/v) at room temperature for 36 hours. The squashy suspension was rinsed with deionized water to remove acid and calcium chloride. The demineralized powder was properly dried in sun, left overnight at 40 °C and was deproteinized with 5% NaOH solution in the ratio of 1:12(w/v) at 90 °C for 24 hours. The deproteinized powder- chitin was washed to neutrality with water, properly dried in sun and left overnight at 40 °C (Rodde, *et al.*, 2008).

### 3.3.2. Deacetylation of Chitin: Preparation of Chitosan

Crab shell chitin with 45% NaOH solution in the ratio of 1:10 (w/v) was stirred at 90 °C in nitrogen atmosphere for 2 hours. The product was cooled to room temperature and washed to neutrality with distilled water by augmentation with pH meter at pH 7. Chitosan thus obtained was properly dried in sun for a few days and left overnight at 40 °C (Dutta, *et al.*, 2004; Yuan, *et al.*, 2011).

## 3.4. Determination of Physicochemical Properties of Chitosan

### 3.4.1. Determination of Moisture Content

Moisture content was gravimetrically determined. Crucible was heated at 105 °C for 15 min, cooled down in desiccator for half an hour and weighed. This process was repeated until getting the constant weight of crucible (m). This process was repeatedly carried out with chitosan in weighed crucible until the constant weight ($m_2$) from initial weight of crucible with chitosan ($m_1$) (Black (Ed.), 1965).

Hence, $moisture\ content(w) = \frac{m_2 - m_1}{m_1 - m} \times 100\ \%$

### 3.4.2. Determination of Degree of Deacetylation (DDA)

#### 3.4.2.1. Acid Base Titration method

Three different solutions were prepared each by dissolving 0.5 g of chitosan in 30 mL of 0.1 M HCl solution for 24 h at room temperature. Each solution with a drop of methyl orange was titrated against 0.1 M NaOH solution as titrant and the neutral point was ensured further by augmenting the solution with pH meter at pH 7 (Jiang, 2001).

Amine percent was calculated with the equation:

$$NH_2\ \% = \frac{(C_1V_1 - C_2V_2) \times 0.016 \times 100}{G\ (100 - w)}$$

where $C_1$ = concentration of HCl solution, $V_1$ = volume of chitosan solution in HCl (titre), $C_2$ = concentration of NaOH solution (titrant), $V_2$ = concurrent burette reading, G = weight of chitosan dissolved and W = moisture content (in percentage).

Then DDA was calculated with the equation:

$$DDA = \frac{NH_2\% \times 100\%}{9.94\%}$$

#### 3.4.2.2. Potentiometric Titration Method

Dried chitosan, 0.2 g was dissolved in 20 mL of 0.1 M HCl solution and 25 mL of distilled water. After stirring for 2 hours, next portion of 25 mL of distilled water was added and stirring was continued at room temperature for 24 hours. Chitosan solution as titre connected to potentiometer was titrated against 0.1 M NaOH solution from burette. DDA (%) was calculated with the equation: $\mathrm{DDA}(\%) = \frac{2.03\ .\ (V_2 - V_1)}{m + 0.0042\ (V_2 - V_1)}$ where $V_1$ and $V_2$ are volumes corresponding to the first and second inflexion points in the titration respectively, m = weight of chitosan (g), 2.03 is coefficient resulting from molecular weight of chitin monomer, 0.0042 is coefficient resulting from the difference between molecular weights of chitin and

chitosan monomer units (Czechowska-Biskup, *et al.*, 2004; Tolimate, *et al.*, 2000; Wojtasz-Pajak, *et al.*, 1998).

### 3.4.2.3. FT-IR Spectroscopic Method

The DDA of crab shell chitosan was determined with FT-IR spectroscopic method using the equation: $DDA = 100 - \left(\frac{A_{1658}}{A_{3364}}\right) 100/1.33$ where $A_{1658}$ $cm^{-1}$ and $A_{3364}$ $cm^{-1}$ are absolute heights of N-H stretch of amide ($A_{NH}$) and hydroxyl absorption bands ($A_{OH}$) respectively (Struszczyk, 1987). The absolute absorption heights were measured after adoption of baselines corresponding to the amide and hydroxyl absorption peaks (figure 13).

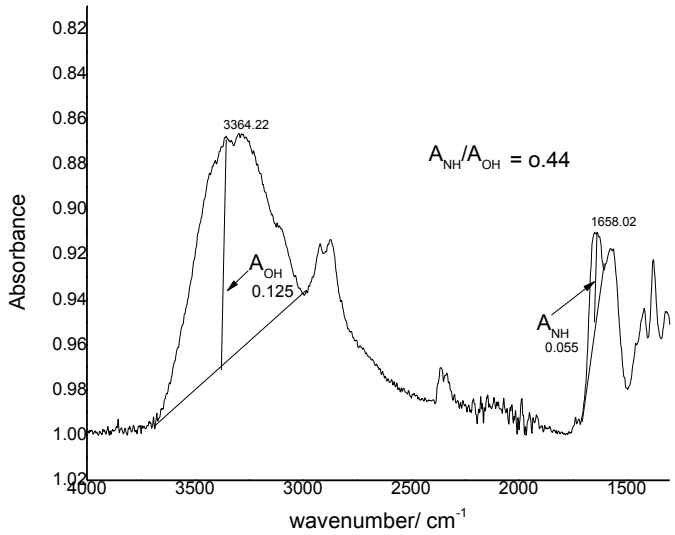


**Figure 13:** A portion of FTIR spectrum of chitosan with the adopted base lines for absolute heights measurement for determination of DDA.

### 3.4.3. Determination of Ash Content

Crucible was heated at 550 °C for half an hour, cooled down to room temperature in desiccator for half an hour and weighed. This process of triplication work was repeated until a constant weight of crucible (m) was obtained. Weight of crucible with chitosan ($m_1$) was taken and it was heated at 550 °C for 3 hours, cooled down to room temperature in desiccator for half an hour and weighed. This process was also repeated until a constant weight of crucible with chitosan ash ($m_2$) was obtained.

Ash content was calculated with the equation (Jiang, 2001)

$$Ash\ content(\%) = \frac{(m_2 - m) \times 100\%}{(m_1 - m)}$$

### 3.4.4. Determination of Molecular Weight (Mw)

Molecular Weight ($M_W$) of chitosan was determined with the help of intrinsic viscosity measurement of its solution in acetic acid and in a mixture of acetic acid with acidic buffer solution using Ostwald's viscometer. So, it was obtained as viscosity average molecular weight.

Chitosan, 1 g was left to be dissolved overnight in 100 mL of 1% acetic acid solution. A mixture of 8 mL of 0.3 M acetic acid and 12 mL of 0.2 M sodium acetate solution to get a buffer of pH 4.74 at 298 K was prepared in accordance with Henderson's equation. Test solutions (a, b, c and d) were prepared by mixing chitosan solution (in 1% acetic acid) and buffer solution (pH 4.74) in the ratio as shown in table 1.

**Table 1:** Preparation of test solutions for viscosity average $M_w$ measurement

| Test solutions | Volume of chitosan solution in 1% acetic acid (mL) | Volume of buffer solution (mL) | Molar concentration (C) in g $mL^{-1}$ |
|---|---|---|---|
| a. | 20 | 0 | 0.01 |
| b. | 15 | 5 | 0.0075 |
| c. | 10 | 10 | 0.0050 |
| d. | 5 | 15 | 0.0025 |

Mean time ($t_2$ in S) for the flow of same volume of each test solution was taken with the help of Ostwald's viscometer. Mean time ($t_1$ in S) taken for the flow of same volume of water was also recorded. For each test solution, specific viscosity ($\eta_{sp}$) and intrinsic viscosity ($\eta$) were calculated. Viscosity Average Molecular Weight (taken as $M_W$) of chitosan was determined with Mark-Houwink equation (Terbojevidh & Cosani, 1997).

## 3.5. Synthesis of Chitosan Thiosemicarbazones

### 3.5.1. Functionalization of chitosan as Chitosan Thiosemicarbazide

The one pot synthetic approach was employed for functionalization of chitosan as chitosan thiosemicarbazide *via* the formation of ammonium dithiocarbamate chitosan and sodium carbethoxydithiocarbamate chitosan with minor modifications in the reported procedure (Muzzarelli, *et al.*, 1982). A mixture of chitosan and ammonium hydroxide in the ratio of 4:5 by their weight in ethanol was stirred for an hour at laboratory temperature. Carbon disulphide (1 mL) was slowly dropped into the mixture and it was stirred for two and half hours to get ammonium dithiocarbamate chitosan. Addition of 1.437 g of sodium chloroacetate in ammonium dithiocarbamate chitosan followed by stirring at room temperature for an hour formed sodium carbethoxydithiocarbamate chitosan. Next, 1.5 mL of hydrazine monohydrate was slowly added and the mixture was stirred further at room temperature for two and half hours. The resulting mixture was filtered through G4 sintered

crucible, residue was completely washed with ethanol to dryness and left overnight at 40 °C to get a light brown powder of the key intermediate, chitosan thiosemicarbazide (Muzzarelli, *et al.*, 1982).

### 3.5.2. Preparation of Chitosan Thiosemicarbazones

An equimolar mixture of chitosan thiosemicarbazide and carboxaldehyde in 10 mL of methanol with 2 drops of acetic acid as catalyst was refluxed at 65 °C for 12 h, the mixture was cooled to room temperature and filtered through G4 sintered crucible. It was properly washed with methanol and the residue was dried overnight at 40 °C to get the respective chitosan thiosemicarbazone analogues. Synthesis of thiosemicarbazone involves condensation of thiosemicarbazide with carboxaldehyde. The one pot synthesis of the intermediate chitosan thiosemicarbazide in overall involves (i) reaction of ammonia monohydrate with chitosan to cause protonation of amino group in chitosan, (ii) reaction with carbon disulphide to form ammonium dithiocarbamate chitosan, and (iii) further reaction of sodium chloroacetate to form sodium carbethoxydithiocarbamate chitosan. The synthetic route involves no step-wise separation and refinement of the intermediates. There is partial functionalization of chitosan as chitosan thiosemicarbazide and hence there is partial incorporation of thiosemicarbazone moiety in C-2 position of constituent chitosan. The free amino groups in non-functionalized chitosan react with carboxaldehyde to introduce the partial Schiff's base character in the product molecules (Zhong, *et al.*, 2010). The overall scheme of synthesis of the compound through the intermediate formation of chitosan thiosemicarbazide is shown in figure 14.

Degree of substitution (DS) was determined with the relevant modification in the method given in literature (Inukai, *et al.*, 1998; Melo, *et al.*, 2002; Pires, *et al.*, 2013; Qin, *et al.*, 2012) according to Degree of substitution (DS) was calculated from the equation $DS = \frac{Mcs \times \%(S)}{3200 - Mtsc \times \%(S)}$ where Mcs is monomeric chitosan weight of 166 for chitosan oligosaccharide (87% DDA) of 173 for high molecular weight crab shell chitosan (71% DDA), %(S) is percentage of sulphur in chitosan functionalized thiosemicarbazone and Mtsc is unit weight of thiosemicarbazone incorporated into chitosan.

## 3.6. Synthesis of Copper(II) chitosan thiosemicarbazones

An equimolar mixture of chitosan functionalized thiosemicarbazone and copper(II) chloride was dissolved in 1% acetic acid solution at pH 6 maintained by the addition of 5% sodium hydroxide solution little at a time. Then, upon stirring for 3 h at 60 °C, the resulting mixture was filtered and the solid mass of the complex separated as residue was desiccated.

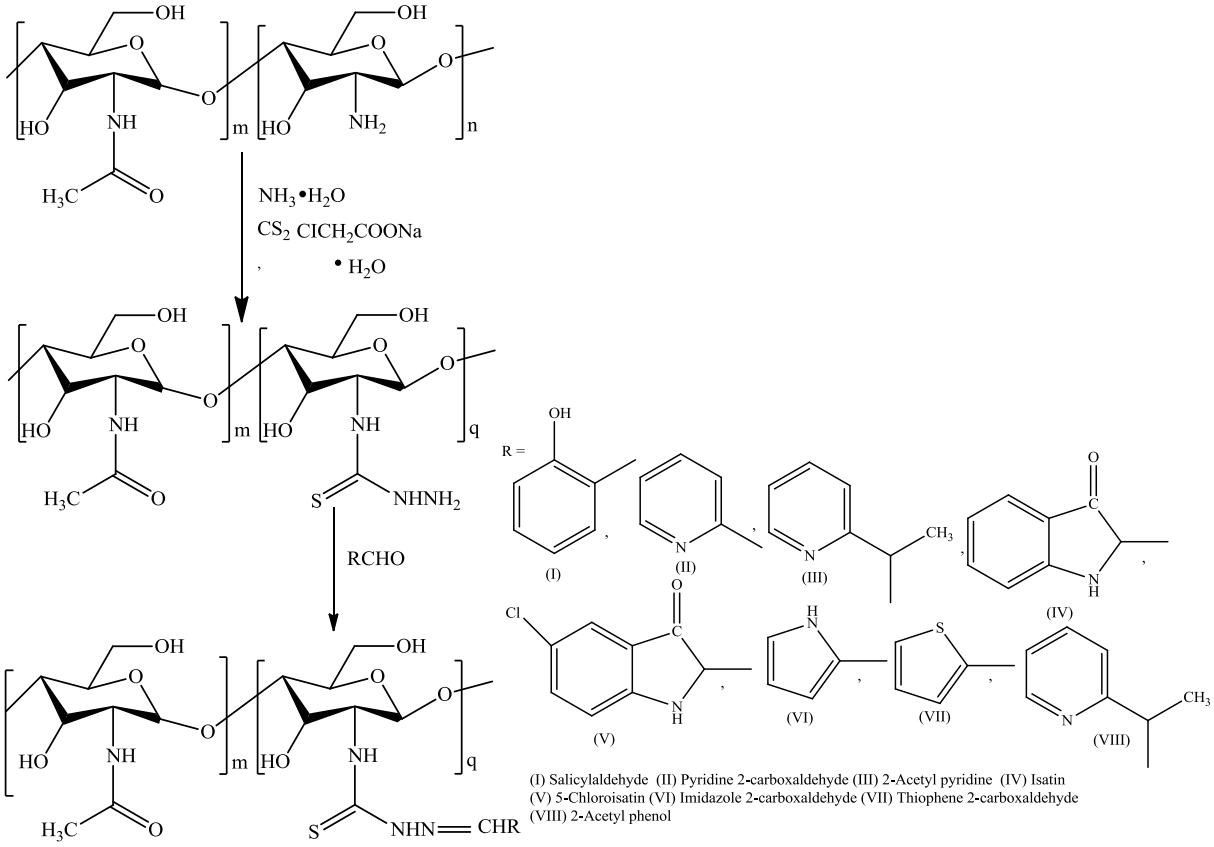


**Figure 14:** Synthetic route of chitosan thiosemicarbazones

## 3.7. Estimation of Chlorine in the Complexes

Copper(II) chitosan thiosemicarbazone complex, 0.025 g was weighed out and spread on a layer of anhydrous sodium carbonate in a nickel crucible. The complex was completely covered by a subsequent layer of anhydrous sodium carbonate, muffled at 900 °C for an hour, and cooled down. Nitric acid solution, 2 N, was added in little instalments until there was no effervescence. The mixture was left overnight and the completion of reaction was confirmed by ceasing of effervescence on further addition of a little amount of 2N nitric acid solution. Chlorine in the complex was then potentiometrically determined upon the argentometric

titration with 0.02 N silver nitrate solution ($Hg/Hg^{+}$, sat. KCl ‖ $Ag^{+}/Ag$) with a salt bridge of agar agar and nitric acid solution (1:5) (Tiwari, *et al.*, 2016).

The titrant volume at the end point was corrected through the blank potentiometric titration with water following the same procedure.

End point of titration = Volume of 0.02 M $AgNO_3$ solution (titrant) = X mL (say)

1000 mL of 1 N $AgNO_3$ solution contain 35.5 g of $Cl^-$ ions.

X mL of 0.02 N $AgNO_3$ solution contain $35.5 \times 0.02 \frac{X}{1000}$ g of $Cl^-$ ions.

= Y g of $Cl^-$ ions (say).

Weight of complex = 0.025 g

$Chlorine\ percentage = \frac{V\ 35.5\ 0.02}{1000} \frac{100}{0.025}$ where V is end point of titration.

## 3.8. Cells Culturing and Colorimetric MTT Assays

The incomplete Roswell Park Memorial Institute (RPMI) media with glutamine, 25 mM 4-(2-hydroxyethyl)-1-piperazineethanesulfonic acid (HEPES), 10% Fetal Bovine Serum (FBS) and 1.2% antibiotic solution of penicillin and streptomycin were mixed for 24 h with 5% carbon dioxide to get the complete RPMI media. The cellular debris was removed by washing with phosphate buffer solution (PBS). The cells were counted, and every well of the 96 well plate was distributed with ~$10^5$ cells. The suspensions of the test samples in 10 mL of DMSO obtained after 72 h stirring were filtered to get the test solutions as filtrate. The concentration of the test solution was obtained by gravimetric calculation. The test solution and 0.5 mg/mL solution of 3-(4,5-dimethylthiazol-2-yl)-2,5-diphenyltetrazolium bromide (MTT) were added in each well, incubated at 37 °C for 4 h until the visible appearance of the purple formazan crystals under the microscope. Upon the removal of MTT and dissolution of formazan crystals in DMSO followed by trituration and incubation for 2 h at 37 °C, the cells were lysed and the purple crystals were well dissolved to get the absorbance measured at 551 nm. The blank and positive control for the study were the media only and the untreated cells respectively. The equation: $\%\ viable\ cells = \frac{\text{Sample abs – Blank abs}}{\text{Control abs – Blank abs}}\ X\ 100$ was used to find the cell viability percentage. The concentration analogous to half the maximum absorbance was taken as half inhibitory concentration ($IC_{50}$) (Kumar, *et al.*, 2018) and the inhibition ratio (IR) was determined as $IR\ \% = \frac{Control\ abs - Sample\ abs}{Control\ abs}\ X\ 100\%$ (Shahneh, *et al.*, 2013; Zheng, *et al.*, 2006).

**CHAPTER 4**

# 4. RESULTS AND DISCUSSION

## 4.1. Chitosan

### 4.1.1. Physicochemical Parameters

The physicochemical parameters of chitosan oligosaccharide (CS) and crab shell chitosan (CCS) are summarized in table 2. Chitosan oligosaccharide (CS) was commercially available as a low $M_w$ (<3000 Da) yellow solid with 87% DDA, whereas crab shell chitosan (CCS) was synthesized as a high $M_w$ off- white solid by alkaline deacetylation of chitin extracted from crab shells. CS was soluble in water, but CCS showed 1% solubility in 1% aqueous acetic acid (w/v) solution upon an extensive stirring for 48 h.

Crab shell chitosan was found to have 71% DDA in average (66.92% from FT-IR spectroscopic method, 70.02 % from acid-base titration and 76.10% from potentiometric titration method) and viscosity average $M_w$ of 350 k Da. The chitosan yield was 31.4%, close to the reported chitosan yield of 32.2% from crab shell wastes upon 2 h deacetylation with 40% sodium hydroxide solution in a solid/solvent ratio of 1:10 (w/v) (Yen, *et al.*, 2009), but higher than crab chitosan yield of 16.7% reported upon 30 min deacetylation with 45% sodium hydroxide solution in a solid/solvent ratio of 1:10 (w/v) (No, *et al.*, 2003).

The moisture content of 7.40% in crab shell chitosan was in agreement with the moisture content of less than 10% in commercial chitosan, attributed to hygroscopicity upon the storage (Khan, *et al.*, 2002; Li, *et al.*, 1992). The ash content of 1% in crab shell chitosan showed reasonably an effective loss of calcium carbonate, as the ash content below 1% has been reported to be an indicator of high effectiveness of demineralization (No & Meyers, 2000). Ash content is an important parameter that affects the solubility and viscosity, and ash content of 1.18% has been found in commercial chitosan (Wang & Kinsella, 1976).

The FT-IR spectroscopy in the mid spectral region of 4000-400 $cm^{-1}$ provides a convenient technique for a qualitative structural elucidation and determination of DDA in chitosan (Brugnerottoa, *et al.*, 2001; Kasaai, 2011; Majtán, *et al.*, 2007; Pearson, *et al.*, 1960). The overall FT-IR spectrum of chitosan resembles the spectrum of cellulose with additional characteristic bands attributed to acetamido and amino group vibrations (Brummer & Cui, 2006). The physicochemical and biological properties of chitosan like crystallinity, hydrophobicity, degradation, and cell response are greatly dependent on DDA (Rinaudo, 2006), that in turn, can be determined by the methods of titrimetric and spectroscopic analysis

(Brugnerottoa, *et al.*, 2001; Heux, *et al.*, 2000; Kasaai, 2011; Peniche, *et al.*, 2008). Acid-base and potentiometric titration are easy to work out methods, but they are limited by solubility of the sample. So, the FT-IR spectroscopic method which can be employed even for insoluble sample without its loss is advantageous (Brugnerottoa, *et al.*, 2001) though it is also limited by the possible inaccuracy in drawing the base line and interferences due to humidity and impurities in the sample (Kasaai, 2011).

Normally, the increase in DDA causes the decrease in $M_w$, that brings about the variations in physicochemical and functional properties (Yen, *et al.*, 2009). The DDA, on the other hand, is affected by extraction conditions viz temperature, chitin/ alkali concentration, reaction time, particle size of chitin and also the native source of chitin in nature (Guo, *et al.*, 2002; Li, *et al.*, 1992; Nemtsey, *et al.*, 2002; Oh, *et al.*, 2001). The physicochemical properties of crab shell chitosan show the reasonably high yield of HMWC with the standard range of moisture and ash content.

**Table 2:** The physicochemical parameters of chitosan oligosaccharide (CS) and crab shell chitosan (CCS)

| Chitosan | Moisture content (%) | Ash content (%) | DDA (%) | $M_w$ (k Da) | Yield (%) |
|---|---|---|---|---|---|
| Chitosan oligosaccharide (CS) | 2-10 | 1.18 | 87 | < 3000 Da | - |
| Crab shell chitosan (CCS) | 7.40 | 1.00 | 71 (in average) | 350 k Da | 31.40 |

### 4.1.2. Characterization

#### 4.1.2.1. Fourier Transform-Infrared (FT-IR) Spectroscopy

The FT-IR spectrum of crab shell chitosan (figure 15) showed the characteristic peaks of polysaccharide *viz.* a weak ν(aliphatic C-H) symmetric stretch at 2923 $cm^{-1}$ and ν(aliphatic C-H) asymmetric stretch at 2873 $cm^{-1}$. The presence of residual N-acetyl groups is confirmed by a sharp characteristic ν(C=O amide I) stretch at 1646 $cm^{-1}$ and the stretching vibration of ν(C-N) type III amide band at 1313 $cm^{-1}$ (Fernandes Queiroz, *et al.*, 2015). Some characteristic peaks are the weak ν(N-H amide II) angular bending deformation vibration at 1557 $cm^{-1}$, the ν($CH_2$) bending at 1423 $cm^{-1}$ and a broad peak attributed to symmetrical deformation vibration of C-H bonds of methyl group at 1377 $cm^{-1}$. The weaker peak at 1146 $cm^{-1}$ indicates the asymmetric stretching vibration of C-O-C bridge. Both the medium absorption band at 1064 $cm^{-1}$ and the sharp band at 1027 $cm^{-1}$ correspond to C-O stretching

(Fernandes Queiroz, *et al.*, 2015). The band at 892 $cm^{-1}$ corresponds to C-O-C symmetric skeletal stretching vibration of chitosan (Fernandes Queiroz, *et al.*, 2015; Pawlak & Mucha, 2003). A broad band in the region 3286-3364 $cm^{-1}$ was attributed to ν(O-H) stretch at 3364 $cm^{-1}$, ν(N-H) stretch at 3286 $cm^{-1}$ and intramolecular hydrogen bonds (Fernandes Queiroz, *et al.*, 2015; Rampino, *et al.*, 2013). The selected FT-IR bands ($cm^{-1}$) of the synthesized chitosan are presented in table 3.

**Table 3:** The selected FT-IR bands ($cm^{-1}$) of the synthesized chitosan (CCS)

| Bands | Vibrational frequency ($cm^{-1}$) |
|---|---|
| ν(O-H) & ν(N-H) stretch | 3286-3364 (broad band) |
| ν(C-H, aliphatic) symmetric stretch | 2923 |
| ν(C-H, aliphatic) asymmetric stretch | 2873 |
| ν(C=O amide I) stretch | 1646 |
| ν(N-H amide II) angular bend deformation | 1557 |
| ν($CH_2$) bend | 1423 |
| ν(C-H) of methyl group, symmetrical deformation | 1377 |
| ν(C-N) type III amide stretch | 1313 |
| ν(C-O-C) bridge, asymmetric stretch | 1146 |
| ν(C-O) stretch | 1027 & 1064 |
| ν(C-O-C) symmetric skeletal stretch | 892 |

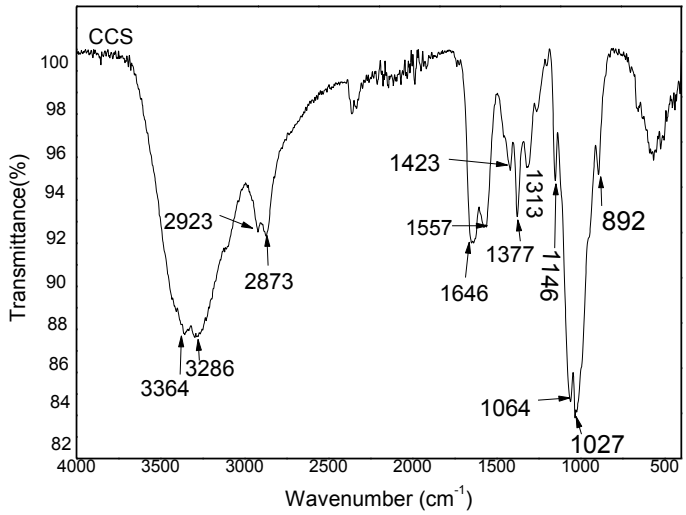


**Figure 15:** FT-IR spectrum of crab shell chitosan

### 4.1.2.2. Solid State $^{13}C$ Nuclear Magnetic Resonance ($^{13}C$ NMR) Spectroscopy

Solid State $^{13}C$ NMR spectrum of crab shell chitosan (figure 16), used to characterize chitosan structure (De Angelis, *et al.*, 1998), showed the chemical shift (δ) signals at 23.07

ppm (methyl carbon of acetamido moiety), 57.50 ppm ($C_2$), 60.92 ppm ($C_6$), 75.70 ppm ($C_3$, $C_5$), 83.45 ppm ($C_4$), 104.57 ppm ($C_1$) of pyranose ring, and 174.29 ppm (C=O, indicative of incomplete deacetylation), in close agreement with the reported chitosan signals at 24-25 ppm (carbon atom of the methyl moieties of the acetamido groups), 57- 60 ppm ($C_2$), 60- 63 ppm ($C_6$), 76-78 ppm ($C_3$, $C_5$), 84 ppm ($C_4$), 106 ppm ($C_1$ of pyranose ring carbons), and 178 ppm (attributed to C=O indicative of incomplete deacetylation) (de Britto, *et al.*, 2007; Qin, *et al.*, 2012). The solid state $^{13}C$ NMR spectral data (δ, ppm) of crab shell chitosan are presented in table 4.

**Table 4:** The solid state $^{13}C$ NMR spectral data (δ, ppm) of crab shell chitosan (CCS)

| Carbon atoms | methyl carbon | C2 | C6 | C3, C5 | C4 | C1 | C=O |
|---|---|---|---|---|---|---|---|
| δ (ppm) | 23.07 | 57.50 | 60.92 | 75.70 | 83.45 | 104.57 | 174.29 |

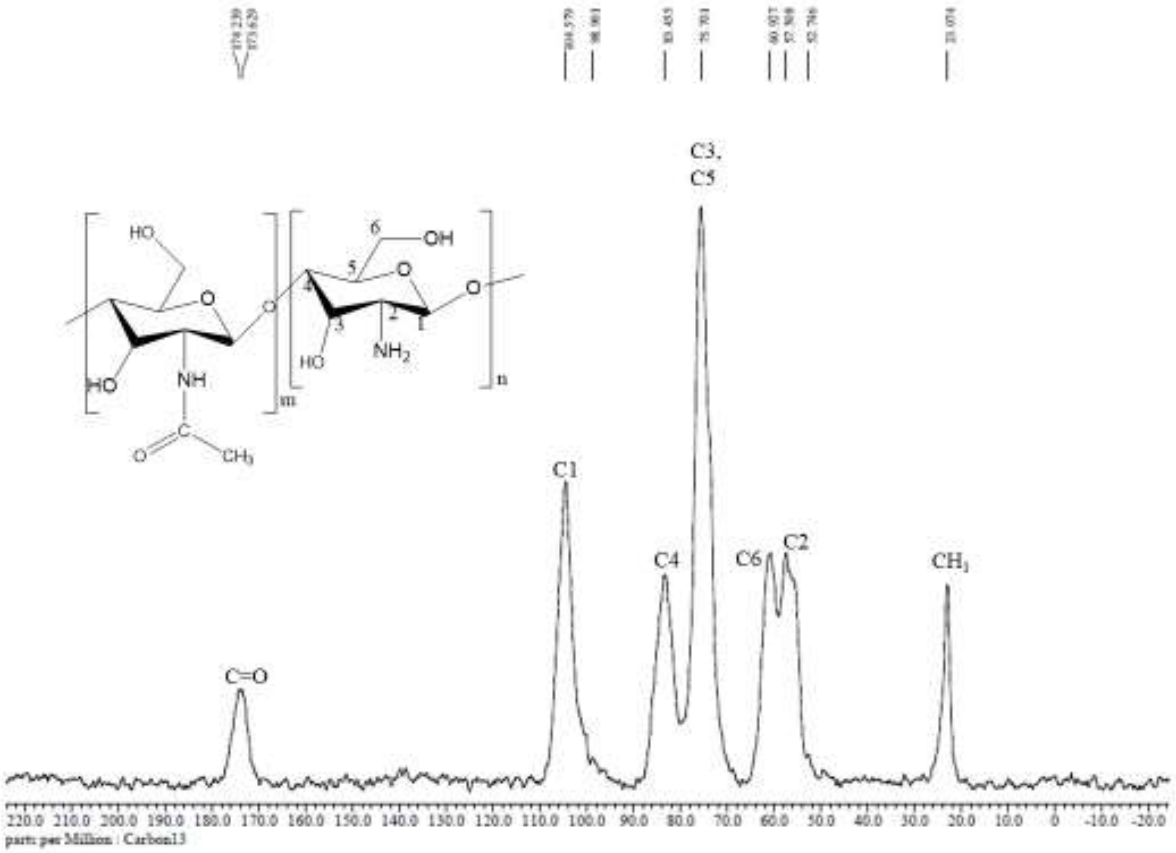


**Figure 16:** Solid State $^{13}C$ NMR spectrum of crab shell chitosan

### 4.1.2.3. Powder X Ray Diffraction (PXRD) Studies

Powder X ray diffractogram of crab shell chitosan (figure 17) showed two crystalline reflection peaks at 2θ = 9.5º and 19.6°, in close agreement with the reported peaks at 10° and 20º for chitosan oligosaccharide (Yen, *et al.*, 2009). This close correlation of peak positions with the reported values without additional crystallinities, suggests that the crab shell chitosan crystallizes in an orthorhombic unit cell (Okuyama, *et al.*, 1997).

The particle size of chitosan (D) as estimated with the help of *Debye- Scherer formula* (Dehaghi, *et al.*, 2014; Kucukgulmez, *et al.*, 2011) was 13.27 nm in average. The broader peak meant the smaller particles and more amorphous form (Kucukgulmez, *et al.*, 2011). The particle size of the synthesized chitosan in proximity to the reported range of 3-12 nm (Kucukgulmez, *et al.*, 2011) showed the aggregation of chitosan in nanocrystalline form. The crystallinity index of crab shell chitosan was 73.53%. Crystallinity of chitosan, though partially affected by the factors like spatial hindrance, hydrophobic force and π-π stacking (Lomadze, *et al.*, 2005) has been found to be mainly dependent on DDA (Bumgardner, *et al.*, 2003; Di Martino, *et al.*, 2005; Hidaka, *et al.*, 1999; Khor & Lim, 2003). The powder X ray diffraction data of crab shell chitosan (CCS) are presented in table 5.

**Table 5:** The powder X ray diffraction data of crab shell chitosan (CCS)

| | |
|---|---|
| 2θ | 9.5°, 19.6° |
| Particle size (D) | 13.27 nm |
| Crystallinity Index (C.I.) | 73.53% |

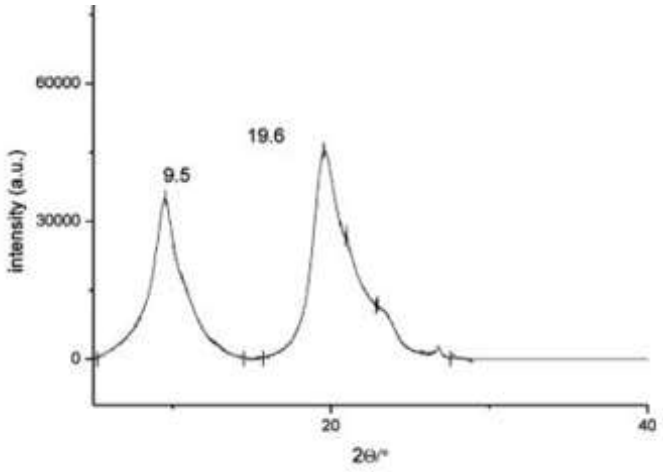


**Figure 17:** Powder X ray diffractogram of crab shell chitosan

#### 4.1.2.4. Elemental Microanalysis

For chitosan with 100% DDA, corresponding to the monomer structure of unit formula weight 161.15, calculated percentages of elements are C, 52.16; H, 9.38; N, 8.69. Elemental microanalysis of crab shell chitosan (71% DDA) with the percentages as C, 41.10; H, 6.00; N, 6.50 is in agreement with the reported values of elemental microanalysis of chitosan with 87 % DDA as C, 40.05; H, 6.41; N, 7.29 (Qin, *et al.*, 2012). The values of calculated C/N ratio of chitosan with 100% deacetylation, crab shell chitosan (71% DDA and $M_w$ 350 k Da) and commercial chitosan oligosaccharide (87% DDA, average $M_w$ <3000 Da) are 6.00:1, 6.32:1 and 5.49:1 respectively. The alkali concentration, reaction conditions and the presence of impurities have been reported to cause the lowering of C/N ratio (Stoscheck,1990; Yen, *et al.*, 2009). The elemental microanalysis of chitosan samples (table 6) shows the comparative and arbitrary variation of C/N ratio with DDA, indicating the effect of other factors such as time of reaction, temperature, alkali concentration on deacetylation and molecular weight distribution of chitosan.

**Table 6:** Elemental (CHN) microanalysis of chitosan samples: calculated (anal. found)

| Samples | DDA(%) | C(%) | H(%) | N(%) | C/N ratio |
|---|---|---|---|---|---|
| Chitosan | 100 | 52.16 | 9.38 | 8.69 | 6.00:1 |
| Crab shell chitosan (CCS) | (71) | (41.10) | (6.00) | (6.50) | 6.32:1 |
| Commercial chitosan (CS) | (87) | (40.05) | (6.41) | (7.29) | 5.49:1 |

#### 4.1.2.5. Thermal Studies

Thermogravimetric/differential thermal analysis (TG/DTA) curves of crab shell chitosan (CCS) (figure 18) and the TG/DTA data of thermal events in CCS summarized in table 7 showed the thermal decomposition in two stages corresponding to 18.82% weight loss due to the loss of water at 190 °C and 63.99 % weight loss due to the disruption of backbone linkage and thermal degradation of glucosamine residue at 200 °C -1000 °C. The abrupt increase in the rate of decomposition (with about 33% weight loss) from 200 °C to 400 °C is an indicative of disruption of chitosan backbone chain. This behavior reasonably agrees with the reported decomposition temperatures of crab shell chitosan at 50 °C- 100 °C and 400 °C- 500 °C (Andrade, *et al.*, 2012; Kumari, *et al.*, 2017) and two stages of weight loss of commercial chitosan: viz 9 % of weight loss at 120 °C due to loss of water and 43% of weight loss at 500

°C due to degradation of main chain of chitosan (Chethan, *et al.*, 2013; De Britto & Campana-Filho, 2004; Xu, *et al.*, 2010). It showed a rapid rate of decomposition from 100 °C to 400 °C and then a steady rate of decomposition, leaving about 17% of the sample as residue of the unsaturated structure at 1000 °C. Such a behavior is attributed to high thermal stability of chitosan (Qu, *et al.*, 2000).

**Table 7:** TG/DTA data of thermal events in CCS

| Temperature(°C) | Weight loss (%) | Thermal events |
|---|---|---|
| 190 | 18.82 | Loss of water |
| 200-400 | 33.00 | Disruption of chitosan backbone chain |
| 400-1000 | 30.99 | Degradation of backbone and glucosamine residue |

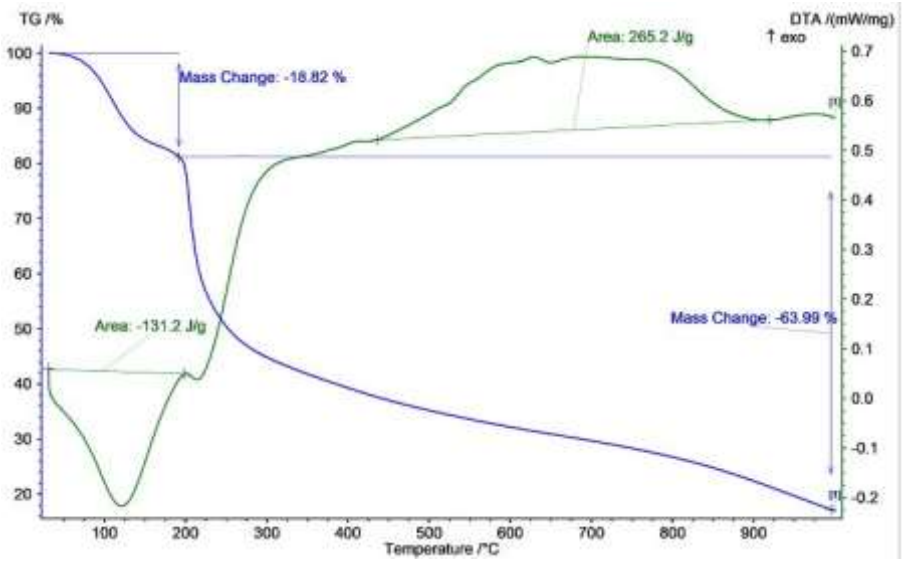


**Figure 18:** TG/DT curves of crab shell chitosan (CCS) showing the thermal events at different temperatures

## 4.2. Chitosan Thiosemicarbazones and their Copper(II) Complexes: Salicylaldehyde and 2-Acetyl phenol Analogues

### 4.2.1. Physical Characteristics

Physical characteristics of salicylaldehyde and 2-acetyl phenol thiosemicarbazones and their copper(II) complexes summarized in table 8 & 9 respectively show that they are thermally stable crystalline solid with melting point above 300 °C. They were partially soluble in 1% aqueous acetic acid and more solubility was observed in commercial chitosan analogues having more DDA. They were obtained in substantial yield *viz.* 32-46% ligands and 66-72% complexes. Commercial chitosan analogues were extractable with about 40% solubility in water.

**Table 8:** Physical characteristics of salicylaldehyde chitosan thiosemicarbazones and their copper(II) complexes

| Compounds | Unit formula | Unit formula weight | Color | m.pt. (°C) | Yield (%) |
|---|---|---|---|---|---|
| CSSTSC | $C_{14}H_{17}N_3O_5S$ | 339 | Yellowish | >300 | 38 |
| CCSSTSC | $C_{14}H_{17}N_3O_5S$ | 339 | Yellowish white | >300 | 32 |
| Cu-CS S TSC | $C_{14}H_{17}N_3O_5SCuCl$ | 438 | Greenish yellow | >300 | 70 |
| Cu-CCS S TSC | $C_{14}H_{17}N_3O_5SCuCl$ | 438 | Greenish yellow | >300 | 67 |

**Table 9:** Physical characteristics of 2-acetyl phenol chitosan thiosemicarbazones and their copper(II) complexes

| Compounds | Unit formula | Unit formula weight | Color | m.pt. (°C) | Yield (%) |
|---|---|---|---|---|---|
| CS AP TSC | $C_{15}H_{19}N_3O_5S$ | 353 | Yellow | >300 | 46 |
| CCS AP TSC | $C_{15}H_{19}N_3O_5S$ | 353 | Yellowish white | >300 | 39 |
| Cu-CS AP TSC | $C_{15}H_{19}N_3O_5SCuCl$ | 452 | Yellowish green | >300 | 72 |
| Cu-CCS AP TSC | $C_{15}H_{19}N_3O_5SCuCl$ | 452 | Yellowish green | >300 | 66 |

### 4.2.2. Characterization

#### 4.2.2.1. Fourier Transform- Infrared (FT-IR) Spectroscopy

The FT-IR spectra of salicylaldehyde and 2-acetyl phenol chitosan thiosemicarbazones (figure 19, 21, 23 & 25) showed a broad translocation due to ν(O-H) and ν(N-H) merged at a range of 3100-3300 $cm^{-1}$ (Qin, *et al.*, 2012; Zhong, *et al.*, 2011). Disappearance of ν(C=O) of amide I at 1645 $cm^{-1}$ (Qin, *et al.*, 2012) and the appearance of new band in the range of 1611-1625 $cm^{-1}$ in the ligands were indicatives of the involvement of C=O group in imine (-C=N-) bond formation (Qin, *et al.*, 2012). Partial involvement of $NH_2$ group in the formation of thiosemicarbazones was shown by ν($NH_2$) at 1555-1567 $cm^{-1}$ (Yadav & Shivakumar, 2012) and ν(C=S) in two separate ranges of 841-1078 $cm^{-1}$ (Tiwari, *et al.*, 2016; Yamaguchi, *et al.*, 1958) and 1360-1380 $cm^{-1}$ (Aneesrahman, *et. al.*, 2019; Joseph, *et al.*, 2006). The existence of thiosemicarbazones in thione form was shown by the absence of ν(C-SH) band at 2500–2600 $cm^{-1}$ (Bharti, *et al.*, 2003). The absorption bands at 660-1100 $cm^{-1}$ were attributed to ν(phenyl) from carboxaldehyde (Qin, *et al.*, 2012) and the bands at 1438-1489 $cm^{-1}$ were corresponding to characteristic stretch ν (CH) of methylene to methyl groups (Kumari, *et al.*,

2016; Kumirska, *et al*., 2010) in the ligands. There was weakening of residual peak due to acetamido moiety of chitin at 1550-1558 $cm^{-1}$ (Zhong, *et al*., 2010).

In the FT-IR spectra of copper(II) complexes (figure 20,22, 24 & 26), the absorption peaks due to ν (OH) and ν (NH) were shifted to lower wave lengths at 3000-3200 $cm^{-1}$ (Qin, *et al*., 2012; Zhong, *et al*., 2011) indicating the involvement of oxygen in coordination. The absence, or else the highly diminished intramolecular hydrogen band ν (OH) at 3284 $cm^{-1}$ in the complexes indicated the deprotonation of phenolic-OH group (Sarker, *et al*., 2019). The ν (phenolic C-O) vibration in the ligands at 1241-1275 $cm^{-1}$ (Ismail, *et al*., 2014) was lowered to 1196-1260 $cm^{-1}$ indicating the involvement of OH group in complex formation. Lowering of ν (C=N) from 1611-1625 $cm^{-1}$ (Qin, *et al*., 2012) in ligand to 1602-1616 $cm^{-1}$ in complexes showed the involvement of C=N group in complex formation. The negative shifting of peaks due to ν (C=S) to 829-1037 $cm^{-1}$ (Wiles, *et al*., 1967) and 1320-1354 $cm^{-1}$ (Joseph, *et al*., 2006) in the corresponding complexes showed the coordination of sulphur with metal ion. The overall impression of IR data (table 10) indicated the partial grafting of thiosemicarbazone group into chitosan, and bonding of metal ion with thiosemicarbazones through phenolic oxygen, imino nitrogen and thione sulphur. This phenomenon accorded with the completion of the coordination sphere of copper(II) ion by mono-deprotonated O,N,S tridentate salicylaldehyde thiosemicarbazone ligand and a chloride ion (Carcelli, *et al*., 2020).

**Table 10:** The selected FT-IR bands ($cm^{-1}$) of chitosan thiosemicarbazones and their complexes: salicylaldehyde and 2-acetyl phenol analogues

| Compounds | ν (C=N) | ν (C=S) | ν ($NH_2$) | ν (phenolic C-O) |
|---|---|---|---|---|
| CSSTSC | 1625 | 1055, 1374 | 1567 | 1268 |
| Cu-CSSTSC | 1616 | 1030, 1324 | 1536 | 1260 |
| CCSSTSC | 1618 | 894, 1380 | 1556 | 1275 |
| Cu-CCSSTSC | 1611 | 860, 1320 | 1533 | 1196 |
| CSAPTSC | 1612 | 1078, 1361 | 1558 | 1251 |
| Cu-CSAPTSC | 1602 | 1037, 1353 | 1563 | 1232 |
| CCSAPTSC | 1611 | 841, 1360 | 1555 | 1241 |
| Cu- CCSAPTSC | 1604 | 829, 1354 | 1557 | 1235 |

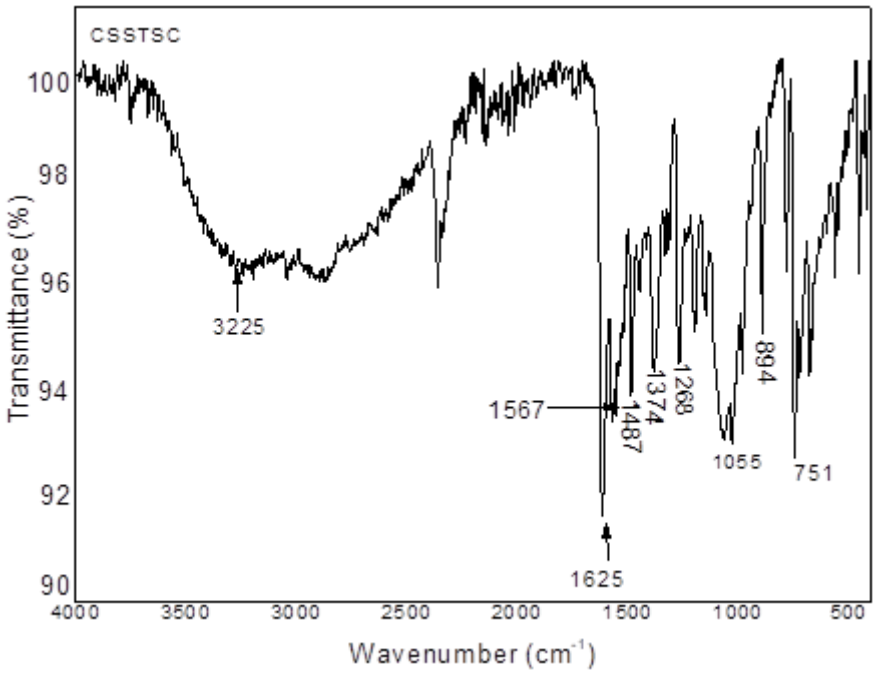


**Figure 19:** FT-IR spectrum of CSSTSC

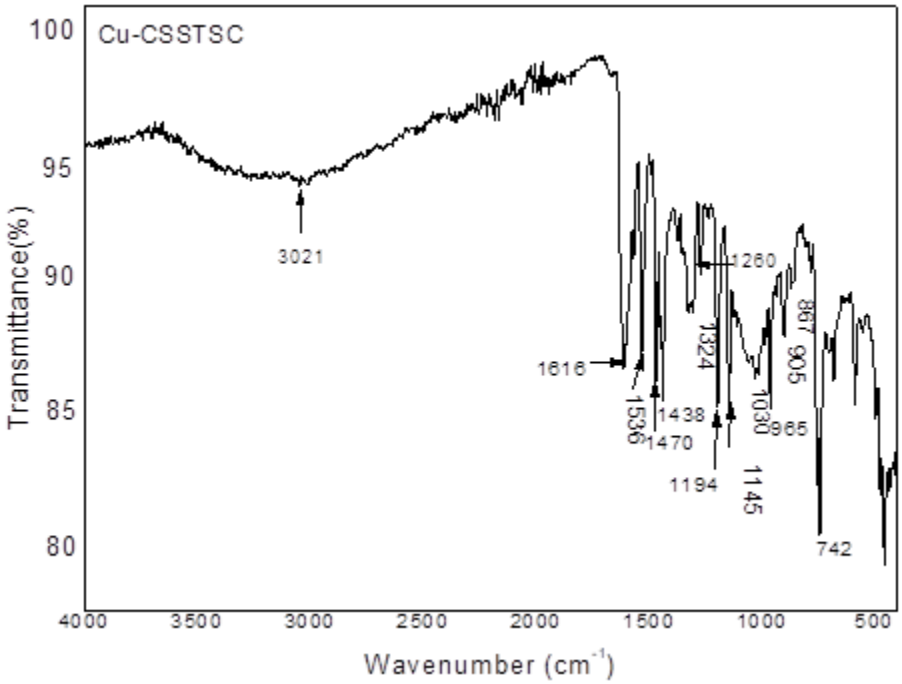


**Figure 20:** FT-IR spectrum of Cu-CSSTSC

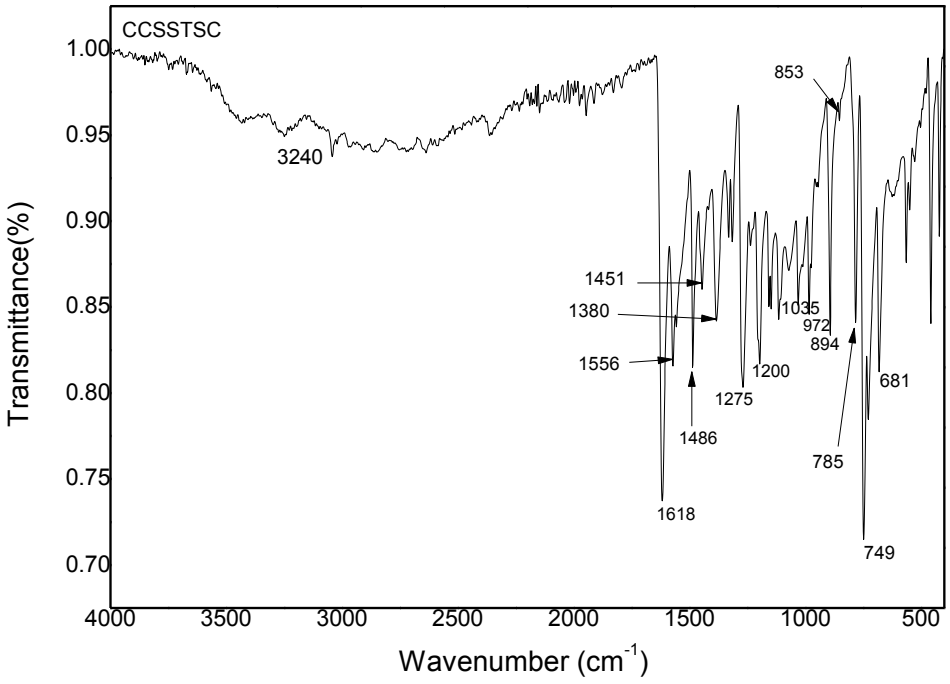


**Figure 21:** FT-IR spectrum of CCSSTSC

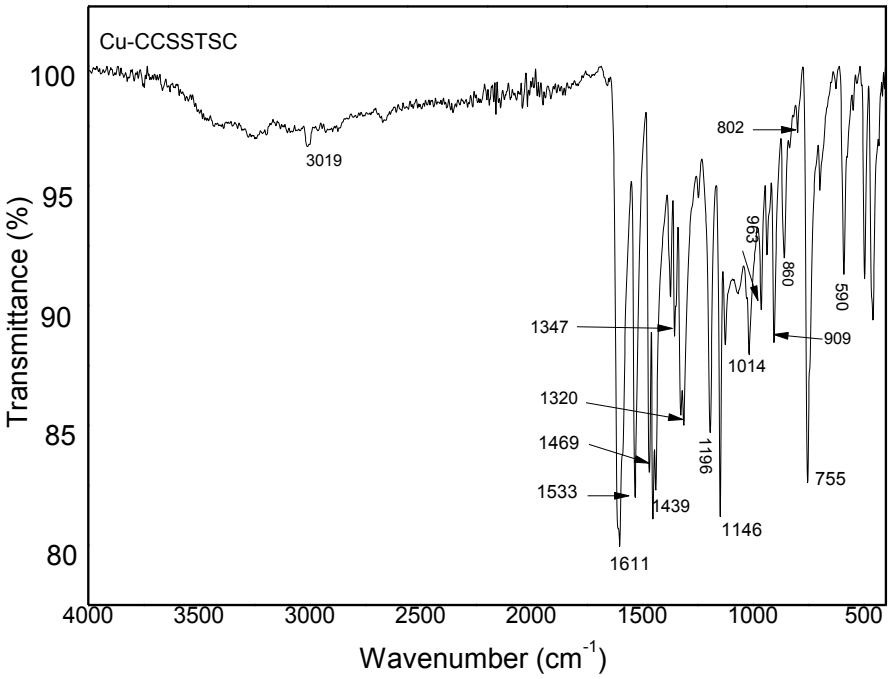


**Figure 22:** FT-IR spectrum of Cu-CCSSTSC

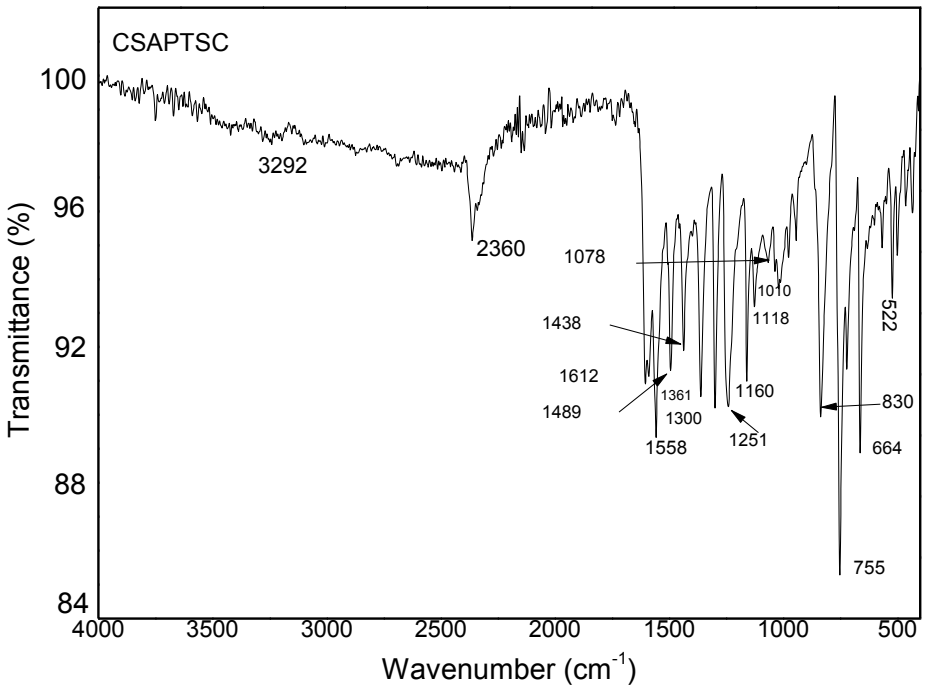


**Figure 23:** FT-IR spectrum of CSAPTSC

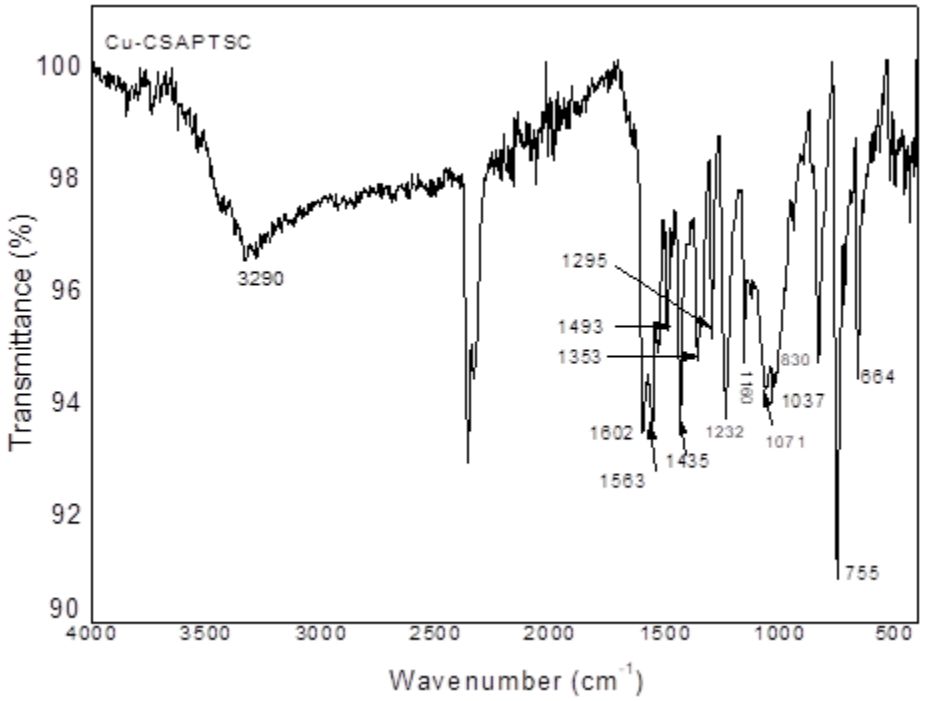


**Figure 24:** FT-IR spectrum of Cu-CSAPTSC

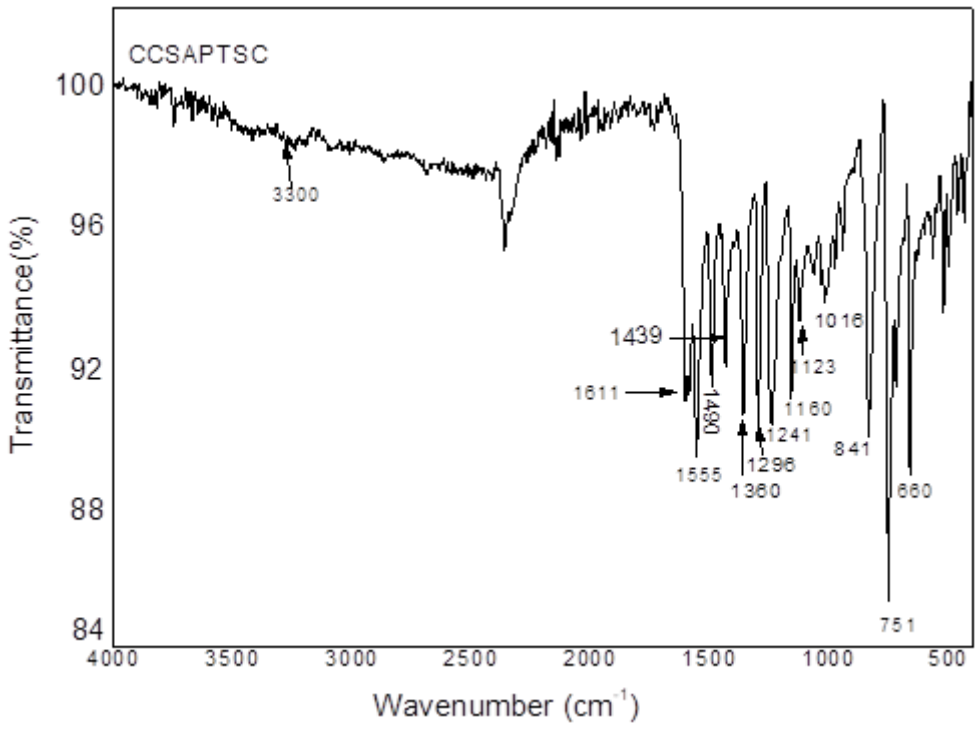


**Figure 25:** FT-IR spectrum of CCSAPTSC

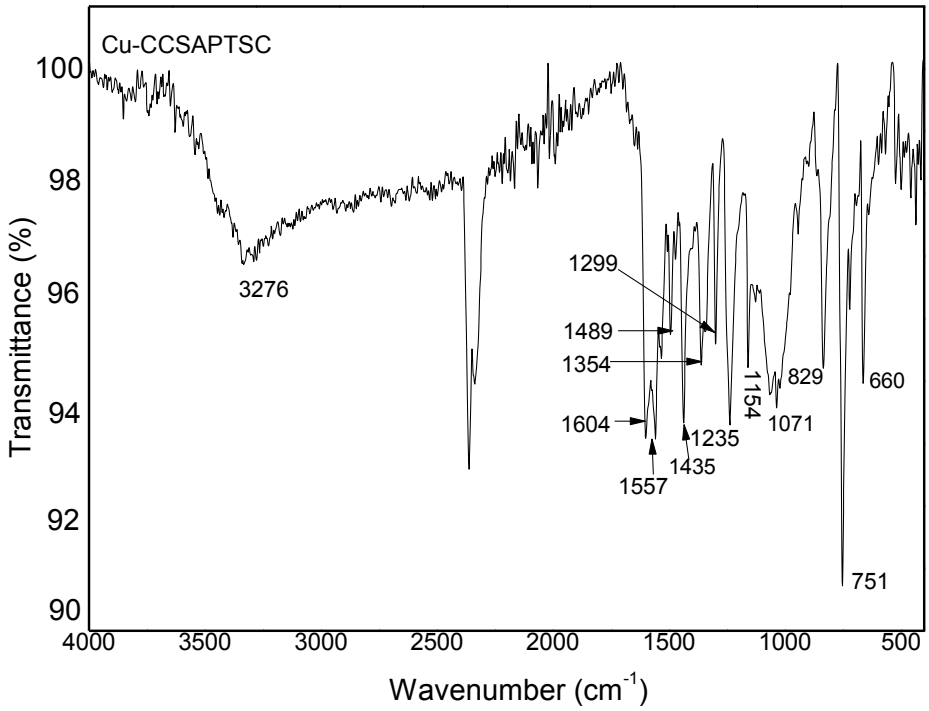


**Figure 26:** FT-IR spectrum of Cu-CCSAPTSC

### 4.2.2.2. Solid State $^{13}$C Nuclear Magnetic Resonance ($^{13}$C NMR) Spectroscopy

Solid state $^{13}$C NMR spectra of chitosan thiosemicarbazones (figure 27, 28, 29 & 30) have been used to elucidate the chitosan ring structure (De Angelis, *et al.*, 1998). The weakening of C2 of chitosan signal at δ=57 ppm or the appearance of C2 signals in its neighbourhood

and the simultaneous appearance of -N=CH signal at δ= 167.40 -173.934 ppm showed the amino group substitution at C2 *viz*. the partial incorporation of C2 towards the imine bond formation (Qin, *et al.*, 2012; Wang, *et al.*, 2016). The partial deacetylation was shown by C=O signals (Wang, *et al.*, 2016) at a range of δ= 172.92-200.941ppm. The characteristic peaks corresponding to ring chitosan in these chitosan thiosemicarbazones were evident from $CH_3$ (22.81-24.62-ppm), C6(61.04-64.956 ppm), C3, C5(73.39-79.731 ppm), C4(83.28-84.44 ppm), and C1(102.01-104.358 ppm) (Qin, *et al.*, 2012; Wang, *et al.*, 2016); and the phenyl carbon signals at δ= 130-160 ppm in CSSTSC, 119-164 ppm in CCSSTSC, 119-162 ppm in CSAPTSC, and 119-162 ppm in CCSAPTSC (Qin, *et al.*, 2012). The broadening of peak at a range of 172.92-200.941 ppm was indicative of the superimposition of C=S and C=O signals (Qin, *et al.*, 2012). These results were in agreement with the formation of thiosemicarbazone *via* the partial introduction of thiosemicarbazone moiety to C2 position of the ring chitosan. The solid state $^{13}C$ NMR spectral data (δ, ppm) of salicylaldehyde and 2-acetyl phenol analogues of chitosan thiosemicarbazones are presented in table 11.

**Table 11:** The solid state $^{13}C$ NMR spectral data (δ, ppm) of chitosan thiosemicarbazones: salicylaldehyde and 2-acetyl phenol analogues

| Compounds | Methyl carbon | C6 | C3, C5 | C4 | C1 | -N=CH | Phenyl carbons | C=S & C=O superimposition |
|---|---|---|---|---|---|---|---|---|
| CSSTSC | 24.62 | 62.14 | 75.81 | 84.44 | 104.36 | 173.23 | 130-160 | 178.96 |
| CCSSTSC | 22.99 | 64.95 | 73.50 | 83.51 | 104.27 | 173.93 | 119-164 | 200.94 |
| CSAPTSC | 23.50 | 62.08 | 75.15 | 83.33 | 102.01 | 168.43 | 119-162 | 176.25 |
| CCSAPTSC | 22.81 | 61.04 | 73.39 | 83.28 | 104.07 | 167.40 | 119-162 | 172.92 |

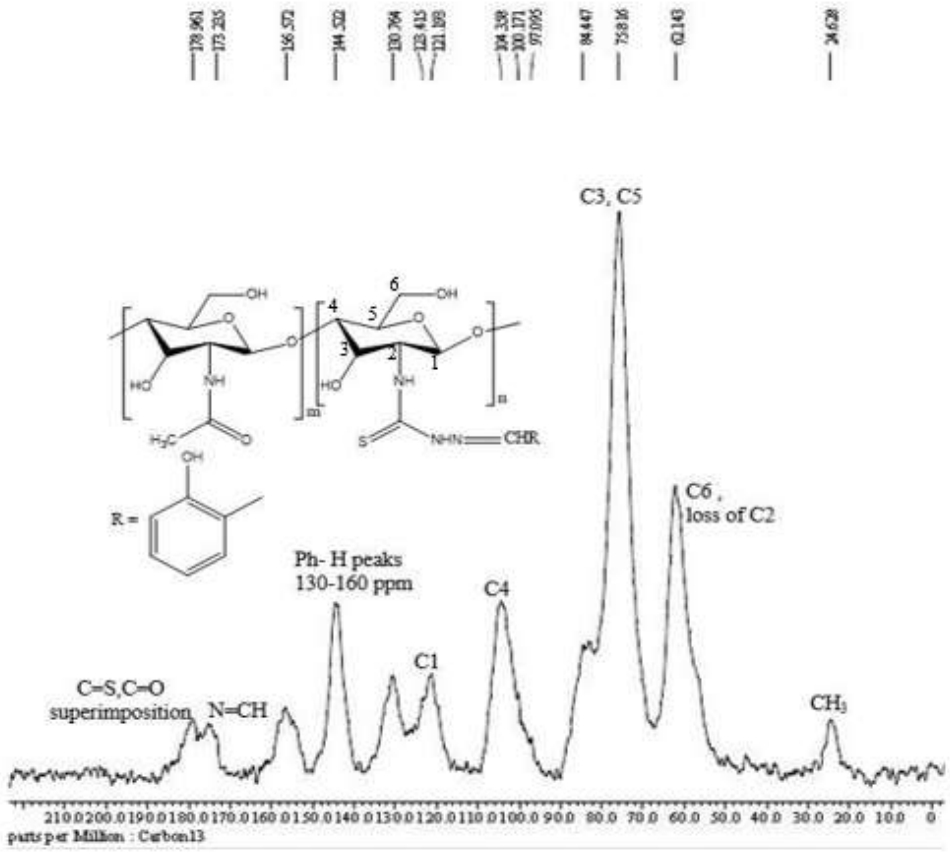


**Figure 27:** $^{13}C$ NMR spectrum of CSSTSC

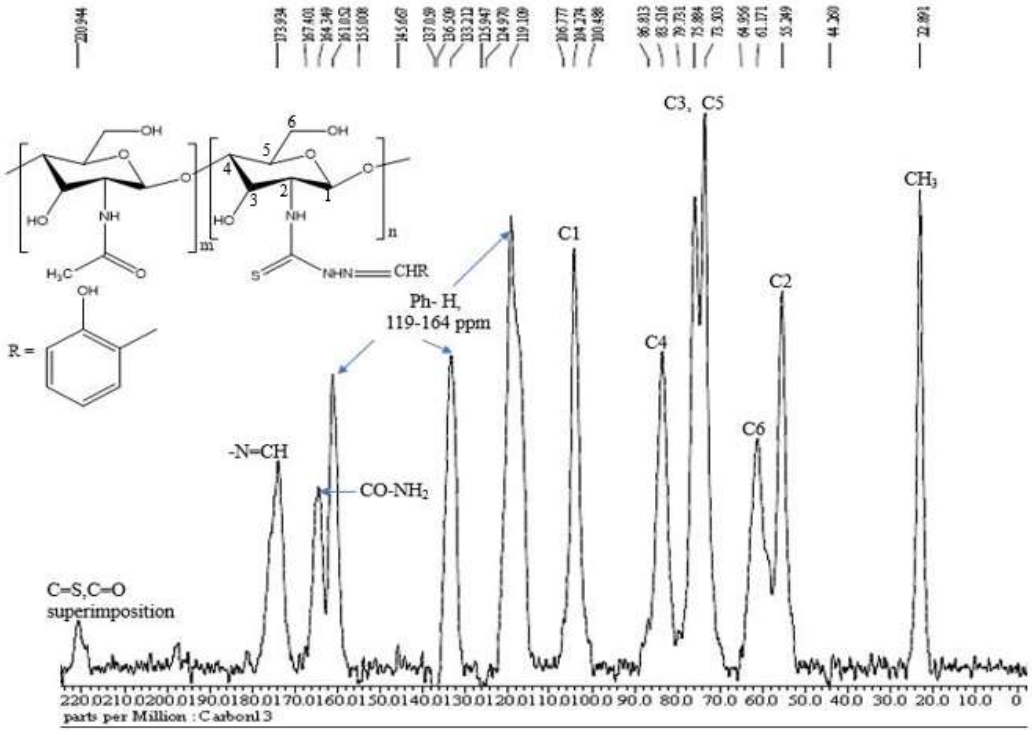


**Figure 28:** $^{13}C$ NMR spectrum of CCSSTSC

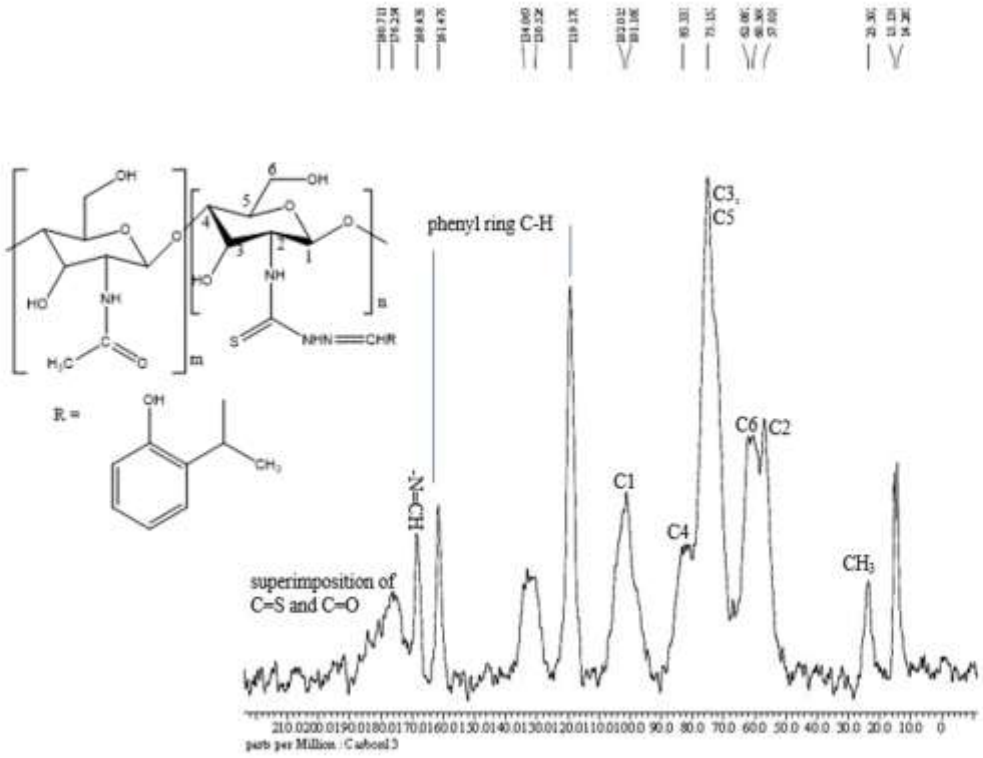


**Figure 29:** $^{13}$C NMR spectrum of CSAPTSC

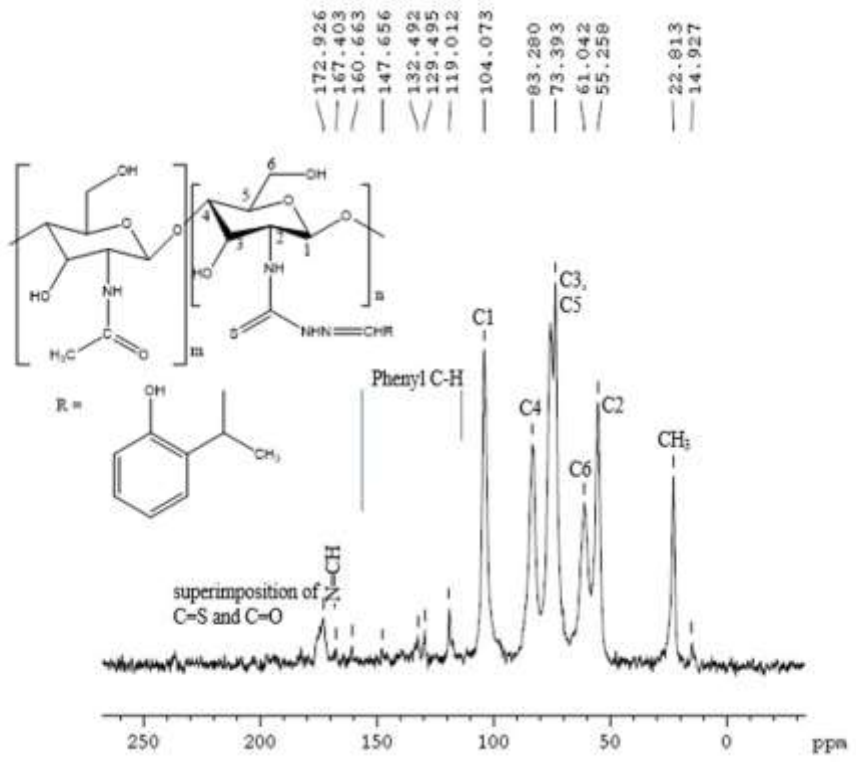


**Figure 30:** $^{13}$C NMR spectrum of CCSAPTSC

### 4.2.2.3. Powder X Ray Diffraction (PXRD) Studies

The X Ray diffractograms of chitosan thiosemicarbazones (figure 31, 32, 33 & 34) with the distinct reflection peaks at 2θ = 15.39-25.30° in CSSTSC, 2θ = 11.39-26.91° in CCSSTSC, 2θ = 8.40°-29. 98° in CSAPTSC, and 2θ = 9.2-29.40° in CCSAPTSC showed the formation of new crystallinity phases due to formation of thiosemicarbazones (Hanumantharao, *et al.*, 2012; Santhakumari, *et al.*, 2010). The incorporation of thiosemicarbazone group in chitosan without destruction of the original crystallinity of chitosan was justifiable from shifting of peaks to neighbourhood of chitosan peaks at 10° and 20° (Qin, *et al.*, 2012; Ramya, *et al.*, 2012) and the change in crystallinity pattern with the appearance of several other peaks (Qin, *et al.*, 2012). The formation of imine group and cleavage of intra-molecular hydrogen bond of chitosan have been reported to bring about the appearance of the new crystalline peaks (Jiao, *et al.*, 2011).

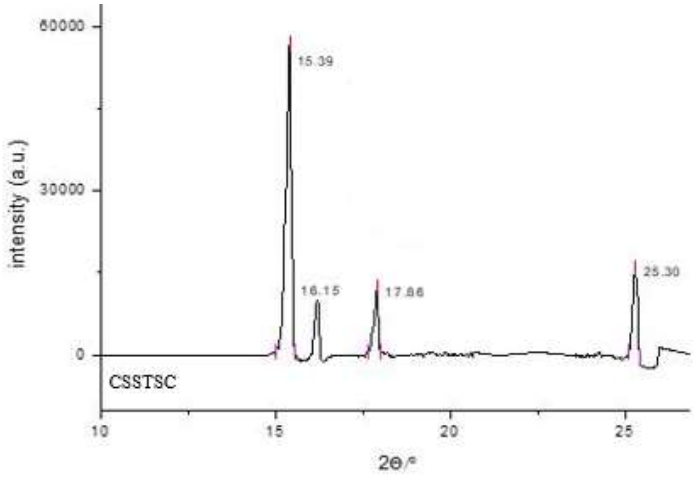


**Figure 31:** X ray diffractogram of CSSTSC

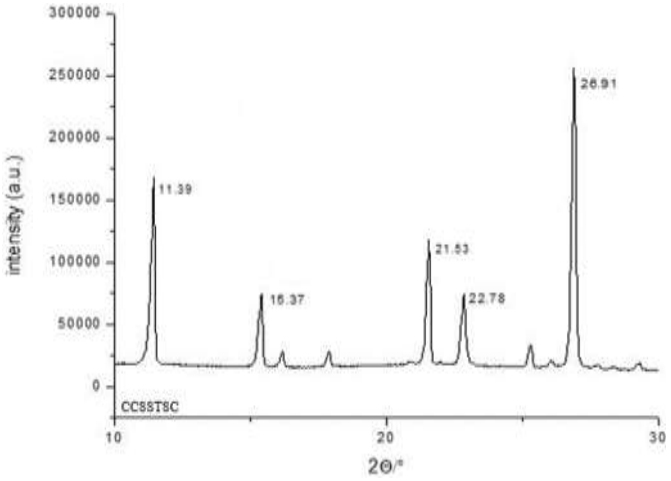


**Figure 32:** X ray diffractogram of CCSSTSC

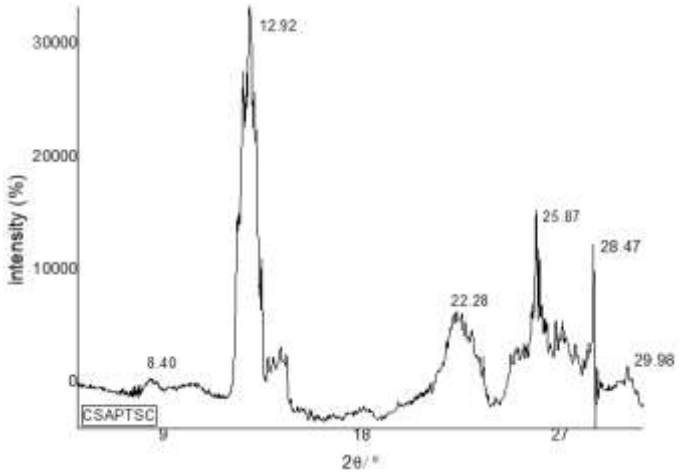


**Figure 33:** X ray diffractogram of CSAPTSC

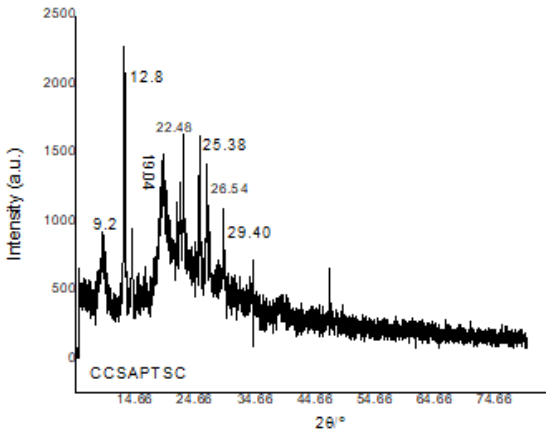


**Figure 34:** X ray diffractogram of CCSAPTSC

The X ray diffractograms of copper(II) chitosan thiosemicarbazone complexes (figure 35, 36, 37 & 38) showed the shifting of crystallinity pattern from that of the respective ligands. New peaks at 2θ = 12.57°,19.98° and 25.07°in Cu-CSSTSC, 2θ = 13.92º,18.89° and 25.36º in Cu-CCSSTSC, 2θ = 14.26°,19.98° and 24.14º in Cu-CSAPTSC, 2θ = 12.96°,19.82°,29.00° and 40.22° in Cu-CCSAPTSC were attributed to the formation of new crystalline phases, chelation of metal ion with different groups of thiosemicarbazone ligand and the destruction of existing crystallinity (Antony, *et al.*, 2012; Dehaghi, *et al.*, 2014; Mekahlia, *et al.*, 2009; Qin, *et al.*, 2012; Wang, *et al.*, 2005). The destruction of hydrogen bonds in chitosan owing to chelation of metal ions with amino or hydroxy group has been reported to bring about the

formation of new crystallinity phases and the subsequent weakening or shifting of crystallinity peaks of chitosan at 10.4° and 19.8° (Wang, *et al.*, 2005).

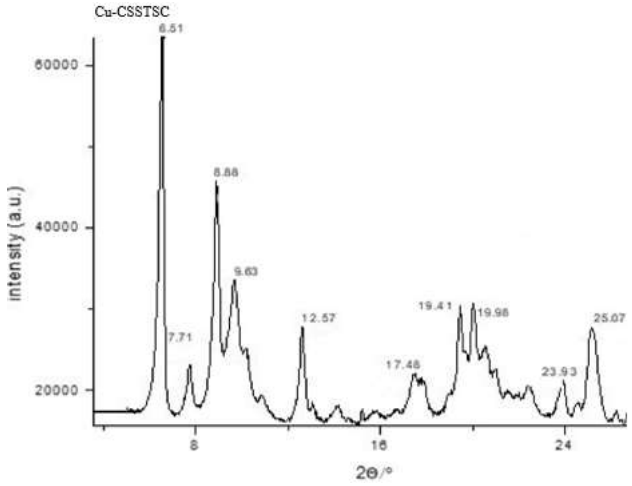


**Figure 35:** X ray diffractogram of Cu-CSSTSC

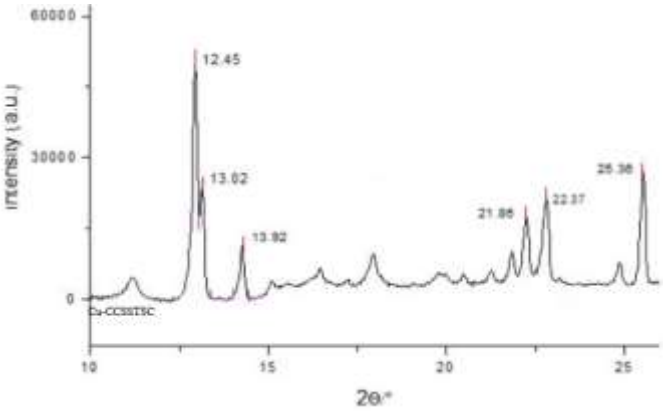


**Figure 36:** X ray diffractogram of Cu-CCSSTSC

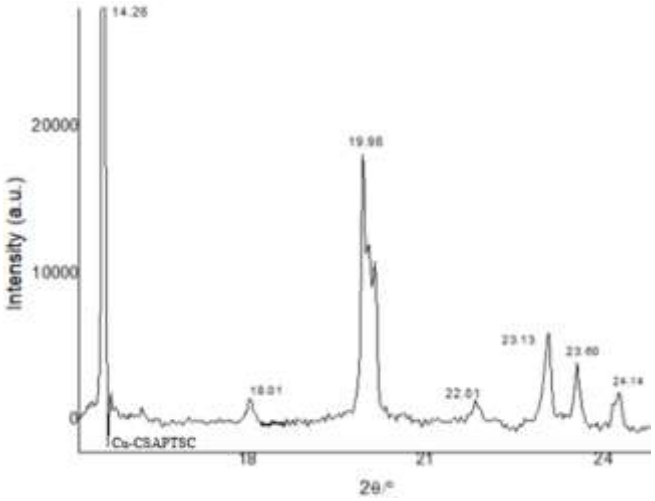


**Figure 37:** X ray diffractogram of Cu-CSAPTSC

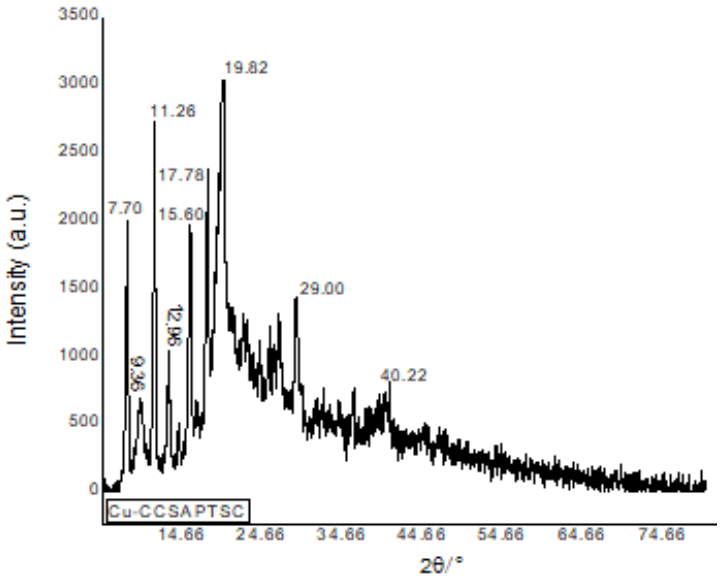


**Figure 38:** X ray diffractogram of Cu-CCSAPTSC

The particle sizes corresponding to highest intensity peaks in X ray diffraction curves from *Debye-Scherrer formula* (Dehaghi, *et al.*, 2014; Kucukgulmez, *et al.*, 2011), and the degree of crystallinity (Kumirska, *et al.*, 2010; Lomadze *et al.*, 2005; Zhang, *et al.*, 2005) as the crystallinity index were determined. The particle sizes of salicylaldehyde-based chitosan thiosemicarbazones (15.53-16.57 nm) were found less than 2-acetyl phenol-based chitosan thiosemicarbazones (22.28-24.76 nm). The crystallinity index was 72.84% in CSSTSC, 71.97% in CCSSTSC, 42.96% in CSAPTSC, and 42.26% in CCSAPTSC. It showed more crystallinity index with the decrease in particle size of the ligands. The particle sizes of copper(II) chitosan thiosemicarbazone complexes were found to be 9.02 nm in Cu-CSSTSC, 10.20 nm in Cu-CCSSTSC, 4.88 nm in Cu-CSAPTSC, and 6.39 nm in Cu-CCSAPTSC. The degree of crystallinity ranged from 45.12-47.77% in salicylaldehyde complexes, and 49.47-51.15% in 2-acetyl phenol complexes. These results showed the decrease in particle size upon the complex formation, but the crystallinity index was not found only dependent on particle size in complexes. The powder X ray diffraction data of chitosan thiosemicarbazones and their copper(II) complexes: salicylaldehyde and 2-acetyl phenol analogues are presented in table 12. Appearance of new crystalline peaks in X ray diffractograms of the complexes showed the shifting of crystallinity pattern from chitosan thiosemicarbazone. Chelation of metal ion with different groups of thiosemicarbazone and the modification in existing crystallinity was shown by overall differences in crystallinity (Jiao, *et al.*, 2011). Further shifting of characteristic peaks derived from chitosan showed the new molecular arrangement in crystalline complexes.

**Table 12:** The powder X ray diffraction data of chitosan thiosemicarbazones and their copper(II) complexes: salicylaldehyde and 2-acetyl phenol analogues

| Compounds | Selected functionality peaks, 2θ | | D (nm) | C.I. (%) |
|---|---|---|---|---|
| | Thiosemicarbazone crystallinity | Chitosan complex crystallinity | | |
| CSSTSC | 15.39°, 16.15°, 17.86°, 25.30° | - | 16.57 | 72.84 |
| Cu-CSSTSC | 6.5º, 7.7°, 8.8º, 9.63°, 17.46°, 19.41°, 23.93° | 12.57°,19.98°,25.07° | 9.02 | 47.77 |
| CCSSTSC | 11.39°, 15.37°, 21.53°, 22.78°, 26.91° | - | 15.53 | 71.97 |
| Cu-CCSSTSC | 9.60°, 12.45°, 13.02°,16.80°, 21.86°, 22.37° | 13.92º,18.89°, 25.36º | 10.20 | 45.12 |
| CSAPTSC | 8.40°,12.92°,22.28°,25.87°,28.47°, 29. 98° | - | 24.76 | 42.96 |
| Cu-CSAPTSC | 18.01°, 22.01°, 23.13°, 23.60° | 14.26°,19.98°, 24.14º | 4.88 | 51.15 |
| CCSAPTSC | 9.2°, 12.8°, 19.04°, 22.48°, 25.38°, 26.54°, 29.40° | - | 22.28 | 42.26 |
| Cu-CCSAPTSC | 7.70°, 11.26°, 15.60°, 17.78° | 12.96°,19.82°,29.00°, 40.22° | 6.39 | 49.47 |

### 4.2.2.4. Elemental Microanalysis

The elemental microanalysis data of salicylaldehyde and 2-acetyl phenol analogues of chitosan thiosemicarbazones and their copper(II) complexes are presented in table 13 and 14. The calculated percentages of elements in the ligands CSSTSC and CCSSTSC with the monomer structure of unit formula weight 339 were found in close agreement with analytically found percentages of elements. The calculated percentages of elements in their complexes with the monomer structure of unit formula weight 438 also accorded with the analytically found percentages of elements and estimated chlorine percentages.

The calculated percentages in CSAPTSC and CCSAPTSC, corresponding to the monomer structure of unit formula weight 353 showed close correspondence with the analytically found percentages of elements. The calculated percentages corresponding to the monomer structure of unit formula weight 452 of their complexes were also in correspondence to the analytically found percentages of elements and estimated chlorine percentages.

The analytically found percentages showed the substantial ranges of DS (Inukai, *et al.*, 1998; Melo, *et al.*, 2002; Pires, *et al.*, 2013; Qin, *et al.*, 2012), with 19.42-19.83% DS in salicylaldehyde chitosan thiosemicarbazones and 31.68-31.74% DS in acetyl phenol chitosan

thiosemicarbazones. The percentages were indicatives of partial substitution of amino group in chitosan by thiosemicarbazone group and the analytically found percentages of elements in the complexes showed the coordination behaviour of chitosan thiosemicarbazones.

The calculated percentages of elements were based on the structures with completely deacetylated ring of chitosan. The DS values showed an agreement with decreased sulphur percentage with some variations in percentages of other elements in the derivatives formed by partial deacetylation of chitin, partial introduction of Schiff base group into chitosan (Qin, *et al.*, 2012), more functionalization of commercial oligo chitosan than high molecular weight crab shell chitosan. The non-functionalized chitosan also forms the complex in a parallel reaction, and this is justified by higher percentage of estimated chlorine than calculated chlorine percentage.

**Table 13:** Elemental (CHNS) microanalysis of chitosan thiosemicarbazones: salicylaldehyde and 2-acetyl phenol analogues: calculated (found)

| Compounds | C(%) | H(%) | N(%) | S(%) | DS(%) |
|---|---|---|---|---|---|
| CSSTSC | 49.55(55.10) | 5.01(5.201) | 12.38(10.00) | 9.43(3.150) | 19.83 |
| CCSSTSC | 49.55(54.216) | 5.01(5.135) | 12.38(10.823) | 9.43(3.021) | 19.42 |
| CSAPTSC | 51.28(53.10) | 5.41(5.87) | 11.96(8.98) | 9.11(4.47) | 31.68 |
| CCSAPTSC | 51.28(52.01) | 5.41(5.74) | 11.96(8.86) | 9.11(4.38) | 31.74 |

**Table 14:** Elemental (CHNS) microanalysis and chlorine estimation in copper(II) chitosan thiosemicarbazones: salicylaldehyde and 2-acetyl phenol analogues: calculated (found)

| Compounds | C(%) | H(%) | N(%) | S(%) | Cl(%) |
|---|---|---|---|---|---|
| Cu-CSSTSC | 38.35(44.04) | 3.88(4.019) | 9.58(7.74) | 7.30(2.214) | 8.10(10.50) |
| Cu-CCSSTSC | 38.35(44.50) | 3.88(5.201) | 9.58(10.325) | 7.30(2.012) | 8.10(10.50) |
| Cu-CSAPTSC | 39.82(44.35) | 4.20(5.104) | 9.29(8.84) | 7.07(2.351) | 7.85(10.05) |
| Cu-CCSAPTSC | 39.82(44.20) | 4.20(5.09) | 9.29(8.902) | 7.07(2.29) | 7.85(10.05) |

### 4.2.2.5. Thermal Studies

Thermogravimetric/differential thermal analysis (TG/DTA) curves of chitosan thiosemicarbazones (figure 39, 40, 41 & 42) and the thermal data presented in table 15

showed the thermal decomposition in two stages corresponding to weight loss due to the loss of water at 145-205 °C and weight loss due to the disruption of backbone linkage and thermal degradation of glucosamine residue at 200-1000 °C. In particular, there was a weight loss of 6.68% at 150 °C in CSSTSC, 5.86% at 205 °C in CCSSTSC, 5.29% at 147 °C in CSAPTSC and 5.36% at 145 °C in CCSAPTSC, and a weight loss of 79% in CSSTSC, 74% in CCSSTSC, 88% in CSAPTSC, and 86% in CCSAPTSC at 200-1000 °C. This behavior reasonably showed analogy with the reported temperature of loss of water in chitosan at 80-160 °C (Kittur, *et al.*, 2002; Qin, *et al.*, 2012) and decomposition temperatures of chitosan at 50-100 °C and 400 – 500 °C (Andrade, *et al.*, 2012; Kumari, *et al.*, 2017). The two stages of weight loss of commercial chitosan *viz* 9% of weight loss at 120 °C due to loss of water and 43% of weight loss at 500 °C due to degradation of main chain of chitosan (Chethan, *et al.*, 2013; De Britto & Campana-Filho, 2004; Xu, *et al.*, 2010) have been reported, and in close agreement to this, there was 4.05-4.88% weight loss due to loss of water at 120 °C and 65-69% weight loss due to chain degradation at 500 °C in chitosan thiosemicarbazones. It showed more degradation of chitosan thiosemicarbazones than chitosan at the moderate heating in the range of 400 °C to 500 °C. There was a rapid rate of decomposition from 100 °C to 400 °C like in chitosan and then a steady rate of decomposition, leaving about 14-15% salicylaldehyde-based ligands and 5-6% 2-acetyl phenol-based ligands as residue of the unsaturated structure at 1000 °C. Such a behavior was eventually attributed to reasonably high thermal stability of thiosemicarbazones (Qu, *et al.*, 2000). The two DTA peaks of chitosan thiosemicarbazones showed the correspondence to TG weight loss in two steps at the range of 25- 200 °C and 400-700 °C.

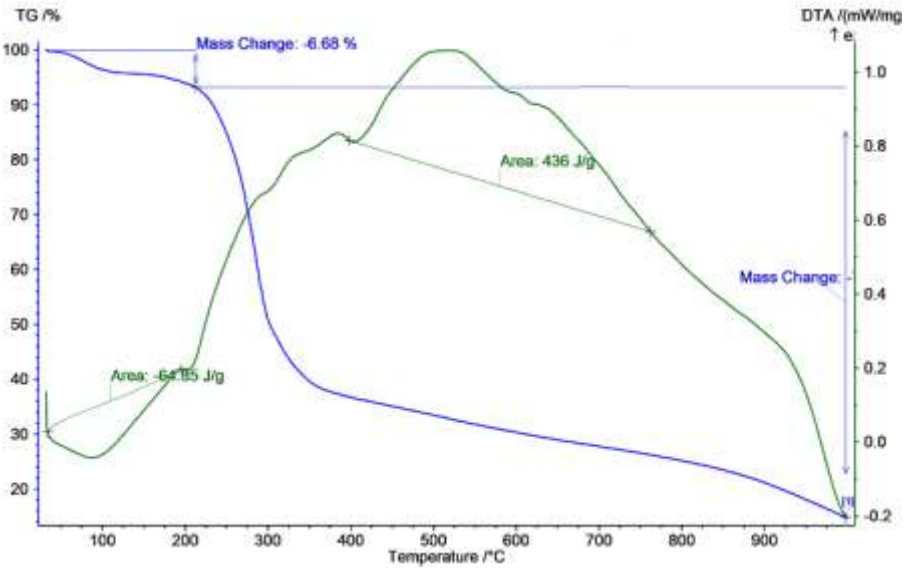


**Figure 39:** TG/DTA curves of CSSTSC showing the thermal events at different temperatures

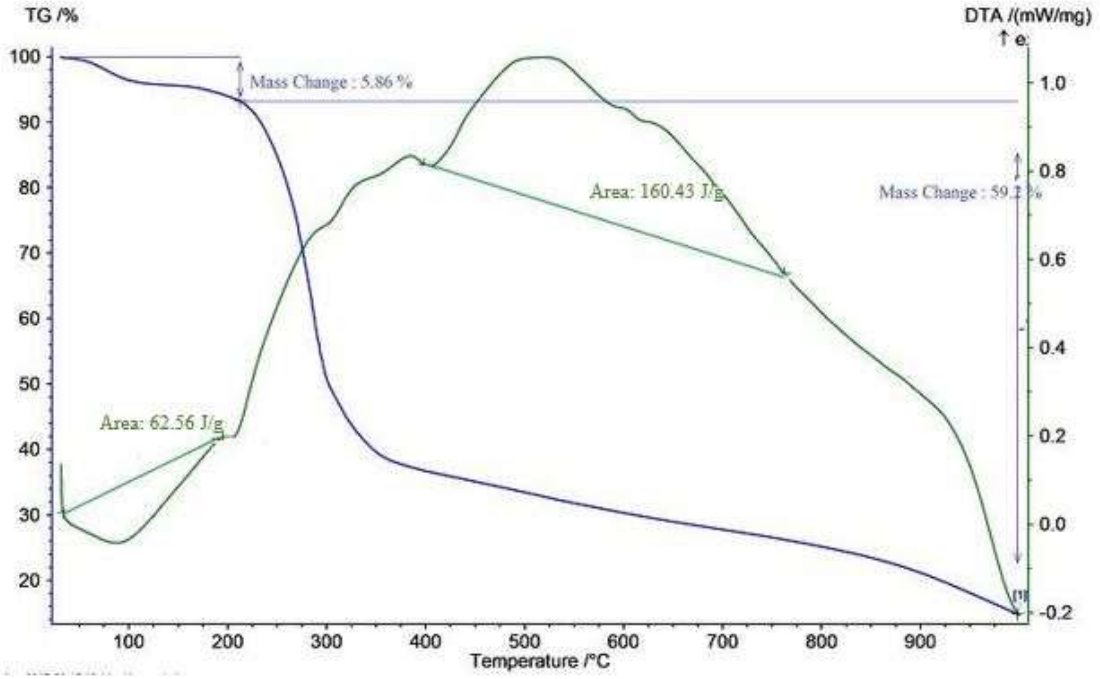


**Figure 40:** TG/DTA curves of CCSSTSC showing the thermal events at different temperatures

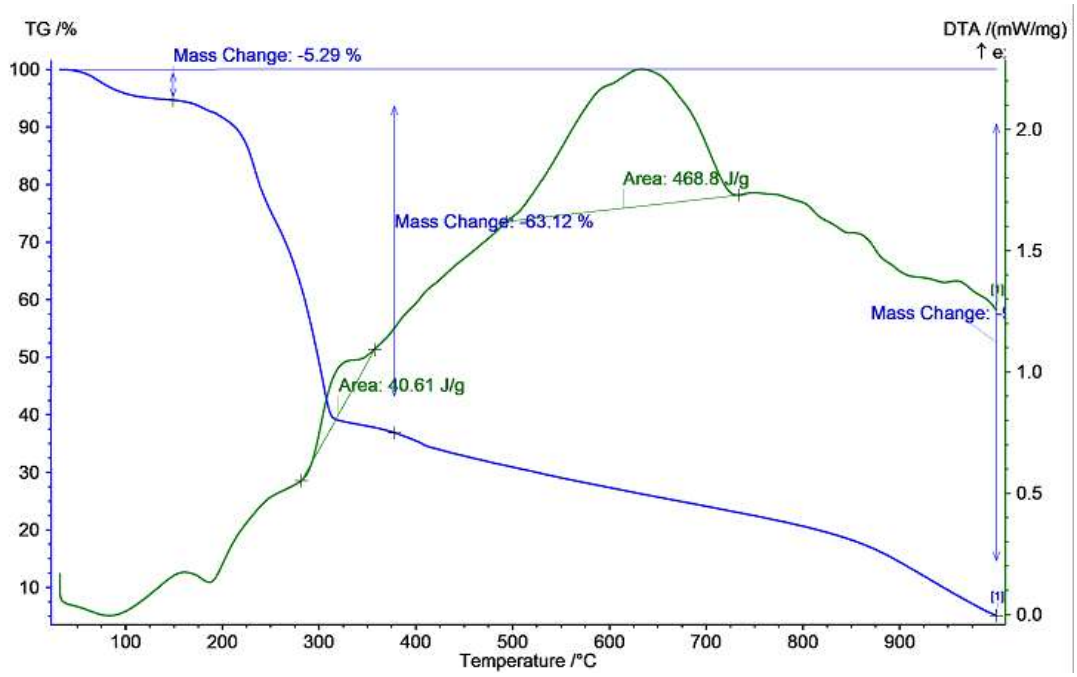


**Figure 41:** TG/DTA curves of CSAPTSC showing the thermal events at different temperatures

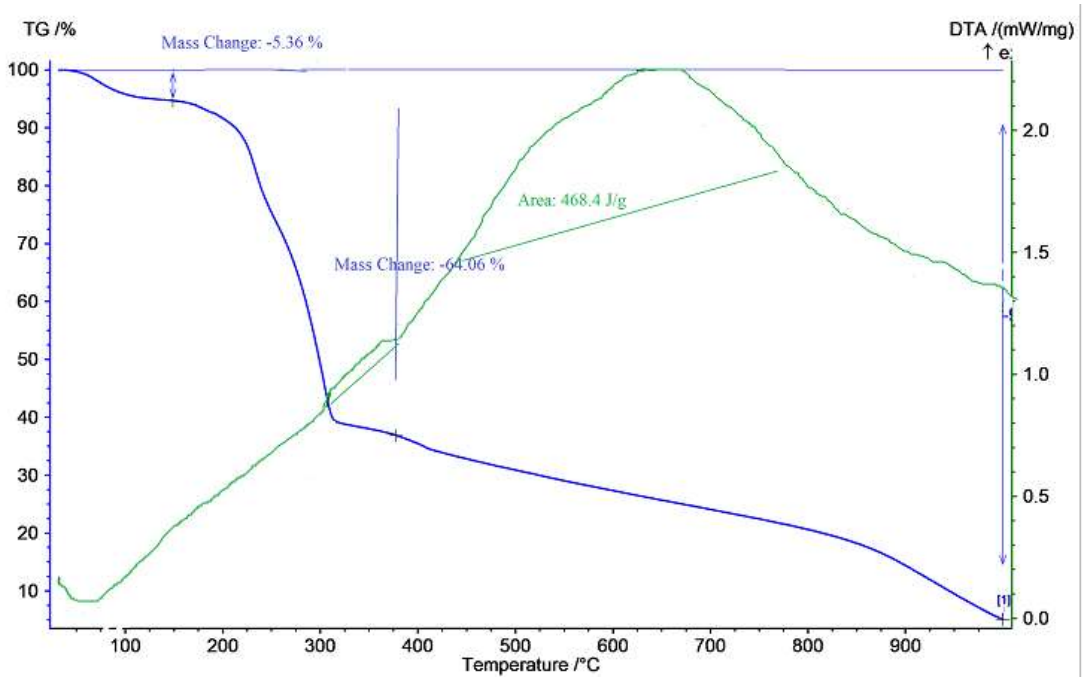


**Figure 42:** TG/DTA curves of CCSAPTSC showing the thermal events at different temperatures

**Table 15:** TG/DTA data of thermal events in chitosan thiosemicarbazones: salicylaldehyde and 2-acetyl phenol analogues

| Compounds | Temperature (°C) | Weight loss (%) | Thermal event | % residue at 1000 °C |
|---|---|---|---|---|
| CSSTSC | 150 | 6.68 | Loss of water | 15 |
| | 200-1000 | 79 | Chain disruption and backbone degradation | |
| CCSSTSC | 205 | 5.86 | Loss of water | 14 |
| | 200-1000 | 74 | Chain disruption and backbone degradation | |
| CSAPTSC | 147 | 5.29 | Loss of water | 5 |
| | 200-1000 | 88 | Chain disruption and backbone degradation | |
| CCSAPTSC | 145 | 5.36 | Loss of water | 6 |
| | 200-1000 | 86 | Chain disruption and backbone degradation | |

The TGA curves of complexes (figure 43, 44, 45 & 46) and the thermal data presented in table 16 showed the weight loss in three steps corresponding to the steady loss of weight up to 150- 200 °C, rapid loss of weight at 200-500 °C, and again a steady loss of weight from 500-1000 °C. In particular, there was a weight loss of 12.66% in Cu-CSSTSC, 1.08% in Cu-CCSSTSC, 5.14% in Cu-CSAPTSC and 1.06% in Cu-CCSAPTSC at 200 °C, and a weight

loss of about 42% in Cu-CSSTSC, 78% in Cu-CCSSTSC, 60% in Cu-CSAPTSC, and 53% in Cu-CCSAPTSC at 200-500 °C. It showed more degradation of complexes at the moderate heating in the lower range of temperature at 200-500 °C and then a steady rate of decomposition, leaving about 15-35% as residue of the unsaturated structure at 700 °C. High molecular weight chitosan complexes were stable up to 200 °C. Such a behaviour was attributed to reasonably standard thermal stability (Kittur, *et al.*, 2002; Qu, *et al.*, 2000) of complexes.

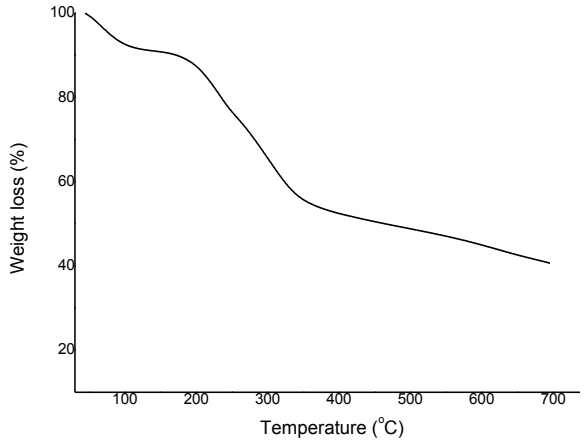


**Figure 43:** TGA curve of Cu-CSSTSC

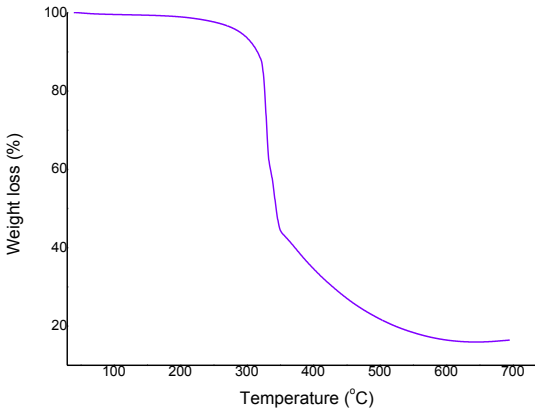


**Figure 44:** TGA curve of Cu-CCSSTSC

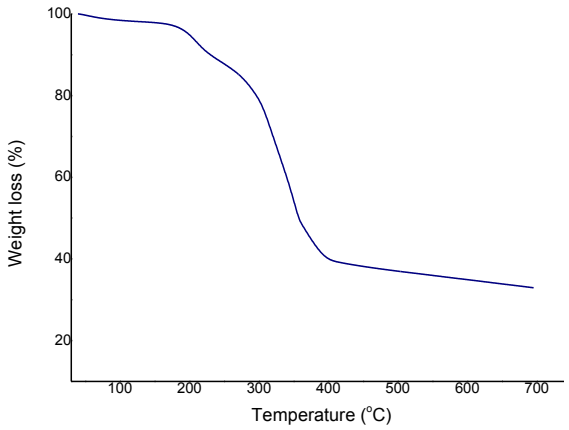


**Figure 45:** TGA curve of Cu-CSAPTSC

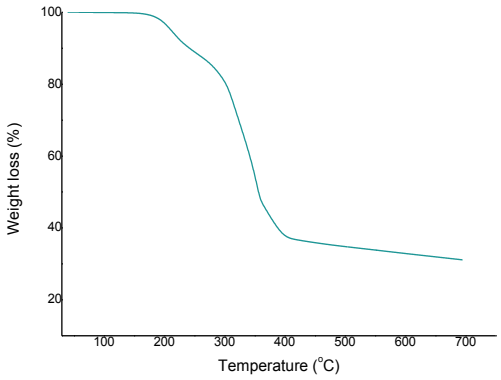


**Figure 46:** TGA curve of Cu-CCSAPTSC

**Table 16:** TGA data of thermal events in copper(II) chitosan thiosemicarbazones: salicylaldehyde and 2-acetyl phenol analogues

| Compounds | Temperature (°C) | Weight loss % | Thermal event | % residue at 700 °C |
|---|---|---|---|---|
| Cu-CSSTSC | 200 | 12.66 | Loss of water | 35 |
| | 200-500 | 42 | Disruption of the chain | |
| | 500-700 | 10 | Further degradation of the backbone | |
| Cu-CCSSTSC | 200 | 1.08 | Loss of water | 15 |
| | 200-500 | 78 | Disruption of the chain | |
| | 500-700 | 06 | Further degradation of the backbone | |
| Cu-CSAPTSC | 200 | 5.14 | Loss of water | 30 |
| | 200-500 | 60 | Disruption of the chain | |
| | 500-700 | 05 | Further degradation of the backbone | |
| Cu-CCSAPTSC | 200 | 1.06 | Loss of water | 30 |
| | 200-500 | 53 | Disruption of the chain | |
| | 500-700 | 16 | Further degradation of the backbone | |

### 4.2.2.6. Magnetic Susceptibility Measurement and Electron Paramagnetic Resonance (EPR) Spectroscopy

Magnetic susceptibility measurement showed the effective magnetic moment ($\mu_{eff}$) values of the complexes in the range of 1.80-1.85 BM, close to spin-only moment of 1.73 BM due to an unpaired electron. This indicated a low spin-spin coupling between unpaired electrons of different copper atoms (Ahmed & Lal, 2017) and some increase in the moment was attributed to large spin orbit coupling constant of cupric ion (Djord jevic, 1960). Magnetic moment of <1.90 BM indicated the square planar or octahedral stereochemistry of the complexes (Figgis, 1958).

The EPR spectra of complexes (figure 47, 48, 49 & 50) were characterizable by axial g tensors (Bennur, *et al.*, 2001) and the non-resolution of hyperfine features due to copper (S =1/2 and I= 3/2) was owing to intermolecular spin-spin interactions and dimeric association of molecules (Bhadbhade & Srinivas, 1993; Suresh, *et al.*, 1996). It meant that the absence of hyperfine splitting was attributed to exchange broadening due to still incomplete separation of paramagnetic centres (Farra, *et al.*, 2011) at a low X-band frequency of 9.8 GHz (Farra, *et al.*, 2011). The values of magnetic moment and g values in EPR spectra are presented in table 17. The EPR spectra corresponding to an unpaired electron in $d_{x^2-y^2}$ orbital of Cu(II) centres were in further agreement with a square planar geometry (Garribba & Micera, 2006), but the g parallel tensors were undetectable due to absence of hyperfine splitting. The g values were

2.07 for Cu-CSSTSC (ν = 9.8623 GHz, $B_o$=3400 Gs = 340 mT), 2.10 for Cu-CCSSTSC (ν =9.8630 GHz, $B_o$ = 3350 Gs = 335 mT), 2.09 for Cu-CSAPTSC (ν =9.8623 GHz, $B_o$ = 3359 Gs = 335.9 mT), and 2.09 for Cu-CCSAPTSC (ν =9.8628 GHz, $B_o$ = 3356 Gs = 335.6 mT). The shifting of g value from $g_e$ (2.0023) that is due to spin orbital coupling of metal orbitals with unpaired electrons has been reported to depend upon the degree of covalency of the complex that is determined by the unpaired electron density at the donor atoms of ligand molecule (Ahmed & Lal, 2017). The absence of half field peak at 1500 Gauss suggesting the absence of two copper centres in the same lacuna indicated the mononuclear structure of the complexes (Patel & Sadasivan, 2017).

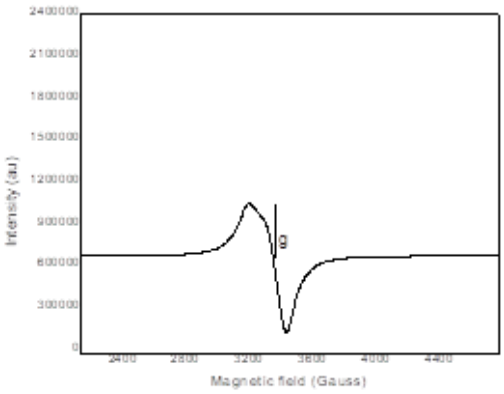


**Figure 47:** EPR spectrum of Cu-CSSTSC

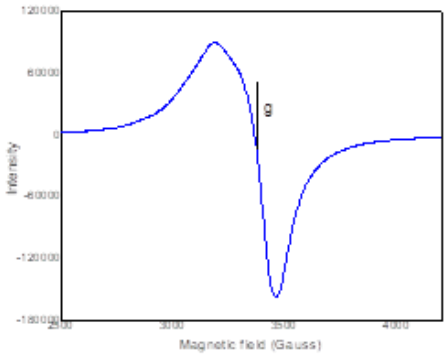


**Figure 48:** EPR spectrum of Cu-CCSSTSC

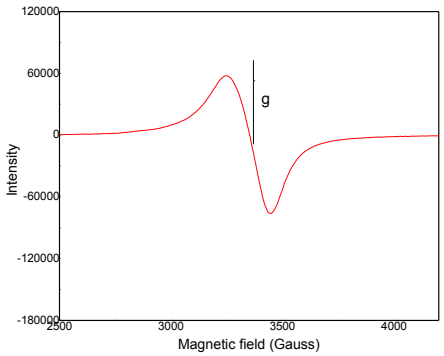


**Figure 49:** EPR spectrum of Cu-CSAPTSC

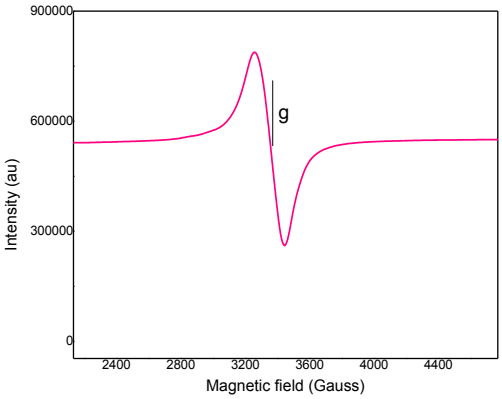


**Figure 50:** EPR spectrum of Cu-CCSAPTSC

**Table 17:** Effective magnetic moments ($\mu_{eff}$) and EPR g values of copper(II) chitosan thiosemicarbazones: salicylaldehyde and 2-acetyl phenol analogues

| Complexes | $\mu_{eff}$, B. M. | EPR g value |
|---|---|---|
| Cu-CSSTSC | 1.80 | 2.07 |
| Cu-CCSSTSC | 1.85 | 2.10 |
| Cu-CSAPTSC | 1.82 | 2.09 |
| Cu-CCSAPTSC | 1.84 | 2.09 |

On the basis of the aforementioned results, the copper(II) complexes were proposed to assume the mononuclear distorted square planar geometry (figure 51). The thione sulphur, azomethine nitrogen, hydroxy group of salicylaldehyde or 2-acetyl phenol moiety, and one chlorine atom were used as the donor sites in coordination with copper(II) ion in the complexes.

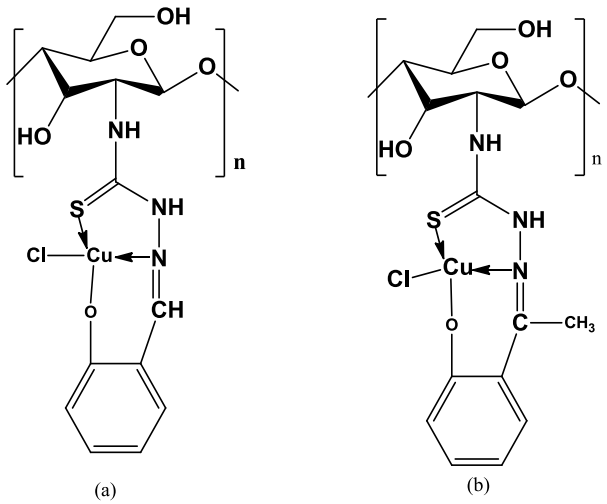


**Figure 51:** Proposed structure of complexes: (a). Cu-CSSTSC and Cu-CCSSTSC. (b). Cu-CSAPTSC and Cu-CCSAPTSC

## 4.3. Chitosan Thiosemicarbazones and their Copper(II) Complexes: Pyridine-2-carboxaldehyde and 2-Acetyl-pyridine Analogues

### 4.3.1. Physical Characteristics

Physical characteristics of pyridine-2-carboxaldehyde and 2-acetyl-pyridine thiosemicarbazones and their copper(II) complexes presented in table 18 & 19 respectively revealed their good yield *viz.* 34-44% of ligands and 66-72% of complexes, high thermal stability, solid crystalline behaviour with the increase in solubility in 1% aqueous acetic acid with increase in DDA, and about 40% water-solubility of commercial chitosan analogues.

**Table 18:** Physical characteristics of pyridine-2-carboxaldehyde chitosan thiosemicarbazones and their copper(II) complexes

| Compounds | Unit formula | Unit formula weight | Color | m.pt. (°C) | Yield (%) |
|---|---|---|---|---|---|
| CSPCTSC | $C_{13}$ $H_{16}$ $N_4O_4S$ | 324 | Yellowish | >300 | 36 |
| CCSPCTSC | $C_{13}$ $H_{16}$ $N_4O_4S$ | 324 | Yellowish white | >300 | 34 |
| Cu-CSPCTSC | $C_{13}$ $H_{16}$ $N_4O_4SCuCl$ | 423 | Greenish | >300 | 67 |
| Cu-CCSPCTSC | $C_{13}$ $H_{16}N_4O_4SCuCl$ | 423 | Greenish | >300 | 66 |

**Table 19:** Physical characteristics of 2-acetyl-pyridine chitosan thiosemicarbazones and their copper(II) complexes

| Compounds | Unit formula | Unit formula weight | Color | m.pt. (°C) | Yield (%) |
|---|---|---|---|---|---|
| CS APR TSC | $C_{14}$ $H_{18}$ $N_4O_4S$ | 338 | Yellow | >300 | 44 |
| CCS APR TSC | $C_{14}$ $H_{18}$ $N_4O_4S$ | 338 | Yellowish white | >300 | 42 |
| Cu-CS APR TSC | $C_{14}$ $H_{18}$ $N_4O_4S$ CuCl | 437 | Yellowish green | >300 | 72 |
| Cu-CCS APR TSC | $C_{14}$ $H_{18}$ $N_4O_4S$ CuCl | 437 | Yellowish green | >300 | 68 |

### 4.3.2. Characterization

#### 4.3.2.1. Fourier Transform- Infrared (FT-IR) Spectroscopy

The FT-IR spectra of pyridine-2-carboxaldehyde and 2-acetyl pyridine chitosan thiosemicarbazones (figure 52, 54, 56 & 58) showed a merging of broad ν (O-H) and ν (N-H) at a range of 3190-3260 $cm^{-1}$ with a broad translocation (Qin, *et al*., 2012; Zhong, *et al*., 2011). The ν (C=O) of amide I at 1645 $cm^{-1}$ (Qin, *et al*., 2012) was found to disappear and a new band was observed in the range of 1621-1653 $cm^{-1}$. This was an indicative of the involvement of C=O group in imine (-C=N-) bond formation (Qin, *et al*., 2012). The simultaneous appearance of ν ($NH_2$) at 1504-1556 $cm^{-1}$ (Kucukgulmez, *et al.*, 2011) and ν (C=S) at 1020-1072 $cm^{-1}$ (Tiwari, *et al.*, 2016; Yamaguchi, *et al.*, 1958) and 1369-1376 $cm^{-1}$ (Aneesrahman, *et. al.*, 2019; Joseph, *et al.*, 2006) showed the partial involvement of $NH_2$ group of chitosan in the formation of thiosemicarbazones. The absorption bands at 600 $cm^{-1}$

(Nanbu, *et al.*, 1999) and 620-622 $cm^{-1}$ were attributed to ν (in plane pyridine ring deformation) (Rapheal, *et al.*, 2007). The partial substitution of amino group in chitosan was shown by weakening of the ν (N-H) bending peak due to primary amine and residual amide II of chitosan at 1566 $cm^{-1}$ (Zhong, *et al.*, 2010) and its negative shifting to 1504-1556 $cm^{-1}$. The peaks with some shifting at 1350-1460 $cm^{-1}$ and 1057-1072 $cm^{-1}$ were attributed to ν (C-H) and ν (C-O-C) in chitosan ring respectively (Yadav, *et al.*, 2020). The absence of ν (C-SH) band at 2500–2600 $cm^{-1}$ showed the more stabilisation of thiosemicarbazone moiety in thione form (Bharti, *et al*., 2003).

The FT-IR spectra of complexes (figure 53, 55, 57 & 59) showed the grafting of thiosemicarbazone moiety to copper(II) ion. There was lowering of ν (C=N) to 1604-1638 $cm^{-1}$ in complex showing the involvement of C=N group in complex formation. There was shifting of ν (C=S) to lower frequency of 1004-1052 $cm^{-1}$ (Tiwari, *et al.*, 2016; Yamaguchi, *et al.*, 1958) and 1363-1367 $cm^{-1}$ (Aneesrahman, *et. al.*, 2019; Joseph, *et al.*, 2006) in the complex showing the coordination of sulphur with metal ion. The coordination through pyridyl ring nitrogen was shown by positive shifting of ν (in plane pyridine ring deformation) to 606-628 $cm^{-1}$ (Rapheal, *et al.*, 2007). Hence, the bonding of metal ion with thiosemicarbazone through azomethine nitrogen, pyridyl nitrogen and thione sulphur was confirmed by the overall IR data (table 20).

**Table 20:** The selected FT-IR bands ($cm^{-1}$) of chitosan thiosemicarbazones and their complexes: pyridine-2-carboxaldehyde and 2-acetyl-pyridine analogues

| Compounds | ν (C=N) | ν (C=S) | ν ($NH_2$) | ν (pyridine ring deformation) |
|---|---|---|---|---|
| CSPCTSC | 1638 | 1070, 1376 | 1539 | 621 |
| Cu-CSPCTSC | 1626 | 1052, 1366 | 1555 | 628 |
| CCSPCTSC | 1653 | 1036, 1374 | 1555 | 622 |
| Cu-CCSPCTSC | 1638 | 1023, 1366 | 1555 | 628 |
| CSAPRTSC | 1639 | 1072, 1369 | 1504 | 620 |
| Cu-CSAPRTSC | 1604 | 1035, 1363 | 1556 | 628 |
| CCSAPRTSC | 1621 | 1020, 1376 | 1544 | 600 |
| Cu-CCSAPRTSC | 1611 | 1004, 1367 | 1548 | 606 |

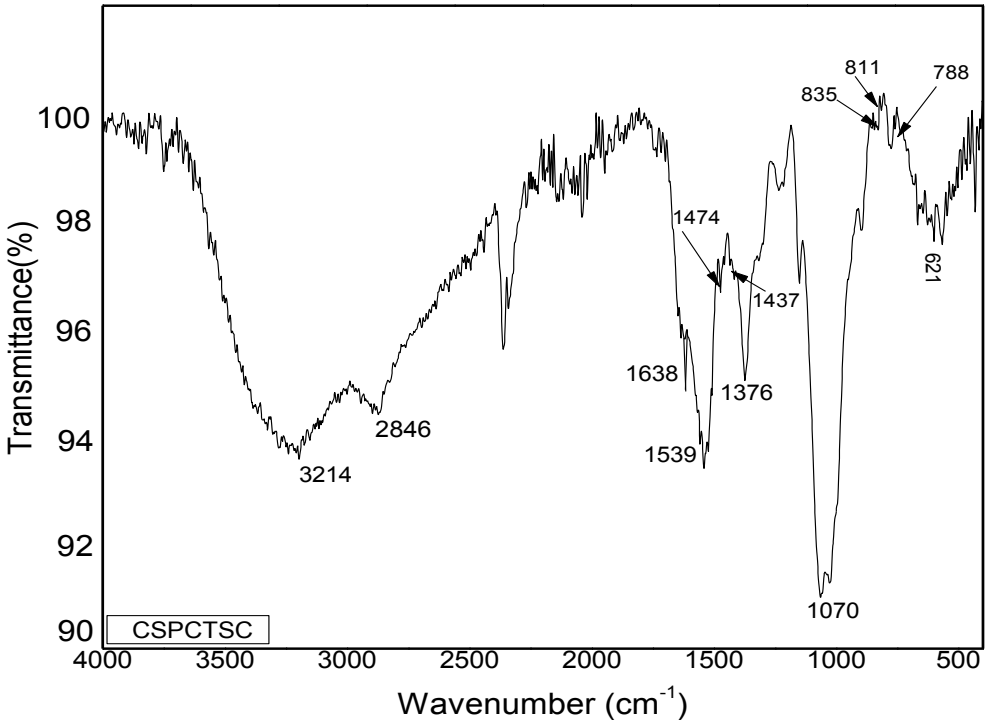


**Figure 52:** FT-IR spectrum of CSPCTSC

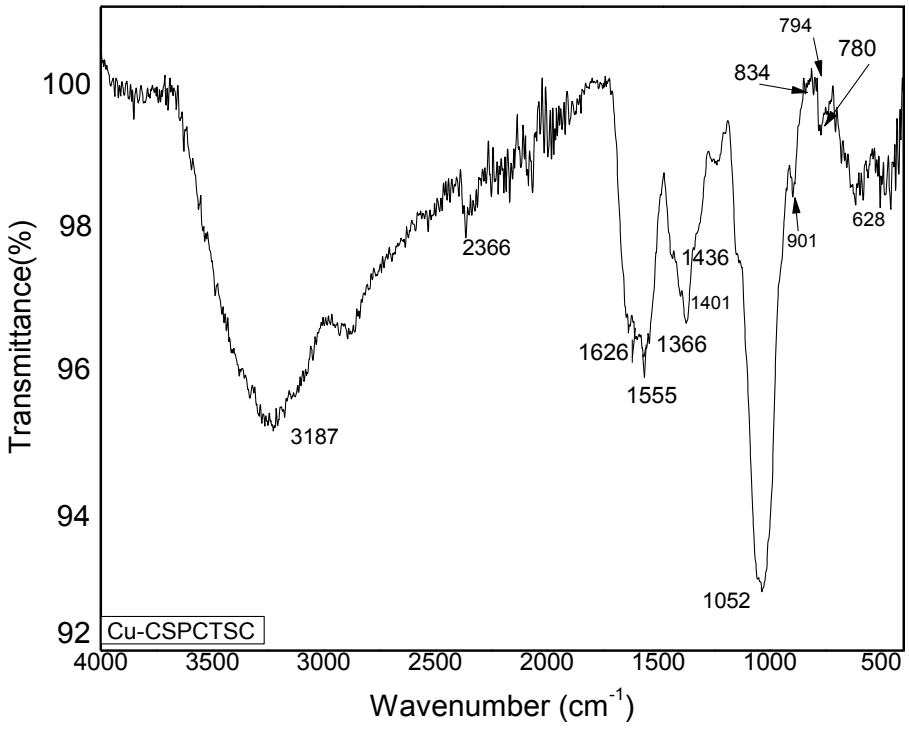


**Figure 53:** FT-IR spectrum of Cu-CSPCTSC

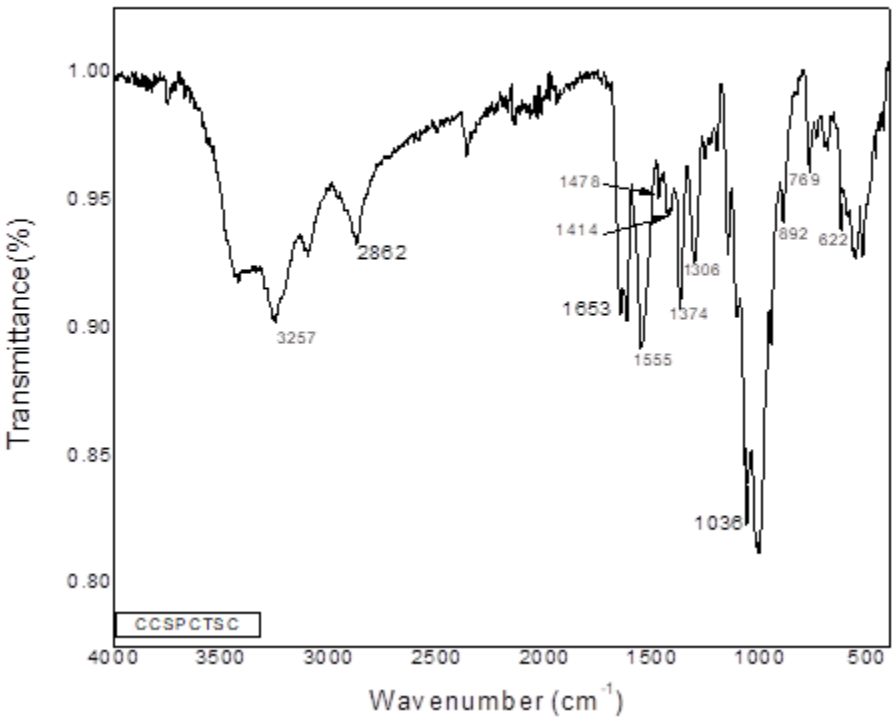


**Figure 54:** FT-IR spectrum of CCSPCTSC

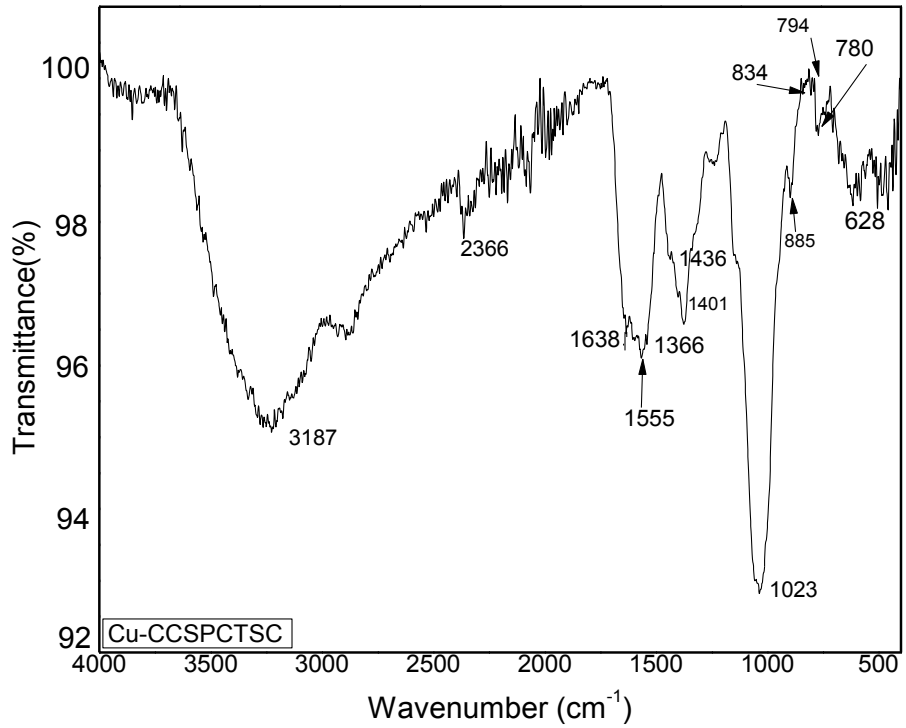


**Figure 55:** FT-IR spectrum of Cu-CCSPCTSC

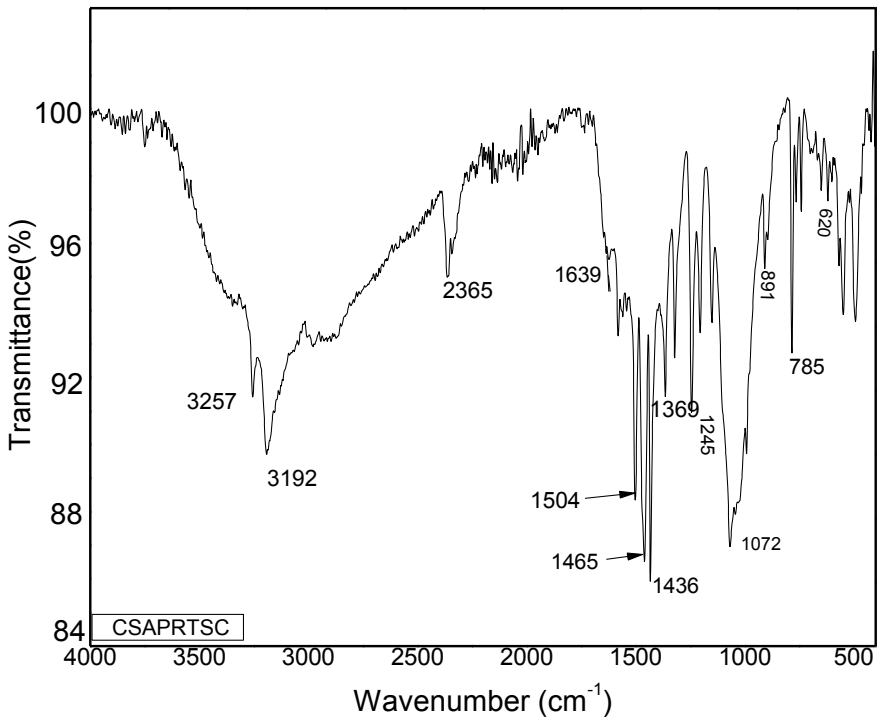


**Figure 56:** FT-IR spectrum of CSAPRTSC

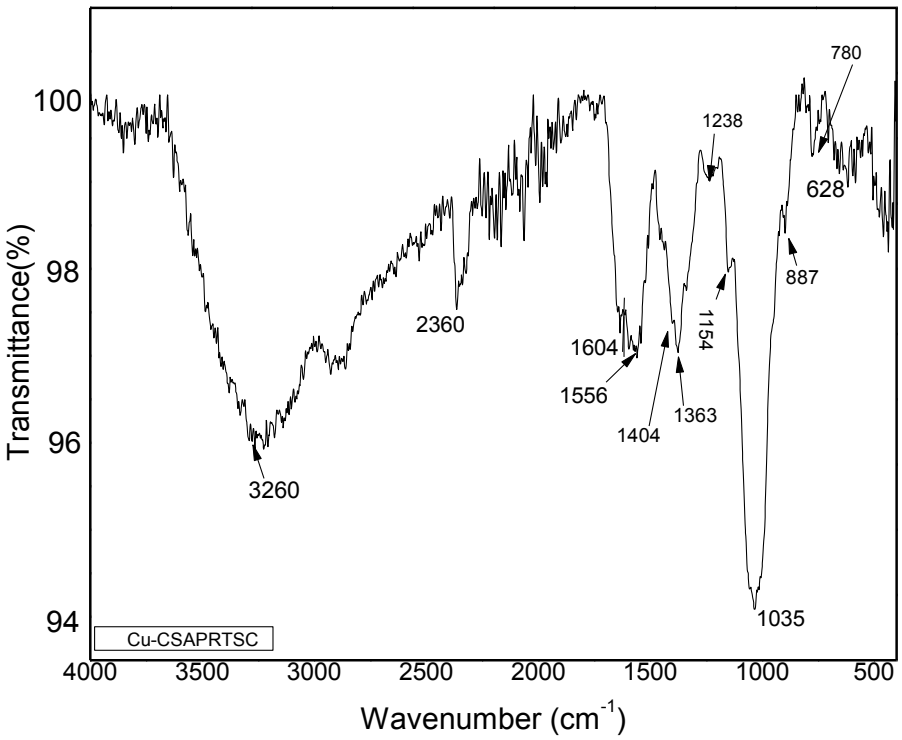


**Figure 57:** FT-IR spectrum of Cu-CSAPRTSC

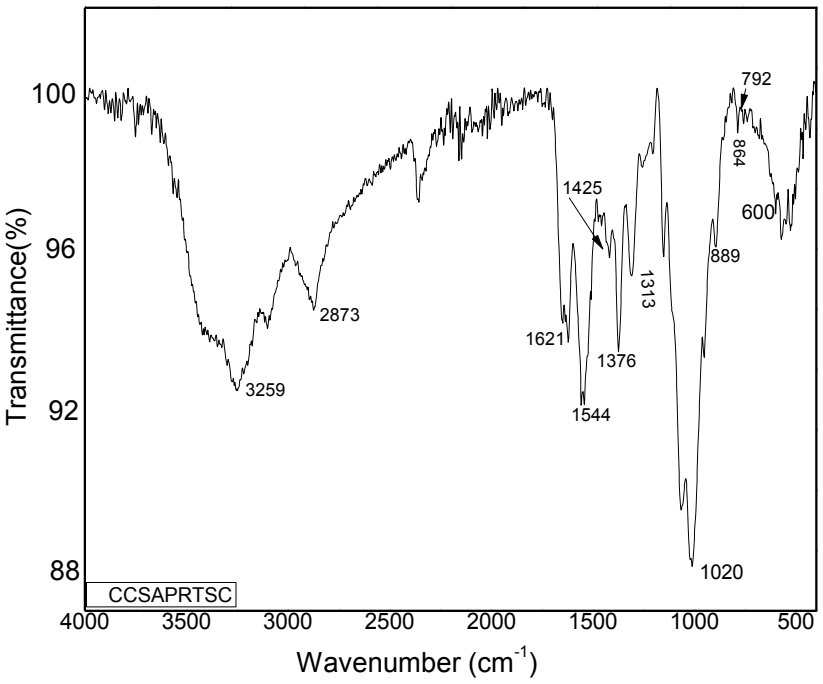


**Figure 58:** FT-IR spectrum of CCSAPRTSC

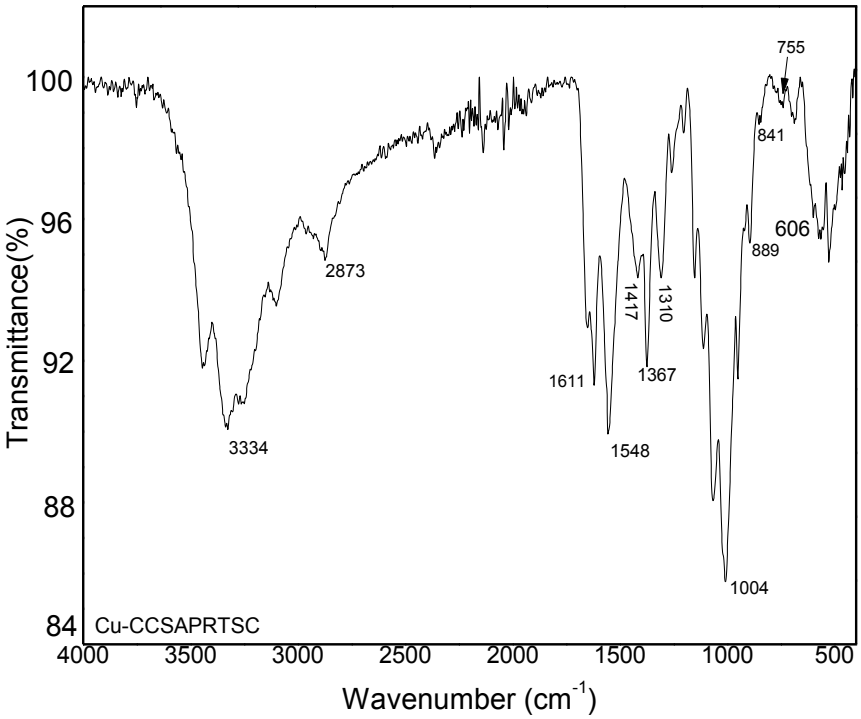


**Figure 59:** FT-IR spectrum of Cu-CCSAPRTSC

### 4.3.2.2. Solid State $^{13}C$ Nuclear Magnetic Resonance ($^{13}C$ NMR) Spectroscopy

Chitosan ring structure and introduction of thiosemicarbazone moiety in C2 position of the ring have been shown by solid state $^{13}C$ NMR spectra of chitosan thiosemicarbazones (figure 60, 61, 62 & 63). The $^{13}C$ NMR spectra with reduction of C2 signal at δ=55.57-57.63 ppm (Qin, *et al.*, 2012; Wang, *et al.*, 2016) indicated the partial involvement of amino group at C2, and the amino group substitution at C2 to give -N=CH was evident from δ= 150.12-169.11 ppm (Qin, *et al.*, 2012). The simultaneous appearance of signals due to C=O (Wang, *et al.*, 2016) at δ= 174.60-178.81 ppm also showed the partial deacetylation of acetamido moiety in chitosan. Other characteristic peaks corresponding to the ring chitosan were $CH_3$(22.72-24.35 ppm), C6(61.13-65.99 ppm), C3, C5(75.33-75.58 ppm), C4(83.26-84.12 ppm), C1(102.74-104.46 ppm) (Qin, *et al.*, 2012; Wang, *et al.*, 2016). The pyridyl carbon signals at δ= 125-140 ppm in CSPCTSC, 125-140 ppm in CCSPCTSC, 119-160 ppm in CSAPRTSC and 116-160 ppm in CCSAPRTSC (Li, Ren, *et al.*, 2013) also showed the grafting of thiosemicarbazone with pyridyl ring. The broadening of peak at δ= 174.60-178.81 ppm was indicative of the superimposition of C=S and C=O signals (Qin, *et al.*, 2012). These results showed the formation of chitosan thiosemicarbazones with partial introduction of thiosemicarbazone group in chitosan. The solid state $^{13}C$ NMR spectral data (δ, ppm) of chitosan thiosemicarbazones: pyridine-2-carboxaldehyde and 2-acetyl-pyridine analogues are presented in table 21.

**Table 21:** The solid state $^{13}C$ NMR spectral data (δ, ppm) of chitosan thiosemicarbazones: pyridine-2-carboxaldehyde and 2-acetyl-pyridine analogues

| Compounds | Methyl carbon | C6 | C3, C5 | C4 | C1 | -N=CH | Pyridyl carbons | C=S & C=O superimposition |
|---|---|---|---|---|---|---|---|---|
| CSPCTSC | 23.90 | 65.99 | 75.33 | 83.88 | 103.41 | 153.90 | 125-140 | 174.60 |
| CCSPCTSC | 22.92 | 61.31 | 75.58 | 83.31 | 104.46 | 150.12 | 125-140 | 175.16 |
| CSAPRTSC | 24.35 | 62.02 | 75.33 | 84.12 | 102.74 | 169.11 | 119-160 | 178.81 |
| CCSAPRTSC | 22.72 | 61.13 | 75.45 | 83.26 | 104.16 | 164.61 | 116-160 | 174.60 |

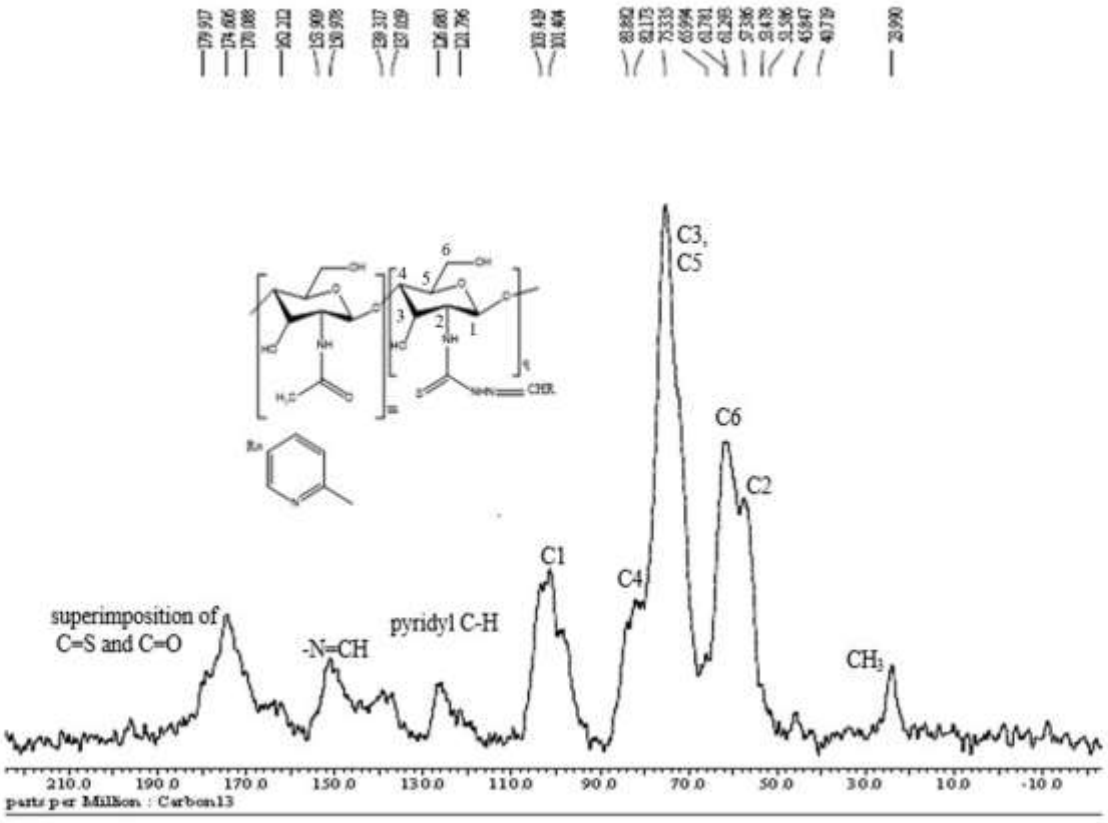


**Figure 60:** $^{13}C$ NMR spectrum of CSPCTSC

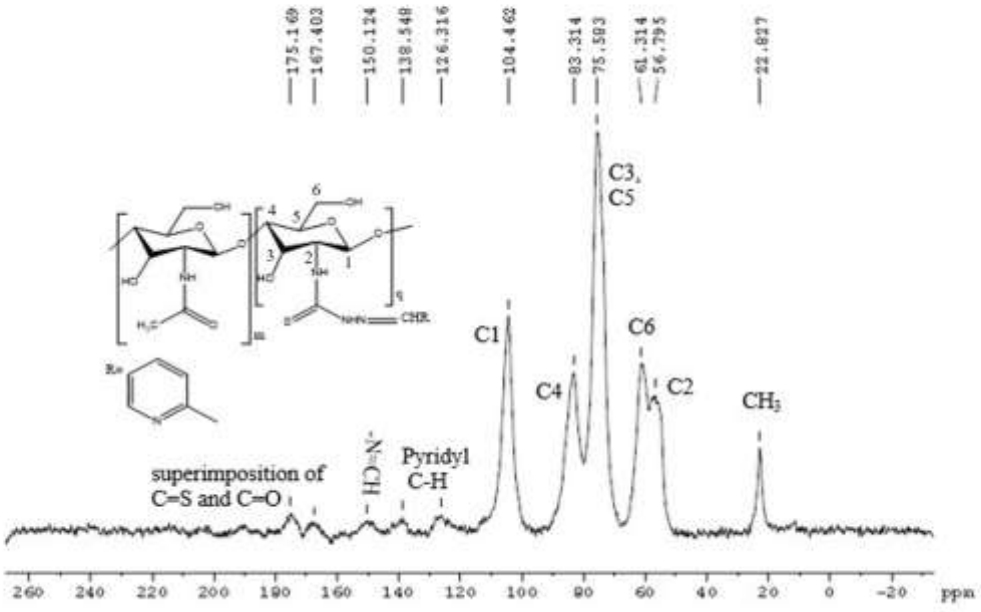


**Figure 61:** $^{13}C$ NMR spectrum of CCSPCTSC

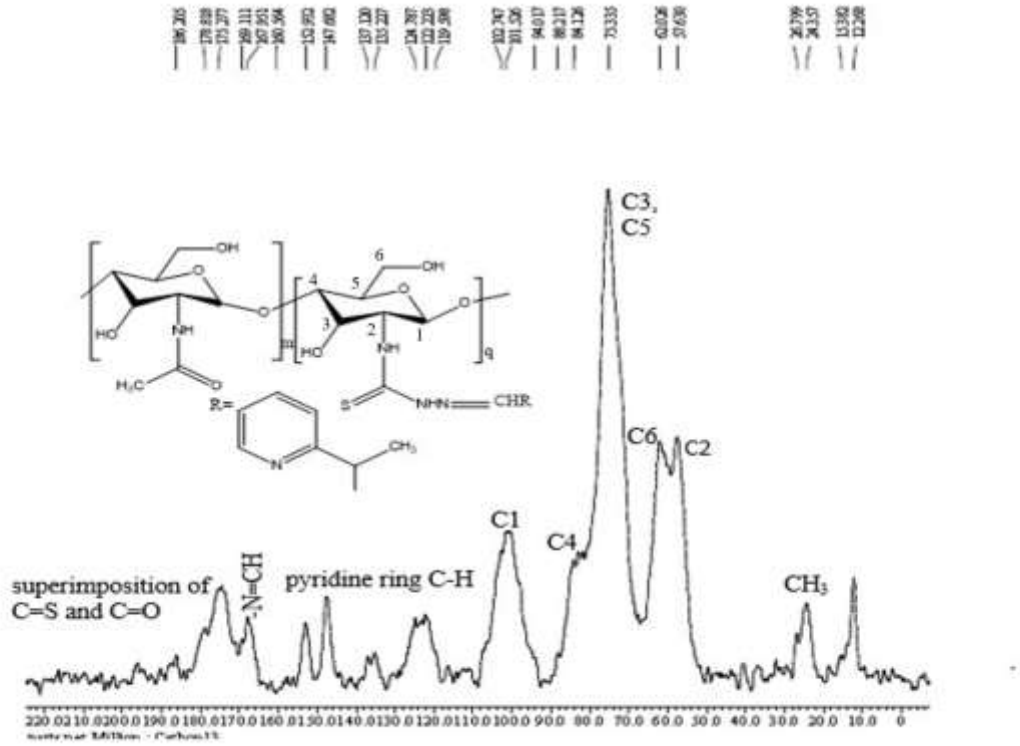


**Figure 62:** $^{13}$C NMR spectrum of CSAPRTSC

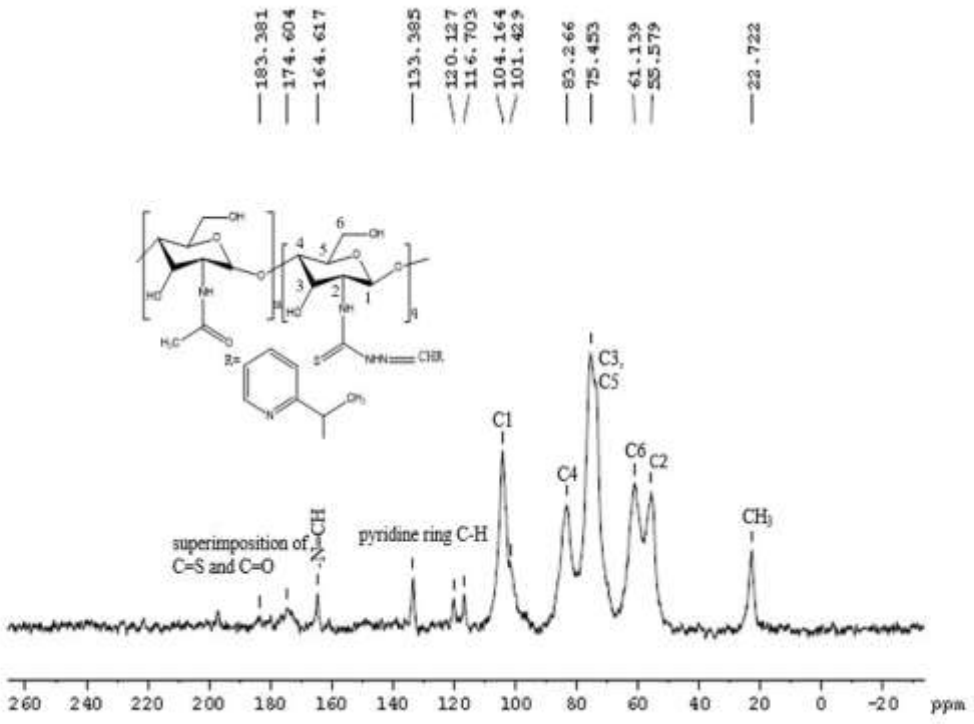


**Figure 63:** $^{13}$C NMR spectrum of CCSAPRTSC

#### 4.3.2.3. Powder X Ray Diffraction (PXRD) Studies

The X ray diffractograms of chitosan thiosemicarbazones (figure 64, 65, 66 & 67) revealed several crystallinity peaks due to thiosemicarbazone moiety at 2θ = 20.10-50.60° in CSPCTSC, 2θ = 6.28-26.48° in CCSPCTSC, 2θ = 25.51-49.74° in CSAPRTSC, and 2θ = 7.06- 27.00° in CCSAPRTSC (Hanumantharao, *et al.*, 2012; Santhakumari, *et al.*, 2010). The appearance of new peaks showing the change in the crystallinity pattern and the shifting of peaks at 10° and 20° due to chitosan (Qin, *et al.*, 2012; Ramya, *et al.*, 2012) showed the grafting of thiosemicarbazone group in chitosan (Qin, *et al.*, 2012) and this process of functionalization of chitosan as chitosan thiosemicarbazone involving the imine group formation and cleavage of intra-molecular hydrogen bond of chitosan caused the appearance of new crystallinity peaks (Jiao, *et al.*, 2011).

As calculated from *Debye-Scherrer formula* (Dehaghi, *et al.*, 2014; Kucukgulmez, *et al.*, 2011), the particle sizes of ligands corresponding to highest intensity peaks in their diffraction curves in a range of 14.98-30.75 nm and the degree of crystallinity as the crystallinity index (Kumirska, *et al.*, 2010; Lomadze *et al.*, 2005; Zhang, *et al.*, 2005) in a range of 56.06-84.85% showed the general trend of increase in crystallinity index with decrease in particle size.

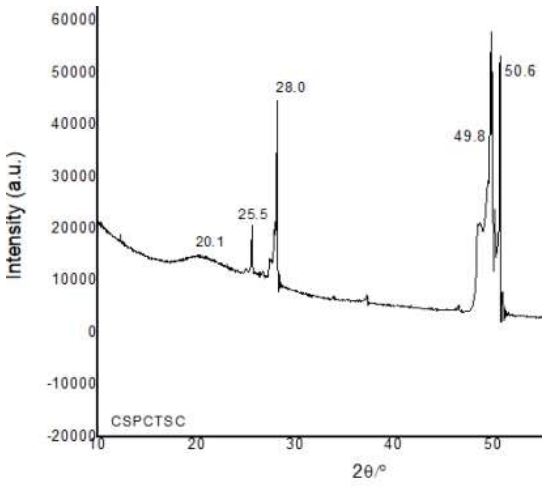


**Figure 64:** X ray diffractogram of CSPCTSC

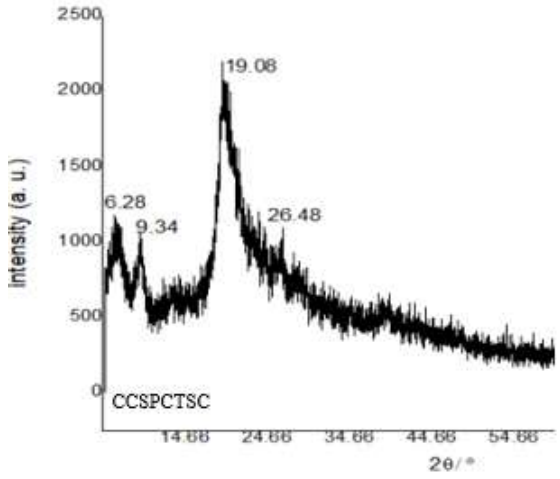


**Figure 65:** X ray diffractogram of CCSPCTSC

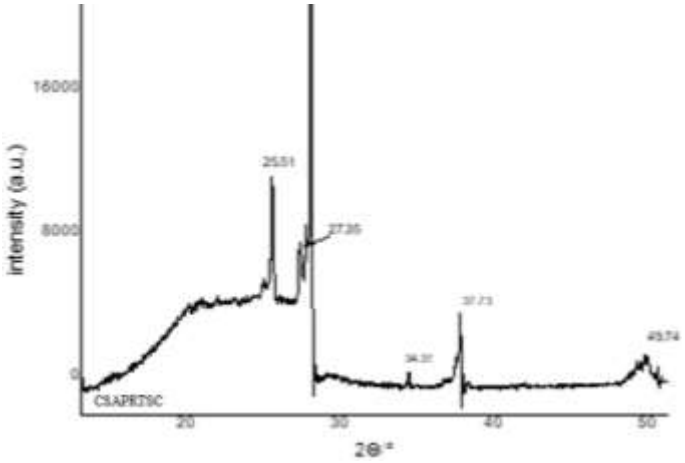


**Figure 66:** X ray diffractogram of CSAPRTSC

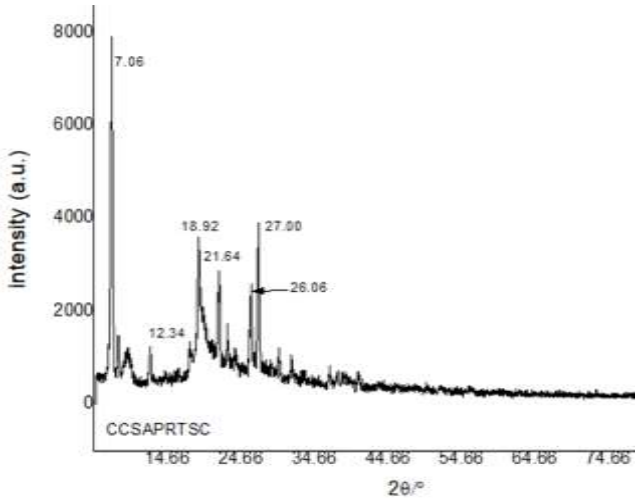


**Figure 67:** X ray diffractogram of CCSAPRTSC

The X ray diffractograms of copper(II) chitosan thiosemicarbazone complexes (figure 68, 69, 70 & 71) showed the shifting of crystallinity pattern from the respective ligands. New peaks at 2θ = 12.92°, 21.79°, 26.68° and 29.57° in Cu-CSPCTSC, 2θ =19.22° and 39.64° in Cu-CCSPCTSC, 2θ = 19.55° and 39.86° in Cu-CSAPRTSC, 2θ = 20.88° and 25.51°in Cu-CCSAPRTSC were attributed to chelation of metal ion with different groups of thiosemicarbazone ligand resulting in the formation of a new crystalline phase (Antony, *et al.*, 2012; Dehaghi, *et al.*, 2014; Mekahlia, *et al.*, 2009; Qin, *et al.*, 2012; Wang, *et al.*, 2005). The original crystallinity of chitosan corresponding to the peaks at 10.4° and 19.8° was not destroyed, but the crystallinity peaks were weakened and shifted due to formation of a new crystalline phase that is attributed to destruction of hydrogen bonds as a result of chelation of metal ions with amino or hydroxy group in chitosan (Wang, *et al.*, 2005).

From *Debye-Scherer formula* (Dehaghi, *et al.*, 2014; Kucukgulmez, *et al.*, 2011), the particle sizes of copper(II) chitosan thiosemicarbazone complexes corresponding to the maximum intensity peak in their X ray diffraction curves, were found to range from 23.91-37.70 nm in pyridine -2-carboxaldehyde-based copper(II) chitosan thiosemicarbazones and 16.01-46.40 nm in 2-acetyl pyridine-based copper(II) chitosan thiosemicarbazones. The degree of crystallinity as the crystallinity index (Kumirska, *et al.*, 2010; Lomadze *et al.*, 2005; Zhang, *et al.*, 2005) was found 47.77-68.87% in pyridine -2-carboxaldehyde -based copper(II) chitosan thiosemicarbazones and, 30.63-39.28% in 2-acetyl pyridine-based copper(II) chitosan thiosemicarbazones.

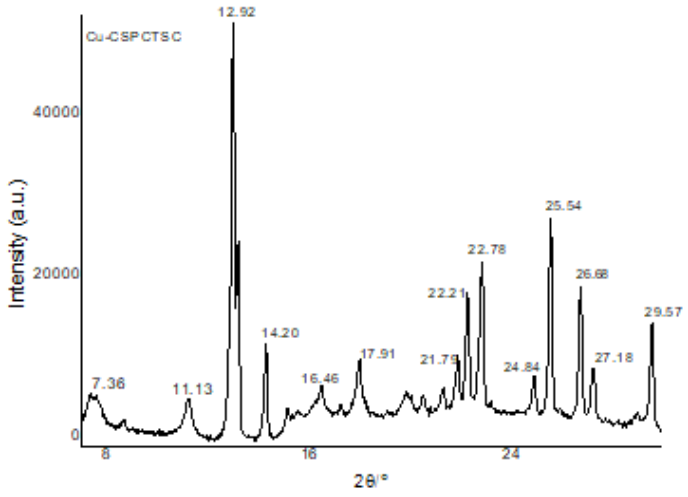


**Figure 68:** X ray diffractogram of Cu-CSPCTSC

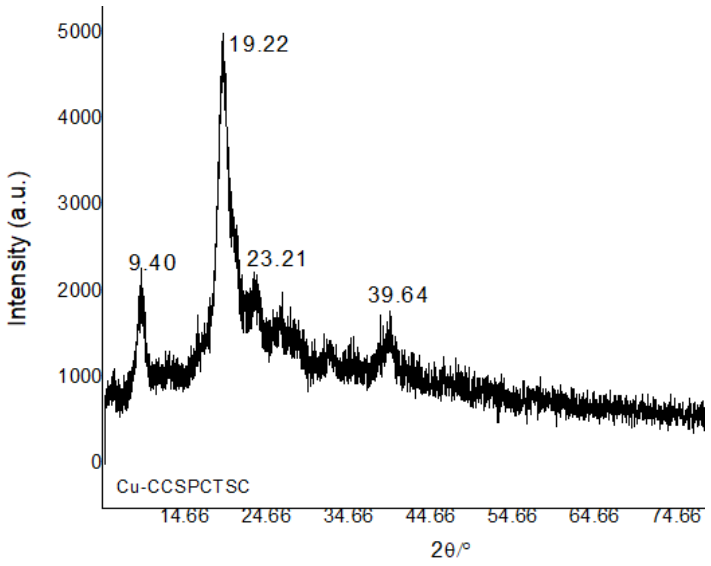


**Figure 69:** X ray diffractogram of Cu-CCSPCTSC

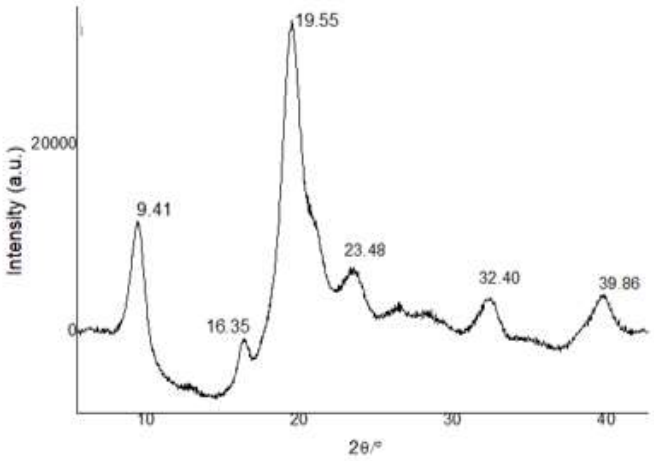


**Figure 70:** X ray diffractogram of Cu-CSAPRTSC

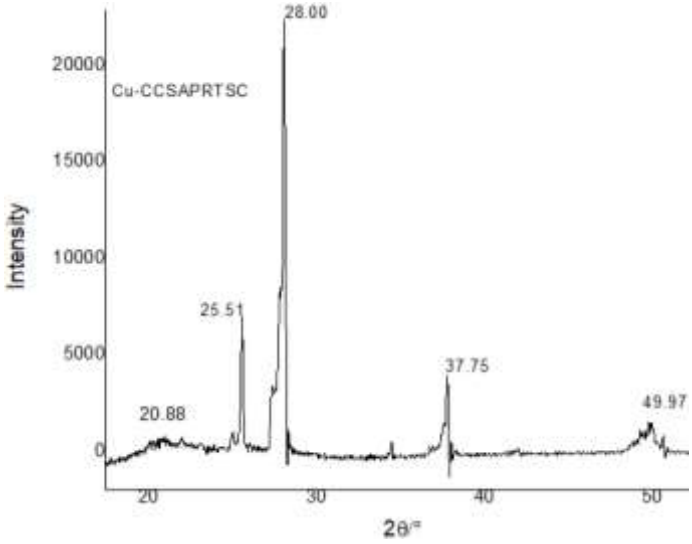


**Figure 71:** X ray diffractogram of Cu-CCSAPRTSC

The powder X ray diffraction data of pyridine-2-carboxaldehyde and 2-acetyl pyridine chitosan thiosemicarbazones and their copper(II) complexes are presented in table 22.

**Table 22:** The powder X ray diffraction data of chitosan thiosemicarbazones and their copper(II) complexes: pyridine-2-carboxaldehyde and 2-acetyl pyridine analogues

| Compounds | Selected functionality peaks, 2θ | | D (nm) | C.I. (%) |
|---|---|---|---|---|
| | Thiosemicarbazone crystallinity | Chitosan complex crystallinity | | |
| CSPCTSC | 20.1°, 25.5°, 28.0°, 49.8°, 50.6° | - | 14.98 | 71.46 |
| Cu-CSPCTSC | 7.36°, 11.13°, 22.21°, 22.78°, 25.54° | 12.92°,21.79°, 26.68°, 29.57° | 37.70 | 47.77 |
| CCSPCTSC | 6.28°, 9.34°, 19.08°, 26.48° | - | 18.24 | 78.21 |
| Cu-CCSPCTSC | 9.40°, 23.21° | 19.22°, 39.64° | | |
| CSAPRTSC | 25.51°,27.35°,28.05°.34.37°,37.73°, 49.74° | - | 26.21 | 56.06 |
| Cu-CSAPRTSC | 9.41°, 16.35°, 23.48°,32.40° | 19.55°, 39.86° | 16.01 | 30.63 |
| CCSAPRTSC | 7.06°,12.34°,18.92°,21.54°,26.06°, 27.00° | - | 30.75 | 84.85 |
| Cu-CCSAPRTSC | 28.00°, 37.75°, 49.97° | 20.88°, 25.51° | 46.40 | 39.28 |

### 4.3.2.4. Elemental Microanalysis

For the ligands CSPCTSC and CCSPCTSC, corresponding to the monomer structure of unit formula weight 324, and for the ligands CSAPRTSC and CCSAPRTSC, corresponding to the monomer structure of unit formula weight 338, the calculated percentages showed the agreement with analytically found percentages of elements when there is partial grafting of thiosemicarbazone group in chitosan. This is further supported by their DS values. Corresponding to the monomer structure of unit formula weight 423 of the pyridine-2-carboxaldehyde-based complexes, and 2-acetyl pyridine-based complexes of unit formula weight 437, the analytically found percentages showed an agreement with the coordination of non-functionalized chitosan as well as thiosemicarbazone ligands with copper(II) ion. This is further supported by higher value of estimated chlorine percentage than the calculated chlorine percentage. The DS values (Inukai, *et al.*, 1998; Melo, *et al.*, 2002; Pires, *et al.*, 2013; Qin, *et al.*, 2012) are indicatives of partial substitution of amino group of chitosan in C2 position and the analytically found percentages of elements in the complexes are in agreement with the simultaneous coordination of chitosan and chitosan thiosemicarbazone with copper(II) ion. The partial deacetylation of chitin, and partial introduction of Schiff base group into chitosan are justifiable with decreased sulphur percentage and some differences

with calculated percentages of other elements, as the calculated percentages were for the respective chitosan thiosemicarbazones with completely deacetylated ring of chitosan (Qin, *et al.*, 2012). The DS values also showed more functionalization of commercial oligo chitosan than high molecular weight crab shell chitosan showing more deacetylation with increase in DDA and decrease in $M_w$. The elemental (CHNS) microanalysis of chitosan thiosemicarbazones: pyridine-2-carboxaldehyde and 2-acetyl pyridine analogues and their copper(II) complexes are presented in table 23 and 24 respectively.

**Table 23:** Elemental (CHNS) microanalysis of chitosan thiosemicarbazones: pyridine-2-carboxaldehyde and 2-acetyl pyridine analogues: calculated (found)

| Compounds | C(%) | H(%) | N(%) | S(%) | DS(%) |
|---|---|---|---|---|---|
| CSPCTSC | 48.14(44.025) | 4.93(5.875) | 17.28(16.069) | 9.87(5.149) | 36.28 |
| CCSPCTSC | 48.14(44.205) | 4.93(5.324) | 17.28(16.321) | 9.87(4.936) | 35.31 |
| CSAPRTSC | 49.70(42.736) | 5.32(5.661) | 16.56(11.029) | 9.46(7.010) | 59.18 |
| CCSAPRTSC | 49.70(42.051) | 5.32(5.65) | 16.56(10.005) | 9.46(5.962) | 47.40 |

**Table 24:** Elemental (CHNS) microanalysis and chlorine estimation in copper(II) chitosan thiosemicarbazones: pyridine-2-carboxaldehyde and 2-acetyl pyridine analogues: calculated (found)

| Compounds | C(%) | H(%) | N(%) | S(%) | Cl(%) |
|---|---|---|---|---|---|
| Cu-CSPCTSC | 36.87(31.75) | 3.78(4.985) | 13.23(9.64) | 7.56(3.222) | 8.39(12.08) |
| Cu-CCSPCTSC | 36.87(32.41) | 3.78(5.427) | 13.23(9.69) | 7.56(3.436) | 8.39(12.08) |
| Cu-CSAPRTSC | 38.44(31.16) | 4.11(4.397) | 12.81(9.65) | 7.32(4.773) | 8.12(10.02) |
| Cu-CCSAPRTSC | 38.44(32.41) | 4.11(5.427) | 12.81(9.69) | 7.32(3.436) | 8.12(10.01) |

### 4.3.2.5. Thermal Studies

Thermogravimetric/differential thermal analysis (TG/DTA) curves of chitosan thiosemicarbazones (figure 72, 73, 74 & 75) and the thermal data presented in table 25 showed, in particular, a weight loss of 14.04% at 173 °C in CSPCTSC, 17.97% at 190 °C in CCSPCTSC, 4.41% at 72 °C followed by an abrupt loss of 49.92% weight due to the disruption of chitosan backbone up to about 440°C in CSAPRTSC and 4.39% at 75 °C followed by an abrupt loss of 48.86 % weight due to the disruption of the backbone up to about 440 °C in CCSAPRTSC. The thermal decomposition was attributed to the loss of water at 100-200 °C and chain degradation followed by the disruption of chitosan backbone at 200-

1000 °C. The chain degradation at 200-1000 °C caused a weight loss of 75% in CSPCTSC, 72% in CCSPCTSC, 74% in CSAPRTSC, and 76% in CCSAPRTSC. These thermal events were in agreement with the reports of loss of water in chitosan at 80-160 °C (Kittur, *et al.*, 2002; Qin, *et al.*, 2012) and decomposition of chitosan at 50-100 °C and 400 – 500 °C (Andrade, *et al.*, 2012; Kumari, *et al.*, 2017). Further, the commercial chitosan has been reported to undergo a weight loss in two stages with 9% of weight loss owing to loss of water at 120 °C and 43% of weight loss owing to chitosan chain degradation at 500 °C (Chethan, *et al.*, 2013; De Britto & Campana-Filho, 2004; Xu, *et al.*, 2010), and in agreement to this, there was 9.20-14.30% weight loss attributed to loss of water at 120 °C and 65-67% weight loss as a result of chain degradation at 500 °C in chitosan thiosemicarbazones. These derivatives were found to undergo more degradation than chitosan at the moderate temperature of 400-500 °C. Meanwhile, they were also found to follow the general trend of decomposition similar to that of chitosan with a rapid rate of decomposition from 100 °C to 400 °C and a steady rate of chain degradation, leaving about 10% CSPCTSC, 9% CCSPCTSC, 13% CSAPRTSC and 12% CCSAPRTSC as residue of the unsaturated structure at 1000 °C. Such a thermal behaviour accorded with a higher thermal stability of thiosemicarbazones (Qu, *et al.*, 2000) and their DTA peaks also showed an agreement with TG weight loss in two steps of 150- 400 °C and 400-900 °C, and an endothermic peak attributed to loss of water from 25-150 °C.

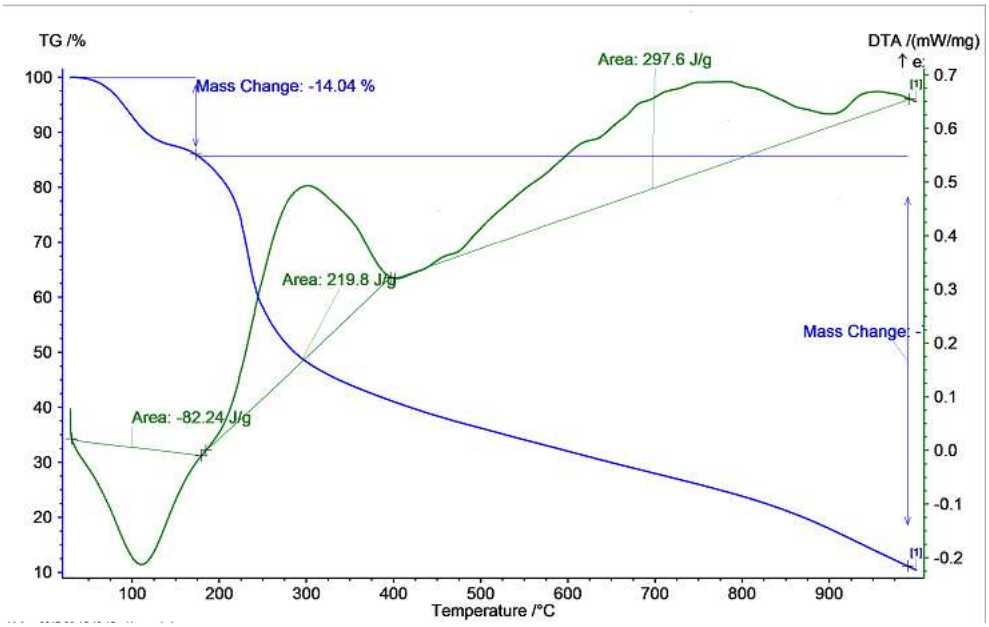


**Figure 72:** TG/DTA curves of CSPCTSC showing the thermal events at different temperatures

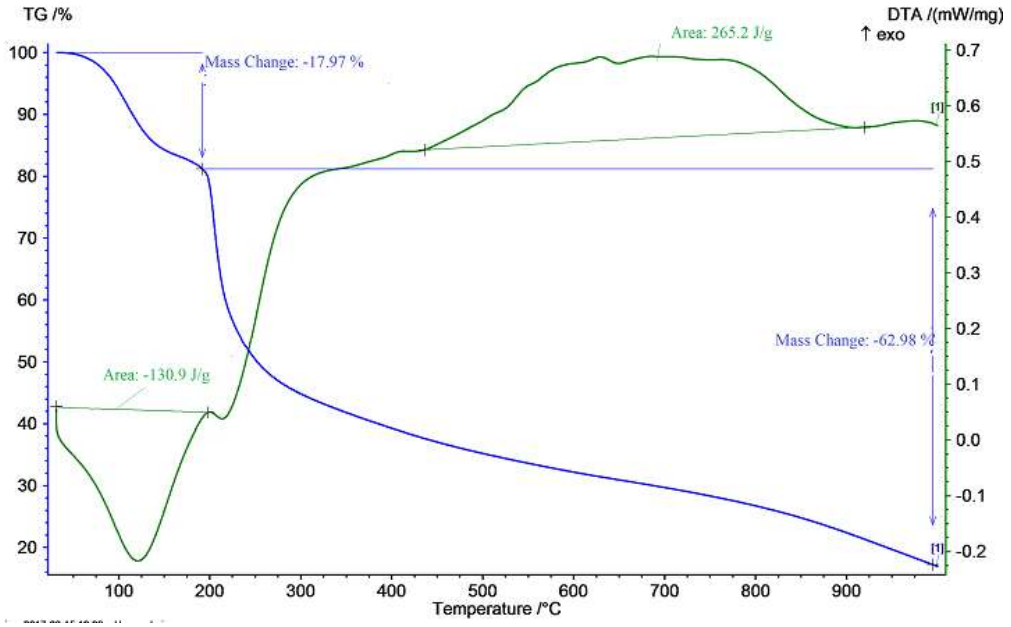


**Figure 73:** TG/DTA curves of CCSPCTSC showing the thermal events at different temperatures

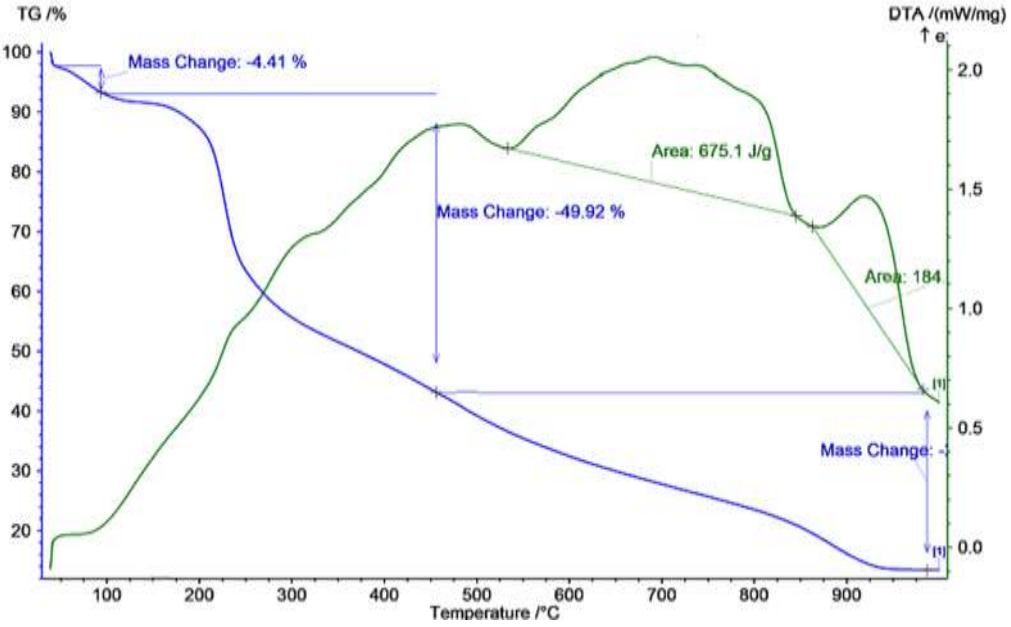


**Figure 74:** TG/DTA curves of CSAPRTSC showing the thermal events at different temperatures

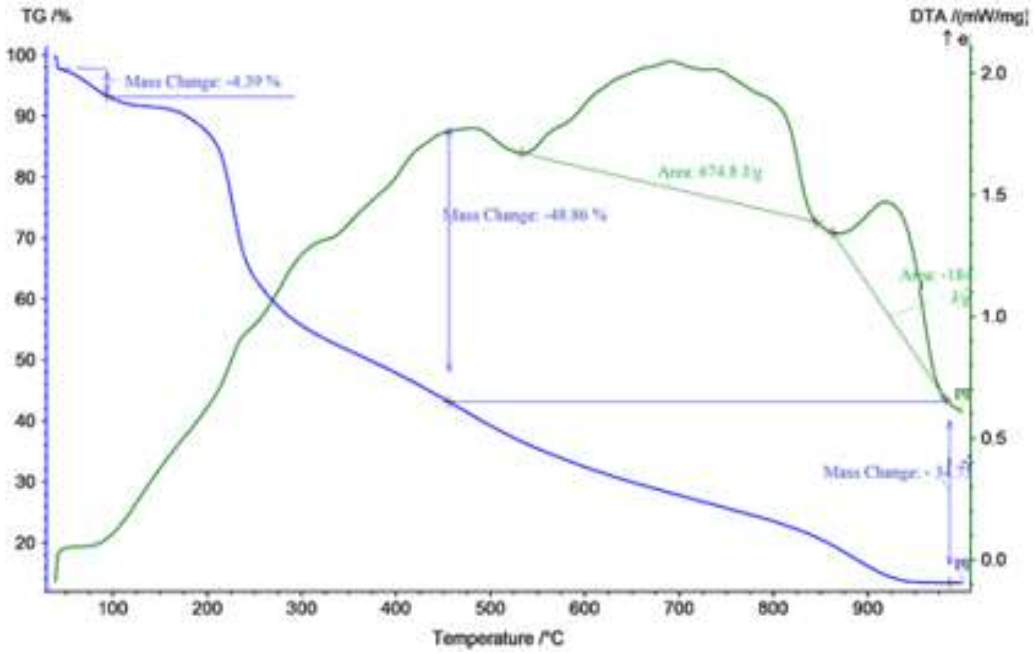


**Figure 75:** TG/DTA curves of CCSAPRTSC showing the thermal events at different temperatures

**Table 25:** TG/DTA data of thermal events in chitosan thiosemicarbazones: pyridine-2-carboxaldehyde and 2-acetyl pyridine analogues

| Compounds | Temperature (°C) | Weight loss (%) | Thermal event | % residue at 1000 °C |
|---|---|---|---|---|
| CSPCTSC | 173 | 14.04 | Loss of water | 10 |
| | 200-1000 | 75 | Chain disruption and backbone degradation | |
| CCSPCTSC | 190 | 17.97 | Loss of water | 9 |
| | 200-1000 | 72 | Chain disruption and backbone degradation | |
| CSAPRTSC | 72<br>440 | 4.41<br>49.92 | Loss of water<br>Abrupt disruption of backbone | 13 |
| | 200-1000 | 74 | Backbone degradation | |
| CCSAPRTSC | 75<br>440 | 4.39<br>48.86 | Loss of water<br>Abrupt disruption of backbone | 12 |
| | 200-1000 | 76 | Backbone degradation | |

The TGA curves of complexes (figure 76, 77, 78 & 79) and the thermal data presented in table 26 showed, in particular, a weight loss of 0.08% in Cu-CSPCTSC, 0.36% in Cu-CCSPCTSC, 5.5% in Cu-CSAPRTSC and 0.81% in Cu-CCSAPRTSC at 200 °C, and a weight loss of about 51.44% in Cu-CSPCTSC, 58.38% in Cu-CCSPCTSC, 39.15% in Cu-CSAPRTSC, and 57.58% in Cu-CCSAPRTSC at 200-500 °C. The curves showed the weight

loss in three steps corresponding to the constant loss of weight up to 150- 200 °C, rapid loss of weight at 200-400 °C, and again a steady loss of weight from 400-700 °C. It showed more degradation of complexes at the moderate heating in the lower range of temperature at 200-500 °C and then a steady rate of decomposition, leaving about 39% Cu-CSPCTSC, 37% Cu-CCSPCTSC, 46% Cu-CSAPRTSC and 37% Cu-CCSAPRTSC as residue of the unsaturated structure at 700 °C. These thermal events showed the standard thermal stability (Kittur, *et al.*, 2002; Qu, *et al.*, 2000) of the complexes.

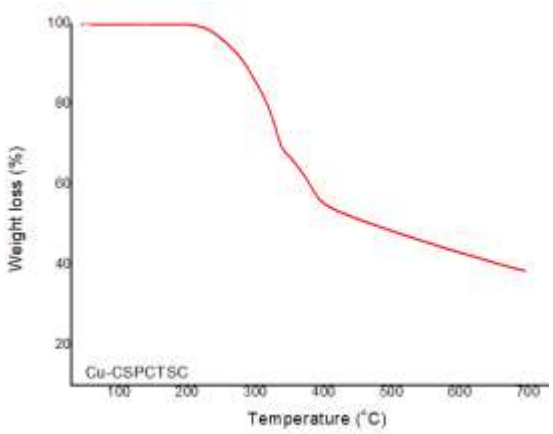


**Figure 76:** TGA curve of Cu-CSPCTSC

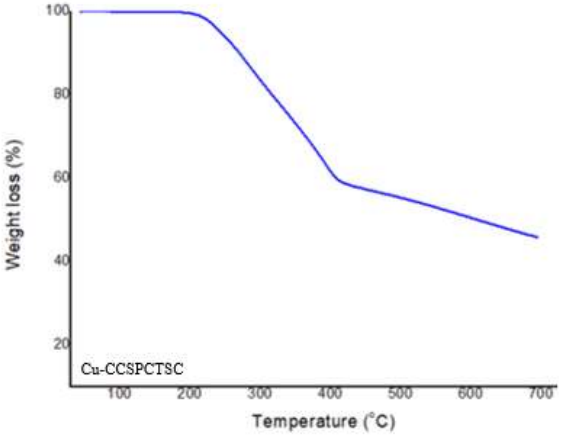


**Figure 77:** TGA curve of Cu-CCSPCTSC

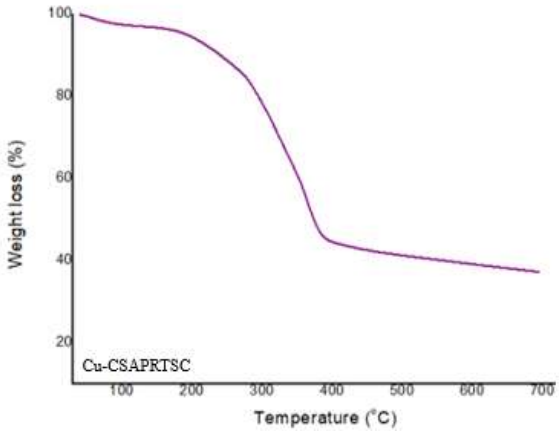


**Figure 78:** TGA curve of Cu-CSAPRTSC

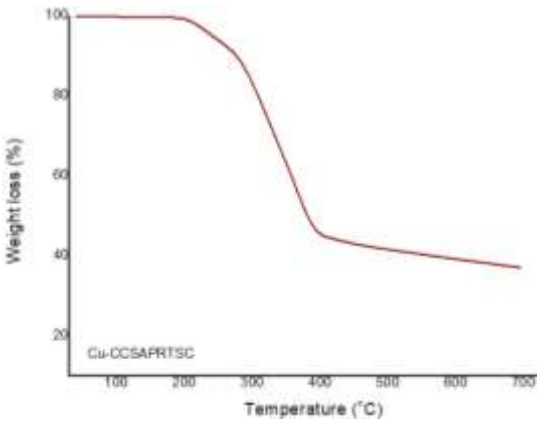


**Figure 79:** TGA curve of Cu-CCSAPRTSC

**Table 26:** TGA data of thermal events in copper(II) chitosan thiosemicarbazones: pyridine-2-carboxaldehyde and 2-acetyl pyridine analogues

| Compounds | Temperature (°C) | Weight loss % | Thermal event | % residue at 700 °C |
|---|---|---|---|---|
| Cu-CSPCTSC | 200 | 0.08 | Loss of water | 39 |
| | 200-500 | 51.44 | Disruption of the chain | |
| | 500-700 | 9.52 | Further degradation of the backbone | |
| Cu-CCSPCTSC | 200 | 0.36 | Loss of water | |

| | | | | |
|---|---|---|---|---|
| | 200-500 | 58.38 | Disruption of the chain | 37 |
| | 500-700 | 4.41 | Further degradation of the backbone | |
| Cu-CSAPRTSC | 200 | 5.50 | Loss of water | 46 |
| | 200-500 | 39.15 | Disruption of the chain | |
| | 500-700 | 9.40 | Further degradation of the backbone | |
| Cu-CCSAPRTSC | 200 | 0.81 | Loss of water | 37 |
| | 200-500 | 57.58 | Disruption of the chain | |
| | 500-700 | 4.61 | Further degradation of the backbone | |

#### 4.3.2.6. Magnetic Susceptibility Measurement and Electron Paramagnetic Resonance (EPR) Spectroscopy

The magnetic susceptibility measurement revealed that the complexes were paramagnetic with the magnetic moment ($\mu_{eff}$) values of 1.80-1.85 BM. The magnetic moment values were fairly above the pure spin-only moment of 1.73 BM due to large spin orbit coupling constant of cupric ion (Djord jevic, 1960) but these values of <1.90 BM indicated the square planar or octahedral geometry of the complexes (Figgis, 1958). The low spin-spin coupling between the unpaired electrons of copper atoms was shown by the values of magnetic moment in a neighbourhood of spin-only moment of 1.73 BM corresponding to an unpaired electron (Ahmed & Lal, 2017).

The EPR spectra of complexes (figure 80, 81, 82 & 83) showed the absence of hyperfine splitting that was attributed to exchange broadening caused by the insufficient separation of paramagnetic centres (Farra, *et al.*, 2011) at a lower frequency of X-band at 9.8 GHz (Farra, *et al.*, 2011). The non-resolution of hyperfine features due to copper (S =1/2 and I= 3/2) was contributed by intermolecular spin-spin interactions and dimeric association of molecules (Bhadbhade & Srinivas, 1993; Suresh, *et al.*, 1996), but the spectra in which the g parallel tensors were undetectable with the absence of hyperfine splitting still possessed the feature to be characterized by axial g tensors (Bennur, *et al.*, 2001) and the spectra in correspondence to an unpaired electron in $d_{x^2-y^2}$ orbital of Cu(II) centres showed the square planar orientation of complexes (Garribba & Micera, 2006). The values of magnetic moment and g values in EPR spectra are presented in table 27. The g values were 2.10 for Cu-CSPCTSC (ν = 9.8623 GHz, $B_o$=3355 Gs = 335.5 mT), 2.09 for Cu-CCSPCTSC (ν =9.8577 GHz, $B_o$ = 3360 Gs = 336 mT), 2.08 for Cu-CSAPRTSC (ν =9.8623 GHz, $B_o$= 3383 Gs = 338.3 mT), and 2.08 for Cu-CCSAPRTSC (ν =9.8621 GHz, $B_o$ = 3383 Gs = 338.3 mT).

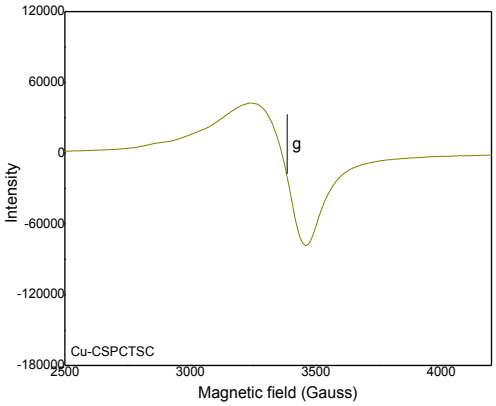


**Figure 80**: EPR spectrum of Cu-CSPCTSC

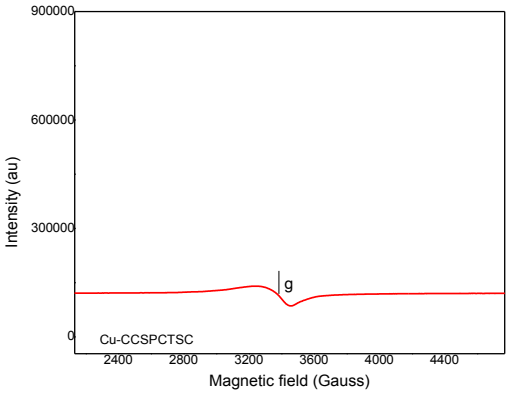


**Figure 81:** EPR spectrum of Cu-CCSPCTSC

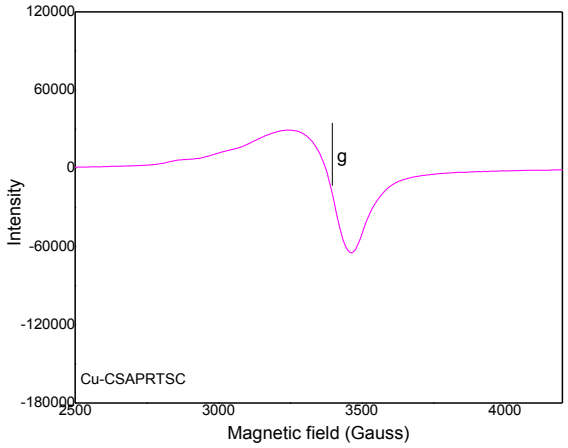


**Figure 82:** EPR spectrum of Cu-CSAPRTSC

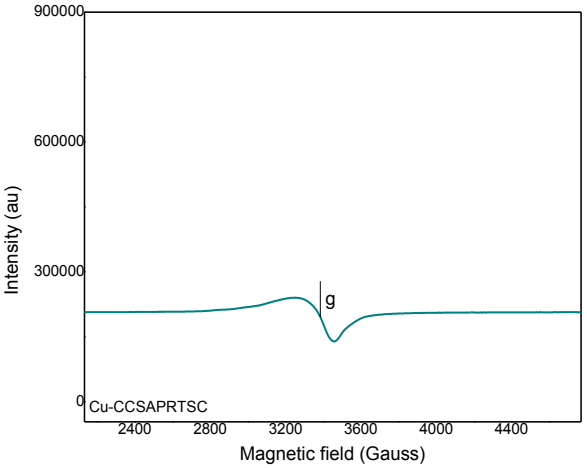


**Figure 83:** EPR spectrum of Cu-CCSAPRTSC

**Table 27:** Effective magnetic moments ($\mu_{eff}$) and EPR g values of copper(II) chitosan thiosemicarbazones: pyridine-2-carboxaldehyde and 2-acetyl pyridine analogues

| Complexes | $\mu_{eff}$, B. M. | EPR g value |
|---|---|---|
| Cu-CSPCTSC | 1.79 | 2.10 |
| Cu-CCSPCTSC | 1.80 | 2.09 |
| Cu-CSAPRTSC | 1.89 | 2.08 |
| Cu-CCSAPRTSC | 1.87 | 2.08 |

The shifting of g value from $g_e$ (2.0023) was attributed to spin orbital coupling with unpaired electrons, and this spin orbital coupling was introduced by covalent behaviour of the complex that was dependent upon the density of unpaired electrons in ligand molecules (Ahmed & Lal, 2017). The absence of half field peak at 1500 Gauss that was indicative of the absence of two copper centres in the same lacuna showed the mononuclear structure of complexes (Patel & Sadasivan, 2017).

The overall results of characterization showed that the thione sulphur, azomethine nitrogen, pyridyl nitrogen of pyridine -2-carboxaldehyde or 2-acetyl-pyridine moiety, and one chlorine atom were used as the donor sites in coordination with copper(II) ion in the complexes that were proposed to assume the mononuclear distorted square planar geometry (figure 84).

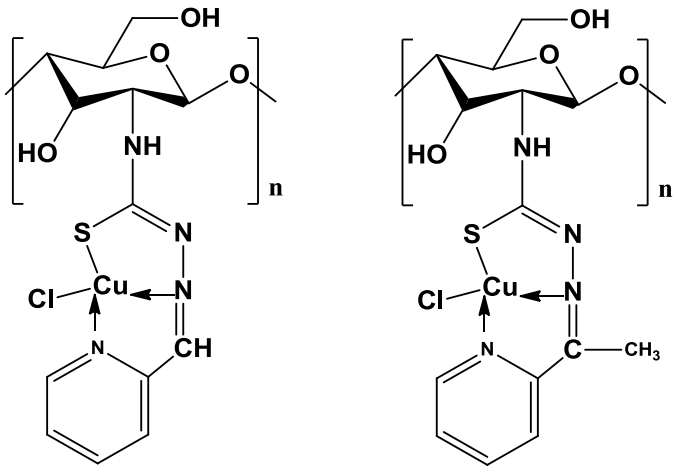


**Figure 84:** Proposed structure of complexes: (a). Cu-CSPCTSC and Cu-CCSPCTSC. (b). Cu-CSAPRTSC and Cu-CCSAPRTSC

## 4.4. Chitosan Thiosemicarbazones and their Copper(II) Complexes: Isatin and 5-Chloroisatin Analogues

### 4.4.1. Physical Characteristics

The physical characteristics of isatin and 5-chloroisatin thiosemicarbazones and their copper(II) complexes, summarized in table 28 & 29 respectively, showed their high yield *viz.* 42-45% ligands and 63-71% complexes, and high thermal stability in crystalline solid state with melting point above 300 °C. They were fairly soluble in 1% acetic acid and the solubility increased with increase in DDA and decrease in $M_w$.

**Table 28:** Physical characteristics of isatin chitosan thiosemicarbazones and their copper(II) complexes

| Compounds | Unit formula | Unit formula weight | Color | m.pt. (°C) | Yield (%) |
|---|---|---|---|---|---|
| CSISTSC | $C_{15}H_{16}N_4O_5S$ | 364 | Red | >300 | 44 |
| CCSISTSC | $C_{15}H_{16}N_4O_5S$ | 364 | Red | >300 | 42 |
| Cu-CSISTSC | $C_{15}H_{16}N_4O_5SCuCl$ | 463 | Yellowish red | >300 | 68 |
| Cu-CCSISTSC | $C_{15}H_{16}N_4O_5SCuCl$ | 463 | Yellowish red | >300 | 63 |

**Table 29:** Physical characteristics of 5-chloroisatin chitosan thiosemicarbazones and their copper(II) complexes

| Compounds | Unit formula | Unit formula weight | Color | m.pt. (°C) | Yield (%) |
|---|---|---|---|---|---|
| CSCLISTSC | $C_{15}H_{16}N_4O_5SCl$ | 399 | Red | >300 | 45 |
| CCSCLISTSC | $C_{15}H_{16}N_4O_5SCl$ | 399 | Red | >300 | 44 |
| Cu-CS CLISTSC | $C_{15}H_{16}N_4O_5SCuCl_2$ | 498 | Yellowish green | >300 | 71 |
| Cu-CCSCLISTSC | $C_{15}H_{16}N_4O_5SCuCl_2$ | 498 | Yellowish green | >300 | 70 |

### 4.4.2. Characterization

#### 4.4.2.1. Fourier Transform- Infrared (FT-IR) Spectroscopy

The FT-IR spectra of isatin and 5-chloroisatin thiosemicarbazones (figure 85, 87, 89 & 91) showed the bands due to isatin ring at 3188-3211 $cm^{-1}$ (broad, ν indole N-H) (Abbas, *et al.*, 2013; Islam & Mohsin, 2007), 1710-1728 $cm^{-1}$ (ν C=O, keto), 1451-1466 $cm^{-1}$ (ν C-C, aromatic) (Islam & Mohsin, 2007), and the bands at 3188-3212 $cm^{-1}$ were merged with ν (N-H, azomethine) (Aneesrahman, *et al.*, 2019) and ν (O-H) stretches (Qin, *et al.*, 2012; Zhong, *et al.*, 2011). The peaks at 1618–1620 $cm^{-1}$ were due to ν (C=N) (Qin, *et al.*, 2012). The ν (C=S) stretches were shown at 884-897 $cm^{-1}$ (Tiwari, *et al.*, 2016; Yamaguchi, *et al.*, 1958) and 1306-1341 $cm^{-1}$ (Aneesrahman, *et. al.*, 2019; Joseph, *et al.*, 2006). The IR spectra also showed the simultaneous appearance of the peaks at 1069-1096 $cm^{-1}$ corresponding to the C=S vibrations (Tiwari, *et al.*, 2016; Yamaguchi, *et al.*, 1958) coupled with other vibrations for the case in which thiocarbonyl group is attached with nitrogen atom (Wiles, *et al.*, 1967). Weakening of the ν (N-H) bending peak due to primary amine and residual amide II of chitosan at 1566 $cm^{-1}$ (Zhong, *et al.*, 2010) and its negative shifting to 1526-1555 $cm^{-1}$ showed partial substitution of amino group in chitosan. The peaks attributed to ν (C-H) and ν (C-O-C) in chitosan ring appeared with some shifting at 1381-1465 $cm^{-1}$ and 1069-1092 $cm^{-1}$ respectively (Yadav, *et al.*, 2020). The existence of thiosemicarbazone in thione form was shown by the absence of ν (C-S-H) stretches at 2500-2600 $cm^{-1}$ (Bharti, *et al.*, 2003).

The FT-IR spectra of the corresponding complexes (figure 86, 88, 90 & 92) showed a negative shift in ν C=O stretches to 1696-1700 $cm^{-1}$, ν (C=N) stretches to 1608-1610 $cm^{-1}$ and ν (C=S) stretches to 870-881 $cm^{-1}$ and 1300-1334 $cm^{-1}$. The ν (C=S) stretches coupled with other vibrations were lowered to 1060-1089 $cm^{-1}$. The selected FT-IR spectral data (table 30) were indicatives of the coordination of thiosemicarbazone to Cu(II) through ONS donor atoms.

**Table 30:** The selected FT-IR bands ($cm^{-1}$) of chitosan thiosemicarbazones and their complexes: isatin and 5-chloroisatin analogues

| Compounds | ν(C=N) | ν(C=S) | ν(C=O) | ν($NH_2$) | ν(indole N-H) of isatin |
|---|---|---|---|---|---|
| CSISTSC | 1620 | 891, 1340 | 1720 | 1526 | 3189 |
| Cu-CSISTSC | 1608 | 881, 1330 | 1696 | 1538 | 3218 |
| CCSISTSC | 1618 | 884, 1341 | 1718 | 1533 | 3211 |
| Cu-CCSISTSC | 1610 | 870, 1334 | 1700 | 1534 | 3263 |
| CSCLISTSC | 1620 | 889, 1308 | 1734 | 1530 | 3188 |
| Cu-CSCLISTSC | 1610 | 878, 1300 | 1727 | 1531 | 3212 |
| CCSCLISTSC | 1618 | 897, 1306 | 1710 | 1555 | 3198 |
| Cu- CCSCLISTSC | 1610 | 872, 1300 | 1700 | 1557 | 3203 |

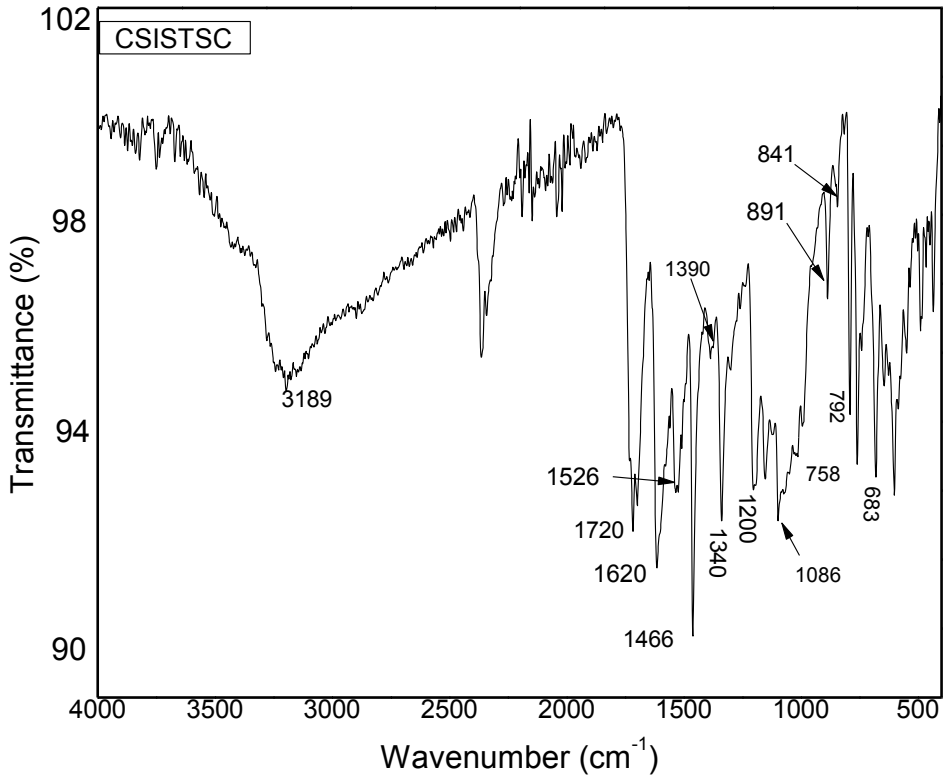


**Figure 85:** FT-IR spectrum of CSISTSC

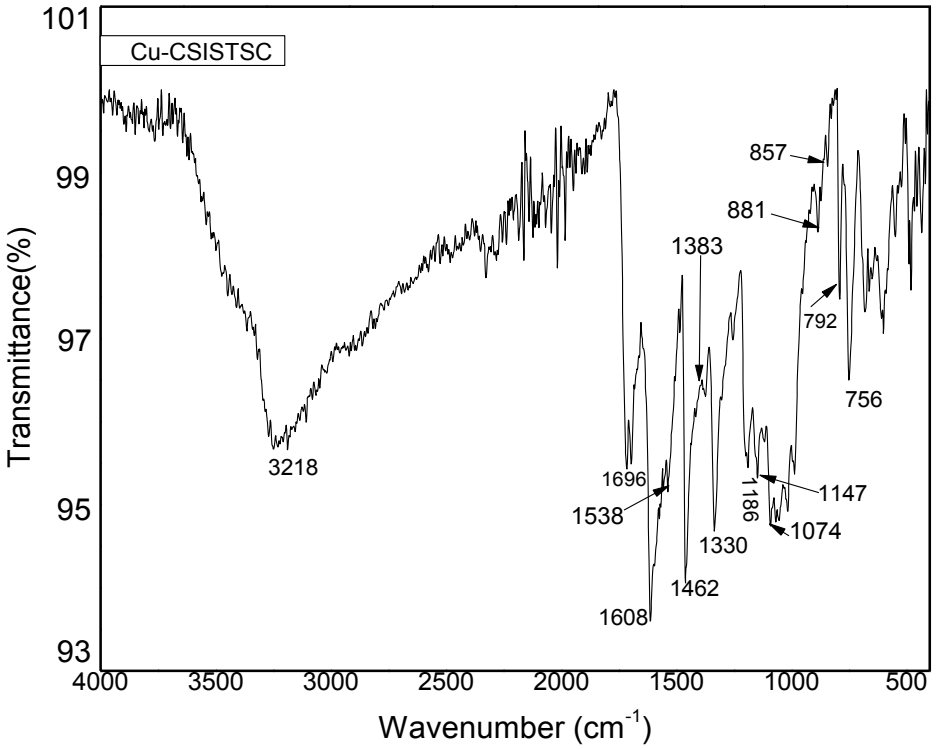


**Figure 86:** FT-IR spectrum of Cu-CSISTSC

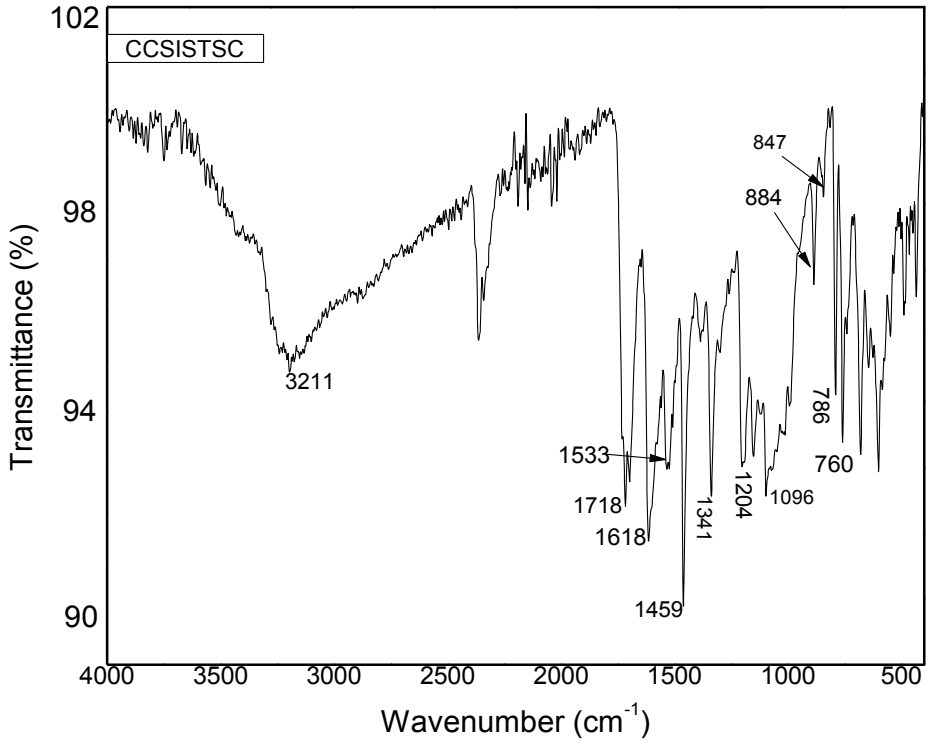


**Figure 87:** FT-IR spectrum of CCSISTSC

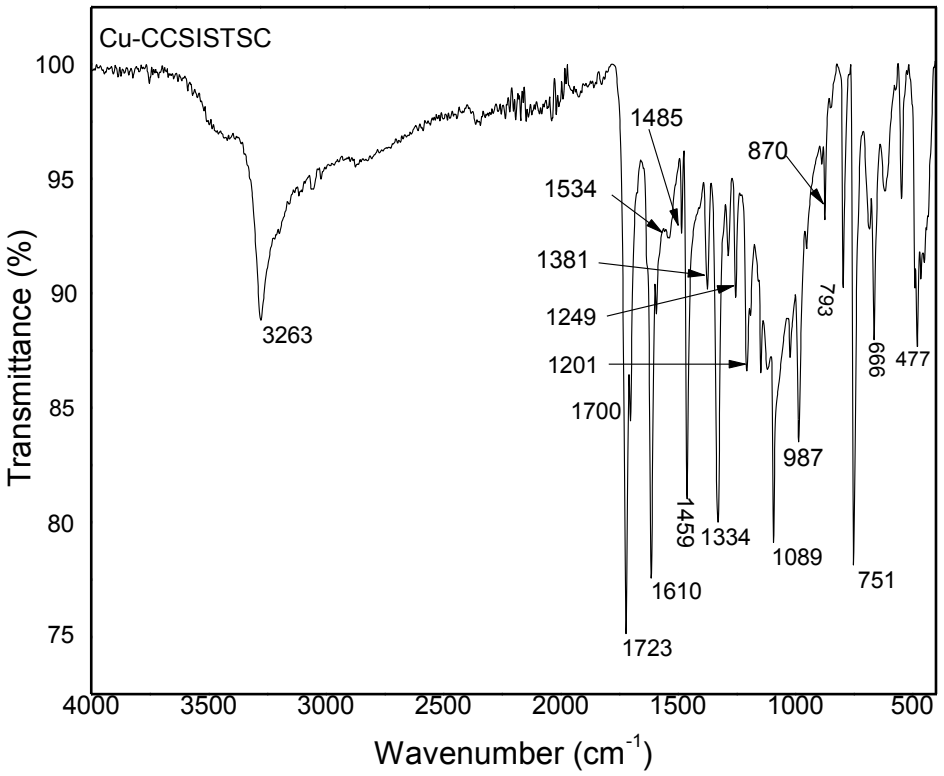


**Figure 88:** FT-IR spectrum of Cu-CCSISTSC

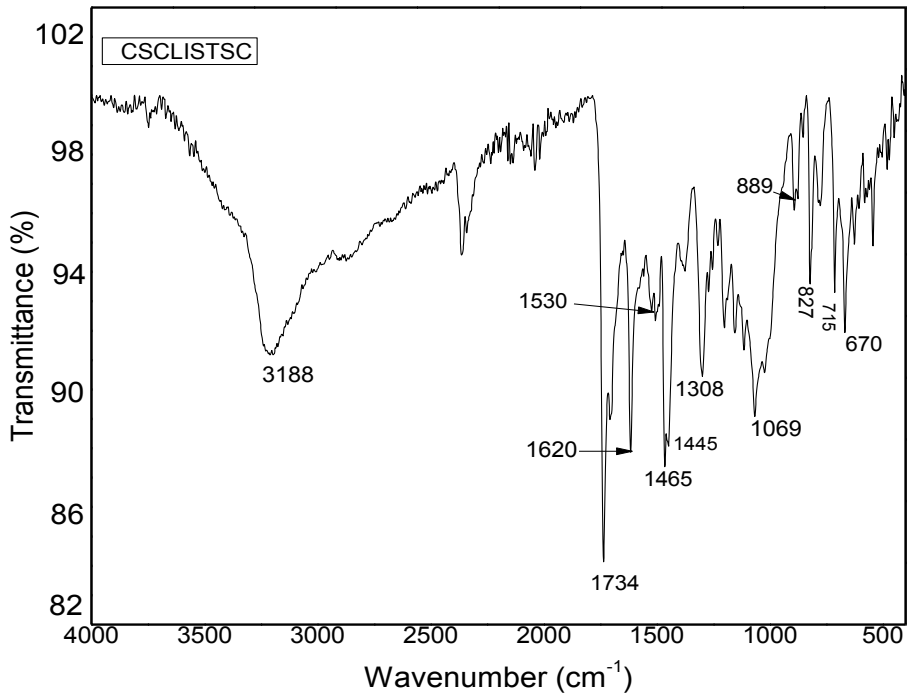


**Figure 89:** FT-IR spectrum of CSCLISTSC

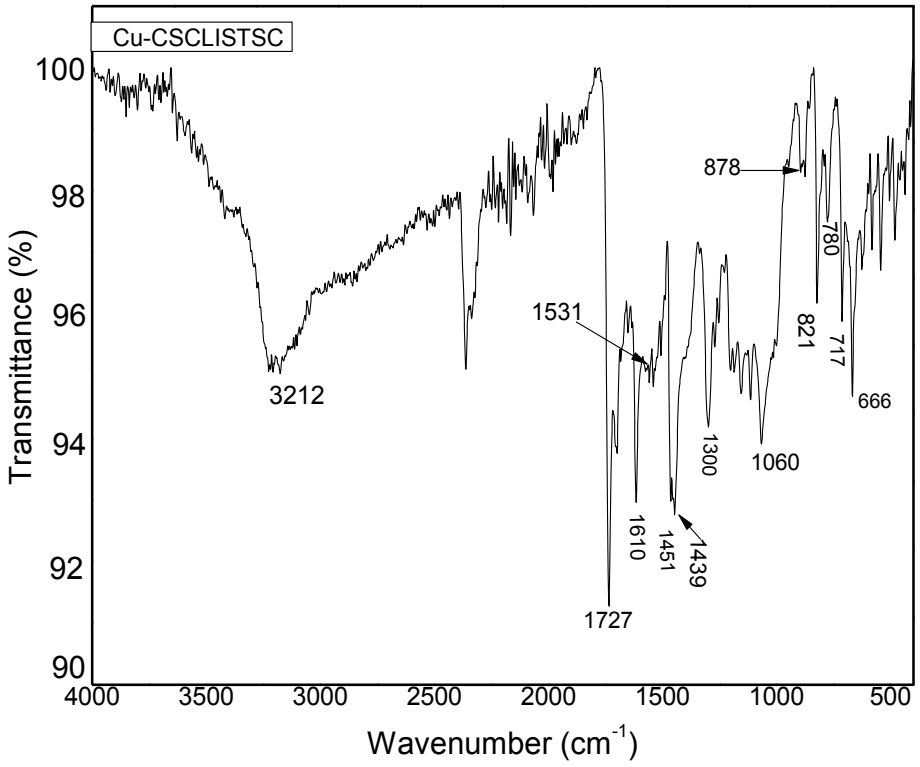


**Figure 90:** FT-IR spectrum of Cu-CSCLISTSC

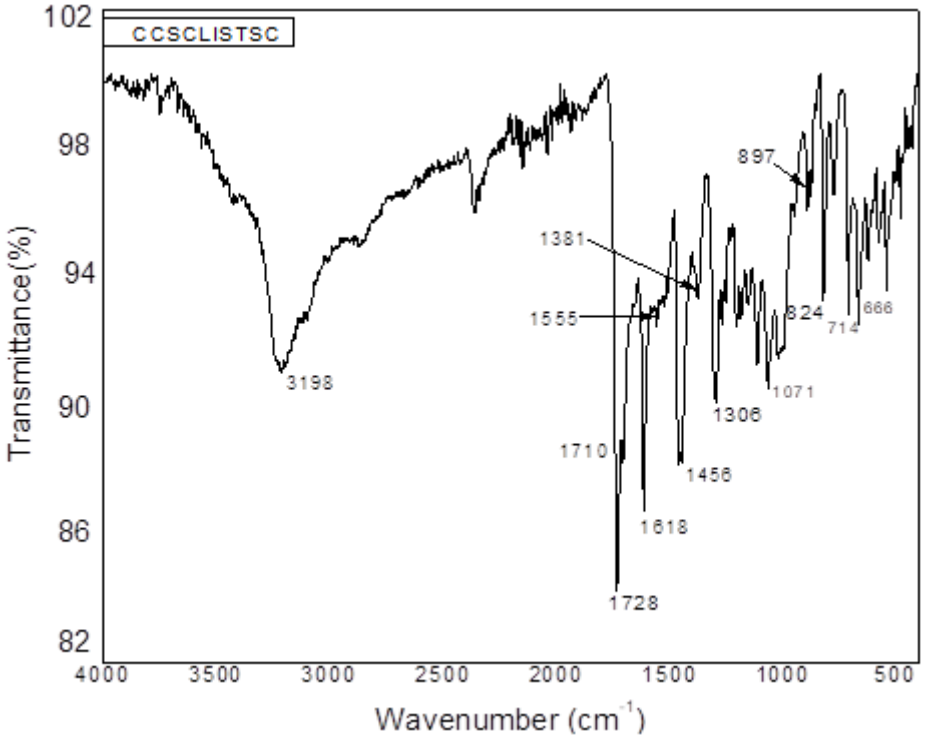


**Figure 91:** FT-IR spectrum of CCSCLISTSC

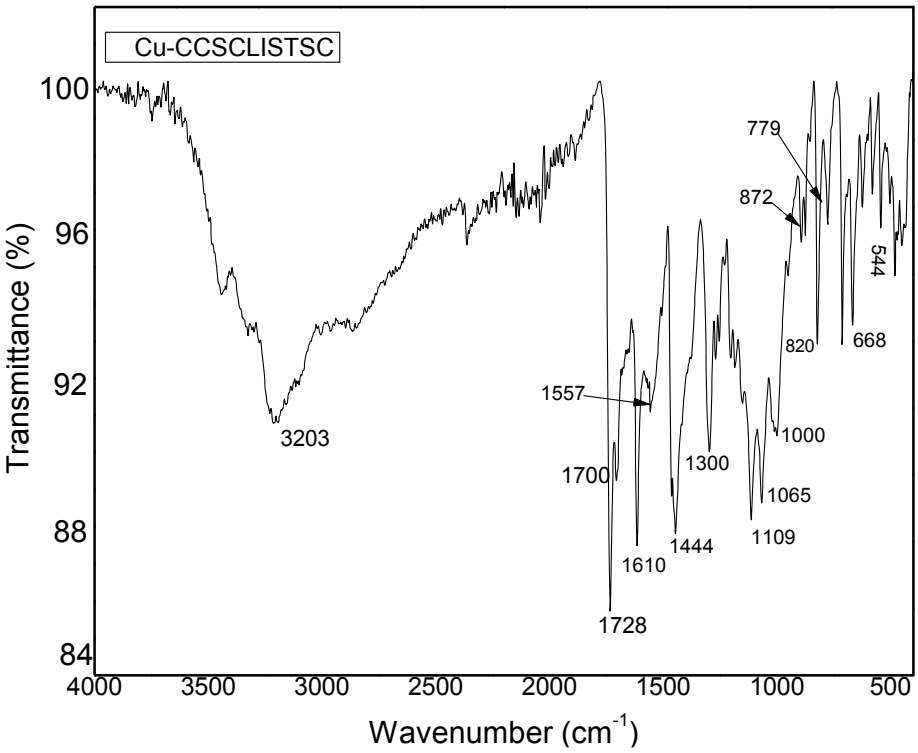


**Figure 92:** FT-IR spectrum of Cu-CCSCLISTSC

### 4.4.2.2. Solid State $^{13}C$ Nuclear Magnetic Resonance ($^{13}C$ NMR) Spectroscopy

Solid state $^{13}C$ NMR spectra of isatin and 5-chloroisatin chitosan thiosemicarbazones (figure 93, 94, 95 & 96) with the spectral data presented in table 31 were used in structural elucidation. The $^{13}C$ NMR spectra with weak C2 signal of chitosan at δ=55.08-57.63 ppm (Qin, *et al.*, 2012; Wang, *et al.*, 2016), -N=CH signals at δ= 164.28-167.25 ppm (Qin, *et al.*, 2012) and the signals due to C=O at δ= 175.09-177.50 (Qin, *et al.*, 2012) showed the partial deacetylation of acetamido group in the ring and the partial involvement of amino group at C2 towards the introduction of thiosemicarbazone group into chitosan. The characteristic peaks $CH_3$ (22.73-24.47 ppm), C6 (61.05-62.33 ppm), C3, C5 (73.59-75.54 ppm), C4 (83.01-84.55 ppm), C1 (102.93-104.94 ppm) were used to confirm the chitosan ring carbon atoms (Qin, *et al.*, 2012; Wang, *et al.*, 2016). The isatin ring carbon signals at δ= 110-149 ppm in CSISTSC, 113-147 ppm in CCSISTSC, 113-142 ppm in CSCLISTSC and 113-142 ppm in CCSCLISTSC (Chohan, *et al.*, 2004) showed the presence of isatin ring in these chitosan thiosemicarbazones. The broadening of peak at δ= 175.09-177.50 ppm was indicative of the superimposition of C=S and C=O signals (Qin, *et al.*, 2012). These results showed the partial substitution of amino group in C2 position of the chitosan ring by thiosemicarbazone moity.

**Table 31:** The solid state $^{13}C$ NMR spectral data (δ, ppm) of chitosan thiosemicarbazones: isatin and 5-chloroisatin analogues

| Compounds | Methyl carbon | C6 | C3, C5 | C4 | C1 | -N=CH | Isatin ring carbons | C=S & C=O superimposition |
|---|---|---|---|---|---|---|---|---|
| CSISTSC | 23.99 | 61.59 | 75.09 | 84.55 | 102.93 | 164.59 | 110-149 | 176.49 |
| CCSISTSC | 22.73 | 61.05 | 75.54 | 83.01 | 104.11 | 167.25 | 113-147 | 177.50 |
| CSCLISTSC | 24.47 | 62.33 | 75.39 | 83.82 | 104.94 | 164.34 | 113-142 | 175.09 |
| CCSCLISTSC | 22.85 | 61.06 | 73.59 | 83.15 | 104.13 | 164.28 | 113-142 | 177.27 |

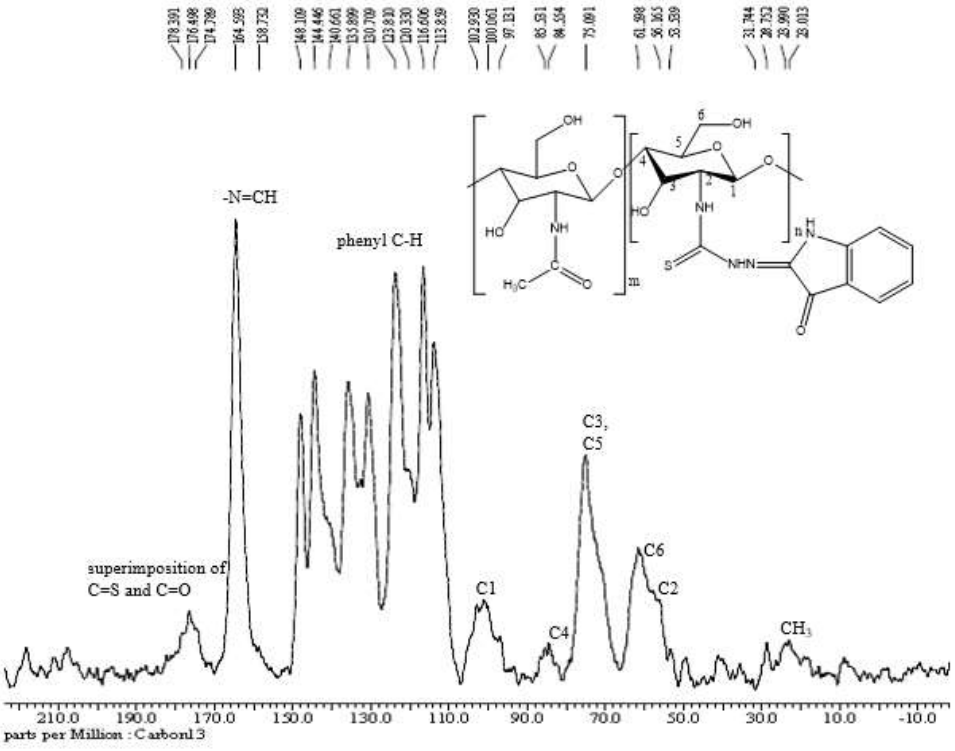


**Figure 93:** $^{13}C$ NMR spectrum of CSISTSC

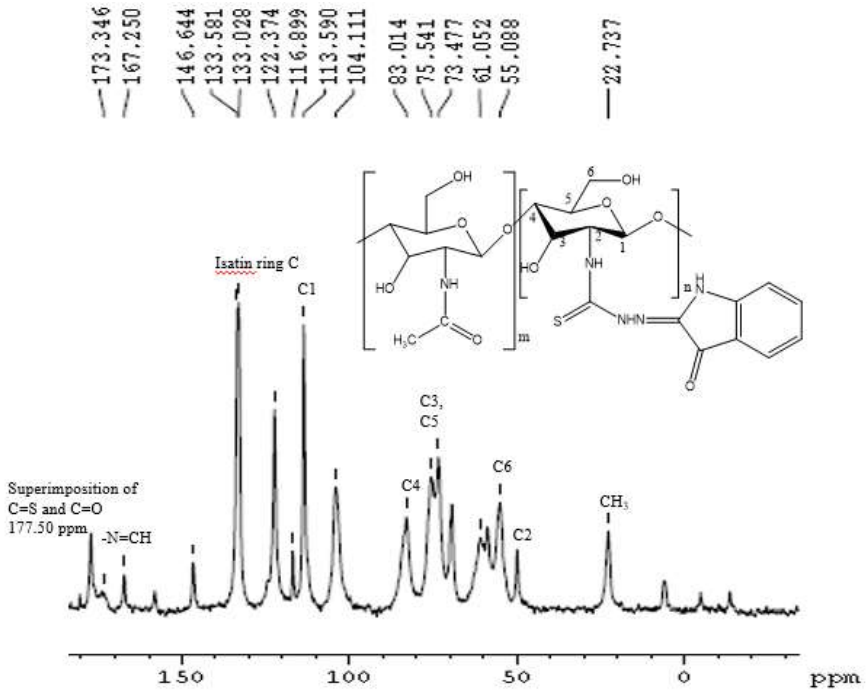


**Figure 94:** $^{13}C$ NMR spectrum of CCSISTSC

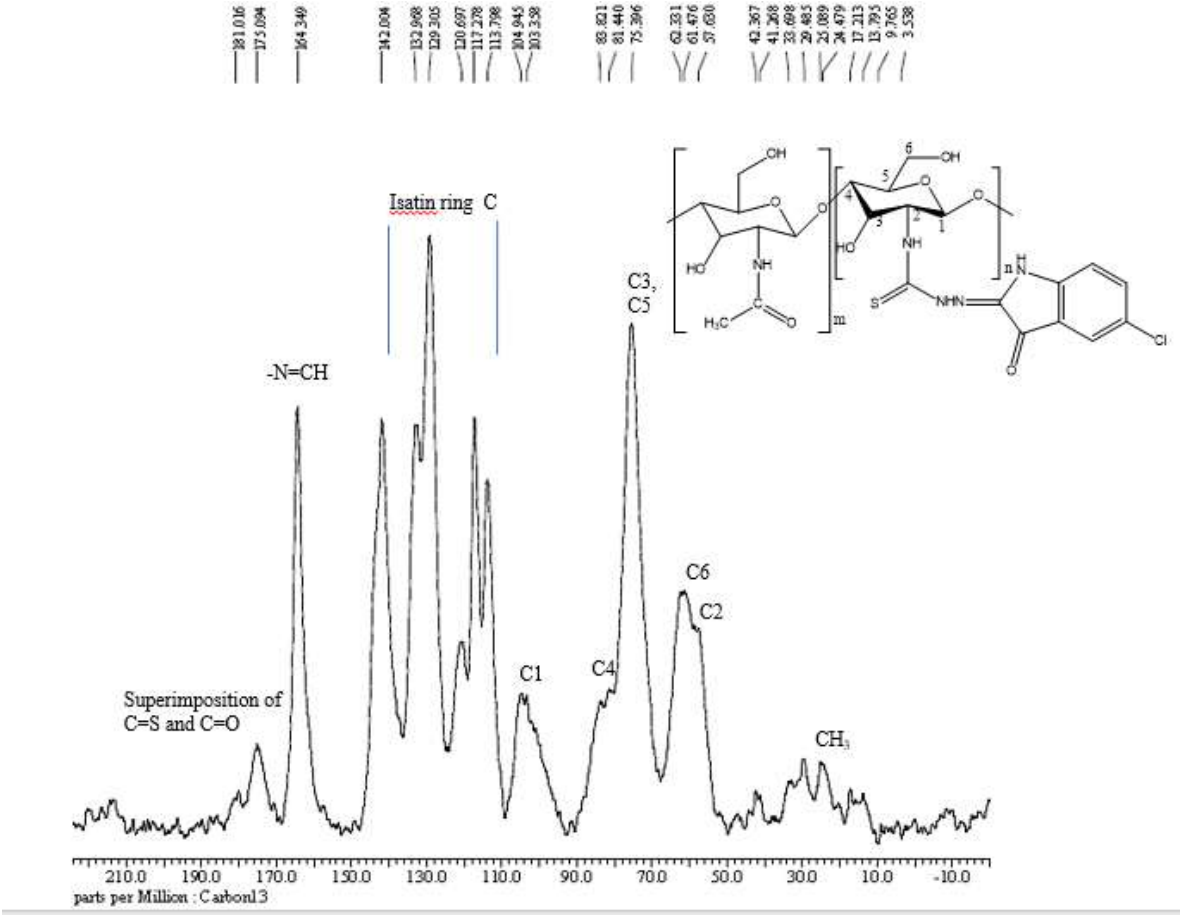


**Figure 95:** $^{13}C$ NMR spectrum of CSCLISTSC

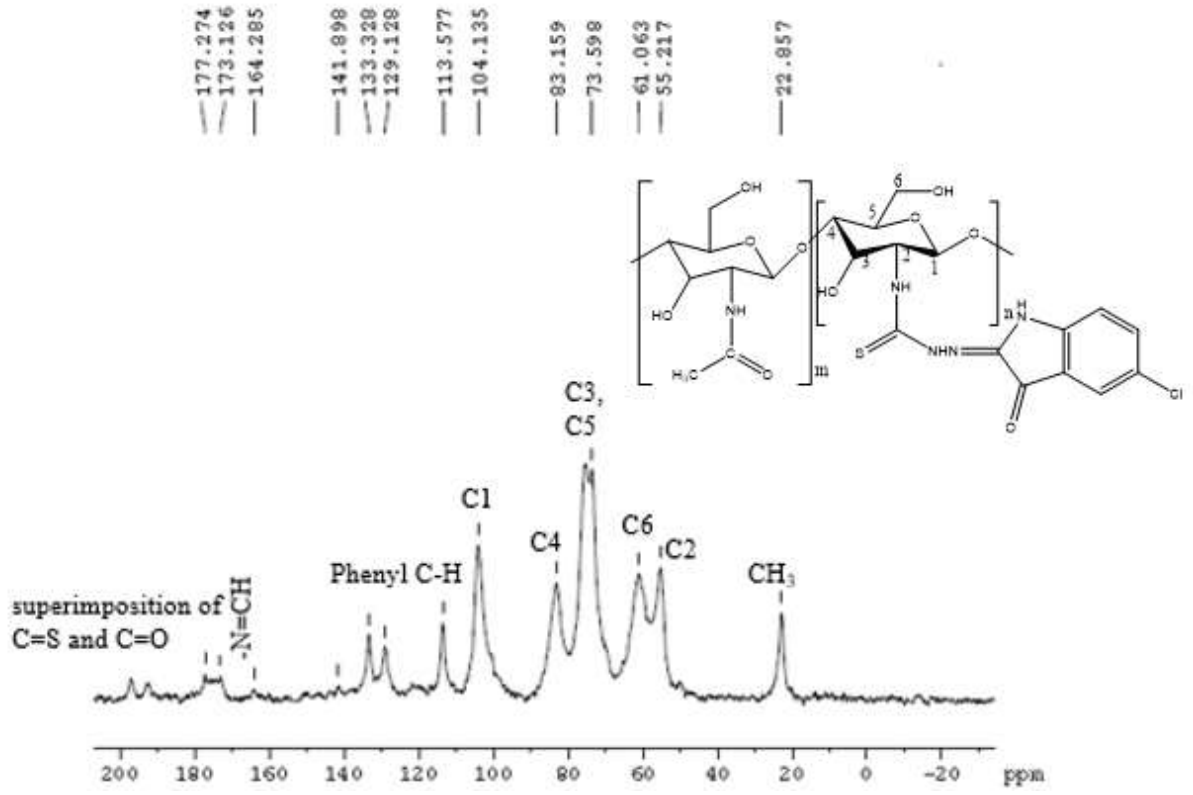


**Figure 96:** $^{13}$C NMR spectrum of CCSCLISTSC

### 4.4.2.3. Powder X Ray Diffraction (PXRD) Studies

The X Ray diffractograms of isatin and 5-chloroisatin based chitosan thiosemicarbazones (figure 97, 98, 99 & 100) showed the peaks in agreement with the reflection peaks obtainable in thiosemicarbazones at 2θ =12.53-49.79° in CSISTSC, 2θ = 7.08-27.12° in CCSISTSC, 2θ = 7.34-48.46° in CSCLISTSC, and 2θ = 9.2-26.14° in CCSCLISTSC (Hanumantharao, *et al.*, 2012; Santhakumari, *et al.*, 2010). The functionalisation of chitosan as chitosan thiosemicarbazones was due to introduction of thiosemicarbazone moiety in chitosan (Qin, *et al.*, 2012) and the shifting of chitosan peaks from 10° and 20° (Qin, *et al.*, 2012; Ramya, *et al.*, 2012). The appearance of new crystallinity peaks in addition to original chitosan crystallinity peaks with some shifting from 10° and 20° has been reported as the implication of imine group formation and the breakage of intra-molecular hydrogen bond of chitosan (Jiao, *et al.*, 2011).

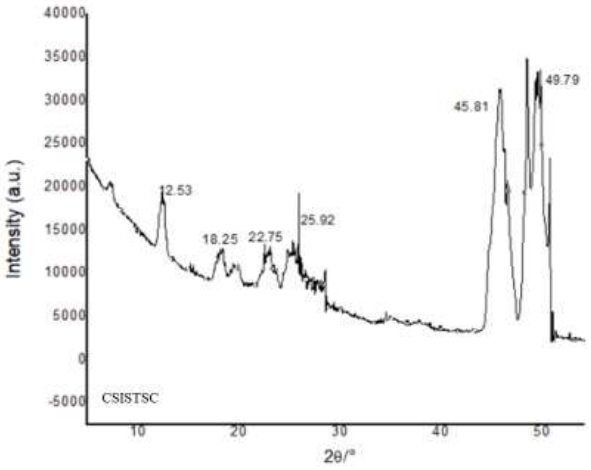


**Figure 97:** X ray diffractogram of CSISTSC

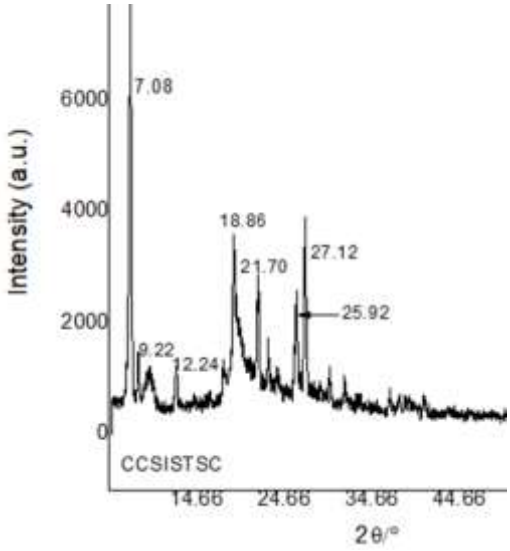


**Figure 98:** X ray diffractogram of CCSISTSC


**Figure 99:** X ray diffractogram of CSCLISTSC

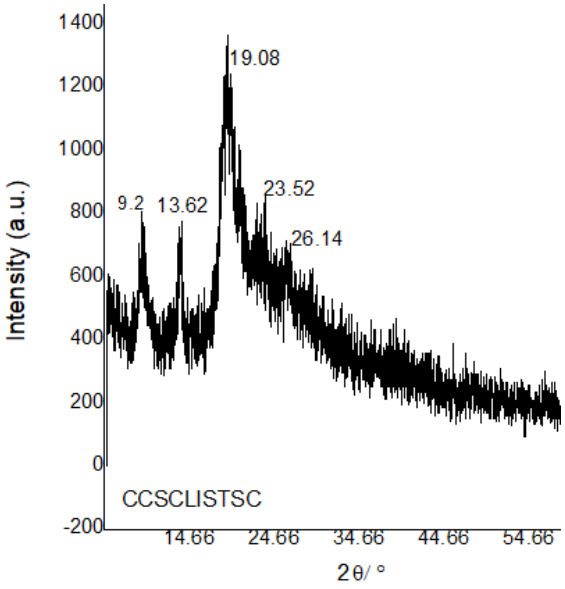


**Figure 100:** X ray diffractogram of CCSCLISTSC

The X ray diffractograms of copper(II) chitosan thiosemicarbazone complexes (figure 101, 102, 103 & 104) showed the new peaks corresponding to new crystallinity phases of chitosan copper(II) complexes showing the chelation of metal ions with different groups of thiosemicarbazone group at 2θ = 19.14°, 33.05° and 39.78°in Cu-CSISTSC, 2θ = 19.80°, 26.98° and 31.54° in Cu-CCSISTSC, 2θ = 20.54°, 26.18°, 30.13°, 36.04° and 39.62° in Cu-CSCLISTSC, 2θ = 35.96° and 39.44° in Cu-CCSCLISTSC (Antony, *et al.*, 2012; Dehaghi, *et al.*, 2014; Mekahlia, *et al.*, 2009; Qin, *et al.*, 2012; Wang, *et al.*, 2005). The deterioration in original crystallinity of chitosan as a result of chelation of metal ions and destruction of hydrogen bonds in chitosan was also shown by shifting and weakening of peaks due to chitosan (Wang, *et al.*, 2005).

Particle sizes, as calculated from *Debye-Scherrer formula* (Dehaghi, *et al.*, 2014; Kucukgulmez, *et al.*, 2011), of ligands corresponding to highest intensity peaks in the diffraction curves of were in a range of 11.55-30.69 nm; and the particle sizes of complexes were at 14.06 -55.49 nm. The degree of crystallinity as the crystallinity index (Kumirska, *et al.*, 2010; Lomadze *et al.*, 2005; Zhang, *et al.*, 2005) was 26.38-85.38% in these ligands, and 33.04-50.83% in their copper(II) complexes. Particle size was found to increase upon the complex formation, and crystallinity index was found independent of particle size, and $M_w$ and DDA.

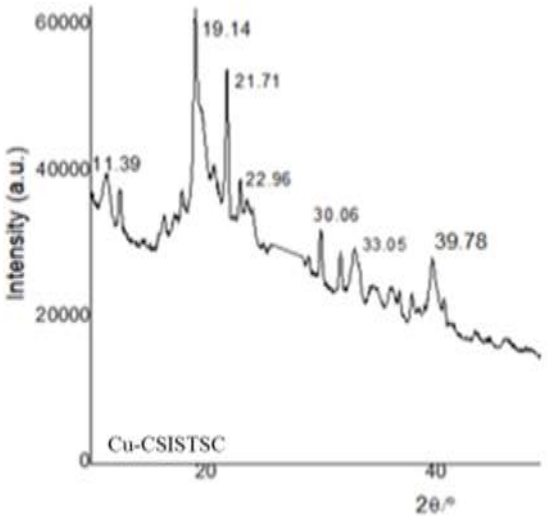


**Figure 101:** X ray diffractogram of Cu-CSISTSC

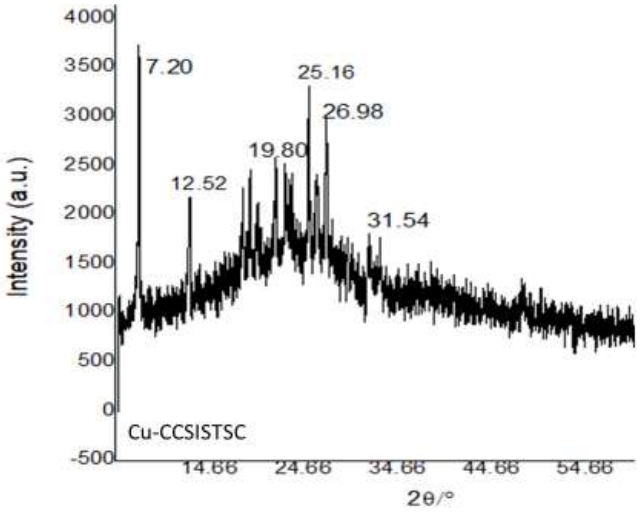


**Figure 102:** X ray diffractogram of Cu-CCSISTSC

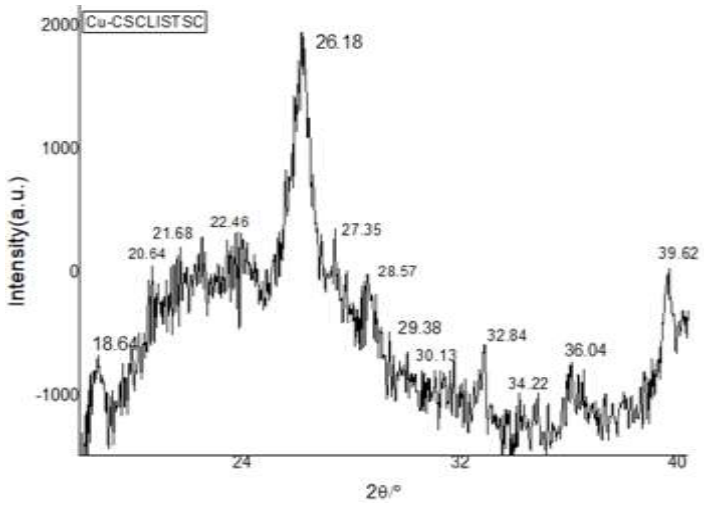


**Figure 103:** X ray diffractogram of Cu-CSCLISTSC

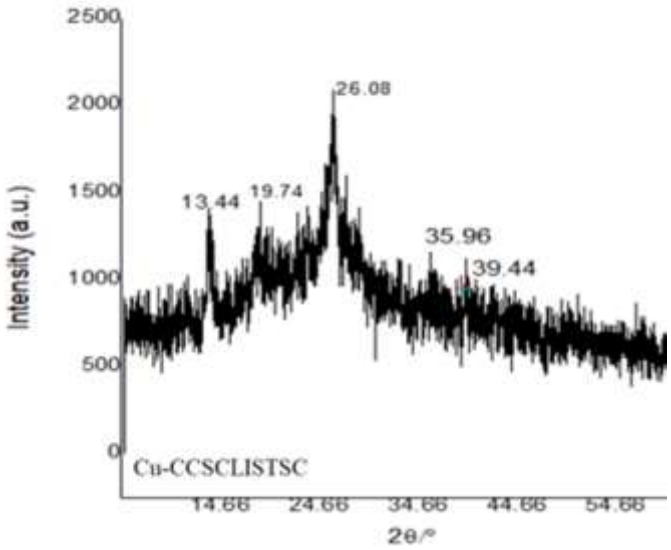


**Figure 104:** X ray diffractogram of Cu-CCSCLISTSC

The powder X ray diffraction data of isatin and 5-chloroisatin analogues of chitosan thiosemicarbazones and their copper(II) complexes are presented in table 32.

**Table 32:** The powder X ray diffraction data of chitosan thiosemicarbazones and their copper(II) complexes: isatin and 5-chloroisatin analogues

| Compounds | Selected functionality peaks, 2θ | | D (nm) | C.I. (%) |
|---|---|---|---|---|
| | Thiosemicarbazone crystallinity | Chitosan complex crystallinity | | |
| CSISTSC | 12.53°, 18.25°, 22.75°, 25.92°, 45.81°, 49.79° | - | 19.50 | 26.38 |
| Cu-CSISTSC | 11.39°, 21.71°, 22.96°, 30.06° | 19.14°,33.05°,39.78° | 45.48 | 34.65 |
| CCSISTSC | 7.08°, 9.22°, 12.24°, 18.86°, 21.70°, 25.92°, 27.12° | - | 30.69 | 85.38 |
| Cu-CCSISTSC | 7.20°, 12.52°,25.16° | 19.80°,26.98°,31.54° | 33.18 | 50.83 |
| CSCLISTSC | 7.34°, 12.61°, 18.25°, 22.98°, 25.82°, 28.47°, 45.92°, 48.46° | - | 11.55 | 67.76 |
| Cu-CSCLISTSC | 18.64°,21.68°,22.46°,27.36°, 28.57°, 29.38°, 32.84°, 34.22° | 20.54°,26.18°,30.13°,36. 04°, 39.62° | 14.06 | 33.04 |
| CCSCLISTSC | 9.2°, 13.62°, 19.08°, 23.52°, 26.14° | - | 17.80 | 48.09 |
| Cu-CCSCLISTSC | 13.44°,19.74°, 26.08° | 35.96°, 39.44° | 55.49 | 44.32 |

### 4.4.2.4. Elemental Microanalysis

The comparative study of calculated percentages of elements in chitosan thiosemicarbazones with completely deacetylated chitosan ring in their structure and the analytically found percentages of elements in the respective derivatives *viz.* isatin chitosan thiosemicarbazones

with monomer structure of unit formula weight 364 (78.80-82.85% DS) and 5-chloroisatin chitosan thiosemicarbazones with the monomer structure of unit formula weight 399 (80.92-91.76% DS) revealed the functionalization of chitosan as chitosan thiosemicarbazones with partial deacetylation and a substantial degree of substitution (Inukai, *et al.*, 1998; Melo, *et al.*, 2002; Pires, *et al.*, 2013; Qin, *et al.*, 2012) of amino group of chitosan by thiosemicarbazone moiety. The coordination behaviour of these derivatives and the formation of copper(II) chitosan complex due to a parallel reaction of copper(II) ion with non-functionalized chitosan was justifiable by the comparative study of the calculated percentages and the analytically found percentages of elements in copper(II) isatin chitosan thiosemicarbazones (monomer structure of unit formula weight 463) and copper(II) 5-chloroisatin chitosan thiosemicarbazones (monomer structure of unit formula weight 498). This phenomenon of simultaneous coordination of chitosan thiosemicarbazones and non-functionalized chitosan with copper(II) was particularly supported by higher value of estimated chlorine percentage than calculated chlorine percentage, and lower sulphur percentage. The elemental analysis data of isatin and 5-chloroisatin analogues of chitosan thiosemicarbazones and their copper(II) complexes are presented in table 33 and 34 respectively.

**Table 33:** Elemental (CHNS) microanalysis of chitosan thiosemicarbazones: isatin and 5-chloroisatin analogues: calculated (found)

| Compounds | C(%) | H(%) | N(%) | S(%) | DS(%) |
|---|---|---|---|---|---|
| CSISTSC | 49.45(47.305) | 4.39(4.165) | 15.38(14.309) | 8.79(7.914) | 82.85 |
| CCSISTSC | 49.45(47.871) | 4.39(4.628) | 15.38(14.406) | 8.79(7.601) | 78.80 |
| CSCLISTSC | 45.11(39.726) | 4.01(4.575) | 14.03(10.876) | 8.02(7.621) | 91.76 |
| CCSCLISTSC | 45.11(41.312) | 4.01(4.687) | 14.03(10.94) | 8.02(7.106) | 80.92 |

**Table 34:** Elemental (CHNS) microanalysis and chlorine estimation in copper(II) chitosan thiosemicarbazones: isatin and 5-chloroisatin analogues: calculated (found)

| Compounds | C(%) | H(%) | N(%) | S(%) | Cl(%) |
|---|---|---|---|---|---|
| Cu-CSISTSC | 38.87(36.37) | 3.45(3.756) | 12.09(11.71) | 6.91(5.798) | 7.66(10.18) |
| Cu-CCSISTSC | 38.87(36.01) | 3.45(3.980) | 12.09(10.974) | 6.91(5.209) | 7.66(9.98) |
| Cu-CSCLISTSC | 36.14(35.09) | 3.21(3.50) | 11.24(10.09) | 6.42(4.998) | 14.25(18.46) |
| Cu-CCSCLISTSC | 36.14(34.88) | 3.21(3.69) | 11.24(10.30) | 6.42(5.79) | 14.25(18.46) |

#### 4.4.2.5. Thermal Studies

Chitosan thiosemicarbazones of isatin and 5-chloroisatin were found to be associated with reasonably high thermal stability as shown by their thermogravimetric/differential thermal analysis (TG/DTA) curves (figure 105, 106, 107 & 108) and their thermal data presented in table 35. The two stages of weight loss corresponding to the loss of water at 100-200 °C and the chain disruption followed by backbone degradation at 200-1000 °C. In particular, there was a weight loss of 6.63% at 154 °C and a further loss by 30.25% at 318 °C in CSISTSC, 6.75% at 152 °C and a further loss by 31.05% at 325 °C in CCSISTSC, no weight loss till 220 °C followed by a loss of 26.63% weight loss at 347 °C and a further loss of 36.36% at 564 °C in CSCLISTSC and 16.80% at 150 °C with a further loss by 40.05% at 620 °C in CCSCLISTSC. There was a weight loss of about 55% in CSISTSC, 56% in CCSISTSC, 50% in CSCLISTSC, and 34% in CCSCLISTSC at 200-1000 °C. These thermal events showed a close correspondence with the reported thermal behaviour of chitosan showing the loss of water at 80-160 °C (Kittur, *et al.*, 2002; Qin, *et al.*, 2012) and the chain weakening and decomposition at 50-100 °C and 400 - 500 °C (Andrade, *et al.*, 2012; Kumari, *et al.*, 2017). One of the ligands CSCLISTSC was stable with no weight loss but in others, there was 6-16% weight loss at 120 °C. There was 47-55% weight loss due to chain degradation at 500 °C. This behaviour was in agreement with the two reported steps of weight loss of commercial chitosan *viz* 9% of weight loss at 120 °C due to loss of water and 43% of weight loss at 500 °C due to degradation of main chain of chitosan (Chethan, *et al.*, 2013; De Britto & Campana-Filho, 2004; Xu, *et al.*, 2010). On moderate heating at 400-500 °C, chitosan thiosemicarbazones were found to undergo more degradation than chitosan. Like chitosan, these derivatives also showed a rapid rate of decomposition at 100-400 °C and then almost a consistent rate of decomposition. The high thermal stability of thiosemicarbazones was further shown by residual mass of about 35% CSISTSC, 34% CCSISTSC, 47% CSCLISTSC and 42% CCSCLISTSC left at 1000 °C (Qu, *et al.*, 2000). The thermal decomposition pattern of chitosan thiosemicarbazones showing the substantial amount of unsaturated structure as residue at the terminal temperature of thermal analysis also accorded with their DTA peaks in an agreement with the TG weight loss in two steps at the range of 150- 400 °C and 400-900 °C.

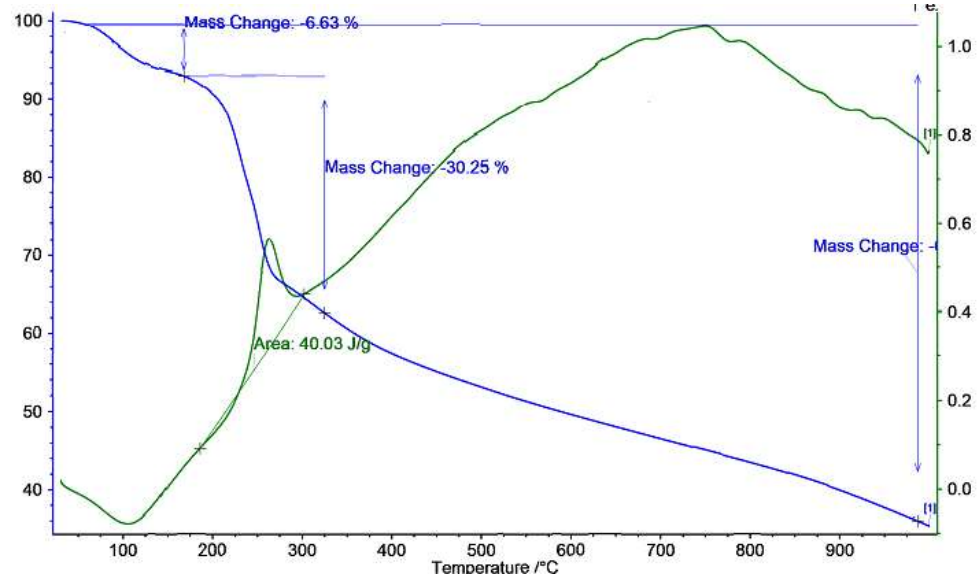


**Figure 105:** TG/DTA curves of CSISTSC showing the thermal events at different temperatures

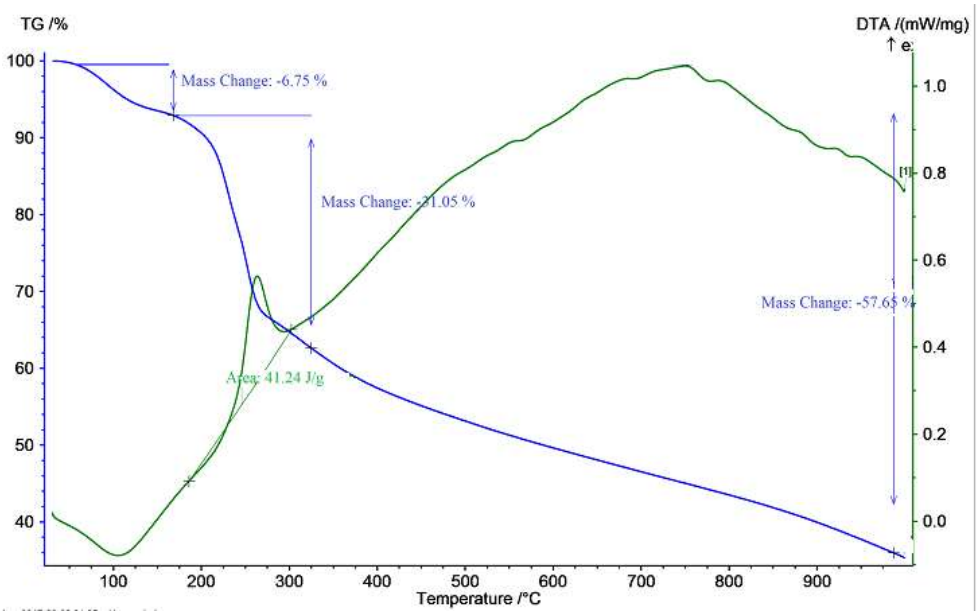


**Figure 106:** TG/DTA curves of CCSISTSC showing the thermal events at different temperatures

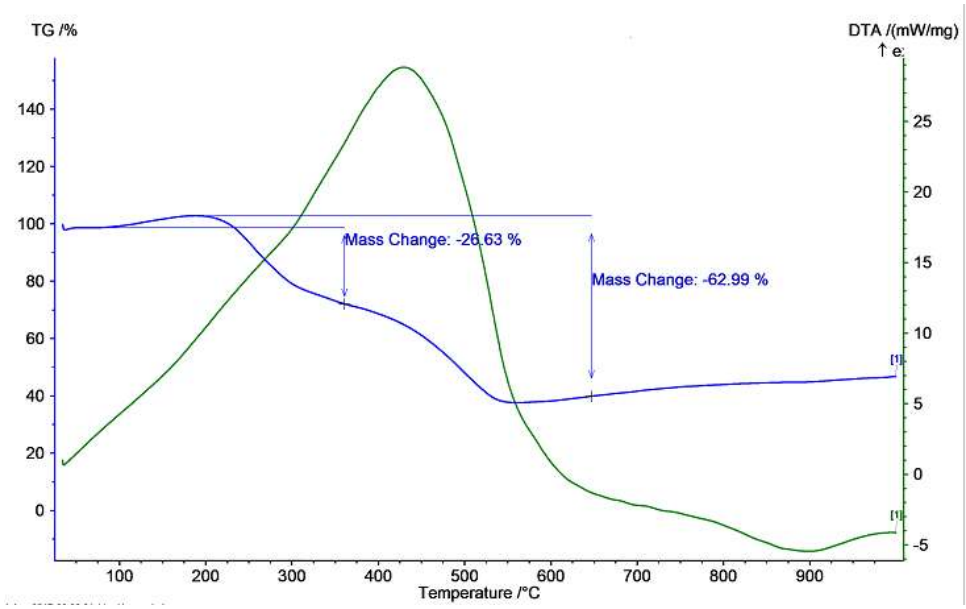


**Figure 107:** TG/DTA curves of CSCLISTSC showing the thermal events at different temperatures

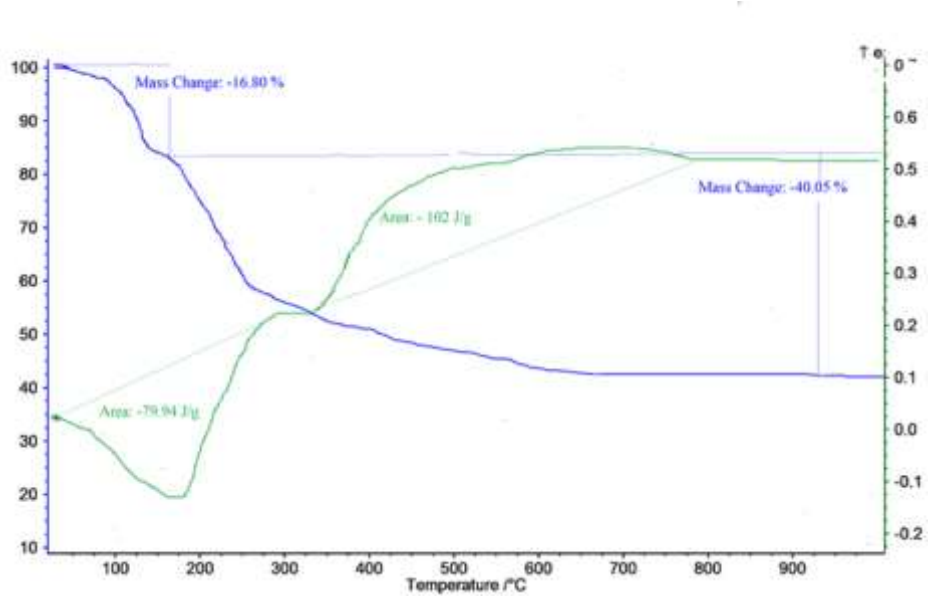


**Figure 108:** TG/DTA curves of CCSCLISTSC showing the thermal events at different temperatures

**Table 35:** TG/DTA data of thermal events in chitosan thiosemicarbazones: isatin and 5-chloroisatin analogues

| Compounds | Temperature (°C) | Weight loss (%) | Thermal event | % residue at 1000 °C |
|---|---|---|---|---|
| CSISTSC | 154 | 6.63 | Loss of water | 35 |
| | 318 | 30.25 | Chain disruption in progress | |
| | 200-1000 | 55 | Backbone degradation | |
| CCSISTSC | 152 | 6.75 | Loss of water | 34 |
| | 325 | 31.05 | Chain disruption in progress | |
| | 200-1000 | 56 | Backbone degradation | |

| | | | | |
|---|---|---|---|---|
| CSCLISTSC | 200<br>347 | -<br>26.63 | Stable up to 200°C<br>Loss of water, and abrupt disruption of backbone | 47 |
| | 200-1000 | 50 | Backbone degradation | |
| CCSCLISTSC | 150<br>620 | 16.80<br>40.05 | Loss of water<br>Chain disruption in progress | 42 |
| | 200-1000 | 34 | Backbone degradation | |

The TGA curves of complexes (figure 109, 110, 111 & 112) with the thermal data presented in table 36 showed their standard thermal stability (Kittur, *et al.*, 2002; Qu, *et al.*, 2000) with the loss of weight in three steps corresponding to the steady loss of weight up to 150- 200 °C, rapid loss of weight at 200-400 °C, and marginal loss of weight from 400-700 °C. In particular, there was a weight loss of 6.62% in Cu-CSISTSC, 6.60% in Cu-CCSISTSC, 2.6% in Cu-CSCLISTSC and 1.5% in Cu-CCSCLISTSC at 200 °C, and a weight loss of about 62.84% in Cu-CSISTSC, 62.86% in Cu-CCSISTSC, 49.97% in Cu-CSCLISTSC, and 49.52% in Cu-CCSCLISTSC at 200-500 °C. So, there was more degradation of complexes in the lower range of temperature at 200-500 °C and then a steady rate of decomposition, leaving about 19% Cu-CSISTSC, 19% Cu-CCSISTSC, 42% Cu-CSCLISTSC and 43% Cu-CCSCLISTSC as residue of the unsaturated structure at 700 °C. The results showed more thermal stability of high molecular weight synthetic chitosan analogues copper(II) thiosemicarbazones.

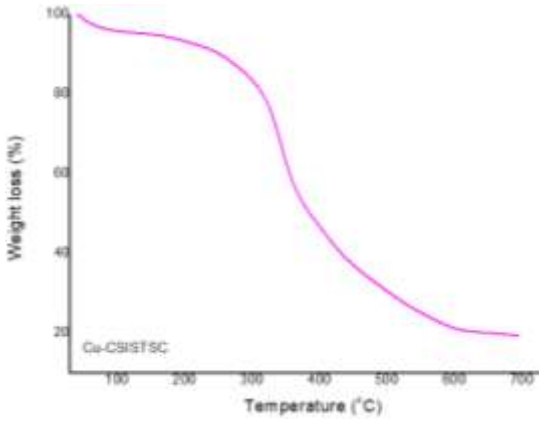


**Figure 109:** TGA curve of Cu-CSISTSC

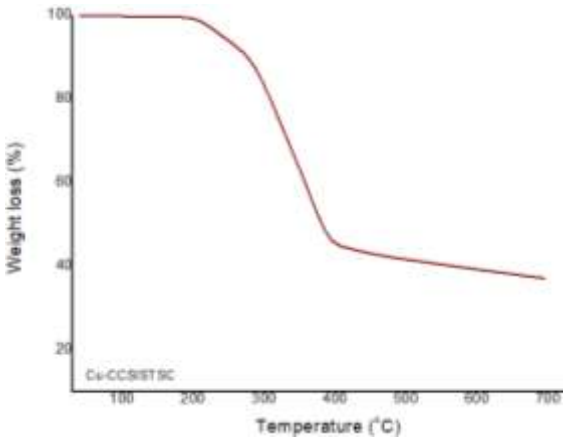


**Figure 110:** TGA curve of Cu-CCSISTSC

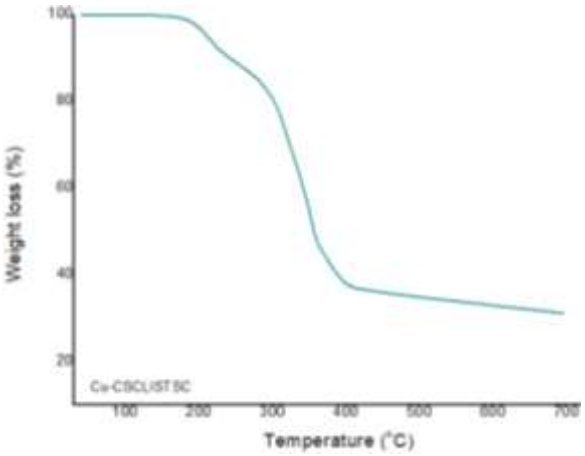


**Figure 111:** TGA curve of Cu-CSCLISTSC

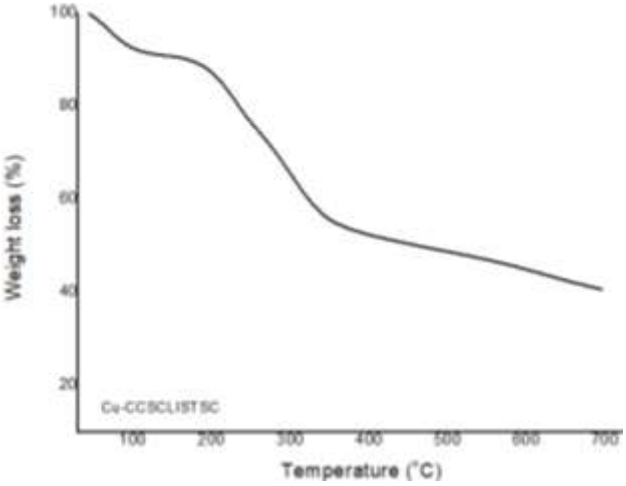


**Figure 112:** TGA curve of Cu-CCSCLISTSC

**Table 36:** TGA data of thermal events in copper(II) chitosan thiosemicarbazones: isatin and 5-chloroisatin analogues

| Compounds | Temperature (°C) | Weight loss % | Thermal event | % residue at 700 °C |
|---|---|---|---|---|
| Cu-CSISTSC | 200 | 6.62 | Loss of water | 19 |
| | 200-500 | 62.84 | Disruption of the chain | |
| | 500-700 | 11.50 | Further degradation of the backbone | |
| Cu-CCSISTSC | 200 | 6.60 | Loss of water | 19 |
| | 200-500 | 62.86 | Disruption of the chain | |
| | 500-700 | 11.82 | Further degradation of the backbone | |
| Cu-CSCLISTSC | 200 | 2.6 | Loss of water | 42 |
| | 200-500 | 49.97 | Disruption of the chain | |
| | 500-700 | 5.71 | Further degradation of the backbone | |
| Cu-CCSCLISTSC | 200 | 1.5 | Loss of water | 43 |
| | 200-500 | 49.52 | Disruption of the chain | |
| | 500-700 | 6.03 | Further degradation of the backbone | |

### 4.4.2.6. Magnetic Susceptibility Measurement and Electron Paramagnetic Resonance (EPR) Spectroscopy

The effective magnetic moment ($\mu_{eff}$) values of the complexes were a little higher at 1.84-1.89 BM than the spin-only moment of 1.73 BM. This was indicative of a low spin-spin coupling between unpaired electrons of different copper atoms (Ahmed & Lal, 2017) and a large spin orbit coupling constant of cupric ion that has been reported to increase the magnetic moment above the spin-only moment (Djord jevic, 1960). However, the magnetic

moments of the complexes were in a range to agree with the square planar or octahedral stereochemistry of the complexes as the magnetic moment values were <1.90 BM (Figgis, 1958).

The EPR spectra of complexes (figure 113, 114, 115 & 116) showed the non-resolution of hyperfine features due to copper (S =1/2 and I= 3/2) showing the presence of intermolecular spin-spin interactions and some degree of dimeric association of molecules (Bhadbhade & Srinivas, 1993; Suresh, *et al.*, 1996). The incomplete separation of paramagnetic centres causing the exchange broadening (Farra, *et al.*, 2011) at low frequency of 9.8 GHz at X-band has been reported to bring about the absence of hyperfine splitting (Farra, *et al.*, 2011). The spectra showed the feature in agreement with the presence of axial g tensors (Bennur, *et al.*, 2001), but the absence of hyperfine splitting made the g parallel tensors undetectable in the spectra. The square planar geometry of complexes was inferred on the basis of the values of magnetic moment below 1.90 BM (Figgis, 1958) and the EPR spectra showing an unpaired electron in d $_{x^2-y^2}$ orbital of Cu(II) centres (Garribba & Micera, 2006). The mononuclear structure of the complexes was justifiable as there was no half field peak at 1500 Gauss showing the presence of only one copper centre in a lacuna (Patel & Sadasivan, 2017). The values of effective magnetic moment and g values in EPR spectra are presented in table 37. The g values were 2.09 for Cu-CSISTSC (ν = 9.8623 GHz, $B_o$=3374 Gs = 337.4 mT), 2.08 for Cu-CCSISTSC (ν = 9.8615 GHz, $B_o$ = 3389 Gs = 338.9 mT), 2.09 for Cu-CSCLISTSC (ν = 9.8621 GHz, $B_o$ = 3368 Gs = 336.8 mT), and 2.07 for Cu-CCSCLISTSC (ν =9.8573 GHz, $B_o$ = 3394 Gs = 339.4 mT). The shifting of g value from $g_e$ (2.0023) was brought about by the spin orbital coupling and such a shifting of g value was dependent upon the covalent nature of complexes (Ahmed & Lal, 2017).

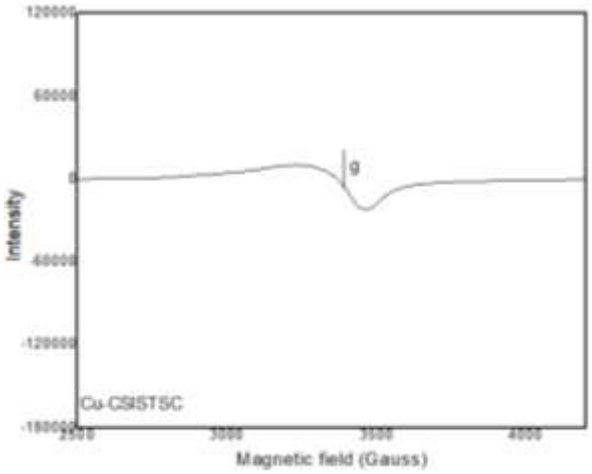


**Figure 113:** EPR spectrum of Cu-CSISTSC

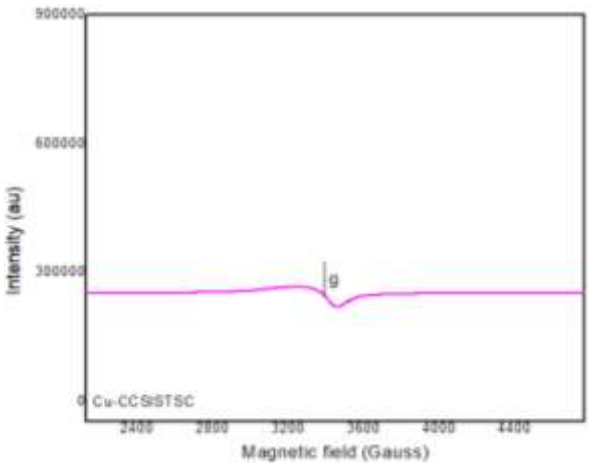


**Figure 114:** EPR spectrum of Cu-CCSISTSC

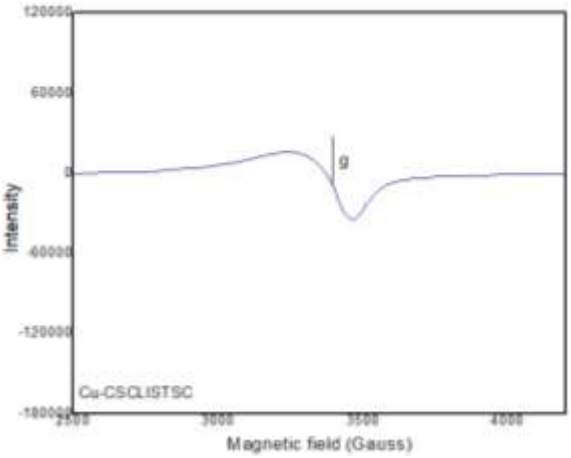


**Figure 115:** EPR spectrum of Cu-CSCLISTSC

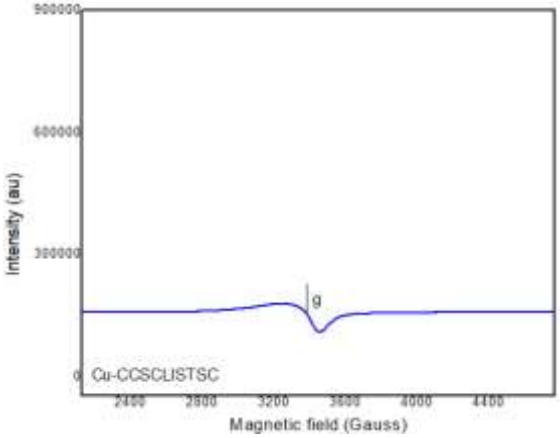


**Figure 116:** EPR spectrum of Cu-CCSCLISTSC

**Table 37:** Effective magnetic moments ($\mu_{eff}$) and EPR g values of copper(II) chitosan thiosemicarbazones: isatin and 5-chloroisatin analogues

| Complexes | $\mu_{eff}$, B. M. | EPR g value |
|---|---|---|
| Cu-CSISTSC | 1.88 | 2.09 |
| Cu-CCSISTSC | 1.84 | 2.08 |
| Cu-CSCLISTSC | 1.88 | 2.09 |
| Cu-CCSCLISTSC | 1.89 | 2.07 |

The results showed the thione sulphur, azomethine nitrogen, oxygen atom of carbonyl moiety and one chlorine atom used as the donor sites in coordination with copper(II) ion in the mononuclear distorted square planar complexes as shown in figure 117.

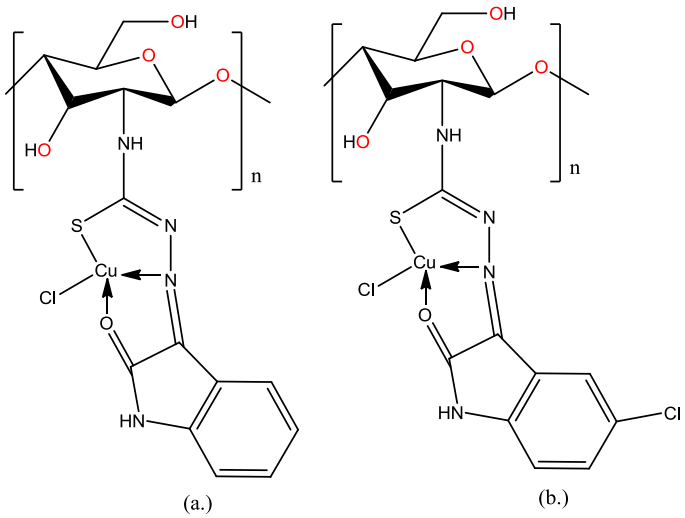


**Figure 117:** Proposed structure of complexes: (a). Cu-CSISTSC and Cu-CCSISTSC. (b). Cu-CSCLISTSC and Cu-CCSCLISTSC

## 4.5. Chitosan Thiosemicarbazones and their Copper(II) Complexes: Imidazole-2-carboxaldehyde and Thiophene-2-carboxaldehyde Analogues

### 4.5.1. Physical Characteristics

Physical characteristics of imidazole-2-carboxaldehyde and thiophene-2-carboxaldehyde thiosemicarbazones and their copper(II) complexes summarized in table 38 and 39 respectively show that the compounds are thermally stable crystalline solid with melting point above 300 °C, obtained in reasonably high yield of 69-75% ligands and 72-81% complexes. They were partially soluble in 1% acetic acid. Commercial chitosan analogues were more soluble in such aqueous acidic media.

**Table 38:** Physical characteristics of imidazole-2-carboxaldehyde chitosan thiosemicarbazones and their copper(II) complexes

| Compounds | Unit formula | Unit formula weight | Color | m.pt. (°C) | Yield (%) |
|---|---|---|---|---|---|
| CSIMTSC | $C_{11}H_{15}N_5O_4S$ | 313 | Yellow | >300 | 73 |
| CCSIMTSC | $C_{11}H_{15}N_5O_4S$ | 313 | Yellowish white | >300 | 71 |
| Cu-CSIMTSC | $C_{11}H_{15}N_5O_4SCuCl$ | 412 | Greenish yellow | >300 | 78 |
| Cu-CCSIMTSC | $C_{11}H_{15}N_5O_4ScuCl$ | 412 | Greenish | >300 | 72 |

**Table 39:** Physical characteristics of thiophene -2-carboxaldehyde chitosan thiosemicarbazones and their copper(II) complexes

| Compounds | Unit formula | Unit formula weight | Color | m.pt. (°C) | Yield (%) |
|---|---|---|---|---|---|
| CSTHPTSC | $C_{12}H_{15}N_3O_4S_2$ | 329 | Yellow | >300 | 75 |
| CCSTHPTSC | $C_{12}H_{15}N_3O_4S_2$ | 329 | Yellowish white | >300 | 69 |
| Cu-CSTHPTSC | $C_{12}H_{15}N_3O_4S_2CuCl_2$ | 463 | Greenish yellow | >300 | 81 |
| Cu-CCSTHPTSC | $C_{12}H_{15}N_3O_4S_2CuCl_2$ | 463 | Greenish | >300 | 77 |

### 4.5.2. Characterization

#### 4.5.2.1. Fourier Transform- Infrared (FT-IR) Spectroscopy

The broad translocations in the FT-IR spectra of chitosan thiosemicarbazone ligands (figure 118, 120, 122 & 124) and complexes (figure 119, 121, 123 & 125) were at 3200-3500 $cm^{-1}$ due to O-H stretching vibration (Zhong, *et al*., 2011), and the ν (N-H) stretches at 3100-3350 $cm^{-1}$ (Sashikala & Shafi, 2014; Zhong, *et al*., 2011) were blended with ν (O-H) stretches. The

bands at 2865-2886 $cm^{-1}$ were attributed to ν (C-H) stretches (Qin, *et al*., 2012). The combination of thiosemicarbazide group NH-CS-NH with C=O group from carboxaldehyde to yield chitosan thiosemicarbazones was evident from the absence of reported band at 1550 $cm^{-1}$ owing to ν (NH-CS-NH) of thiosemicarbazide (Qin, *et al*., 2012). The combination of amino group at C2 position of chitosan with C=O group from carboxaldehyde to give the (C=N–) bonds was evident from the absence of ν (C=O) stretch of chitosan at 1645 $cm^{-1}$, the presence of weak residual peaks due to acetamido moiety of chitin at 1550-1558 $cm^{-1}$ (Zhong, *et al.*, 2010) and the appearance of (C=N–) bands at 1619-1627 $cm^{-1}$ (Sashikala & Shafi, 2014; Saud, *et al*., 2019; Sharma, *et al*., 2005; Triana-Guzmán, *et al.*, 2018; Zhong, *et al*., 2010). The partial functionalization of chitosan as chitosan thiosemicarbazones was shown by the persistence of primary ν (NH) bends at 1540-1555 $cm^{-1}$ (Silva, *et al*., 2015; Zhong, *et al*., 2011). The appearance of strong to medium ν (C=S) bands at the range of 1072 to 1160 $cm^{-1}$ *viz.* in agreement with the reported frequency of ν (C=S) at 1028 to 1082 $cm^{-1}$ (Bharti, *et al*., 2003), 1098 to 1112 $cm^{-1}$ (Sharma, *et al*., 2005), 1165 $cm^{-1}$ (Alomar, *et al*., 2009), and the disappearance of ν (C-SH) band at a range of 2500 to 2600 $cm^{-1}$ were indicatives of the continuation of the thione form of thiosemicarbazones (Bharti, *et al*., 2003). The peaks at the range of 1370 to 1381 $cm^{-1}$ in imidazole-2-carboxaldehyde chitosan thiosemicarbazones and at 1315 $cm^{-1}$ in thiophene-2-carboxaldehyde chitosan thiosemicarbazones also accorded with the frequency range of ν (C=S) stretches (Aneesrahman, *et. al.*, 2019; Joseph, *et al.*, 2006). The absorption bands at 1003-1116 $cm^{-1}$ showed the asymmetric stretching vibration of the C–O–C skeleton (Qin, *et al*., 2012).

There was lowering of ν (C=N) by 7 to 25 $cm^{-1}$ from 1619-1627 $cm^{-1}$ in uncoordinated thiosemicarbazones to 1602-1618 $cm^{-1}$ in their respective complexes, and this confirmed the coordination with metal ion from azomethine nitrogen (Singh & Mishra,1986). There was lowering of ν (C=S) bands by 10-14 $cm^{-1}$ from 1072–1160 $cm^{-1}$ in chitosan thiosemicarbazones to 1058-1150 $cm^{-1}$ in their respective complexes, and this indicated the sulphur atom in coordination with metal ion (Bharti, *et al*., 2003). Further, the coordination of sulphur in copper(II) chitosan imidazole-2-thiosemicarbazones was also indicated by 5-21 $cm^{-1}$ lowering of ν (C=S) bands from 1370-1381 $cm^{-1}$ in imidazole-2-thiosemicarbazones to 1349-1376 $cm^{-1}$ in the respective complexes. The coordination of sulphur in copper(II) chitosan thiophene 2-carboxaldehyde thiosemicarbazones was also indicated by 8-9 $cm^{-1}$ lowering of ν (C=S) bands from 1315 $cm^{-1}$ in thiophene-2-carboxaldehyde thiosemicarbazones to 1306-1307 $cm^{-1}$ in their respective complexes. There were no changes in ν (C–S–C) of thiophene ring at the narrow range of 704 to 706 $cm^{-1}$ (Mathew, *et al*., 2016)

in thiophene-2-carboxaldehyde thiosemicarbazones and the respective complexes. It showed the non-participation of the ring sulphur of thiophene in coordination with metal ion (Bharti, *et al*., 2003). The non-participation of the ring sulphur of thiophene in coordination with metal ion was also shown by no shifting of ν (C=S) band at 1377 $cm^{-1}$ (Aneesrahman, *et. al*., 2019; Joseph, *et al*., 2006) in thiophene-2-carboxaldehyde thiosemicarbazones and their respective complexes. The ν (N–H) broad band stretches remained almost unaltered by coordination. The thionic sulphur possesses more nucleophilic character than the ring sulphur in thiophene. Consequently, there is coordination of thionic sulphur instead of sulphur atom of thiophene with copper(II) ion (Bharti, *et al*., 2003). The bands at the range of 1438 to 1446 $cm^{-1}$ in chitosan imidazole-2-thiosemicarbazones were due to ν (C-N) stretches in the ring of imidazole (Madanagopal, *et al*., 2017), and these frequencies were also owed by ν (C=C) and ν (C=N) stretches (Madanagopal, *et al*., 2017). The downward shifting of these stretches by 21-28 $cm^{-1}$ to 1417-1418 $cm^{-1}$ in the respective complexes indicated that there is predominant development of double bond character in (C=N) bond inside the ring as a result of resonance, and there is involvement of imidazole ring nitrogen in coordination (Munde, *et al*., 2009). Further, the involvement of imidazole ring vibration associated to an active frequency was shown by the presence of its peak with a strong intensity (Madanagopal, *et al*., 2017). The mutual neutralization of metal-ligand charges in copper(II) chitosan imidazole-2-thiosemicarbazones was attributed to thiolate sulphur coordination. Hence, the terdentate nature of chitosan imidazole-2-thiosemicarbazones is justifiable in the light of deprotonation of H-N-C=S group that makes sulphur exist in thiolate form (Joseph, *et al*., 2004). The FT-IR spectral data (table 40 & 41) showed that chitosan imidazole-2-carboxaldehyde thiosemicarbazones were NNS terdentate and thiophene-2-carboxaldehyde chitosan thiosemicarbazones were NS bidentate ligands to copper(II) ion.

**Table 40:** The selected FT-IR bands ($cm^{-1}$) of chitosan thiosemicarbazones and their complexes: imidazole-2-carboxaldehyde analogues

| Compounds | ν(C=N) | ν(C=S) | ν(C-N, imidazole) | ν(N-H) |
|---|---|---|---|---|
| CSIMTSC | 1619 | 1072, 1381 | 1446 | 1540 |
| Cu-CSIMTSC | 1605 | 1058, 1376 | 1418 | 1547 |
| CCSIMTSC | 1627 | 1060, 1370 | 1438 | 1541 |
| Cu-CCSIMTSC | 1602 | 1050, 1349 | 1417 | 1555 |

**Table 41:** The selected FT-IR bands ($cm^{-1}$) of chitosan thiosemicarbazones and their complexes: thiophene-2-carboxaldehyde analogues

| Compounds | ν(C=N) | ν(C=S) | ν (C–S–C) (ring) of thiophene | ν(N-H) |
|---|---|---|---|---|
| CSTHPTSC | 1625 | 1072, 1315 | 706 | 1555 |
| Cu-CSTHPTSC | 1618 | 1061, 1306 | 706 | 1557 |
| CCSTHPTSC | 1624 | 1072, 1315 | 705 | 1541 |
| Cu- CCSTHPTSC | 1614 | 1061, 1307 | 704 | 1543 |

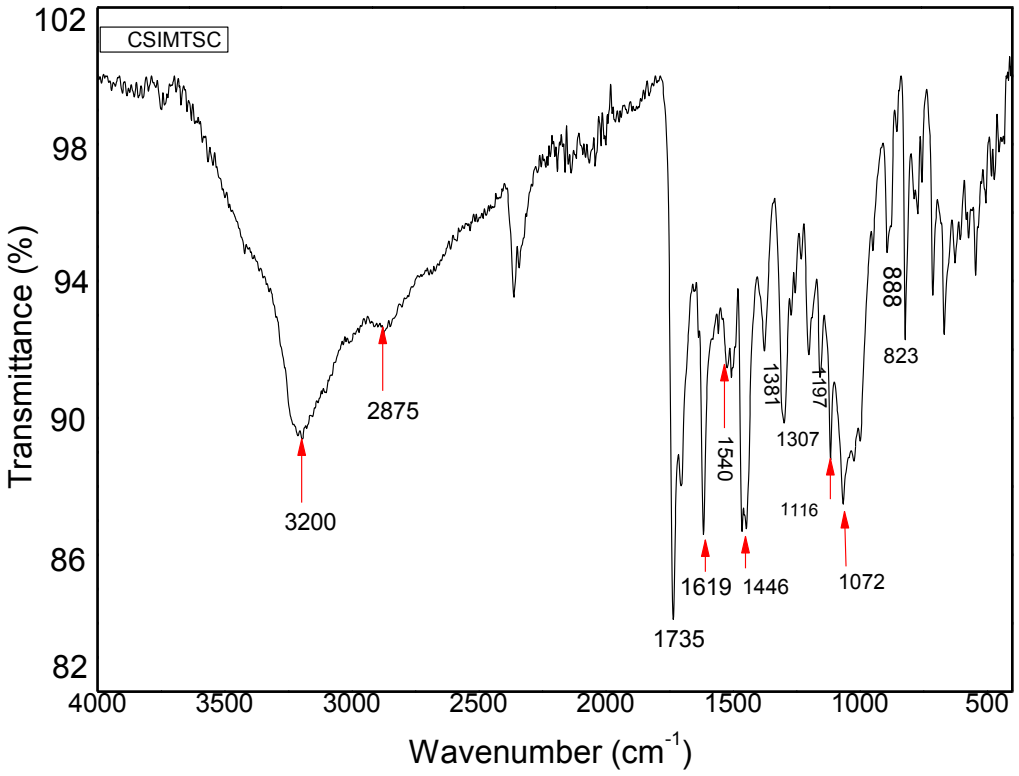


**Figure 118:** FT-IR spectrum of CSIMTSC

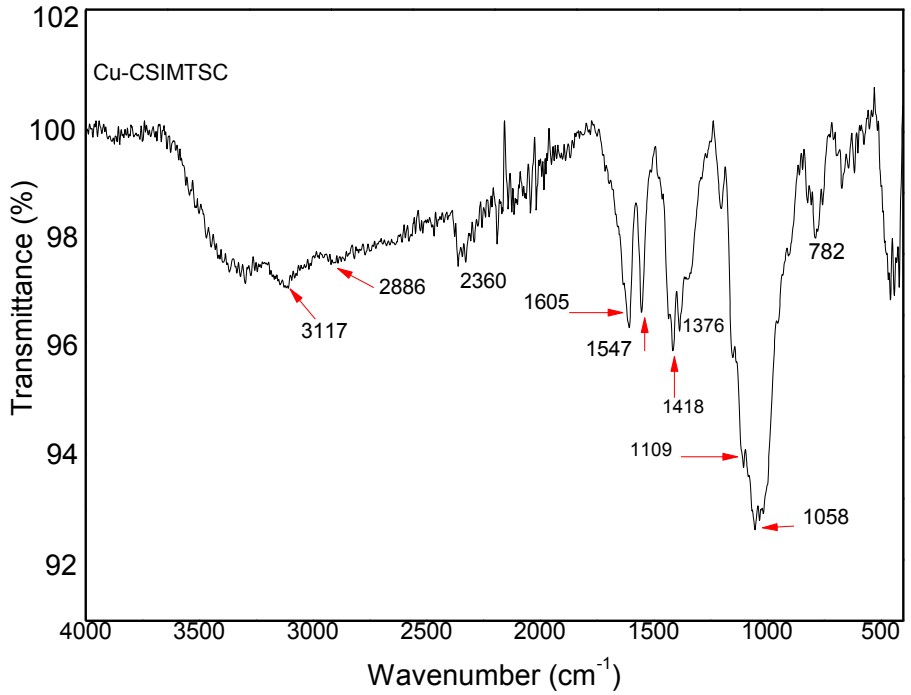


**Figure 119:** FT-IR spectrum of Cu-CSIMTSC

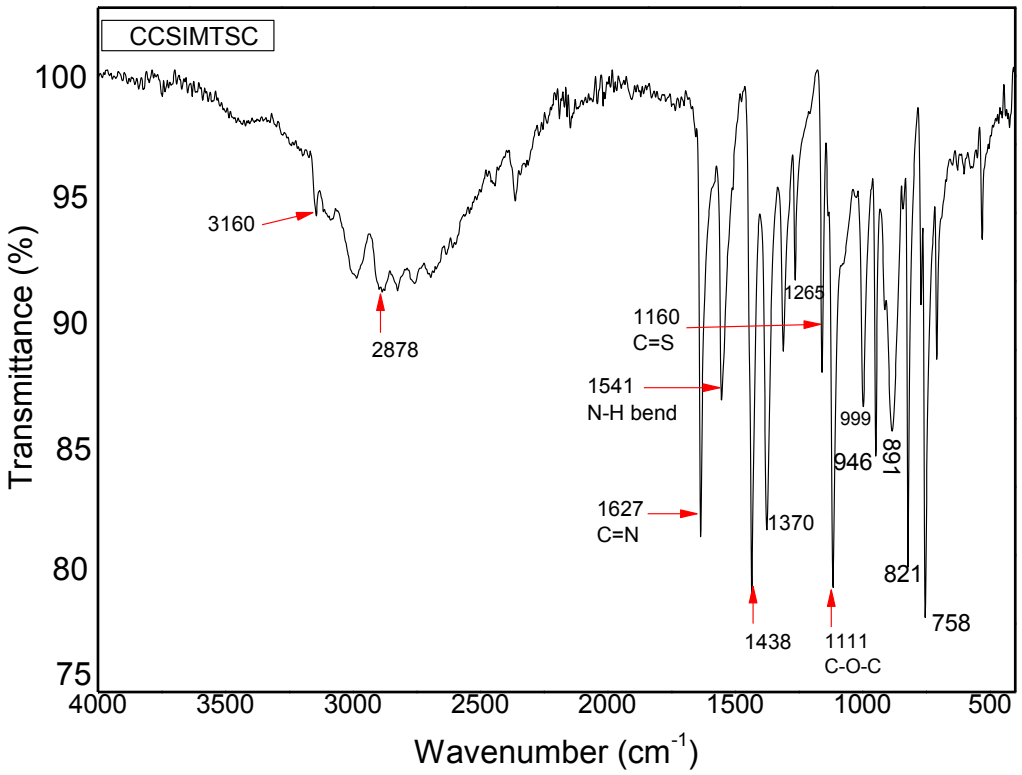


**Figure 120:** FT-IR spectrum of CCSIMTSC

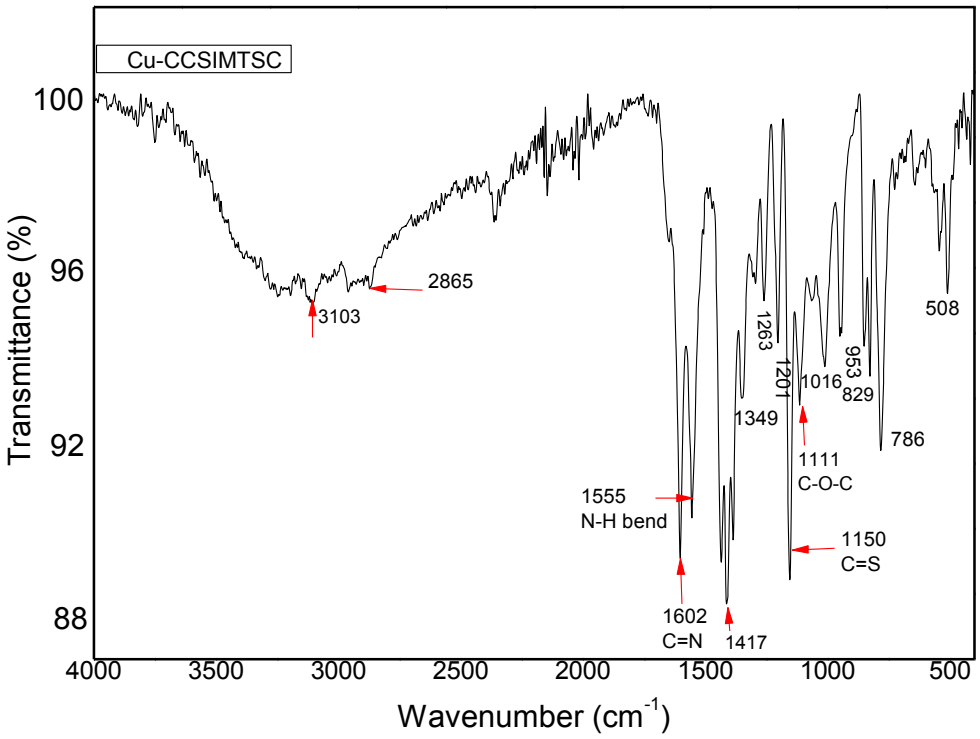


**Figure 121:** FT-IR spectrum of Cu-CCSIMTSC

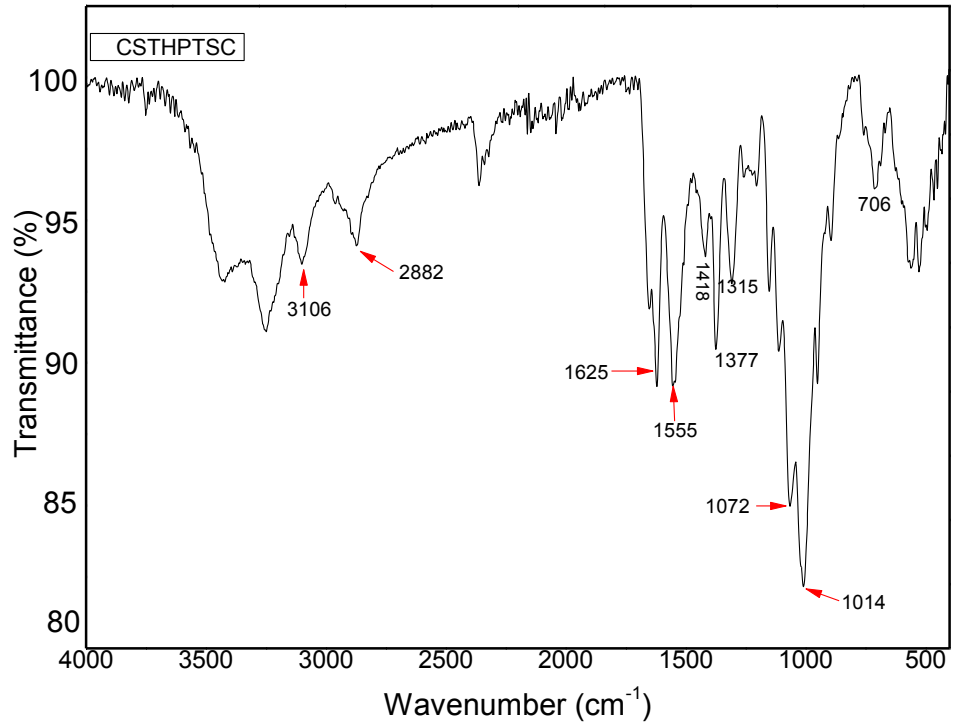


**Figure 122:** FT-IR spectrum of CSTHPTSC

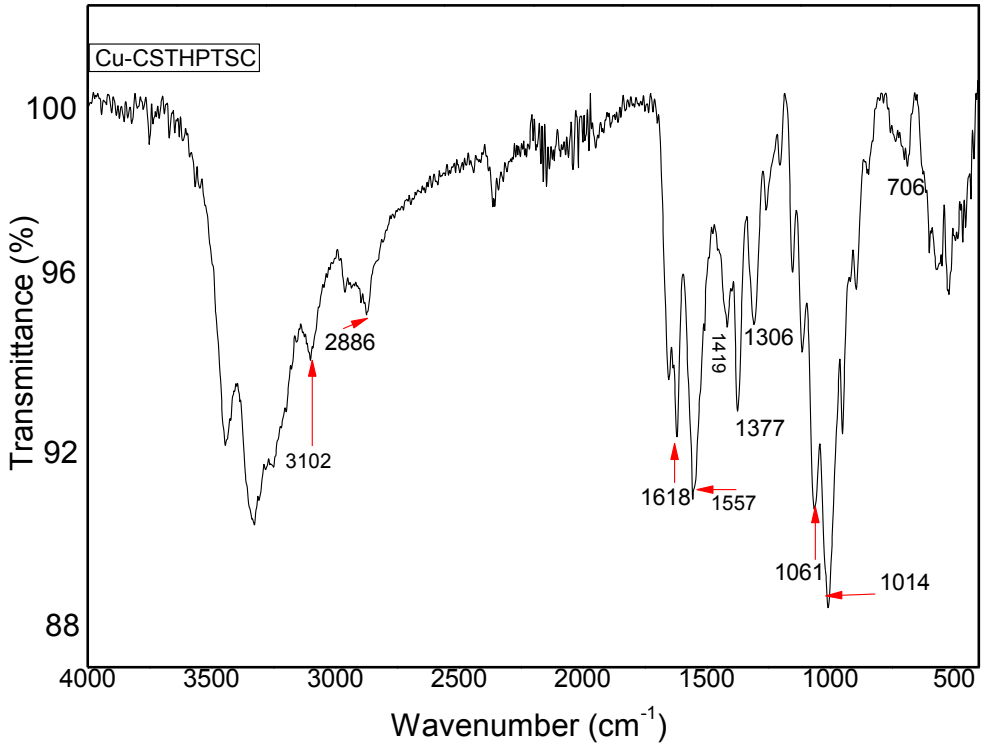


**Figure 123:** FT-IR spectrum of Cu-CSTHPTSC

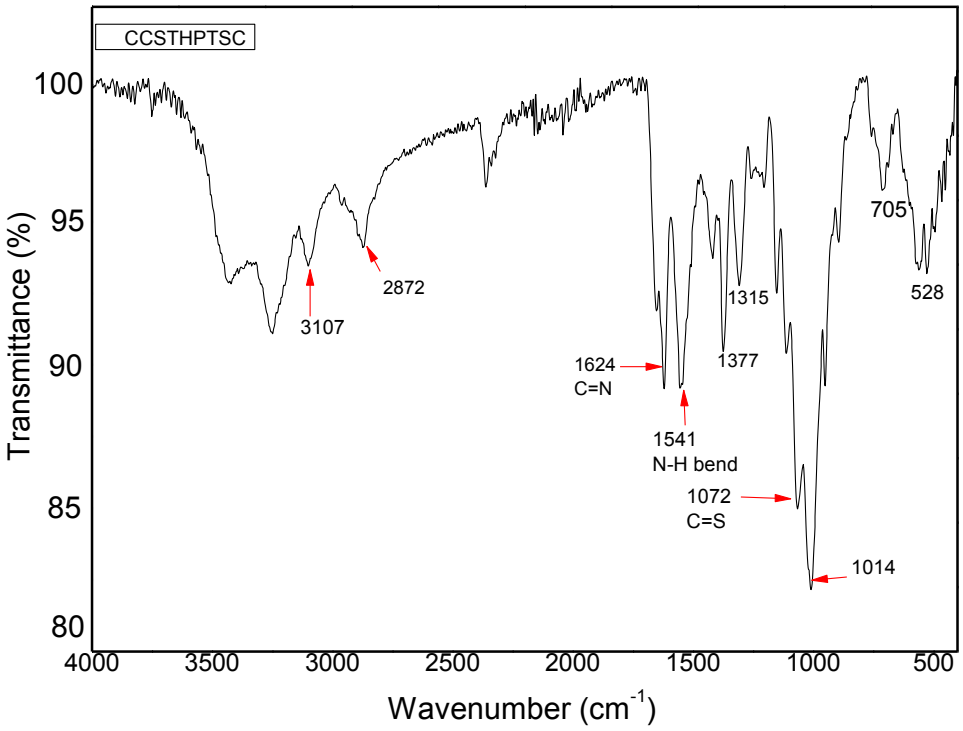


**Figure 124:** FT-IR spectrum of CCSTHPTSC

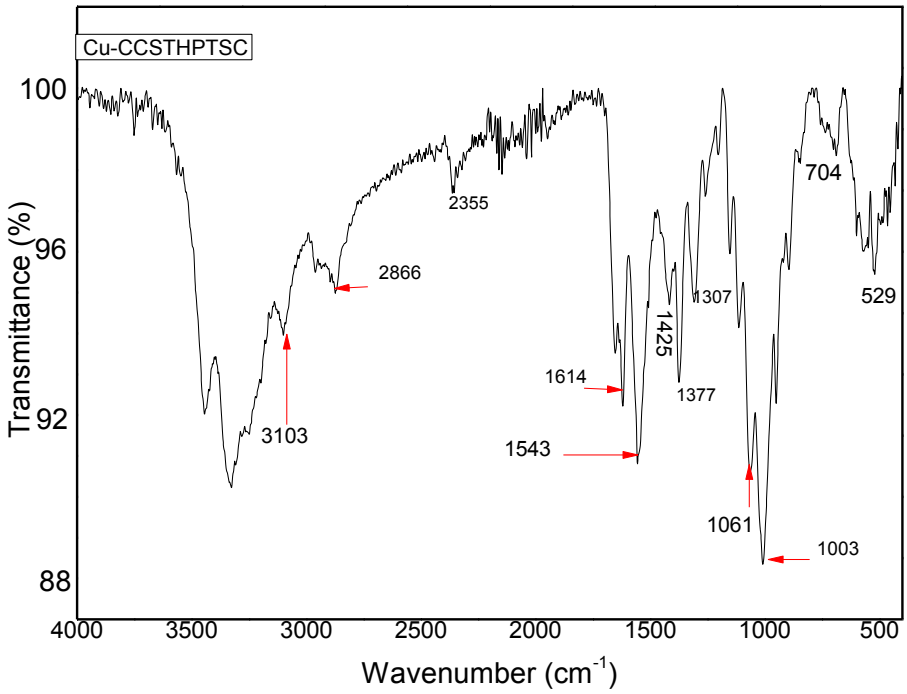


**Figure 125:** FT-IR spectrum of Cu-CCSTHPTSC

### 4.5.2.2. Solid State $^{13}$C Nuclear Magnetic Resonance ($^{13}$C NMR) Spectroscopy

The solid state $^{13}$C NMR spectra of chitosan imidazole-2-thiosemicarbazones and chitosan thiophene-2-thiosemicarbazones (figure 126, 127, 128 & 129) were used to endorse the structural distribution of carbon atoms in ring chitosan and chitosan functionalized thiosemicarbazone derivatives (De Angelis, *et al.*, 1998). The spectra showed the distinguishing signals owing to carbon atoms in chitosan moiety of the compounds *viz.* $CH_3$(22.81-24.11 ppm), C6(60.93-62.57 ppm), C3, C5(74.53-76.84 ppm), C4(82.72-84.36 ppm), C1(103.05-105.12 ppm) (Qin, *et al.*, 2012). The $^{13}$C NMR signals due to carbon atom of C=S at δ=170-180 ppm and azomethine carbon at δ= 140 ppm have been reported as the typical signals due to thiosemicarbazones (El-Atawy, *et al.*, 2019). The signal at δ= 178 ppm is ascribed to carbonyl carbon atom (Qin, *et al.*, 2012) and the broadening of this peak has been reported to be caused by the superimposition of C=S and C=O signals (Qin, *et al.*, 2012). The $^{13}$C NMR signals at δ= 139.19-174.34 ppm were ascribed to the carbon atom in -N=CH group of chitosan thiosemicarbazone (Qin, *et al.*, 2012). The broadening of peaks at 174.97-178.36 ppm was ascribed to superimposition of C=S &C=O groups (Qin, *et al.*, 2012). Further, the signals owing to carbon atoms of imidazole ring appeared at δ= 119-162 ppm (Bouchmella, *et al.*, 2008) and the signals owing to thiophene ring carbon atoms were produced at 116-140 ppm (Martinez, *et al.*, 1989). The absence of C2 signal in CSIMTSC and the presence of substituted C2 signals of the chitosan ring at 56.24 in CCSIMTSC, 57.20

ppm in CSTHPTSC, and 55.10 in CCSTHPTSC showed the involvement of C2 of chitosan in functionalization as chitosan thiosemicarbazone (Qin, *et al*., 2012). The $^{13}C$ NMR spectral data of imidazole-2-carboxaldehyde analogues of chitosan thiosemicarbazones and thiophene-2-carboxaldehyde analogues of chitosan thiosemicarbazones are shown in table 42 and 43 respectively.

**Table 42:** The solid state $^{13}C$ NMR spectral data (δ, ppm) of chitosan thiosemicarbazones: imidazole-2-carboxaldehyde analogues

| Compounds | Methyl carbon | C6 | C3, C5 | C4 | C 1 | -N=CH | Imidazole ring carbons | C=S & C=O superimposition |
|---|---|---|---|---|---|---|---|---|
| CSIMTSC | 24.03 | 62.57 | 75.81 | 84.36 | 104.35 | 171.18 | 119-162 | 178.36 |
| CCSIMTSC | 23.91 | 62.05 | 74.53-76.84 | 84.10 | 105.12 | 174.34 | 119-162 | 178.36 |

**Table 43:** The solid state $^{13}C$ NMR spectral data (δ, ppm) of chitosan thiosemicarbazones: thiophene-2-carboxaldehyde analogues

| Compounds | Methyl carbon | C6 | C3, C5 | C4 | C1 | -N=CH | Thiophene ring carbons | C=S & C=O superimposition |
|---|---|---|---|---|---|---|---|---|
| CSTHPTSC | 24.11 | 61.23 | 75.21 | 82.72 | 103.05 | 139.19 | 116-140 | 174.97 |
| CCSTHPTSC | 22.81 | 60.93 | 75.55 | 83.19 | 104.05 | 164.45 | 116-140 | 175.70 |

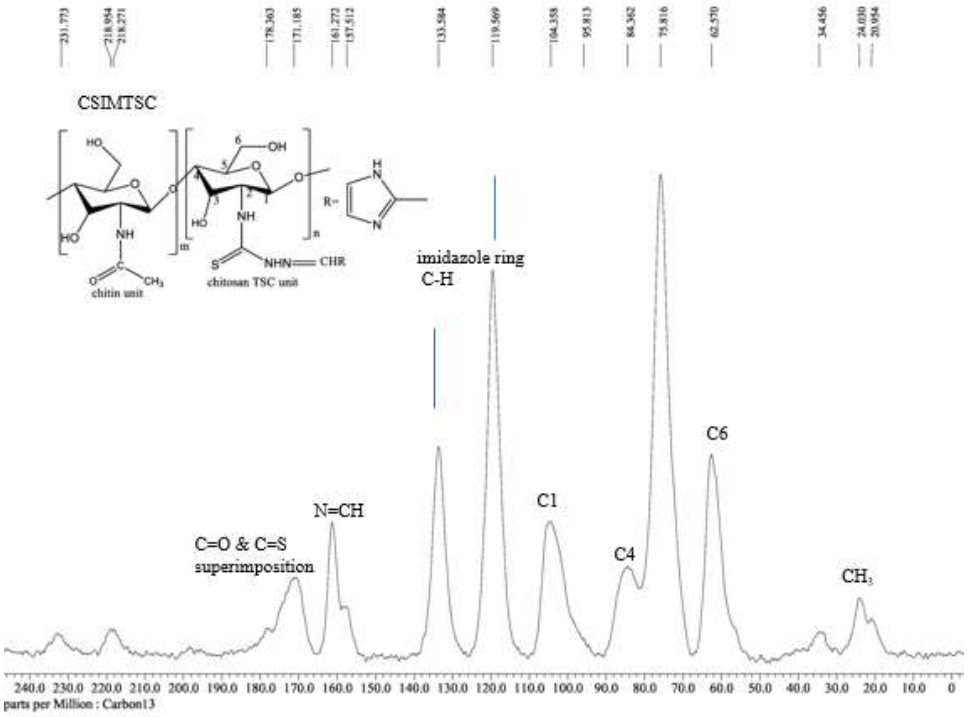


**Figure 126:** $^{13}C$ NMR spectrum of CSIMTSC

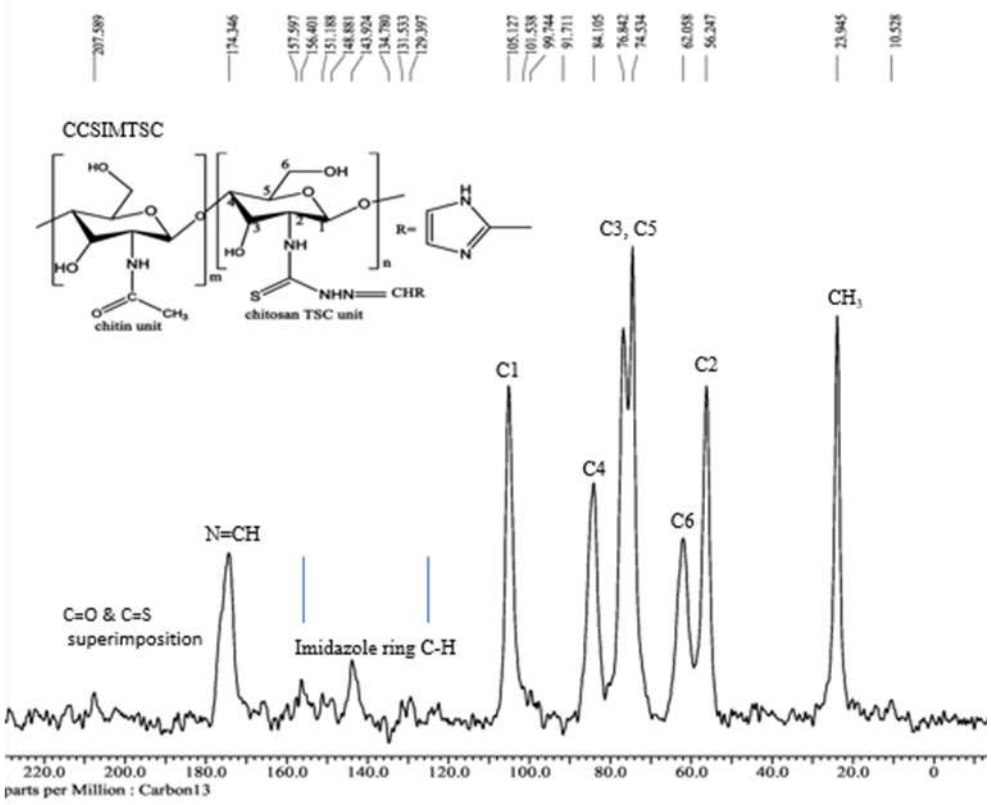


**Figure 127:** $^{13}$C NMR spectrum of CCSIMTSC

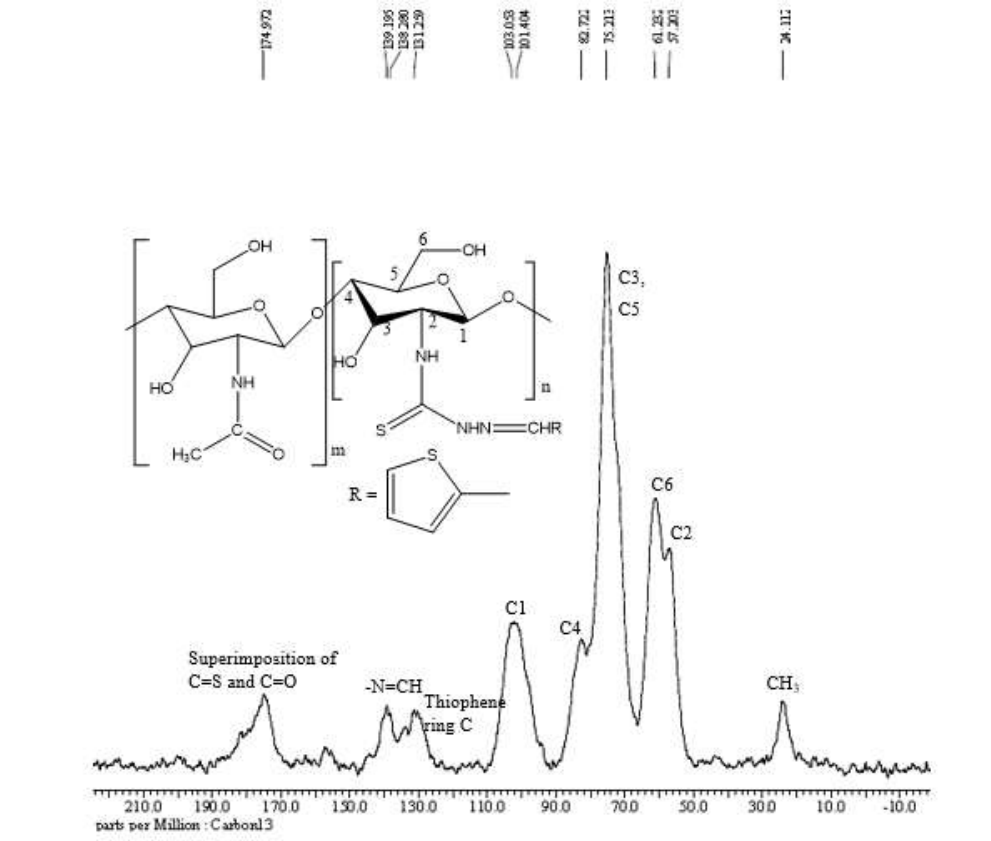


**Figure 128:** $^{13}$C NMR spectrum of CSTHPTSC

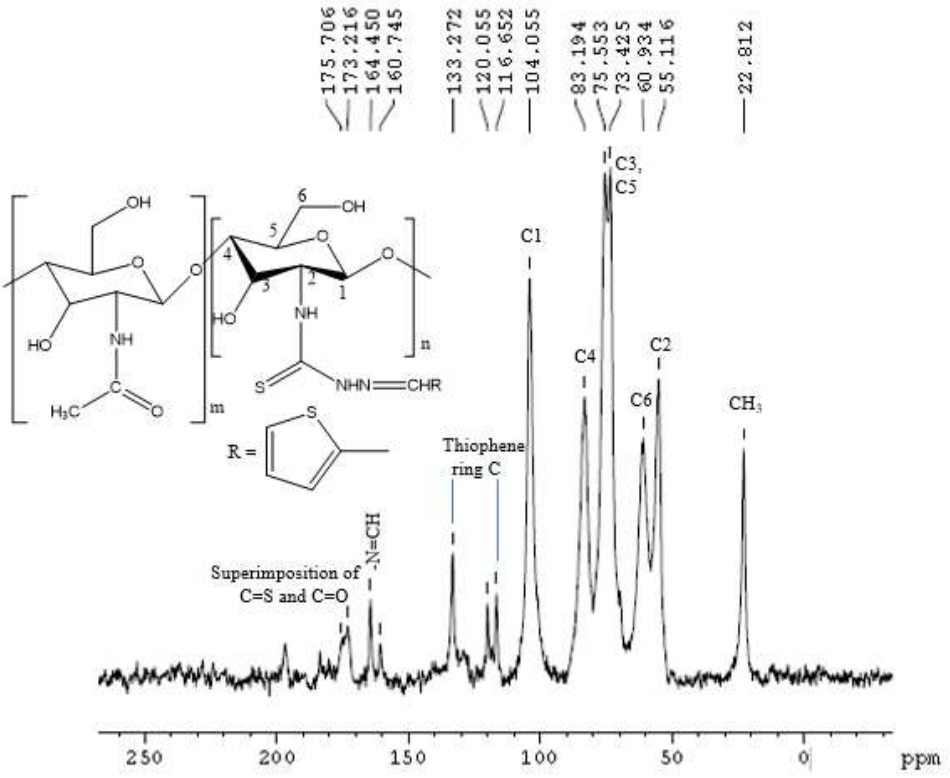


**Figure 129:** $^{13}$C NMR spectrum of CCSTHPTSC

### 4.5.2.3. Powder X Ray Diffraction (PXRD) Studies

The X Ray diffractograms of chitosan thiosemicarbazones (figure 130, 131, 132 & 133) showed the shifting of chitosan peaks from 10° and 20° (Qin, *et al.*, 2012; Ramya, *et al.*, 2012) and the presence of additional peaks owing to higher crystallinity produced with the grafting of chitosan to thiosemicarbazones (Qin, *et al.*, 2012). These peaks attributed to additional crystallinity phases were in accordance with the reported peaks of thiosemicarbazones (Hanumantharao, *et al.*, 2012; Santhakumari, *et al.*, 2010) at 2θ = 7.77-23.66° in CSIMTSC, 2θ = 9.12-31.10° in CCSIMTSC, 2θ = 13.23-26.73° in CSTHPTSC, and 2θ = 6.62-38.94° in CCSTHPTSC. The incorporation of chitosan in thiosemicarbazone was associated with the breakage of intra-molecular hydrogen bonds in chitosan and the emergence of imine group to give chitosan functionalized thiosemicarbazone with more crystallinity peaks (Jiao, *et al.*, 2011).

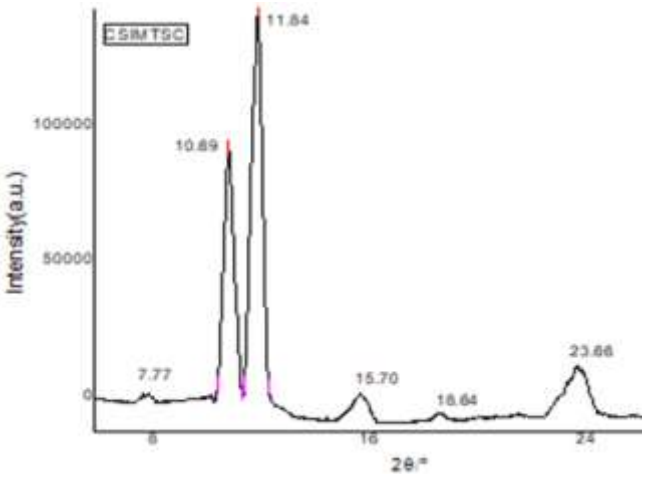


**Figure 130:** X ray diffractogram of CSIMTSC

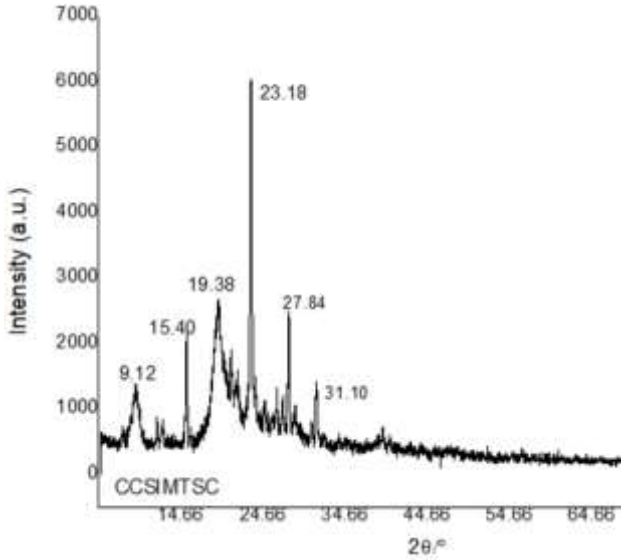


**Figure 131:** X ray diffractogram of CCSIMTSC

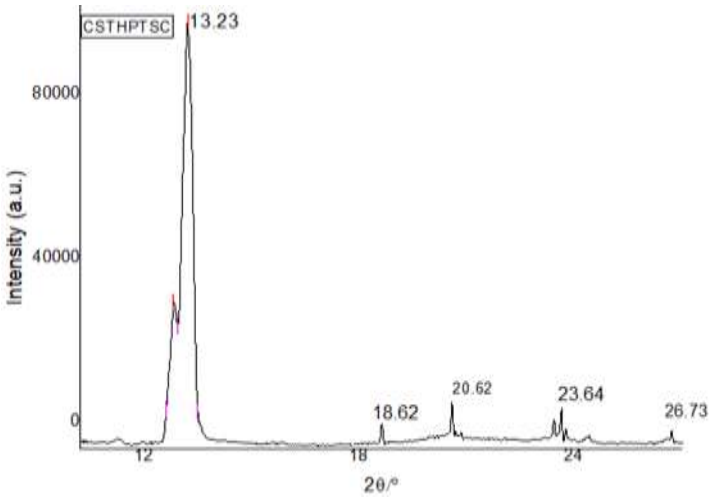


**Figure 132:** X ray diffractogram of CSTHPTSC

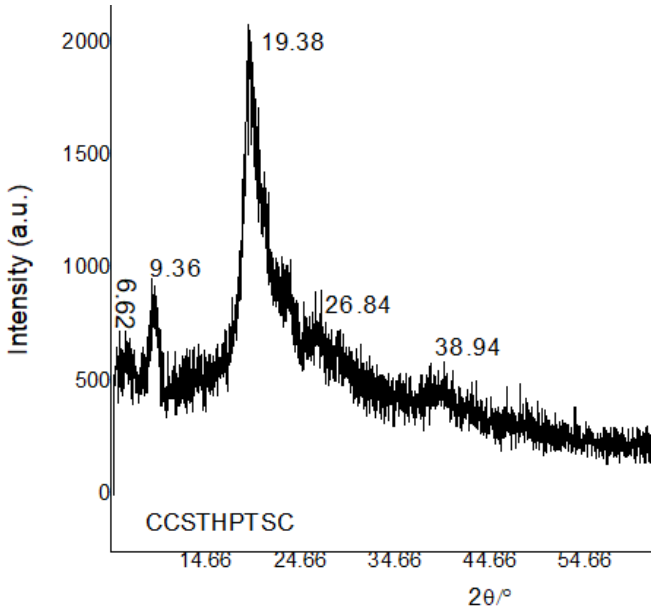


**Figure 133:** X ray diffractogram of CCSTHPTSC

As revealed by X ray diffractograms of copper(II) chitosan thiosemicarbazone complexes (figure 134, 135, 136 & 137) with the new peaks at 2θ = 19.55°, 26.47°, 31.88° and 34.11° in Cu-CSIMTSC, 2θ = 19.34°, 25.88° and 39.28° in Cu-CCSIMTSC, 2θ = 19.96° and 25.78° in Cu-CSTHPTSC, 2θ = 26.40° and 40.04° in Cu-CCSTHPTSC (Antony, *et al.*, 2012; Dehaghi, *et al.*, 2014; Mekahlia, *et al.*, 2009; Qin, *et al.*, 2012; Wang, *et al.*, 2005), the crystallinity peaks showed the shiftings from the free chitosan thiosemicarbazones owing to co-ordination of metal ion. The changes in crystallinity pattern were revealed by the emergence of new peaks and the relocation of original chitosan crystallinity peaks. These changes in crystallinity have been attributed to chelation with metal ion and then the cleavage of hydrogen bonds in chitosan (Wang, *et al.*, 2005).

The particle sizes of ligands were at 17.03-30.31 nm range and the particle sizes of corresponding complexes were at 16.58-32.72 nm range, as determined by using *Debye-Scherrer formula* applied for the peak with the highest intensity peak in the respective diffractograms (Dehaghi, *et al.*, 2014; Kucukgulmez, *et al.*, 2011). The degree of crystallinity as the crystallinity index (Kumirska, *et al.*, 2010; Lomadze *et al.*, 2005; Zhang, *et al.*, 2005) was 62.11-87.41% in ligands and 24.33-54.39% in complexes.

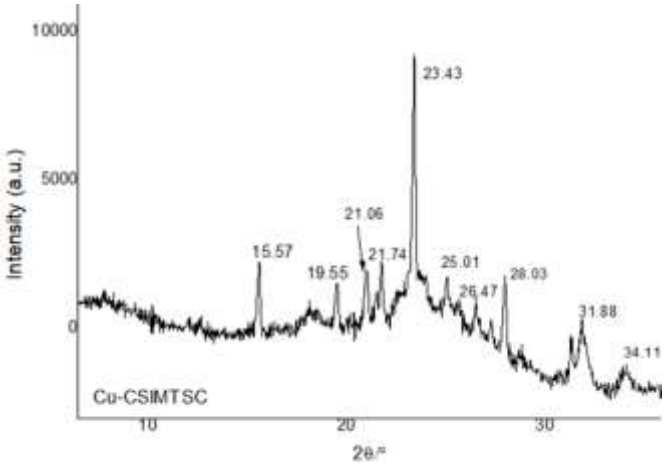


**Figure 134:** X ray diffractogram of Cu-CSIMTSC

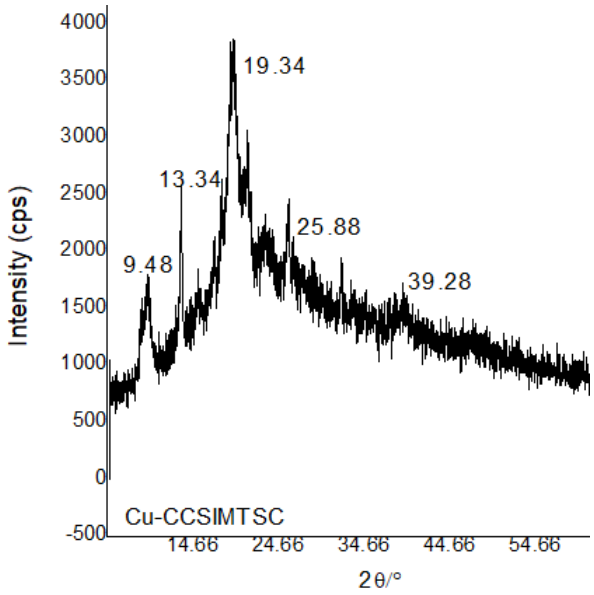


**Figure 135:** X ray diffractogram of Cu-CCSIMTSC

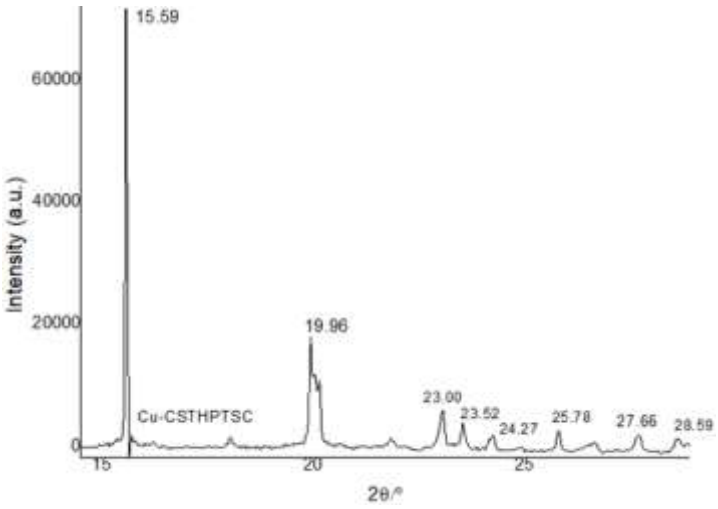


**Figure 136:** X ray diffractogram of Cu-CSTHPTSC

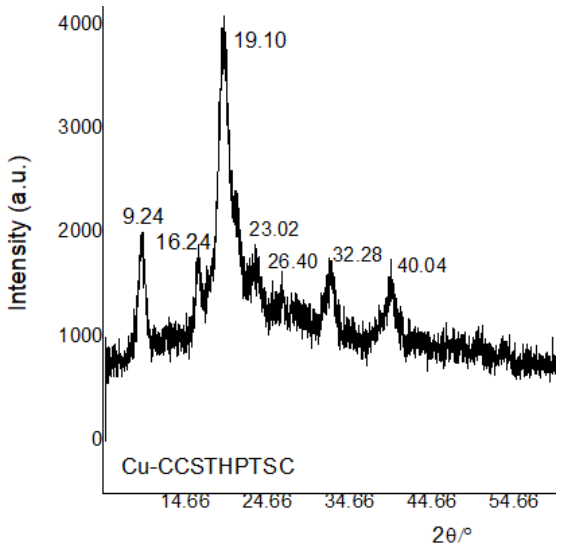


**Figure 137:** X ray diffractogram of Cu-CCSTHPTSC

The powder X ray diffraction data of imidazole-2-carboxaldehyde and thiophene-2-carboxaldehyde analogues of chitosan thiosemicarbazones and their copper(II) complexes are presented in table 44.

**Table 44:** The powder X ray diffraction data of chitosan thiosemicarbazones and their copper(II) complexes: imidazole-2-carboxaldehyde and thiophene-2-carboxaldehyde analogues

| Compounds | Selected functionality peaks, 2θ | | D (nm) | C.I. (%) |
|---|---|---|---|---|
| | Thiosemicarbazone crystallinity | Chitosan complex crystallinity | | |
| CSIMTSC | 7.77°, 10.69°, 11.54°, 15.70°, 18.64°, 23.66° | - | 30.31 | 70.77 |
| Cu-CSIMTSC | 15.57°,21.06°,21.74°,23.43°, 25.01°,28.03° | 19.55°,26.47°,31.88°,34.11° | 26.22 | 24.33 |
| CCSIMTSC | 9.12°, 15.40°, 19.38°, 23.18°, 27.84°, 31.10° | - | 27.76 | 87.41 |
| Cu-CCSIMTSC | 9.48°, 13.34° | 19.34°,25.88°,39.28° | 32.72 | 28.28 |
| CSTHPTSC | 13.23°, 18.62°, 20.62°, 23.64°, 26.73° | - | 17.89 | 62.11 |
| Cu-CSTHPTSC | 15.59°,23.00°, 23.52°, 24.27°, 27.66°, 28.59° | 19.96°, 25.78° | 31.10 | 49.84 |
| CCSTHPTSC | 6.62°, 9.36°, 19.38°, 26.84°, 38.94° | - | 17.03 | 68.00 |
| Cu-CCSTHPTSC | 9.24°, 16.24°, 19.10°, 23.02°, 32.28° | 26.40°, 40.04° | 16.58 | 54.39 |

#### 4.5.2.4. Elemental Microanalysis

The functionalization of chitosan as chitosan thiosemicarbazone through a partial substitution of amino group of chitosan by thiosemicarbazone moiety was confirmed by the correlational study of analytically found and calculated percentages of elements in chitosan imidazole-2-carboxaldehyde thiosemicarbazones (DS 20.18-22.63% and unit formula weight 313), and chitosan thiophene-2-carboxaldehyde thiosemicarbazones (DS 63.48-64.14% and unit formula weight 329). The correlation of the calculated percentages of elements with their analytically found percentages in copper(II) imidazole-2-carboxaldehyde chitosan thiosemicarbazones (unit formula weight 412) and copper(II) thiophene-2-carboxaldehyde chitosan thiosemicarbazones (unit formula weight 463) showed the complexing behavior of chitosan thiosemicarbazones and non-functionalized chitosan in parallel reactions with copper(II) ion. The DS values (Inukai, *et al.*, 1998; Melo, *et al.*, 2002; Pires, *et al.*, 2013; Qin, *et al.*, 2012) were the indicatives of partial incorporation of thiosemicarbazone moiety in chitosan to give chitosan functionalized thiosemicarbazones. The DS values from 20.18-22.63% in imidazole based thiosemicarbazones and 63.48-64.14% in thiophene based thiosemicarbazones meant higher introduction of Schiff base group into chitosan in thiophene chitosan thiosemicarbazones. The higher extent of functionalization of chitosan oligosaccharide than crab shell chitosan as chitosan thiosemicarbazone was shown by the DS values (Qin, *et al.*, 2012). It was not practicable to quantitatively ascertain the contribution of different structural factors fixed on the basis of DDA and DS values and hence the monomeric structural formula weight of completely deacetylated chitosan was taken into account to get the calculated percentages of elements in both the chitosan thioseemicarbazones and their copper(II) complexes. Upon the correlative study with the calculated percentages, the decreased values of analytically found percentages of sulphur were found in agreement with the corresponding DDA and DS values showing the partial deacetylation of chitin and partial grafting of thiosemicarbazone moiety into chitosan. The extent of functionalization corresponding to the given DS values were influenced by DDA of chitosan constituent and $M_w$ of carboxaldehyde moiety in chitosan thiosemicarbazones. The Schiff base addition with partial incorporation of thiosemicarbazone moiety into chitosan leaves some non-functionalized chitosan that reacts parallelly with with copper(II) chloride to give copper(II) chitosan complex.The higher values of the estimated chlorine percentages than the respective values of calculated chlorine percentages in copper(II) chitosan thiosemicarbazone complexes also justify this process of the simultaneous formation of copper(II)-chitosan (Adhikari, Garai, Khanal, *et al.*, 2021; Adhikari, Garai, Khanal, *et al.*,

2022; Adhikari, Garai, Thapa, *et al.*, 2022). The elemental analysis data of imidazole-2-carboxaldehyde and thiophene-2-carboxaldehyde analogues of chitosan thiosemicarbazones and their copper(II) complexes are presented in table 45 and 46 respectively.

**Table 45:** Elemental (CHNS) microanalysis of chitosan thiosemicarbazones: imidazole-2-carboxaldehyde and thiophene-2-carboxaldehyde analogues: calculated (found)

| Compounds | C(%) | H(%) | N(%) | S(%) | DS(%) |
|---|---|---|---|---|---|
| CSIMTSC | 41.90(40.30) | 5.43(5.07) | 22.21(23.75) | 10.17(3.61) | 22.63 |
| CCSIMTSC | 41.90(48.85) | 5.43(7.10) | 22.21(19.05) | 10.17(3.2) | 20.18 |
| CSTHPTSC | 43.49(36.14) | 5.17(5.24) | 12.68(8.91) | 19.35(14.96) | 64.14 |
| CCSTHPTSC | 43.49(36.19) | 5.17(5.20) | 12.68(9.01) | 19.35(14.60) | 63.48 |

**Table 46:** Elemental (CHNS) microanalysis and chlorine % in copper(II) chitosan thiosemicarbazones: imidazole-2-carboxaldehyde and thiophene-2-carboxaldehyde analogues: calculated (found)

| Compounds | C(%) | H(%) | N(%) | S(%) | Cl(%) |
|---|---|---|---|---|---|
| Cu-CSIMTSC | 31.89(30.80) | 4.14(4.22) | 16.90(15.48) | 7.74(2.41) | 8.56(12.20) |
| Cu-CCSIMTSC | 31.89(31.32) | 4.14(5.34) | 16.90(14.35) | 7.74(2.01) | 8.56(12.78) |
| Cu-CSTHPTSC | 30.94(23.59) | 3.68(3.86) | 9.02(5.76) | 13.77(9.63) | 15.22(16.62) |
| Cu-CCSTHPTSC | 30.94(25.03) | 3.68(4.01) | 9.02(8.96) | 13.77(12.99) | 15.22(16.20) |

#### 4.5.2.5. Thermal Studies

The thermogravimetric and differential thermal analysis (TG/DTA) curves of chitosan functionalized thiosemicarbazones (figure 138, 139, 140 & 141) and the data associated with the thermal events presented in table 47 revealed a weight loss of 7.14% at 148 °C and then 44% from 150-350 °C in CSIMTSC, weight loss of 7.58% at 144 °C and then 44 % at 150-350 °C in CCSIMTSC, weight loss of 9.16% at 146 °C and then 52.30% at 468 °C in CSTHPTSC and weight loss of 9.2% at 145 °C with further loss of 50.8% at 466 °C in CCSTHPTSC. There was an overall loss of weight by about 80% in CSIMTSC, 80% in CCSIMTSC, 75% in CSTHPTSC, and 76% in CCSTHPTSC at the temperature range from 200 to 1000 °C. In an agreement with the loss of water in chitosan reported to occur at 80-160 °C (Kittur, *et al.*, 2002; Qin, *et al.*, 2012) and its decomposition at 50-100 °C and 400 - 500 °C (Andrade, *et al.*, 2012; Kumari, *et al.*, 2017), the thermal degradation was found to occur in two steps of weight loss owing to loss of water at 100-200 °C and weight loss owing to the disruption and degradation of the chain at 200-1000 °C. The chitosan

thiosemicarbazones showed 5-7% weight loss at 120 °C due to loss of water, and 60-63% weight loss at 500 °C due to backbone degradation, and this behavior showed an analogy with the literature reports of 9% weight loss at 120 °C due to loss of water and 43% weight loss at 500 °C due to backbone degradation in chitosan (Chethan, *et al.*, 2013; De Britto & Campana-Filho, 2004; Xu, *et al.*, 2010). These derivatives showed an abrupt rate of decomposition with nearly 65% weight loss from 100-550 °C like the reported thermal events in chitosan (Khalid, *et al.*, 2002). Then, the decomposition was steady and a solid residue of about 5% CSIMTSC, 7% CCSIMTSC, 15% CSTHPTSC and 14% CCSTHPTSC was left as the unsaturated and degraded mass at 1000 °C. These thermal events showed substantially higher thermal stability of chitosan thiosemicarbazones (Qu, *et al.*, 2000), but these results showed more degradation of chitosan thiosemicarbazzones than chitosan at 400-500 °C. These TG peaks of chitosan thiosemicarbazones corresponding to the weight loss events in two steps at 100-300 °C and then at 450-900 °C accorded with the energy loss with decomposition and degradation as shown by DTA curves.

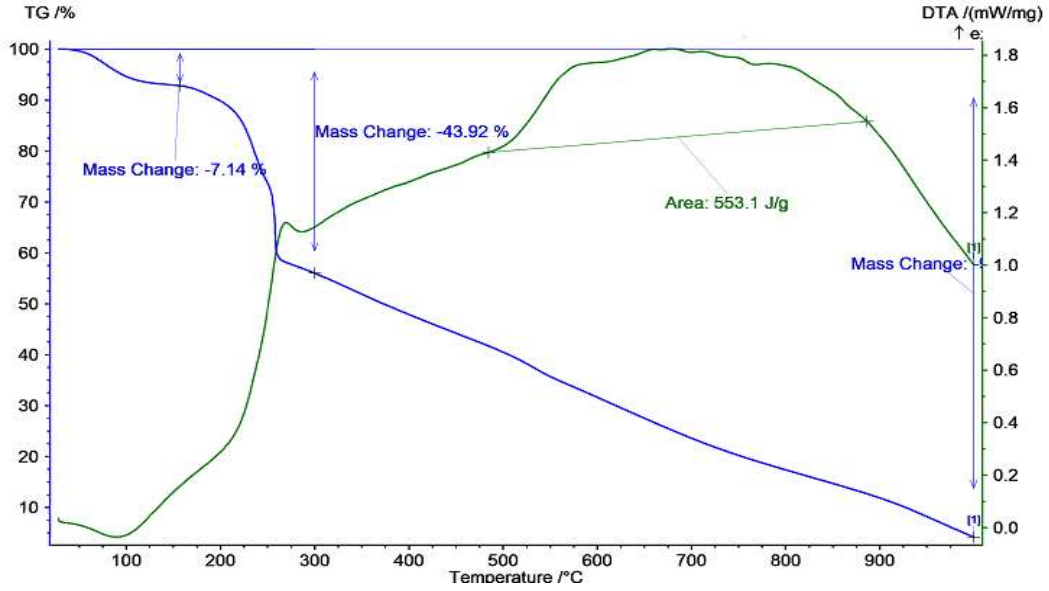


**Figure 138:** TG/DTA curves of CSIMTSC showing the thermal events at different temperatures

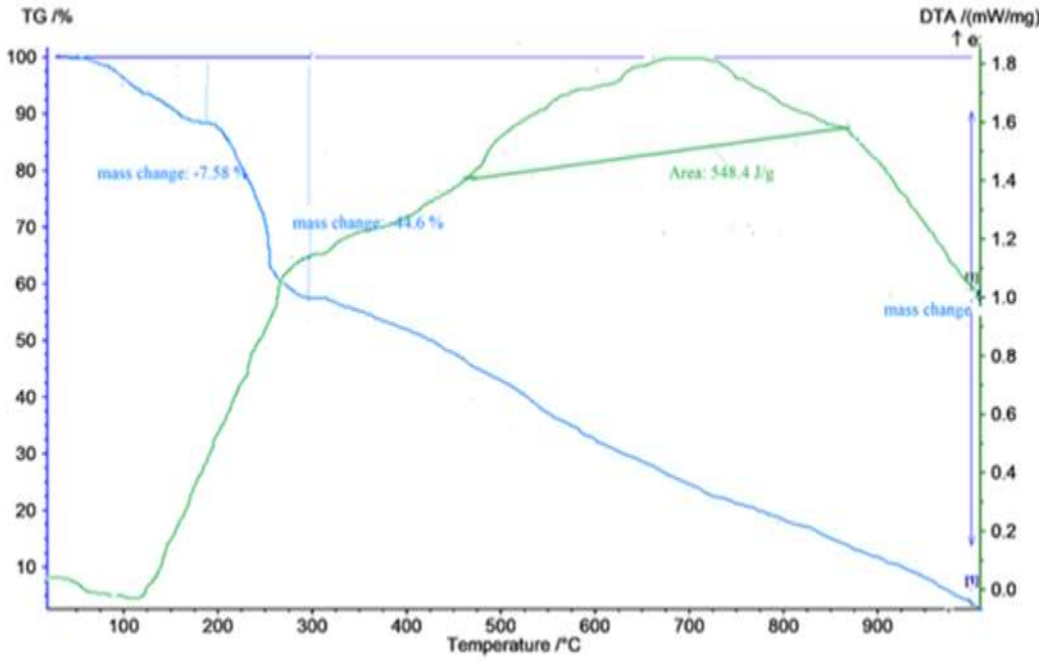


**Figure 139:** TG/DTA curves of CCSIMTSC showing the thermal events at different temperatures

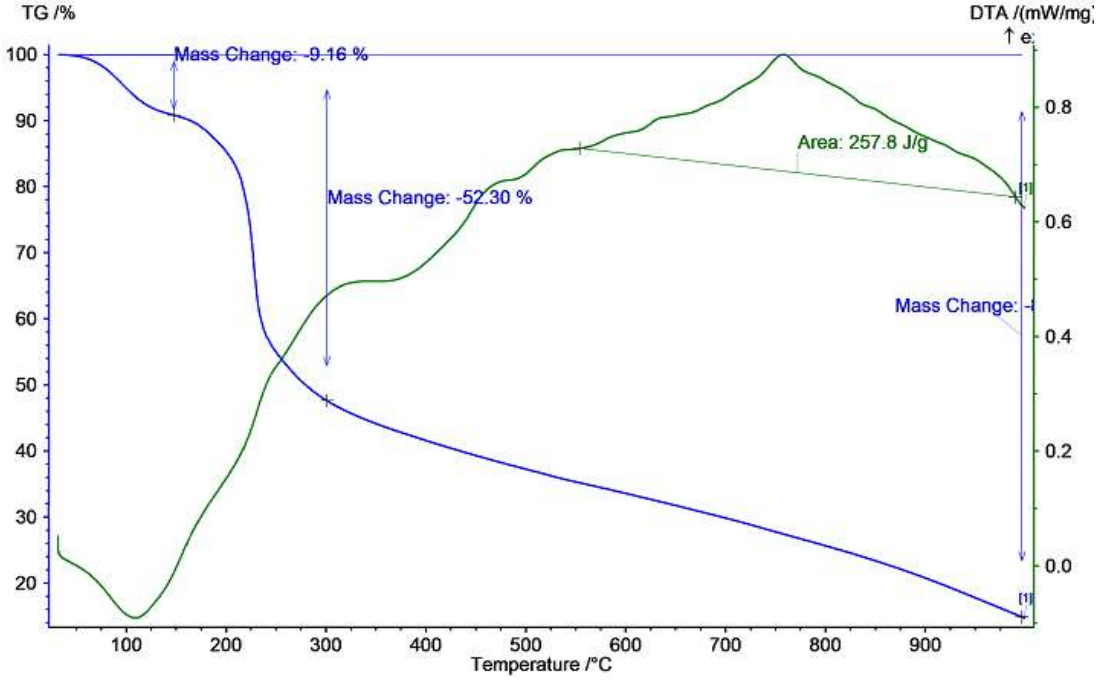


**Figure 140:** TG/DTA curves of CSTHPTSC showing the thermal events at different temperatures

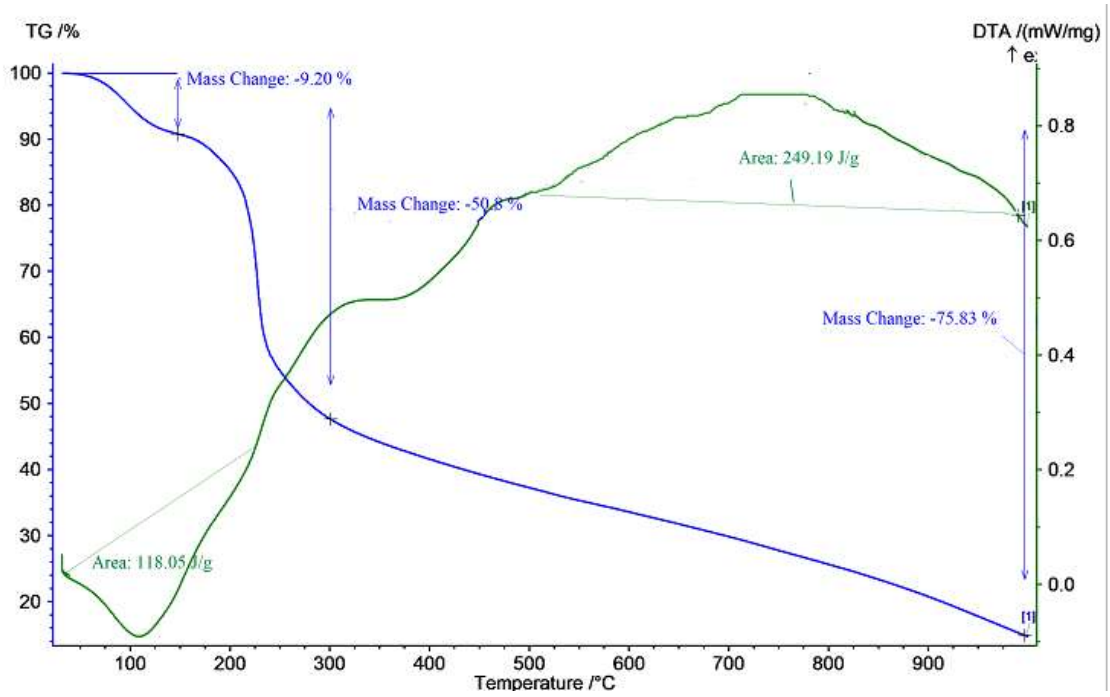


**Figure 141:** TG/DTA curves of CCSTHPTSC showing the thermal events at different temperatures

**Table 47:** TG/DTA data of thermal events in chitosan thiosemicarbazones: imidazole-2-carboxaldehyde and thiophene-2-carboxaldehyde analogues

| Compounds | Temperature (°C) | Weight loss (%) | Thermal event | % residue at 1000 °C |
|---|---|---|---|---|
| CSIMTSC | 148 | 7.14 | Loss of water | 5 |
| | 150-350 | 44 | Chain disruption in progress | |
| | 200-1000 | 80 | Chain disruption and backbone degradation | |
| CCSIMTSC | 144 | 7.58 | Loss of water | 7 |
| | 150-350 | 44 | Chain disruption in progress | |
| | 200-1000 | 80 | Chain disruption and backbone degradation | |
| CSTHPTSC | 146 | 9.16 | Loss of water | 15 |
| | 150-468 | 43 | Abrupt disruption of backbone | |
| | 200-1000 | 75 | Chain disruption and backbone degradation | |
| CCSTHPTSC | 145 | 9.20 | Loss of water | 14 |
| | 150-466 | 42 | Chain disruption in progress | |
| | 200-1000 | 76 | Chain disruption and backbone degradation | |

Thermogravimetric analysis/ differential thermal analysis/differential thermal gravimetry (TGA/DTA/DTG) curves of copper(II) chitosan thiosemicarbazones (figure 142, 143, 144 &

145) at 25-730 °C showed the thermal behavior that has been summarized with the corresponding thermal data in table 48. Variations in decomposition pattern with the weight loss in multiple steps were shown by the TG curves of these complexes. The progressive increase in the rate of decomposition and chitosan chain degradation was observed at 100-300 °C with about 23% weight loss in Cu-CSIMTSC, 19% weight loss in Cu-CCSIMTSC, 30% weight loss in Cu-CSTHPTSC and 43% weight loss in Cu-CCSTHPTSC. Glucosamine chain was found degraded with about 45% weight loss at 300-600 °C in Cu-CSIMTSC, 54% abrupt weight loss at 300-400 °C in Cu-CCSIMTSC, 41% continuous weight loss at 200-500 °C in Cu-CSTHPTSC, and 70.45% major loss in weight at 200-500 °C in Cu-CCSTHPTSC (Jiao, *et al.*, 2011; Khalid, *et al.*, 2002). There was a steady rise till 450 °C and broad exothermic peak at 450–560 °C in DTA curve of Cu-CSIMTSC and a steady rise till 300 °C and an exothermic peak at 300-400 °C in DTA curve of Cu-CCSIMTSC. The steady decomposition and degradation were observed after 600 °C in Cu-CSIMTSC, and after 500 °C in Cu-CCSIMTSC. The solid residue of about 22% of the sample in Cu-CSIMTSC and about 15% of sample in Cu-CCSIMTSC were found at at 700 °C. The DTA curve of Cu-CSTHPTSC showed a slow increase till 305 °C, broad exothermic peak at a point corresponding to 425 °C within the range of 350-500 °C and an exothermic hump at 504 °C. The DTA of Cu-CCSTHPTSC showed the exothermic peaks at 273 °C and 383 °C with the humps at 200-425 °C. The steady rate of degradation of the chain was observed after 550 °C in Cu-CSTHPTSC and after 450 °C in Cu-CCSTHPTSC. The solid residual masses of unsaturated structure at 700 °C were 35% of the sample in Cu-CSTHPTSC and 19% of sample in Cu-CCSTHPTSC. The data of thermal studies in overall showed a significant stability (Kittur, *et al.*, 2002; Qu, *et al.*, 2000) of copper(II) complexes.

The stages of thermal degradation as mentioned above were further supported by the DTG curves with a weight loss of 0.27 mg/min at 257 °C, 0.50 mg/min at 546 °C in Cu-CSIMTSC, 1.26 mg/min at 106 °C in Cu-CCSIMTSC, 252 µg/min at 203 °C, 217 µg/min at 415 °C, 95 µg/min at 505 °C in Cu-CSTHPTSC, and 0.81 mg/min at 255 °C, 0.32 mg/min at 380 °C in Cu-CCSTHPTSC.

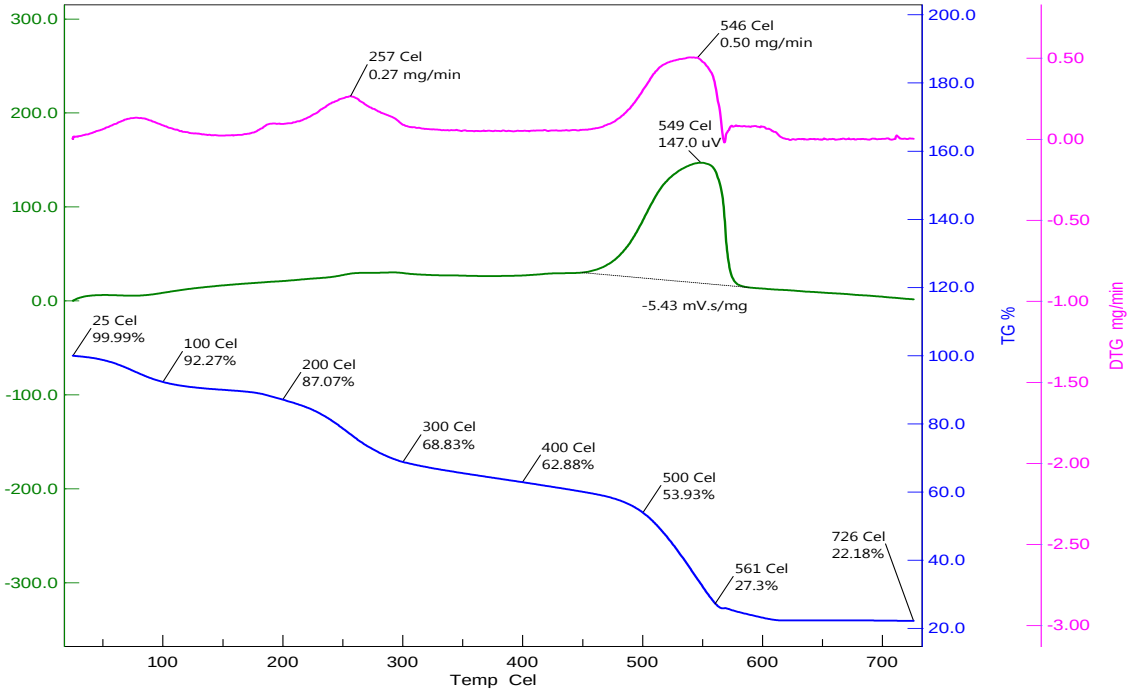


**Figure 142:** TG/DTA/DTG curves of Cu-CSIMTSC

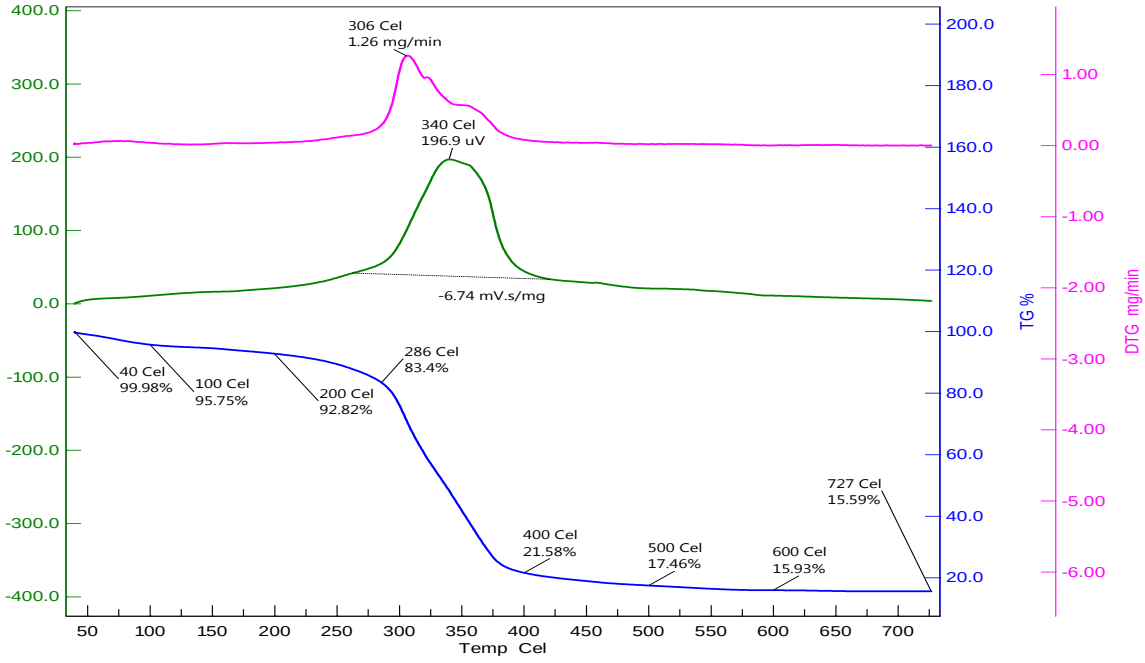


**Figure 143**: TG/DTA/DTG curves of Cu-CCSIMTSC

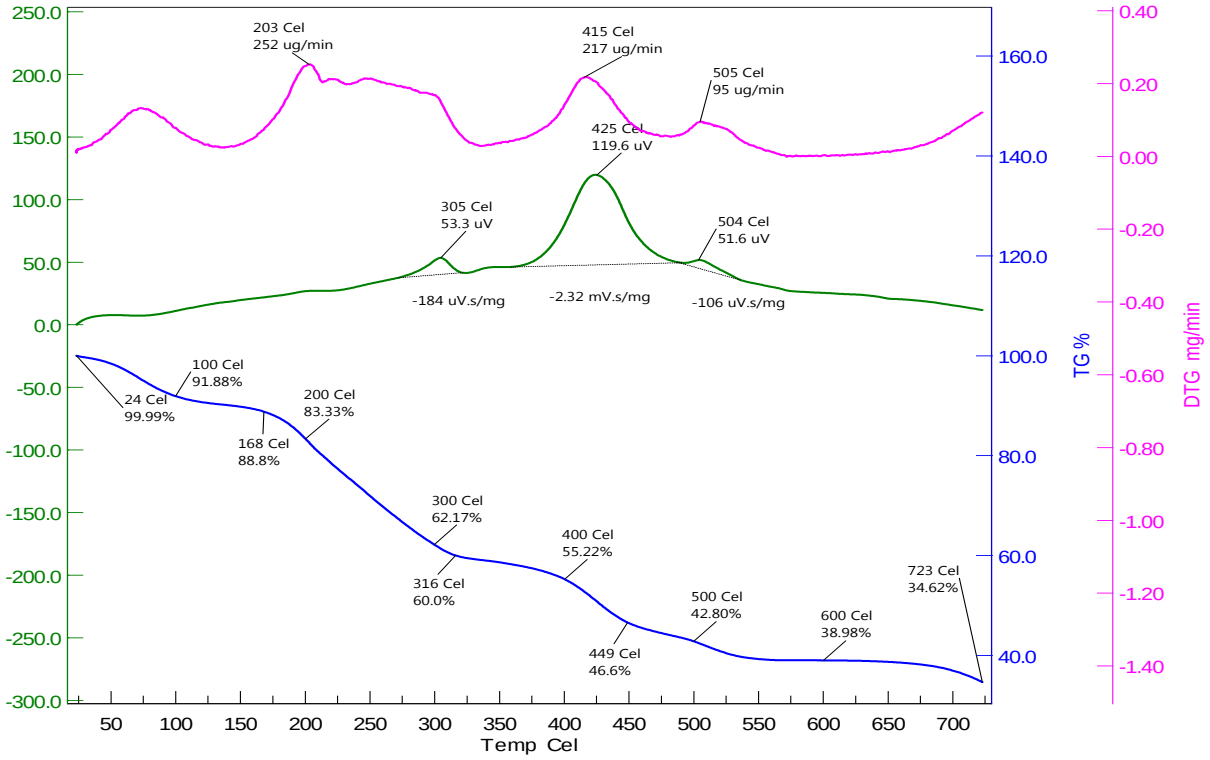


**Figure 144:** TG/DTA/DTG curves of Cu-CSTHPTSC

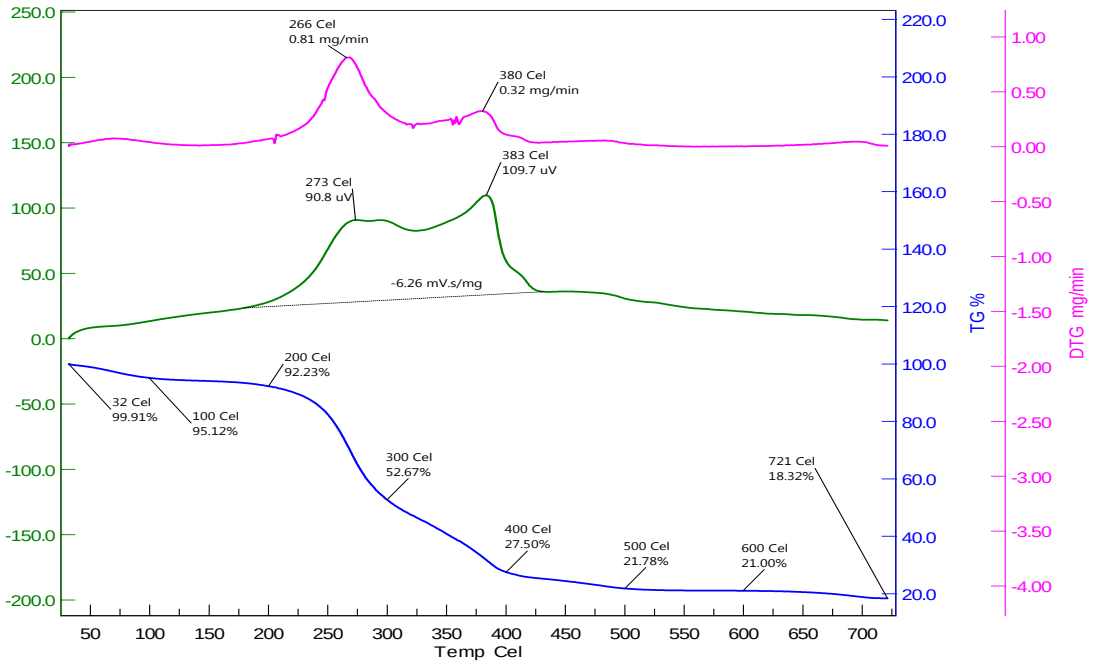


**Figure 145:** TG/DTA/DTG curves of Cu-CCSTHPTSC

**Table 48:** TG/DTA data of thermal events in copper(II) chitosan thiosemicarbazones: imidazole-2-carboxaldehyde and thiophene-2-carboxaldehyde analogues

| Compounds | Temperature (°C) | Weight loss % | Thermal event | % residue at 700 °C |
|---|---|---|---|---|
| Cu-CSIMTSC | 25-300 | 31 | Loss of water and chain disruption | |
| | 300-500 | 15.4 | Chain disruption and degradation | |
| | 500-600 | 29 | Degradation of glucosamine backbone | 22 |
| | 600-700 | 2.6 | Steady rate of backbone degradation | |
| Cu-CCSIMTSC | 25-286 | 16.5 | Loss of water and chain disruption | |
| | 286-400 | 61.6 | Degradation of glucosamine backbone | |
| | 400-700 | 7 | Steady rate of backbone degradation | 15 |
| Cu-CSTHPTSC | 25-300 | 37.8 | Loss of water and chain disruption | |
| | 300-600 | 23.2 | Chain disruption and degradation | |
| | 600-700 | 4 | Further degradation of the backbone | 35 |
| Cu-CCSTHPTSC | 25-200 | 7.6 | Loss of water and chain disruption initiation | 19 |
| | 200-400 | 64.4 | Chain disruption and degradation | |
| | 400-700 | 9.2 | Further degradation of the backbone | |

### 4.5.2.6. Magnetic Susceptibility Measurement and Electron Paramagnetic Resonance (EPR) Spectroscopy

The complexes showed the values of effective magnetic moment ($\mu_{eff}$) in the range at 1.84-1.89 BM. These values of magnetic moment below 1.90 BM were the indicatives of a stereochemical orientation to maintain the square planar or octahedral geometry (Figgis, 1958). The low spin-spin coupling in between the unpaired electrons in the central copper atom was justifiable with the magnetic moment values in the close neighborhood of 1.73 BM taken as the spin-only moment (Ahmed & Lal, 2017). The cupric ion with relatively more spin orbit coupling (Djord jevic, 1960) contributes to elevate the effective magnetic moment values some above the spin only moment.

The EPR spectra of these copper(II) chitosan thiosemicarbazones (figure 146, 147, 148 & 149) in agreement with the axial g tensors (Bennur, *et al.*, 2001) showed the intermolecular interactions among the spin moments, and some extent of dimeric association of molecules was indicated by the absence of hyperfine resolution owing to copper (S =1/2 and I= 3/2) (Bhadbhade & Srinivas, 1993; Suresh, *et al.*, 1996). The absence of hyperfine resolution showed the spectral exchange broadening attributed to paramagnetic centres in considerable proximity to each other (Farra, *et al.*, 2011) and this process was prevalent in the X-band

spectra at the frequency of 9.8 GHz (Farra, *et al.*, 2011). The spectra also showed an unpaired electron present in d $_{x^2-y^2}$ orbital of copper(II) centres in a molecular orientation of square planar geometry (Garribba & Micera, 2006). Due to absence of hyperfine splitting, the g parallel tensors were undetected, and the g values were 2.10 for Cu-CSIMTSC (ν = 9.8623 GHz, $B_o$=3350 Gs = 335.0 mT), 2.09 for Cu-CCSIMTSC (ν = 9.8630 GHz, $B_o$ = 3360 Gs = 336.0 mT), 2.09 for Cu-CSTHPTSC (ν = 9.8621 GHz, $B_o$ = 3380 Gs = 338.0 mT), and 2.08 for Cu-CCSTHPTSC (ν = 9.8617 GHz, $B_o$ = 3394 Gs = 339.4 mT). The spin orbital coupling with unpaired electrons due to which the g values were more than $g_e$ (2.0023) has been reported to be determined by the density of unpaired electrons in ligand and the degree of covalent character in the complexes (Ahmed & Lal, 2017). The absence of a half field peak at 1500 Gauss in the spectra was critically an indicative of the complexes with mononuclear structure (Patel & Sadasivan, 2017). The magnetic moment and g values in EPR spectra are presented in table 49.

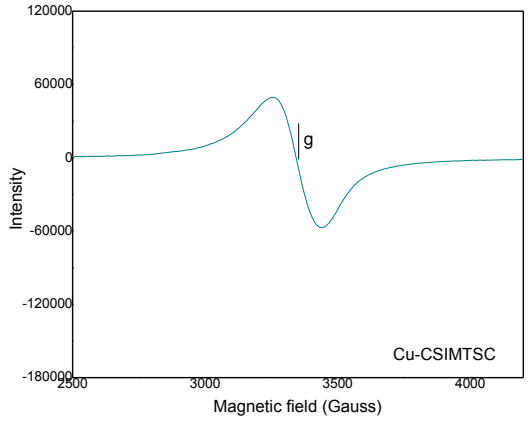


**Figure 146:** EPR spectrum of Cu-CSIMTSC

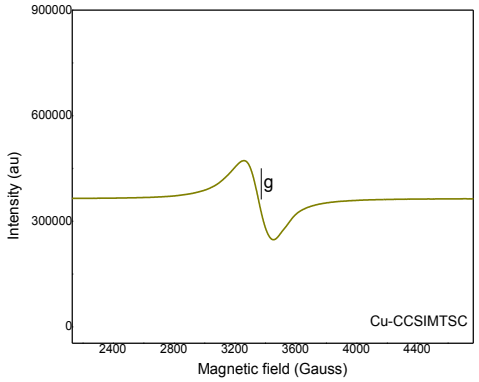


**Figure 147:** EPR spectrum of Cu-CCSIMTSC

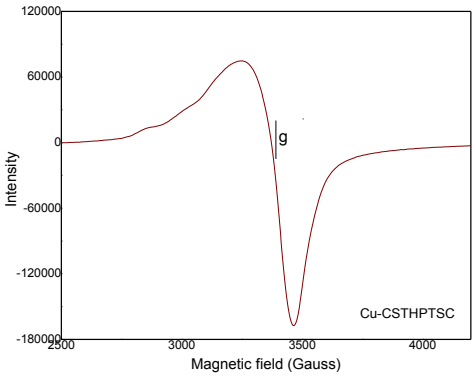


**Figure 148:** EPR spectrum of Cu-CSTHPTSC

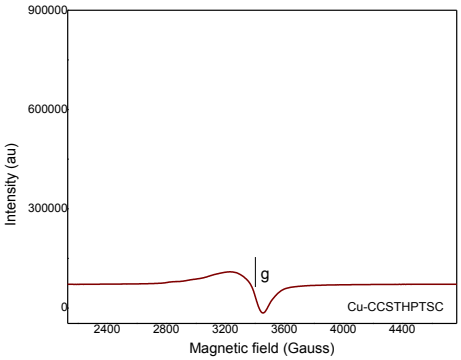


**Figure 149:** EPR spectrum of Cu- CCSTHPTSC

**Table 49:** Effective magnetic moments ($\mu_{eff}$) and EPR g values of copper(II) chitosan thiosemicarbazones: imidazole-2-carboxaldehyde and thiophene-2-carboxaldehyde analogues

| Complexes | $\mu_{eff}$, B. M. | EPR g value |
|---|---|---|
| Cu-CSIMTSC | 1.89 | 2.10 |
| Cu-CCSIMTSC | 1.87 | 2.09 |
| Cu-CSTHPTSC | 1.88 | 2.09 |
| Cu-CCSTHPTSC | 1.84 | 2.08 |

The structures of the complexes with the mononuclear and distorted square planar geometry (figure 150) proposed on the basis of above discussion show that the thione sulphur, azomethine nitrogen and heterocyclic nitrogen of chitosan imidazole 2-thiosemicarbazones and one chlorine atom were involved in coordination with copper(II) ion in Cu-CSIMTSC and Cu-CCSIMTSC. The thione sulphur and azomethine nitrogen atom of chitosan thiophene 2-thiosemicarbazones and two chlorine atoms were involved in coordination with copper(II) ion in Cu-CSTHPTSC and Cu-CCSTHPTSC.

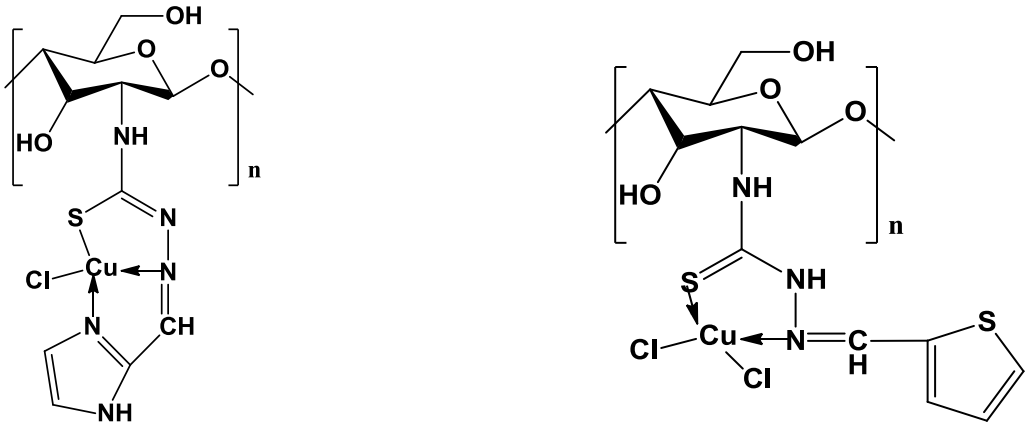


**a.** **b.**

**Figure 150:** Proposed structure of complexes (a): Cu-CSIMTSC and Cu-CCSIMTSC (b): Cu-CSTHPTSC and Cu-CCSTHPTSC

## 4.6. Anticancer Activity of Chitosan, Chitosan Thiosemicarbazones and their Copper(II) Complexes

### 4.6.1. General Discussion

Biomaterial chitosan as a cationic polysaccharide that undergoes protonation in acidic medium shows many applications and remarkable bioactivity (Da Sacco & Masotti, 2010; Khoushab & Yamabhai, 2010; Mathur & Narang, 1990; Percot, *et al.*, 2003; Tao, *et al.*, 2021;

Yuan, *et al.*, 2011). Its anticancer activity with minimal toxicity on healthy cells (Wimardhani, *et al.*, 2014) has been found to depend upon $M_w$ and DDA (Park, *et al.*, 2011). In agreement with the literature reports of remarkable tumor growth inhibitory of chitosan oligosaccharide (Harish Prashanth & Tharanathan, 2005; Maeda & Kimura, 2004; Park, *et al.*, 2011; Qin, Du, Xiao, Li, & Gao, 2002; Wang, *et al.*, 2008; Yamada, *et al.*, 2007), the oligo chitosan with low $M_w$ and high DDA and its thiosemicarbazones were found to show more antiproliferative activity against the tumorigenic and cancer cell lines *in vitro*. The pH sensitive anti-tumor drug delivery system based on chitosan has been reported to enhance the target delivery to tumor cells (Tao, *et al.*, 2021). The atomic interaction of doxorubicin with the polymer brings about the enhancement in its release profile to cancer cells (Li, *et al.*, 2020). Further, the activity was found enhanced upon the grafting of thiosemicarbazone moiety in chitosan, and such activity was substantially affected by the nature of carboxaldehyde in thiosemicarbazone. The results showed the higher anticancer potential of thiosemicarbazones with a heterocyclic ring nitrogen of a five membered ring as an active moiety, and this was an indicative of specific structure-activity relation. The results also accorded with the synthesis of chitosan derivatives upon the chemical modification, and the rational involvement of acetamido and amino groups towards their enhanced biological activity (Batista, *et al.*, 2006; Jayakumar, *et al.*, 2007; Jayakumar, Chennazhi, *et al.*, 2010; Jayakumar, Prabaharan, *et al.*, 2010). Anticancer activity of chitosan thiosemicarbazones can be conveniently linked to their antioxidant behaviour attributed to abstraction of hydrogen from free radicals due to amino and hydroxyl groups attached to C-2, C-3 and C-6 positions of the pyranose ring (Xie, *et al.*, 2001), as a result of weakening of intermolecular and intramolecular hydrogen bonds, and interaction of C=S and N-H groups with free radicals (Zhong, *et al.*, 2010) that would be an etiological agent of age-related disease like cancer (Gordon, 1996; Halliwell, *et al.*, 1995).

The α-(N)-heterocyclic carboxaldehyde thiosemicarabazone derivatives with antitumor activity (Moore & Sartorelli, 1989) were synthesized by the chemical mitigation in the heterocyclic ring system and substituents (Agrawal & Sartorelli, 1969; Brockman, *et al.*, 1956; French & Blantz Jr., 1966; French & Blantz Jr., 1971; Klayman, *et al.*, 1979). In particular, such derivatives were obtained from imidazole-2-carboxaldehyde, pyridine-2-carboxaldehyde, 2-acetyl pyridine, isatin, and 5-chloroisatin. Antioxidant effects attributed to scavenging of ROS and activation of a battery of detoxifying proteins (Kinsella, *et al.*, 1993) are crucial to retard the progress of immune system decline and cancer (Mc Cord, 2000; Rao,

*et al.*, 2006) and such effects have been shown by low molecular weight chitosan derivatives (Ji, *et al.*, 2007). Chemical modification and cellular internalization of chitosan through the cell membrane owing to its cationic nature and reactive functional groups (Gavhane, *et al.*, 2013) could bring about the enhanced scavenging effect of thiosemicarbazone-chitosan and the antioxidant effects have been reported to increase with the decrease in $M_w$ of chitosan (Zhong, *et al.*, 2010). Further, the antitumor activity mechanistically linked to the cellular pathways of scavenging the cancer-causing free radicals (Zhong, *et al.*, 2010) has been found to be exhibited by chitosan thiosemicarbazones.

### 4.6.2. Antitumorigenic Activity against MDCK Cell Line *in vitro*

Madin-Darby Canine Kidney (MDCK) cells, isolated from a male cocker spaniel kidney have been reported to show transformation into a continuous cell line (Frank, 1982; Mills, *et al.*, 1989). So, the cell line established by S. H. Madin and N. B. Darby in 1958 assumes the ability of indefinite proliferation. The MDCK cells that are commercially obtained from the canine kidney cells have been reported to go through the neoplastic transformation by the *in vitro* immortalization of cells as the tumorigenic phenotype (Omeir, *et al.*, 2011). The MDCK cyst model formation and growth have been found to be inhibited by oligo chitosan at 100-500 µg/mL concentration (Tuangpholkrung, *et al.*, 2018), and an increment in cellular permeation through the cell surfaces and the subsequent cellular cytotoxicity enhancement have been shown to be obtained by chitosan tailoring *via* functionalization and complex formation (Adhikari & Yadav, 2018). In accordance with these reports, the current work was centred at novel tailoring of chitosan functionalized thiosemicarbazones, and their copper(II) complexes, and the study of their *in vitro* inhibitory activity against the growth and proliferation of Madin-Darby Canine Kidney (MDCK) cell line. The MDCK cell line, different from the early cell populations of non tumorigenic type (Omeir, *et al.*, 2015), was found to propagate with the immortalized and tumorigenic phenotypic expression upon the culture in complete media. The progression towards tumorigenicity and the utilitarian aspects of tumorigenic canine cell lines have been reported in literatures but how the mammalian cells undergo neoplastic transformation is still unclear (Omeir, *et al.*, 2015). The inhibition profiles against the antitumorigenic MDCK cell line by chitosan, chitosan functionalized thiosemicarbazones and copper(II) chitosan thiosemicarbazone complexes are shown in table 50, 51 and 52 respectively. The $IC_{50}$ values were calculated from linear approximation of cell viability% versus concentration of the sample curve, and as the concentration (x) at which the

cell viability is 50% from the equation of linear trendline y = mx + c where m is slope of the trendline, c is intercept, y is 50 corresponding to half the viable cell percentage.

**Table 50:** Inhibition profile of MDCK cell line proliferation by chitosan oligosaccharide (CS) and crab shell chitosan (CCS)

| Compounds | Cell viability% (at 50-400 $\mu gmL^{-1}$) | $IC_{50}$ ($\mu gmL^{-1}$) | IR% (at 50-400 $\mu gmL^{-1}$) |
|---|---|---|---|
| CS | 91-62 | >400 | 9-38 |
| CCS | 96-78 | >400 | 4-22 |

**Table 51:** Inhibition profile of MDCK cell line proliferation by chitosan oligosaccharide thiosemicarbazones (CS TSC series) and their copper(II) complexes

| Compounds | Cell viability% (at 50-400 $\mu gmL^{-1}$) | $IC_{50}$ ($\mu gmL^{-1}$) | IR% (at 50-400 $\mu gmL^{-1}$) |
|---|---|---|---|
| CSSTSC | 80-28 | 334 | 20-72 |
| Cu-CSSTSC | 83-25 | 258 | 17-75 |
| CSAPTSC | 60-30 | 336 | 40-70 |
| Cu-CSAPTSC | 91-30 | 312 | 09-70 |
| CSPCTSC | 81-38 | 375 | 19-62 |
| Cu-CSPCTSC | 85-35 | 342 | 15-65 |
| CSAPRTSC | 81-45 | 381 | 19-55 |
| Cu-CSAPRTSC | 81-41 | 322 | 19-59 |
| CSISTSC | 63-34 | 351 | 37-66 |
| Cu-CSISTSC | 71-18 | 220 | 29-82 |
| CSCLISTSC | 91-43 | 335 | 09-57 |
| Cu-CSCLISTSC | 72-36 | 285 | 28-64 |
| CSIMTSC | 82-24 | 275 | 18-76 |
| Cu-CSIMTSC | 58-23 | 263 | 42-77 |
| CSTHPTSC | 54-40 | 364 | 46-60 |
| Cu-CSTHPTSC | 71-40 | 338 | 29-60 |

**Table 52:** Inhibition profile of MDCK cell line proliferation by crab shell chitosan thiosemicarbazones (CCS TSC series) and their copper(II) complexes

| Compounds | Cell viability% (at 50-400 $\mu gmL^{-1}$) | $IC_{50}$ ($\mu gmL^{-1}$) | IR% (at 50-400 $\mu gmL^{-1}$) |
|---|---|---|---|
| CCSSTSC | 81-59 | >400 | 19-41 |
| Cu-CCSSTSC | 84-46 | 391 | 16-54 |
| CCSAPTSC | 75-33 | 356 | 25-67 |

| | | | |
|---|---|---|---|
| Cu-CCSAPTSC | 80-34 | 354 | 20-66 |
| CCSPCTSC | 89-57 | >400 | 11-43 |
| Cu-CCSPCTSC | 96-57 | >400 | 04-43 |
| CCSAPRTSC | 91-43 | 335 | 09-57 |
| Cu-CCSAPRTSC | 83-25 | 274 | 17-75 |
| CCSISTSC | 54-31 | 358 | 46-69 |
| Cu-CCSISTSC | 97-22 | 205 | 03-78 |
| CCSCLISTSC | 81-28 | 334 | 19-72 |
| Cu-CCSCLISTSC | 93-25 | 270 | 07-75 |
| CCSIMTSC | 87-55 | >400 | 13-45 |
| Cu-CCSIMTSC | 82-49 | 394 | 18-51 |
| CCSTHPTSC | 68-52 | >400 | 32-48 |
| Cu-CCSTHPTSC | 94-31 | 293 | 06-69 |

### 4.6.3. Anticancer Activity against MCF-7 Cancer Cell Line *in vitro*

MCF-7 stands as an acronym of Michigan Cancer Foundation-7, USA where it was obtained as the human breast cancer cell line through pleural effusion from a breast carcinoma by H. Soule and co-workers (Soule, *et al.*, 1973). Owing to necessity of molecular level research to define prognosis and treatment of breast cancer that appears as a critical health problem and frequent malignancy in woman, MCF-7 has been a commonly used cancer cell line attracting a high interest of researchers since its establishment in 1973 (Comsa, *et al.*, 2015). The ultrafine chitosan nano shuttles have been found to decrease viability of MCF-7 cells *in vitro* and their enhanced cytotoxicity is promising towards intracellular organelles drug delivery (Faris, *et al.*, 2021). Chitosan has been found to show different cytotoxicity and antiproliferative effect in different cell lines in a dose dependent manner and in particular, its *in vitro* inhibitory effect on MCF-7 cell line with $IC_{50}$ values of 348 µg/mL (Ghaly, *et al.*, 2018) and 1.68-1.76 $mgmL^{-1}$ *viz*. 1680-1760 µg/mL (Abedian, *et al.*, 2019) in separate studies showed the suitability of selecting MCF-7 cell line with variation of chitosan cytotoxicity towards it for the current study. In addition to its use in anticancer therapeutics, the functionalized chitosan shows a wide utility in multistage specific and controlled delivery systems of nanomedicines (Jhaveri, *et al.*, 2021). For instance, the synthetic miRNA loaded chitosan nanoparticles have been found as a non-toxic material to bring about the substantial decrease in viability of MCF-7 cells (Rizkita, *et al.*, 2021). Chitosan/ polylactide nanoparticles have been found useful in therapeutical delivery of tamoxifen for the treatment of breast cancer (Gomillion, 2019).

The anticancer activity profiles of chitosan, chitosan functionalized thiosemicarbazones and copper(II) chitosan thiosemicarbazone complexes against MCF-7 cell line are shown in table 53, 54 and 55 respectively. The $IC_{50}$ values were calculated from linear approximation of cell viability% versus concentration of the sample curve, and as the concentration (x) at which the cell viability is 50% from the equation of linear trendline y = mx + c where m is slope of the trendline, c is intercept, y is 50 corresponding to half the viable cell percentage.

**Table 53:** Inhibition profile of MCF-7 cell line proliferation by chitosan oligosaccharide (CS) and crab shell chitosan (CCS)

| Compounds | Cell viability% (at 50-400 $\mu gmL^{-1}$) | $IC_{50}$ ($\mu gmL^{-1}$) | IR% (at 50-400 $\mu gmL^{-1}$) |
|---|---|---|---|
| CS | 91-44 | 370 | 9-56 |
| CCS | 83-33 | >400 | 18-38 |

**Table 54:** Inhibition profile of MCF-7 cell line proliferation by chitosan oligosaccharide thiosemicarbazones (CS TSC series) and their copper(II) complexes

| Compounds | Cell viability% (at 50-400 $\mu gmL^{-1}$) | $IC_{50}$ ($\mu gmL^{-1}$) | IR% (at 50-400 $\mu gmL^{-1}$) |
|---|---|---|---|
| CSSTSC | 82-44 | 343 | 18-56 |
| Cu-CSSTSC | 90-33 | 222 | 10-67 |
| CSAPTSC | 79-39 | 341 | 21-61 |
| Cu-CSAPTSC | 84-20 | 262 | 16-80 |
| CSPCTSC | 96-44 | 281 | 04-57 |
| Cu-CSPCTSC | 86-44 | 278 | 14-56 |
| CSAPRTSC | 85-48 | 355 | 15-52 |
| Cu-CSAPRTSC | 65-39 | 352 | 35-61 |
| CSISTSC | 68-42 | 370 | 32-58 |
| Cu-CSISTSC | 56-13 | 220 | 44-87 |
| CSCLISTSC | 75-32 | 306 | 25-68 |
| Cu-CSCLISTSC | 85-32 | 282 | 15-68 |
| CSIMTSC | 75-32 | 368 | 25-68 |
| Cu-CSIMTSC | 72-19 | 277 | 28-81 |
| CSTHPTSC | 79-43 | 369 | 21-57 |
| Cu-CSTHPTSC | 87-39 | 318 | 13-61 |

**Table 55:** Inhibition profile of MCF-7 cell line proliferation by crab shell chitosan thiosemicarbazones (CCS TSC series) and their copper(II) complexes

| Compounds | Cell viability% (at 50-400 $\mu gmL^{-1}$) | $IC_{50}$ ($\mu gmL^{-1}$) | IR% (at 50-400 $\mu gmL^{-1}$) |
|---|---|---|---|
| CCSSTSC | 78-49 | 393 | 22-51 |

| | | | |
|---|---|---|---|
| Cu-CCSSTSC | 76-48 | 390 | 24-52 |
| CCSAPTSC | 80-52 | >400 | 20-48 |
| Cu-CCSAPTSC | 74-16 | 212 | 26-84 |
| CCSPCTSC | 78-51 | >400 | 22-49 |
| Cu-CCSPCTSC | 70-18 | 231 | 30-82 |
| CCSAPRTSC | 69-42 | 365 | 31-58 |
| Cu-CCSAPRTSC | 69-39 | 352 | 46-62 |
| CCSISTSC | 84-43 | 384 | 16-57 |
| Cu-CCSISTSC | 84-41 | 356 | 16-59 |
| CCSCLISTSC | 83-42 | 367 | 17-58 |
| Cu-CCSCLISTSC | 84-34 | 309 | 16-66 |
| CCSIMTSC | 83-58 | >400 | 17-42 |
| Cu-CCSIMTSC | 82- 57 | >400 | 18-43 |
| CCSTHPTSC | 82-52 | >400 | 26-48 |
| Cu-CCSTHPTSC | 85-34 | >400 | 14-49 |

### 4.6.4. Anticancer Activity Assessment: Graphical Analysis

The general impressions observable from the graphical representations of correlative inhibition of CS & CCS (figure 151), CSTSC series of ligands & their copper(II) complexes (figure 152-159), and CCSTSC series of ligands & their copper(II) complexes (figure 160-167) against the tumorigenic MDCK cell line and MCF-7 cancer cell line are (i) higher activity of chitosan oligosaccharide than high molecular weight crab shell chitosan, (ii) higher activity of chitosan functionalized thiosemicarbazones than native chitosan, and (iii) anticancer activity enhancement upon the complex formation.

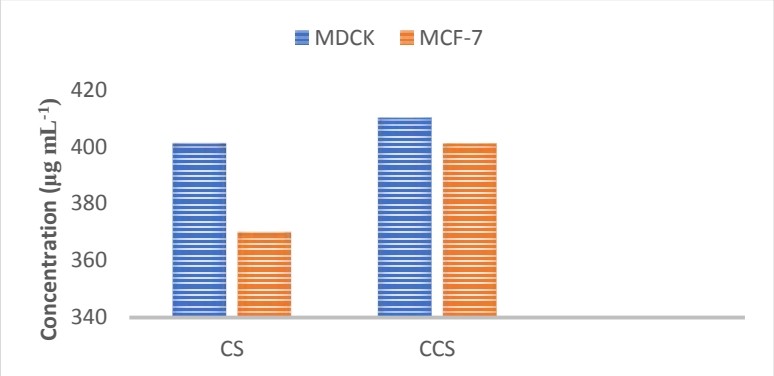


**Figure 151:** Correlative inhibition of CS and CCS against MDCK and MCF-7 cell lines ($IC_{50}$ values)

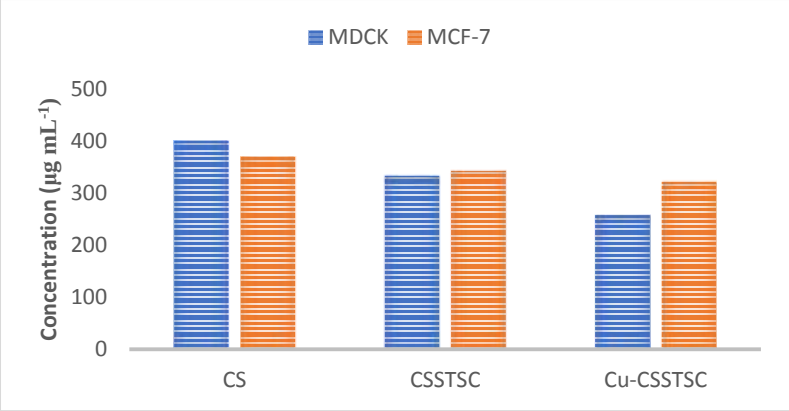


**Figure 152:** Correlative inhibition of CS, CSSTSC and Cu-CSSTSC against MDCK and MCF-7 cell lines ($IC_{50}$ values)

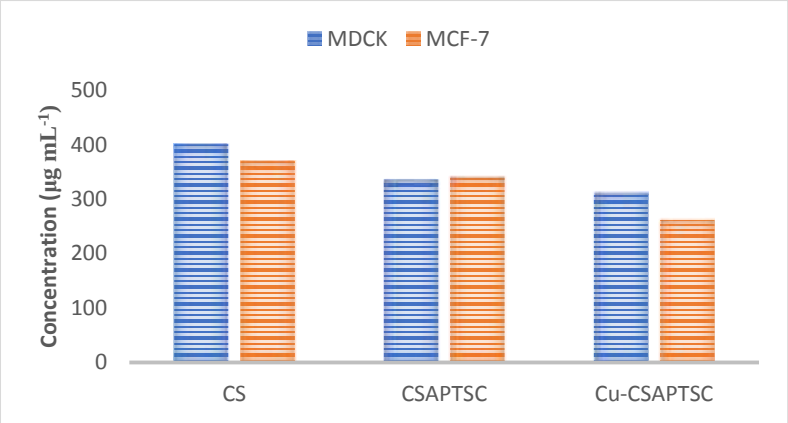


**Figure 153:** Correlative inhibition of CS, CSAPTSC and Cu-CSAPTSC against MDCK and MCF-7 cell lines ($IC_{50}$ values)

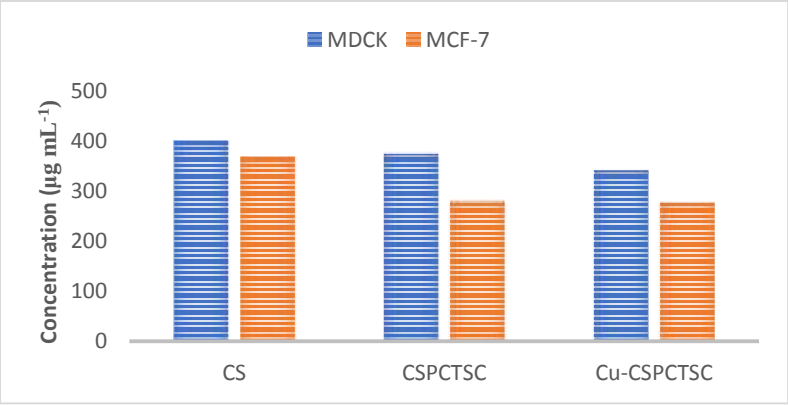


**Figure 154:** Correlative inhibition of CS, CSPCTSC and Cu-CSPCTSC against MDCK and MCF-7 cell lines ($IC_{50}$ values)

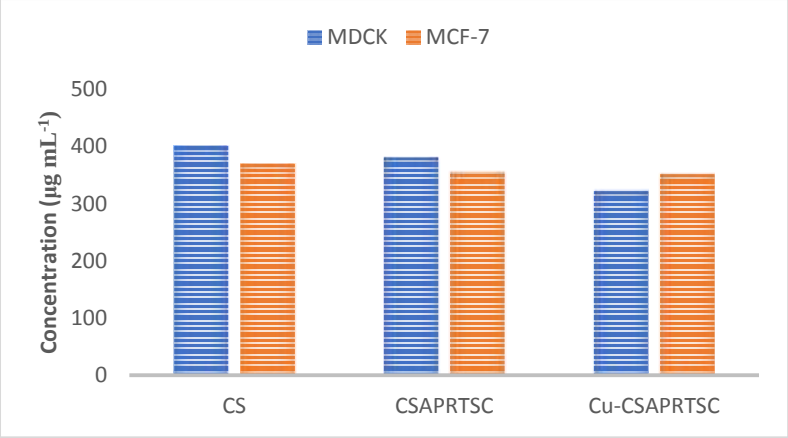


**Figure 155:** Correlative inhibition of CS, CSAPRTSC and Cu-CSAPRTSC against MDCK and MCF-7 cell lines ($IC_{50}$ values)

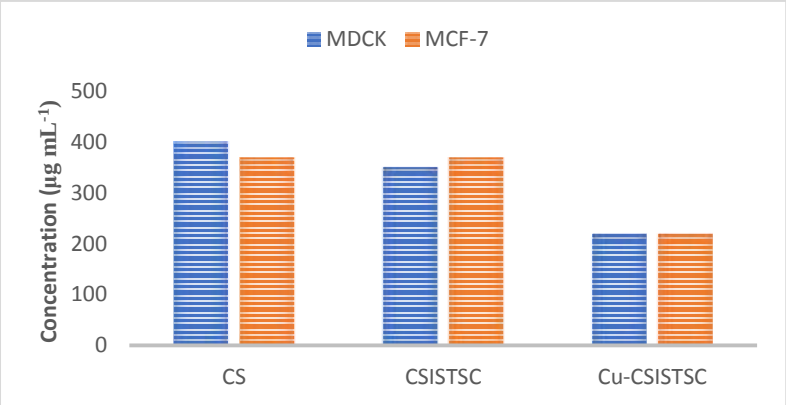


**Figure 156:** Correlative inhibition of CS, CSISTSC and Cu-CSISTSC against MDCK and MCF-7 cell lines ($IC_{50}$ values)

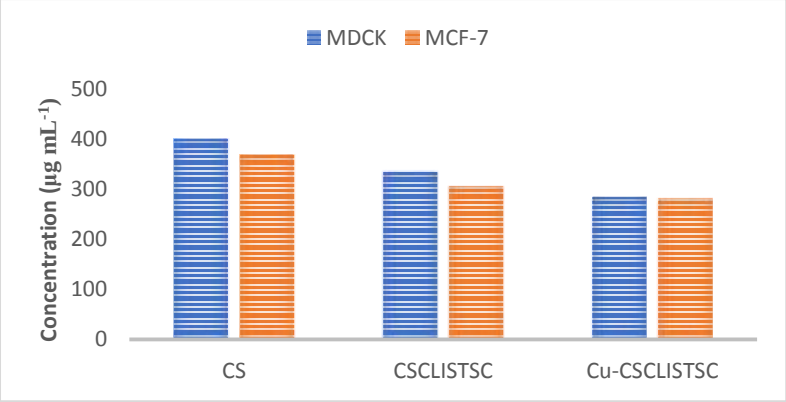


**Figure 157:** Correlative inhibition of CS, CSCLISTSC and Cu-CSCLISTSC against MDCK and MCF-7 cell lines ($IC_{50}$ values)

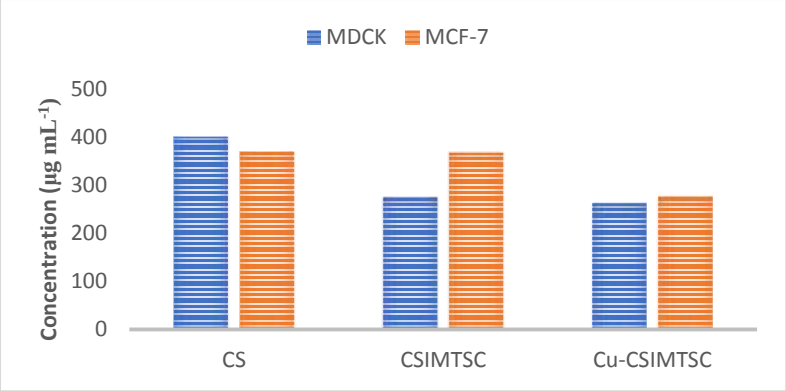


**Figure 158:** Correlative inhibition of CS, CSIMTSC and Cu-CSIMTSC against MDCK and MCF-7 cell lines ($IC_{50}$ values)

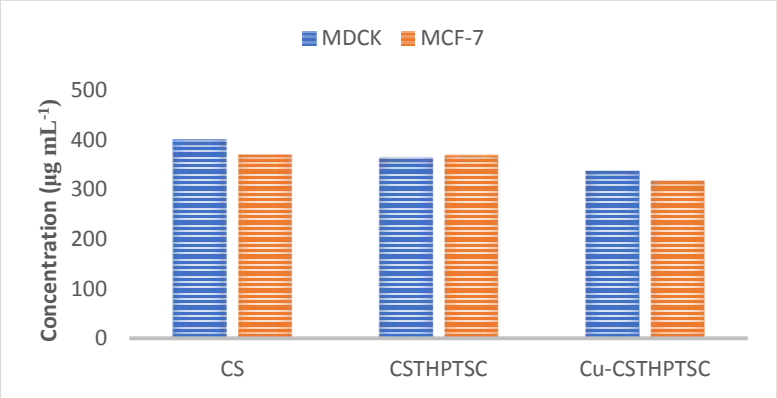


**Figure 159:** Correlative inhibition of CS, CSTHPTSC and Cu-CSTHPTSC against MDCK and MCF-7 cell lines ($IC_{50}$ values)

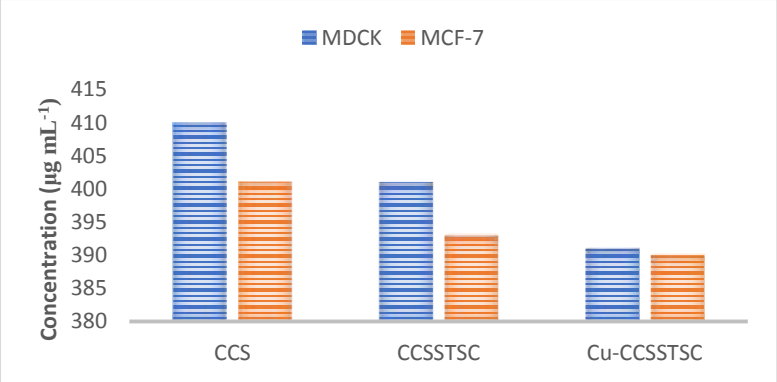


**Figure 160:** Correlative inhibition of CCS, CCSSTSC and Cu-CCSSTSC against MDCK and MCF-7 cell lines ($IC_{50}$ values)

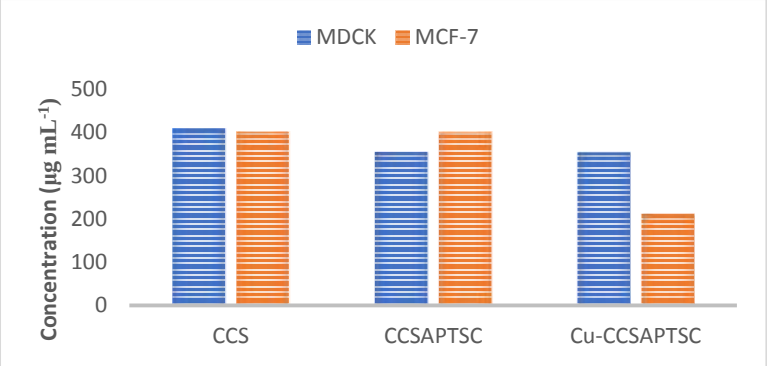


**Figure 161:** Correlative inhibition of CCS, CCSAPTSC and Cu-CCSAPTSC against MDCK and MCF-7 cell lines ($IC_{50}$ values)

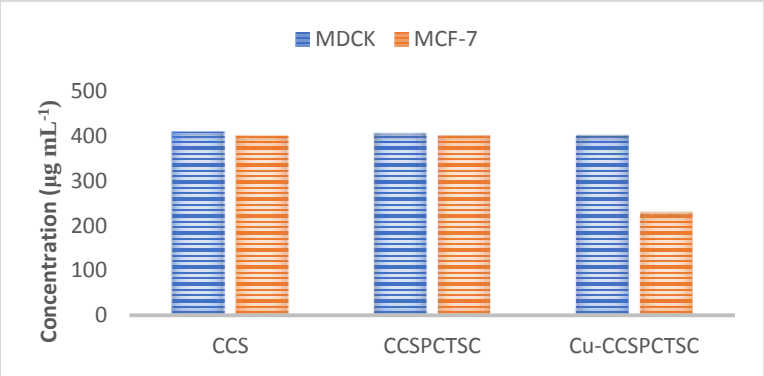


**Figure 162:** Correlative inhibition of CCS, CCSPCTSC and Cu-CCSPCTSC against MDCK and MCF-7 cell lines ($IC_{50}$ values)

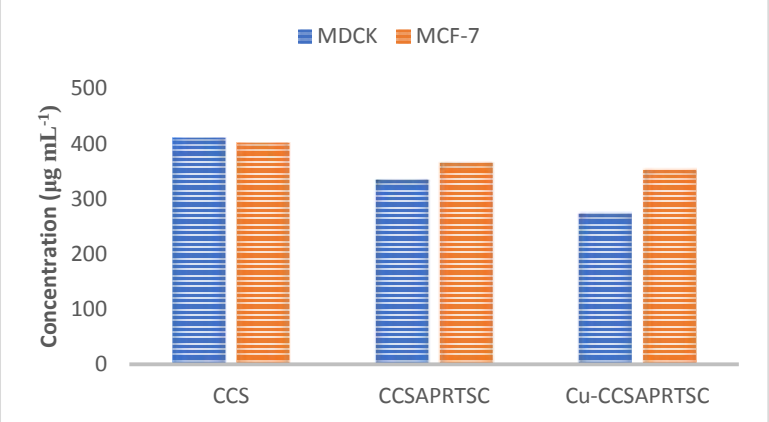


**Figure 163:** Correlative inhibition of CCS, CCSAPRTSC and Cu-CCSAPRTSC against MDCK and MCF-7 cell lines ($IC_{50}$ values)

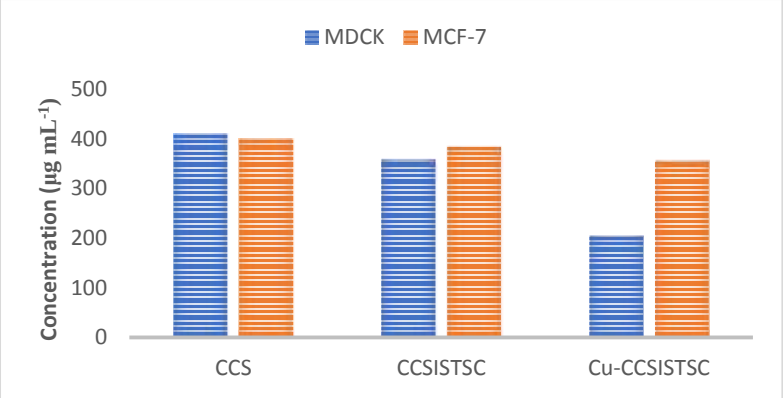


**Figure 164:** Correlative inhibition of CCS, CCSISTSC and Cu-CCSISTSC against MDCK and MCF-7 cell lines ($IC_{50}$ values)

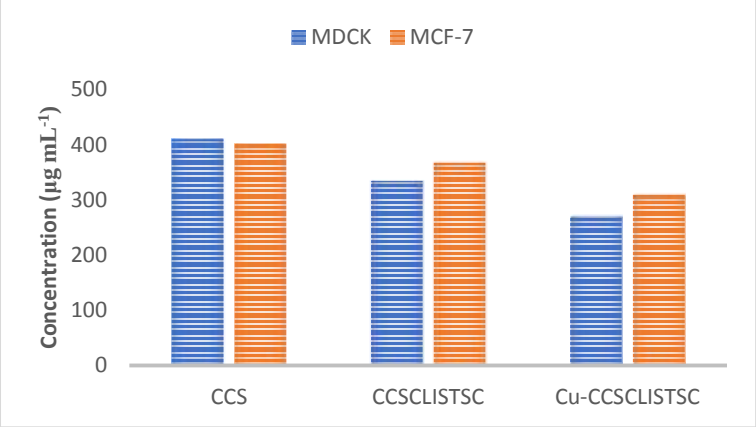


**Figure 165:** Correlative inhibition of CCS, CCSCLISTSC and Cu-CCSCLISTSC against MDCK and MCF-7 cell lines ($IC_{50}$ values)

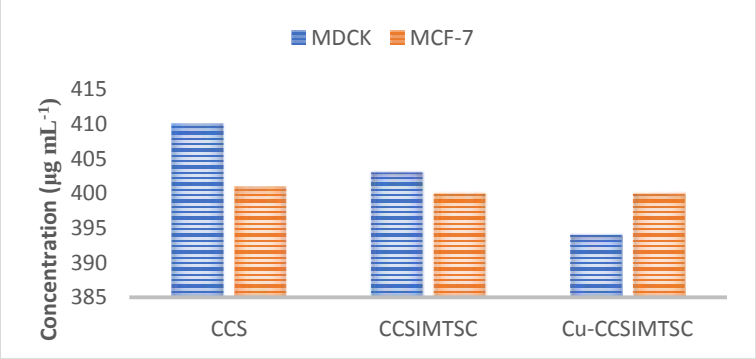


**Figure 166:** Correlative inhibition of CCS, CCSIMTSC and Cu-CCSIMTSC against MDCK and MCF-7 cell lines ($IC_{50}$ values)

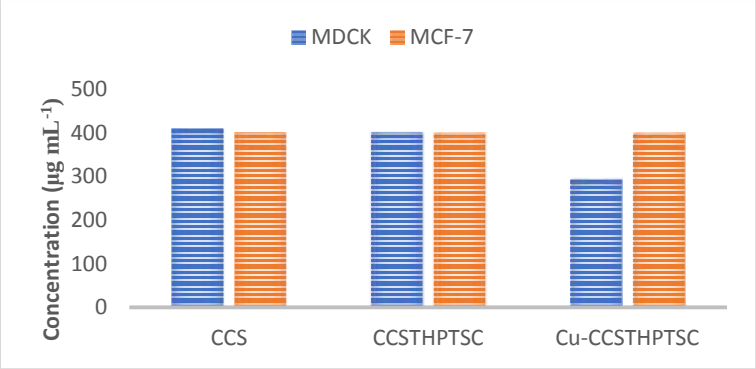


**Figure 167:** Correlative inhibition of CCS, CCSTHPTSC and Cu-CCSTHPTSC against MDCK and MCF-7 cell lines ($IC_{50}$ values)

### 4.6.5. Anticancer Activity of Chitosan and its Derivatives: An Overview on the Mechanism of Action

Medicinal property of chitosan has been reported to get enhanced by its modification through blending or drug loading (Zhang, *et al.*, 2020). In an aqueous bio environment, water molecules can make their way between the chitosan molecules in a drug-loaded chitosan dressing and the volume of the dressing increases. This process leads to the release of drug to bio environment (Brannon-Peppas,1990; Brannon-Peppas & Peppas, 1990). The inherent anticancer activity of chitosan and its derivatives follows the antiangiogenic performance, immunoenhancement, antioxidant defence mechanism and cellular apoptotic pathways (Adhikari & Yadav, 2018).

The interference to mutual regulation of pro-angiogenic and anti-angiogenic factors under the pathological conditions (Jiang, *et al.*, 2015) brings about the development of cancer cells, and this process is of tumor angiogenesis has been reported to be mediated by chitosan nanoparticles (Xu, Wen, & Xu, 2009).

Chitosan also acts by tumor growth inhibitory mechanism in which the immunological system is enhanced through the enhancement of natural killer activity (Kuppusami & Karuppaiah, 2013; Maeda & Kimura, 2004). The selective accumulation of chitosan nanoparticles in tumor cells owing to enhanced permeation and retention (EPR) effect has been found to reduce the multidrug resistance induced by p-glycoprotein (Ai, *et al.*, 2017; Ramasamy, *et al.*,2017). The inhibition of cell proliferation by chitosan oligosaccharide has been found to involve lowering the number of cells in S phase to decrease the rate of DNA synthesis (Shen, *et al.*, 2009). Square planar geometry of chitosan-metal complex has been found favorable towards the interaction of metal ion to cause more scavenging of oxidative

free radicals (Yin, *et al.*, 2004), and the cleavage of DNA that brings about the antitumor activity can also be induced by the interaction of free donor atoms (Zheng, *et al.*, 2006). The biocompatibility of copper(II) chitosan complexes is associated to protonation of amino group of chitosan that increases due to the chelation with copper(II) ion and introduces the interaction with anionic plasma membrane of cancer cells (Qi, *et al.*, 2004; Zheng, *et al.*, 2006).

The anticancer pathways of chitosan thiosemicarbazone might be associated to its antioxidant activity as a result of weakening of hydrogen bonds and interaction of C=S and N-H groups with free radicals (Zhong, *et al.*, 2010). The processes of scavenging of reactive oxygen species (ROS), and activation of a battery of detoxifying proteins are crucial to cause the natural antioxidant effects to retard the progress of many age-related diseases (Kinsella, *et al.*, 1993). The antineoplastic activity of α-(N)-heterocyclic carboxaldehyde thiosemicarabazones (HCTs) is attributed to inhibition of ribonucleotide reductase (RR) activity (Moore & Sartorelli, 1989).

The activity against the human breast cancer cell lines has been reported to be due to its antiproliferative behaviour (Jiang, *et al.*, 2011) and the anticancer pathways in cancer cell lines were found to be associated with the reduction in mitochondrial membrane potential, membrane lipid peroxidation triggering and neutralization of charge on cell surfaces (Qi, *et al.*, 2007). Apoptotic effect of chitosan was found to be associated with modulation of death receptor expression and caspase-8 (14) or caspase-3 activation (Hasegawa, *et al.*, 2001). Due to electrostatic attraction of protonated chitosan towards more negatively charged surfaces of cancer cells, chitosan can disrupt the cancer cell membrane and inflammatory cytokines like IL-6 and IL-8 are secreted (Zhang, *et al.*, 2010). The membrane damaging effect of chitosan and mitogenic effect of cytokines cannot be comprehended by cancer cells. In addition to this process, cancer cells can also be attacked by a specific extracellular receptor or by endocytosis (Wiegand, *et al.*, 2010; Wimardhani, *et al.*, 2012).

# CHAPTER 5

## 5. CONCLUSIONS AND RECOMMENDATIONS

The higher anticancer activity of chitosan oligosaccharide (CS) than high molecular weight crab shell chitosan (CCS) and the more enhanced activity against the MCF-7 cancer cell line than tumorigenic MDCK cell line were observable. Chemical modification of chitosan as chitosan functionalized thiosemicarbazones was found to invariably enhance the activity, and this activity was more enhanced in chitosan oligosaccharide analogues.

There was concentration dependent rise in IR%, and oligo chitosan thiosemicarbazones were found to show more inhibition of cell growth than the high molecular weight crab shell chitosan. Copper(II) chitosan thiosemicarbazone complexes showed an enhanced activity than the respective chitosan thiosemicarbazones, showing the copper(II) complex formation as a significant way to get the antitumorigenic and anticancer derivatives of enhanced activity *in vitro*. The antitumorigenic and anticancer activity enhancement was found more in the complexes of chitosan oligosaccharide than high molecular weight crab shell chitosan analogues. The results are in harmony with the reports that copper(II) thiosemiicarbazones impart higher cytotoxic effects than thiosemicarbazones possibly owing to their inherent redox properties (Ferrari, *et al.*, 1999; West & Liberta,1993) and the current study leaves the treasure of data for further mechanistic investigations.

The higher activity towards MCF-7 than MDCK cell line showed the selective permeability of these chitosan biomaterials through the more negatively charged cancer cell membranes and the alteration of electrical charge on these cancer cell membranes (Cure,1991; Zhou, *et al.*, 2015) for the purpose of therapeutic intervention. In particular, both CS and CCS showed less than 50% inhibition at 400 µg/mL concentration towards MDCK cell line. But, MCF-7 cell line appeared more sensitive with its 56% inhibition at 400 µg/mL concentration by CS, and there was higher inhibition of MCF-7 cancer cell line than MDCK cell line by CCS at 400 µg/mL. The chitosan derivatives with $IC_{50}$ below 348µg/mL (taken as a marginal value from literature) are recommended as more potent anticancer formulations than the derivatives with less than 50% inhibition at 400 µg/mL.

On the basis of the results, the current work is anticipated to leave the area of further investigation of the mechanistic approaches of anticancer activity of these chitosan

derivatives and their nano composites/blends against MCF-7 cancer cells. The results of the cellular uptake level of antioxidant chitosan oligosaccharide and crab shell chitosan *in vitro* (Adhikari, Garai, Marasini, *et al.*, 2021) and anticancer activity of chitosan functionalized thiosemicarbazones and their copper(II) complexes (Adhikari, Garai, Khanal, *et al.*, 2021; Adhikari, Garai, Khanal, *et al.*, 2022; Adhikari, Garai, Thapa, *et al.*, 2022) are indicatives of the necessity of *in vivo* experimental studies and the development of chitosan drug formulations in the future. The results have been found crucial to be recommended for the further investigation of the cellular pathways of their anticancer activity, and the assessment of therapeutically effective and safe chitosan based anticancer preparation.

# CHAPTER 6

## 6. SUMMARY

Chitin is a homopolymer of N-acetyl glucosamine units linked through β (1→4) linkages. This biopolymer, most abundant after cellulose, was extracted from exoskeleton of crabs, and the deacetylation of chitin produced a value-added material called chitosan as a copolymer of N-acetyl and N-deacetyl α-(1, 4) glucosamine units. The synthesized chitosan showed standard range of physicochemical parameters as reported in literatures. Owing to presence of amino and acetamido groups, chitosan was functionalized as carboxaldehyde thiosemicarbazones as versatile ligands to copper(II) ion, and the assessment of their physical characteristics showed the sustainability of chitosan resources in preparation of chitosan thiosemicarbazone from carboxaldehyde moiety. The thiosemicarbazone ligands were structurally elucidated by elemental and PXRD analysis, FT-IR and $^{13}C$ NMR spectroscopic tools. The formation, features of coordination sphere and geometrical orientation of copper(II) chitosan thiosemicarbazones were established with the help of elemental and PXRD analysis, FT-IR, $^{13}C$ NMR, and EPR spectroscopic tools. The paramagnetic behaviour of complexes was confirmed by magnetic susceptibility measurement. With the help of thermogravimetric and thermal analysis, the derivatives were found thermally stable showing almost the same thermal events and degradation behaviour as chitosan. Chitosan thiosemicarbazones of different carboxaldehyde moieties were found to exhibit the exclusive electron pair donation to copper(II) ion of cupric chloride from azomethine nitrogen and thione sulphur to give the complexes with the distorted square planar geometry proposed on the basis of the overall impression made from characterization data interpretation. The heterocyclic nitrogen in pyridine and imidazole moiety, oxygen from carbonyl group of isatin moiety and deprotonated hydroxyl group of salicylaldehyde moiety were found to be involved as coordination sites. But, the heterocyclic sulphur from thiophene ring was not found to be involved in coordination with copper(II) ion.

Anticancer activity of chitosan and its derivatives with their mechanism of action (Adhikari, & Yadav, 2018) was thoroughly reviewed to assess the hitherto reported derivatization through functionalization of chitosan, and complex formation *via* the functionalized derivatives of chitosan. On this basis, the research was motivated towards the tailoring of

chitosan based anticancer derivatives. The functionalization of chitosan as chitosan thiosemicarbazone of different carboxaldehydes with anticancer potency was found to impart a synergistic anticancer behaviour *in vitro* and their copper(II) complexes were reasonably expected to show the enhancement in anticancer activity. So, the work comprised of synthesis, and characterization of chitosan thiosemicarbazones of chitosan oligosaccharide and crab shell chitosan from eight different carboxaldehyde moieties and their copper(II) complexes, and then the study of their *in vitro* anticancer activity against tumorigenic MDCK and MCF-7 cancer cell lines. The MDCK cell line was taken to observe the cytotoxicity profile of the compounds against the cells that have recently passed through the tumorigenic development, and MCF-7 cancer cell line was selected on the basis of previous works on it (Abedian, *et al.*, 2019; Ghaly, *et al.*, 2018) motivated by more permeability of chitosan nano shuttles through the more negatively charged MCF-7 cell surfaces and cellular pathways of anticancer activity shown by chitosan biomaterials (Comsa, *et al.*, 2015; Cure,1991; Faris, *et al.*, 2021; Zhou, *et al.*, 2015).

The results of MTT assay revealed (i) enhancement in antitumorigenic and anticancer activity of chitosan upon the functionalization as chitosan thiosemicarbazone, (ii) relatively higher activity of chitosan oligosaccharide derivatives than crab shell chitosan analogues, (iii) increase in anticancer activity upon the complex formation, (iv) more inhibition of MCF-7 cancer cell line than tumorigenic MDCK cell line, and (v) close anticancer effects of different carboxaldehyde chitosan thiosemicarbazones and their copper(II) complexes, and (vi) more potent antitumorigenic and anticancer activity *in vitro* shown by compounds with $IC_{50}$ less than 348 $\mu gmL^{-1}$ .

As per aforementioned statements, the research study on 'synthesis, characterization, and anticancer activity of chitosan thiosemicarbazones and their copper(II) complexes' has been restated in terms of the following chapter wise summary of this thesis work:

Chapter 1 of this thesis introduces the etiological aspects of cancer pathophysiology and proliferation, pathways of anticancer activity with a special discussion on cellular apoptotic and antiangiogenic, enzymatic, antioxidant and immunoenhancing mechanisms of action, fundamentals of chitin and chitosan chemistry, and biologically important structural analysis of thiosemicarbazones and chitosan-metal complexes. Further, the chapter opens up with rationale and objectives of research study, the background and scope in favour of its cutting-edge perspectives and limitations on the way of chitosan-based anticancer drug development strategy.

Chapter 2 of the thesis mentions a critical, specific and in-depth review on synthetic approaches and the putative mechanisms of action of anticancer activity of chitosan and its various derivatives obtained by functionalisation through involvement of amino group in ring chitosan. Further, the chapter shows an acquaintance with nano chitosan and its anticancer activity, and anticancer clinical study and trials of chitin and chitosan derivatives.

Chapter 3 of the thesis enumerates the materials and methods of synthesis through functionalization of commercial oligo chitosan and high molecular weight crab chitosan as chitosan thiosemicarbazones and preparation of the corresponding copper(II) chitosan thiosemicarbazone complexes. It involves determination of physicochemical properties of synthesized chitosan, measurement of data by spectroscopic and analytical tools of characterization, and laboratory manuals of the measurements of physical properties, and the protocols of cells culturing and colorometric MTT assay of the compounds against tumorigenic MDCK cell line and MCF-7 cancer cell line.

Chapter 4 of the thesis presents the results and discussion. It shows the physicochemical properties of the compounds, that are affected by their mode of synthesis, molecular weight and DDA of chitosan. It gives the characterization of compounds with overall interpretation of FT-IR, $^{13}C$ NMR, PXRD, and EPR spectroscopic data and the data of elemental microanalysis, magnetic susceptibility measurement and thermal analysis to justify the formation and elucidate the bonding and structure of chitosan thiosemicarbazone ligands and their copper(II) complexes. The results of MTT assay of chitosan functionalized thiosemicarbazones and their copper(II) complexes against the MDCK tumorigenic and MCF-7 cancer cell lines have been analysed and compared to assess their relative anticancer activities. Further, it contains a literature report and a brief insight into the mechanism of action of anticancer activity of chitosan and chitosan derivatives against the tumorigenic MDCK and MCF-7 cancer cell lines.

Chapter 5 of the thesis gives the conclusive statements on the strategy of the synthesis of chitosan functionalized thiosemicarbazones and their copper(II) complexes, and their relative activity against the tumorigenic and cancer cell lines. It leaves the area of further research on the mechanistic study of anticancer activity of some more potent chitosan functionalized biomaterials, and their copper(II) complexes recommending the necessity of their *in vivo* clinical studies and trials.

# REFERENCES


Abbas, S. Y., Farag, A. A., Ammar, Y. A., Atrees, A. A., Mohamed, A. F., & El-Henawy, A. A. (2013). Synthesis, characterization and antiviral activity of novel fluorinated isatin derivatives. *Monatshefte für Chemie*, 144(11): 1725–1733.

Abedian, Z., Moghadamnia, A. A., Zabihi, E., Pourbagher, R., Ghasemi, M., Nouri, H. R., Tashakorian, H., & Jenabian, N. (2019). Anticancer properties of chitosan on osteosarcoma, breast cancer and cervical cancer cell lines. *Caspian Journal of Internal Medicine*, 10(4): 439-446.

Abou Alfa, G. K., Schwartz, L., Ricci, S., Amadori, D., Santoro, A., Figer, A., Greve, J. D., Douillard, J-Y., Lathia, C., Schwartz, B., Taylor, I., Moscovici, M., & Saltz, L. B. (2006). Phase II study of sorafenib in patients with advanced hepatocellular carcinoma. *Journal of Clinical Oncology*, 24(26): 4293-4300.

Adhikari, H. S., & Yadav, P. N. (2018). Anticancer Activity of Chitosan, Chitosan Derivatives, and Their Mechanism of Action. *International Journal of Biomaterials*, 2018: 1-29, Article no. 2952085.

Adhikari, H. S., Garai, A., Khanal, C., Adhikari, R., & Yadav, P. N. (2021). Imidazole-2-carboxaldehyde Chitosan Thiosemicarbazones, and Their Copper(II) Complexes: Synthesis, Characterization, and Antitumorigenic Activity against Madin-Darby Canine Kidney Cell Line. *Asian Journal of Chemistry*, 33(5): 969-976.

Adhikari, H. S., Garai, A., Khanal, C., Adhikari, R., & Yadav, P. N. (2022). Low and High Molecular Weight Chitosan Analogues of Imidazole-2-Thiosemicarbazones and Their Copper(II) Complexes: Synthesis, Characterization, and Antitumorigenic Activity *in vitro*. In chapter 12: *Challenges and Advances in Chemical Science*: *B. P. International*, vol. 8, 121-137. DOI: 10.9734/bpi/cacs/v8/15406D.

Adhikari, H. S., Garai, A., Marasini, B. P., Adhikari, R., & Yadav, P. N. (2021). Synthesis and Characterization of High Molecular Weight Chitosan, and Antioxidant Activity of Its Chitosan Oligosaccharide Encapsulation. *Journal of Nepal Chemical Society (JNCS)*, 42(1): 29-38.

Adhikari, H. S., Garai, A., Thapa, M., Adhikari, R., & Yadav, P. N. (2022). Chitosan functionalized thiophene-2-thiosemicarbazones, and their copper(II) complexes: synthesis,

characterization, and anticancer activity. *Journal of Macromolecular Science, Paryt A: Pure and Applied Chemistry*, 59(3), 211-227. DOI: 10.1080/10601325.2021.2022982.

Agarwal, M., Agarwal, M. K., Shrivastav, N., Pandey, S., Das, R., & Gaur, P. (2018). Preparation of Chitosan Nanoparticles and their *In-vitro* Characterization. *International Journal of Life Sciences Scientific Research*, 4(2): 1713-1720.

Agrawal, K. C., & Sartorelli, A. C. (1969). Potential antitumor agents. II. Effects of modifications in the side chain of 1-formylisoquinoline thiosemicarbazone. *Journal of Medicinal Chemistry*, 12(5): 771-774.

Ahmed, A., & Lal, R. A. (2017). Synthesis, characterization and electrochemical studies of copper(II) complexes derived from succinoyl- and adipoyldihydrazones. *Arabian Journal of Chemistry*, 10: S901–S908.

Ahn, E.Y., Pan, G., Vickers, S. M., & McDonald, J. M. (2002). IFN-gamma upregulates apoptosis-related molecules and enhances Fas-mediated apoptosis in human cholangiocarcinoma. *International Journal of Cancer*, 100(4): 445-451.

Ai, J-W., Liao, W., & Ren, Z-L. (2017). Enhanced anticancer effect of copper-loaded chitosan nanoparticles against osteosarcoma, *RSC Advances*, 7(26):15971-15977.

Alomar, K., Khan, M. A., Allain, M., & Bouet, G. (2009). Synthesis, crystal structure and characterization of 3-thiophene aldehyde thiosemicarbazone and its complexes with cobalt(II), nickel(II) and copper(II). *Polyhedron*, 28(7): 1273–1280.

Alves, N. M., & Mano, J. F. (2008). Chitosan derivatives obtained by chemical modifications for biomedical and environmental applications. *International Journal of Biological Macromolecules*, 43(5): 401-414.

Ambs, S., Merriam, W. G., Bennett, W. P., Felly-Bosco, E., Ogunfusika, M. O., Oser, S. M., Klein, S., Shields, P. G., Billiar, T. R., & Harris, C. C. (1998). Frequent nitric oxide synthase-2 expression in human colon adenomas: implication for tumor angiogenesis and colon cancer progression. *Cancer Research*, 58(2): 334-341.

Andrade, S., Ladchumananandasivam, R., Rocha, B., Belarmino, D., & Galvão, A. (2012). The use of exoskeletons of shrimp (*Litopenaeus vanammei*) and crab (*Ucides cordatus*) for the extraction of chitosan and production of nanomembrane. *Materials Sciences and Applications*, 3(7): 495–508.

Andreadis, C., Vahtsevanos, K., Sidiras, T., Thomaidis, I., Antoniadis, K., & Mouratidou, D. (2003). 5-Fluorouracil and cisplatin in the treatment of advanced oral cancer. *Oral Oncology*, 39(4): 380-385.

Aneesrahman, K. N., Ramaiah, K., Rohini, G., Stefy, G. P., Bhuvanesh, N. S. P., & Sreekanth, A. (2019). Synthesis and characterisations of copper(II) complexes of 5-methoxyisatin thiosemicarbazones: Effect of N-terminal substitution on DNA/protein binding and biological activities. *Inorganica Chimica Acta*, 492: 131-141.

Anitha, A., Chennazhi, K. P., Nair, S. V., & Jayakumar, R. (2012). 5-Flourouracil Loaded *N*, *O*-Carboxymethyl Chitosan Nanoparticles as an Anticancer Nanomedicine for Breast Cancer. *Journal of Biomedical Nanotechnology*, 8(1): 29-42.

Anitha, A., Maya, S., Deepa, N., Chennanzhi, K. P., Nair, S. V., & Jayakumar, R. (2012). Curcumin-Loaded *N*,*O*-Carboxymethyl Chitosan Nanoparticles for Cancer Drug Delivery. *Journal of Biomaterials Science, Polymer Edition*, 23(11): 1381-1400.

Antony, R., Theodore David, S., Karuppasamy, K., Saravanan, K., Thanikaikarasan, S., & Balakumar, S. (2012). Structural, Surface, Thermal and catalytic Properties of Chitosan Supported Copper(II) Mixed Ligand Complex Materials. *Journal of Surface Engineered Materials and Advanced Technology*, 2: 284-291.

Arkenau, H- T., Carden, C. P., & de Bono, J. S. (2008). Targeted agents in cancer therapy. *Medicine*, 36(1): 33-37.

Arnesano, F., & Natile, G. (2008). Platinum on the road: Interactions of antitumoral cisplatin with proteins. *Pure and Applied Chem***is**try, 80(12): 2715-2725.

Aruna, U., Rajalakshmi, R., Indira Muzib Y., Vinesha, V., Sushma, M., Vandana, K. R., & Vijay Kumar, N. (2013). Role of Chitosan Nanoparticles in Cancer Therapy. *International Journal of Innovative Pharmaceutical Research*, 4(3): 318– 324.

Astolfi, L., Ghiselli, S., Guaran, V., Chicca, M., Simoni, E., Olivetto, E., Lelli, G., & Martini, A. (2013). Correlation of adverse effects of cisplatin administration in patients affected by solid tumours: A retrospective evaluation. *Oncology Reports*, 29(4): 1285–1292.

Aulitzky, W., Gasti, G., Aulitzky, W. E., Herold, M., Kemmler, J., Mull, B., Frick, J., & Huber, C. (1989). Successful treatment of metastatic renal cell carcinoma with a biologically active dose of recombinant interferon-gamma. *Journal of Clinical Oncology*, 7(12): 1875-1884.

Bagheri-Yarmand, R., Liu, J. F., Ledoux, D., Morere, J. F., & Crepin, M. (1997). Inhibition of human breast epithelial HBL100 cell proliferation by a dextran derivative (CMDB7): interference with the FGF2 autocrine loop. *Biochemical and Biophysical Research Communications*, 239(2): 424-428.

Baldrick, P. (2010). The safety of chitosan as a pharmaceutical excipient. *Regulatory Toxicology and Pharmacology*, 56(3): 290–299.

Bartek, J., & Lukas, J. (2001). Mammalian G1- and S-phase checkpoints in response to DNA damage. *Current Opinion in Cell Biol*ogy, 13(6): 738-747.

Batista, M. K. S., Pinto, L. F., Gomes, C. A. R., & Gomes, P. (2006). Novel highly-soluble peptide–chitosan polymers: Chemical synthesis and spectral characterization. *Carbohydrate Polymers*, 64(2)**:** 299-305.

Benjamin, M. M., & Khalil, R. A. (2012). Matrix Metalloproteinase Inhibitors as Investigative Tools in the Pathogenesis and Management of Vascular Disease. *Experientia Supplementum* (*EXS)*, 103: 209-279.

Bennur, T. H., Srinivas, D., & Ratnasamy, P. (2001). EPR spectroscopy of copper and manganese complexes encapsulated in zeolites. *Microporous and Mesoporous Materials*, 48: 111-118.

Beraldo, H., & Gambinob, D. (2004). The wide pharmacological versatility of semicarbazones, thiosemicarbazones and their metal complexes. *Mini Reviews in Medicinal Chemistry*, 4(1): 31-39.

Bhadbhade, M. M., & Srinivas, D. (1993). Effects on molecular association, chelate conformation, and reactivity toward substitution in copper Cu(5-X-salen) complexes, salen2- = N,N'-ethylenebis(salicylidenaminato), X = H, $CH_3O$, and Cl: synthesis, x-ray structures, and EPR investigations. *Inorganic Chemistry*, 32(24): 5458-5466.

Bharti, N., Shailendra, Sharma, S., Naqvi, F., & Azam, A. (2003). New palladium(II) complexes of 5-nitrothiophene-2-carboxaldehyde thiosemicarbazones: Synthesis, Spectral Studies and In Vitro Anti-amoebic Activity. *Bioorganic and Medicinal Chemistry*, 11(13): 2923–2929.

Bisht, S., & Maitra, A. (2009). Dextran-doxorubicin/chitosan nanoparticles for solid tumor therapy. *Wiley Interdisciplinary Reviews: Nanomedicine and Nanobiotechnology*, 1(4): 415–425.

Bittoun, P., Avramoglou, T., Vassy, J., Crepin, M., Chaubet, F., & Fermandjian, S. (1999). Low-molecular-weight dextran derivatives (f-CMDB) enter the nucleus and are better cell-growth inhibitors compared with parent CMDB polymers. *Carbohydrate Research*, 322(3-4): 247-255.

Bittoun, P., Bagheri-Yarmand, R., Chaubet, F., Crepin, M., Jozefonvicz, J., & Fermandjian, S. (1999). Effects of the binding of a dextran derivative on fibroblast growth factor 2: secondary structure and receptor-binding studies. *Biochemical Pharmacol*ogy, 57(12): 1399-1406.

Boncel, S., Maczka, M., Koziol, K. K. K., Motyka, R., & Walczak, K. Z. (2010). Symmetrical and unsymmetrical $\alpha,\omega$-nucleobase amide-conjugated systems. *Beilstein Journal of Organic Chemistry*, 6(34): doi:10.3762/bjoc.6.34.

Bondarenko, O., Juganson, K., Ivask, A., Kasemets, K., Mortimer, M., & Kahru, A. (2013). Toxicity of Ag, CuO and ZnO nanoparticles to selected environmentally relevant test organisms and mammalian cells in vitro: a critical review. *Archives of Toxicology*, 87(7): 1181-1200.

Bouchmella, K., Dutremez, S. G., Alonso, B., Mauri, F., & Gervais, C. (2008). $^{1}$H,$^{13}$C, and$^{15}$N Solid-State NMR Studies of Imidazole- and Morpholine-Based Model Compounds Possessing Halogen and Hydrogen Bonding Capabilities. *Crystal Growth and Design*, 8(11): 3941–3950.

Brannon-Peppas, L. (1990). Preparation and Characterization of Crosslinked Hydrophilic Networks. *Studies in polymer science, Elsevier*, 8: 45–66.

Brannon-Peppas, L., & Peppas, N. A. (1990). The Equilibrium Swelling Behavior of Porous and Non-porous Hydrogels, *Studies in Polymer Science, Elsevier*, 8: 67–102.

Brockman, R. W., Thomson, J. R., Bell, M. J., & Skipper, H. (1956). Observations on the antileukemic activity of pyridine-2-carboxaldehyde thiosemicarbazone and thiocarbohydrazone, *Cancer Research*, 16(2): 167-170.

Brown, P. D. (1998). Matrix metalloproteinases in gastrointestinal cancer. *Gut*, 43(2): 161-163.

Brugnerottoa, J., Lizardi, J., Goycoolea, F. M., Argüelles-Monal, W., Desbrières, J., & Rinaudo, M. (2001). An infrared investigation in relation with chitin and chitosan characterization. *Polymer*, 42(8): 3569-3580.

Brummer, Y., & Cui, S. W. (2006). Detection and Determination of Polysaccharides in Food. *Food Polysaccharides and their Applications, A. M. Stephen, G. O. Phillips, P. A. Williams, Eds.; CRC: Boca Raton,* pp. 675-712.

Bumgardner, J. D., Wiser, R., Gerard, P. D., Bergin, P., Chestnutt, B., Marin, M., Ramsey, V., Elder, S. H., & Gilbert, J. A. (2003). Chitosan: potential use as a bioactive coating for orthopaedic and craniofacial/dental implants. *Journal of Biomaterial Science Polymer Edition,* 14(5): 423-438.

Burkatovskaya, M., Tegos, G. P., Swietlik, E., Demidova, T. N., Castano, A. P., & Hamblin, M. R. (2006). Use of chitosan bandage to prevent fatal infections developing from highly contaminated wounds in mice. *Biomaterials*, 27(22): 4157–4164.

C. A. Black (Ed.) (1965). Methods of Soil Analysis: Part I, Physical and mineralogical properties. *American Society of Agronomy, Madison, Wisconsin,* pp. 671-698.

Carcelli, M., Tegoni, M., Bartoli, J., Marzano, C., Pelosi, G., Salvalaio, M., Rogolino, D., & Gandin, V. (2020). In vitro and in vivo anticancer activity of tridentate thiosemicarbazone copper complexes: Unravelling an unexplored pharmacological target. *European Journal of Medicinal Chemistry*, 194: 1-15, Article no. 112266.

Carreno-Gomez, B., & Duncan, R. (1997). Evaluation of the biological properties of soluble chitosan and chitosan microspheres. *International Journal of Pharmaceutics*, 148(2): 231-240.

Casas, J. S., Garcia-Tasende, M. S., & Sordo, J. (2000). Main group metal complexes of semicarbazones and thiosemicarbazones. A structural review. *Coordination Chemistry Reviews*, 209(1): 197-261.

Castagnino, E., Ottaviani, M. F., Cangiotti, M., Morelli, M., Casettari, L., & Muzzarelli, R. A. A. (2008). Radical scavenging activity of 5-methylpyrrolidinone chitosan and dibutyryl chitin. *Carbohydrate Polymers*, 74(3): 640–647.

Chang, L., Kamata, H., Solinas, G., Luo, J. L., Maeda, S., Venuprasad, K., Liu, M. C., & Karin, M. (2006). The E3 ubiquitin ligase itch couples JNK activation to TNF alpha-induced cell death by inducing c-FLIP(L) turnover. *Cell*, 124(3): 601-613.

Chappey, O. N., Niel, E., Wautier, J-L., Hung, P. P., Dervichian, M., Cattan, D., & Scherrmann, J. M. (1993). Colchicine disposition in human leukocytes after single and multiple oral administration. *Clinical Pharmacology & Therapeutics*, 54: 360-367.

Chen, P. N., Chu, S. C., Chiou, H. L., Chiang, C. L., Yang, S. F., & Hsieh, Y. S. (2005). Cyanidin 3-glucoside and peonidin 3-glucoside inhibit tumor cell growth and induce apoptosis in vitro and suppress tumor growth *in vivo*. *Nutrition and Cancer*, 53(2): 232-243.

Chen, P. N., Chu, S. C., Chiou, H. L., Kuo, W. H., Chiang, C. L., & Hsieh, Y. S. (2006). Mulberry anthocyanins, cyanidin 3-rutinoside and cyanidin 3-glucoside, exhibited an inhibitory effect on the migration and invasion of a human lung cancer cell line. *Cancer Letters*, 235(2): 248-259.

Chen, P. N., Kuo, W. H., Chiang, C. L., Chiou, H. L., Hsieh, Y. S., & Chu, S. C. (2006). Black rice anthocyanins inhibit cancer cells invasion via repressions of MMPs and u-PA expression. *Chemico-Biological Interactions*, 163(3): 218-229.

Chen, X.-G., & Park, H.-J. (2003). Chemical characteristics of O-carboxymethyl chitosans related to the preparation conditions. *Carbohydrate Polymers*, 53(4): 355-359.

Chethan, P. D., Vishalakshi, B., Sathish, L., Ananda, K., & Poojary, B. (2013). Preparation of substituted quaternized aryl furan chitosan derivatives and their antimicrobial activity. *International Journal of Biological Macromolecules*, 59: 158–164.

Chohan, Z. H., Pervez, H., Rauf, A., Khan, K. M., & Supuran, C. T. (2004). Isatin-derived Antibacterial and Antifungal Compounds and their Transition Metal Complexes. *Journal of Enzyme Inhibition and Medicinal Chemistry*, 19(5): 417-423.

Comsa, Ş., Cimpean, A. M., & Raica, M. (2015). The Story of MCF-7 Breast Cancer Cell Line: 40 years of Experience in Research. *Anticancer Research*, 35(6): 3147-3154.

Cortes, J., & Vidal, M. (2012). Beyond taxanes: the next generation of microtubule-targeting agents. *Breast Cancer Research and Treatment*, 133: 821-830.

Cory, J. G., & Sato, A. (1983). Regulation of ribonucleotide reductase activity in mammalian cells. *Molecular and Cellular Biochemistry*, 53(1-2): 257-266.

Crick, F. (1970). Central Dogma of Molecular Biology. *Nature*, 227: 561-563.

Crielaard, B. J., van der Wal, S., Lammers, T., Le, H. T., Hennink, W. E., Schiffelers, R. M., Storm, G., & HAM Fens, M. (2011). A polymeric colchicinoid prodrug with reduced toxicity and improved efficacy for vascular disruption in cancer therapy. *International Journal of Nanomedicine*, 6: 2697-2703.

Cure, J. C. (1991). Cancer an electrical phenomenon. *Resonant*, 1(1).

Czechowska-Biskup, R., Ulanski, P., Rosiak, J. M., Kumor, A., Kozak-Michalowska, I., Lorence, J., & Meler, J. (2004). Examination of plant fat-and cholesterol binding by chitosan of various molecular weights- preliminary data. *H. Struszczyk (ed.) Progress on Chemistry and Application of Chitin and its Derivatives*, X, Lodz: 121-130.

Da Sacco, L., & Masotti, A. (2010). Chitin and Chitosan as Multipurpose Natural Polymers for Groundwater Arsenic Removal and $As_2O_3$ Delivery in Tumor Therapy. *Marine Drugs*, 8(5): 1518-1525.

De Angelis, A. A., Capitani, D., & Crescenzi, V. (1998). Synthesis and $^{13}C$ CP-MAS NMR characterization of a new chitosan-based polymeric network. *Macromolecules*, 31: 1595–1601.

de Britto, D., & Assis, O. B. G. (2007). A novel method for obtaining a quaternary salt of chitosan. *Carbohydrate Polymers*, 69: 305–310.

De Britto, D., & Campana-Filho, S. P. (2004). A kinetic study on the thermal degradation of N, N, N-trimethylchitosan. *Polymer Degradation and Stability*, 84(2): 353–361.

Dehaghi, S. M., Rahmanifar, B., Moradi, A. M., & Azar, P. A. (2014). Removal of permethrin pesticide from water by chitosan–zinc oxide nanoparticles composite as an adsorbent. *Journal of Saudi Chemical Society*, 18: 348-355.

Di Benedetto, M., Kourbali, Y., Starzec, A., Vassy, R., Jozefonvicz, J., Perret, G., Crepin, M., & Kraemer, M. (2001). Sodium phenylacetate enhances the inhibitory effect of dextran derivative on breast cancer cell growth *in vitro* and in nude mice. *British Journal of Cancer*, 85(6): 917-923.

Di Benedetto, M., Starzec, A., Colombo, B. M., Briane, D., Perret, G. Y., Kraemer, M., & Crepin, M. (2002). Aponecrotic, antiangiogenic and antiproliferative effects of a novel dextran derivative on breast cancer growth *in vitro* and *in vivo*. *British Journal of Pharmacology*, 135(8): 1859-1871.

Di Benedetto, M., Starzec, A., Vassy, R., Perret, G. Y., & Crepin, M. (2008). Distinct heparin binding sites on VEGF165 and its receptors revealed by their interaction with a non sulfated glycoaminoglycan (NaPaC). *Biochimica et Biophysica Acta*, 1780(4): 723-732.

Di Benedetto, M., Starzec, A., Vassy, R., Perret, G. Y., Crepin, M., & Kraemer, M. (2003). Inhibition of epidermoid carcinoma A 431 cell growth and angiogenesis in nude mice by

early and late treatment with a novel dextran derivative. *British Journal of Cancer*, 88(12): 1987-1994.

Di Martino, A., Sittinger, M., & Risbud, M. V. (2005). Chitosan: a versatile biopolymer for orthopaedic tissue-engineering. *Biomaterials*, 26(30): 5983-5990.

Djord jevic, C. (1960). Magnetic Susceptibilities of Some Square Four-Covalent and Tetragonal Six-Covalent Complexes of Divalent Copper. *Croatica Chemica Acta*, 32(4): 183-187.

Dou, J., Ma, P., Xiong, C., Tan, C., & Du, Y. (2011). Induction of apoptosis in human acute leukemia HL-60 cells by oligochitosan through extrinsic and intrinsic pathway. *Carbohydrate Polymers*, 86(1): 19-24.

Dutta, P. K., Dutta, J., & Tripathi, V. S. (2004). Chitin and chitosan: Chemistry, properties and application. *Journal of Scientific and Industrial Research*, 63: 20-31.

Eberhart, C. E., Coffey, R. J., Radhika, A., Giardiello, F. M., Ferrenbach, S., & Du Bois, R. N. (1994). Up-regulation of cyclooxygenase 2 gene expression in human colorectal adenomas and adenocarcinomas. *Gastroenterology*, 107(4): 1183-1188.

Ebert, L. M., Meuter, S., & Moser, B. (2006). Homing and Function of Human Skin γδ T Cells and NK Cells: Relevance for Tumor Surveillance. *The Journal of Immunology*, 176(7): 4331-4336.

Effros, R. B. (2003). Genetic alterations in the ageing immune system: impact on infection and cancer. *Mechanisms of Ageing and Development*, 124(1): 71-77.

Eggermont, A. M., Schraffordt Koops, H., Lienard, D., Kroon, B. B., van Geel, A. N., Hoekstra, H. J., & Lejeune, F. J. (1996). Isolated limb perfusion with high-dose tumor necrosis factor-alpha in combination with interferon-gamma and melphalan for nonresectable extremity soft tissue sarcomas: a multicenter trial. *Journal of Clinical Oncology*, 14(10): 2653-2665.

El-Atawy, M. A., Omar, A. Z., Hagar, M., & Shashir, E. M. (2019). Transalkylidation reaction: green, catalyst-free synthesis of thiosemicarbazones and solving the NMR conflict between their acyclic structure and intramolecular cycloaddition products. *Green Chemistry Letters and Reviews*, 12(3): 364-376.

Eske Corporation S.A.C. (2017). Randomized Clinical Trial Evaluating the Use of the Laser-assisted Immunotherapy (LIT/inCVAX) in Advanced Breast Cancer. Retrieved November

21, 2018 from https://ClinicalTrials.gov/ct2/show/NCT03202446, ClinicalTrials.gov Identifier: NCT03202446.

Falck, J., Mailand, N., Syljuasen, R. G., Bartek, J., & Lukas, J. (2001). The ATM-Chk2-Cdc25A checkpoint pathway guards against radioresistant DNA synthesis. *Nature*, 410(6830): 842-847.

Fangkangwanwong, J., Sae-liang, N., Sriworarat, C., Sereemaspun, A., & Chirachanchai, S. (2016). Water-Based Chitosan for Thymine Conjugation: A Simple, Efficient, Effective, and Green Pathway to Introduce Cell Compatible Nucleic Acid Recognition. *Bioconjugate Chemistry*, 27(10): 2301–2306.

Faris, T., Harisa, G. I., Alanazi, F. K., Badran, M. M., Alotaibi, A. M., Almanea, H., Alqahtani, A. S., & Samy, A. M. (2021). Cytotoxicity of Chitosan Ultrafine Nanoshuttles on the MCF-7 Cell Line as a Surrogate Model for Breast Cancer. *Current Drug Delivery*, 18(1): 19-30.

Farra, R., Thiel, K., Winter, A., Klamroth, T., Po¨ppl, A., Kelling, A., Schilde, U., Taubert, A., & Strauch, P. (2011). Tetrahalidocuprates(II)—structure and EPR spectroscopy. Part 1: Tetrabromidocuprates(II). *New Journal of Chemistry*, 35: 2793–2803.

Fernandes Queiroz, M., Melo, K., Sabry, D., Sassaki, G., & Rocha, H. (2015). Does the Use of Chitosan Contribute to Oxalate Kidney Stone Formation?. *Marine Drugs*, 13: 141–158.

Fernandes, J. C., Sereno, J., Garrido, P., Parada, B., Cunha, M. F. X., Reis, F., Pintado, M. E., & Santos-Silva, A. (2012). Inhibition of bladder tumor growth by chitooligosaccharides in an experimental carcinogenesis model. *Marine Drugs*, 10(12): 2661-2675.

Fernig, D. G., & Gallagher, J. T. (1994). Fibroblast growth factors and their receptors: An information network controlling tissue growth, morphogenesis and repair. *Progress in Growth Factor Research*, 5(4): 353-377.

Ferrari, M. B., Capacchi, S., Pelosi, G., Reffo, G., Tarasconi, P., Albertini, R., Pinelli, S., & Lunghi, P. (1999). Synthesis, structural characterization and biological activity of helicin thiosemicarbazone monohydrate and a copper(II) complex of salicylaldehyde thiosemicarbazone, *Inorganica Chimica Acta*, 286(2): 134–141.

Figgis, B. N. (1958). Magnetic Properties of Spin-Free Transition Series Complexes. *Nature*, 182: 1568-1570.

Folkman, J. (1972). Anti-angiogenesis: new concept for therapy of solid tumors. *Annals of Surgery*, 175(3): 409-416.

Folkman, J. (1995). Clinical applications of research on angiogenesis. *The New England Journal of Medicine*, 333: 1757-1763.

Folkman, J. (1996). New perspectives in clinical oncology from angiogenesis research. *European Journal of Cancer*, 32A(14): 2534-2539.

Folkman, J. (1997). Angiogenesis and angiogenesis inhibition: an overview. Experientia Supplementum (*EXS)*, 79:1-8.

Frank, A. L. (1982). Selected laboratory aspects of influenza surveillance. *Yale Journal of Biology and Medicine*, 55: 201-205.

French, F. A., & Blantz Jr, E. J. (1966). The Carcinostatic Activity of Thiosemicarbazones of Formyl Heteroaromatic Compounds.[1] III. Primary Correlation. *Journal of Medicinal Chemistry*, 9(4): 585-589.

French, F. A., & Blantz Jr, E. J. (1971). Chemotherapy studies on experimental mouse tumors X. *Cancer Chemotherapy Reports Part 2*, 2: 199-235.

Friedel, G., Pastorino, U., Ginsberg, R. J., Goldstraw, P., Johnston, M., Pass, H., Putnam, J. B., & Toomes, H. (2002). Results of lung metastasectomy from breast cancer: prognostic criteria on the basis of 467 cases of the international registry of lung metastases. *European Journal of Cardiothoracic Surgery*, 22: 335-344.

Fuertes, M. A., Alonso, C., & Perez., J. M. (2003). Biochemical Modulation of Cisplatin Mechanisms of Action: Enhancement of Antitumor Activity and Circumvention of Drug Resistance. *Chemical Reviews*, 103(3): 645-662.

Garribba, E., & Micera, G. (2006). The Determination of the Geometry of Cu(II) Complexes: An EPR Spectroscopy Experiment. *Journal of Chemical Education*. 83(8): 1229-1232.

Gaur, U., Sahoo, S. K., De, T. K., Ghosh, P. C., Maitra, A., & Ghosh, P. K. (2000). Biodistribution of fluoresceinated dextran using novel nanoparticles evading reticuloendothelial system. *International Journal of Pharmaceutics*, 202(1-2): 1–10.

Gavhane, Y. N., Gurav, A. S., & Yadav, A. V. (2013). Chitosan and Its Applications: A Review of Literature. *International journal of research in pharmaceutical and biomedical sciences*, 4(1): 312-331.

Gervelas, C., Avramoglou, T., Crepin, M., & Jozefonvicz, J. (2002). Growth inhibition of human melanoma tumor cells by the combination of sodium phenylacetate (NaPA) and substituted dextrans and one NaPA-dextran conjugate. *Anticancer Drugs*, 13(1): 37-45.

Ghaly, C. A. F., Bakaar, A., & Mohamed, A. F. (2018). In vitro Assessment of Anticancer Activity of Shrimp Derived Chitosan and Related Apoptotic Profile Alteration. *Journal of the Egyptian Society of Parasitology*, 48(2): 379-388.

Gomillion, C. T. (2019). Assessing the potential of chitosan/polylactide nanoparticles for delivery of therapeutics for triple-negative breast cancer treatment. *Regenerative Engineering and Translational Medicine*, 5(1): 61-73.

Gordon, M. H. (1996). Characterization of food — Emerging methods: Ed. A. G. Gaonkar. Elsevier Science, Amsterdam. *Food Chemistry*, 57: 587.

Grenha, A., Grainger, C. I., Dailey, L. A., Seijo, B., Martin, G. P., Remuñán-López, C., & Forbes, B. (2007). Chitosan nanoparticles are compatible with respiratory epithelial cells *in vitro*. *European Journal of Pharmaceutical Sciences*, 31(2): 73–84.

Gritsch, L., Lovell, C., Goldmann, W. H., & Boccaccini, A. R. (2018). Fabrication and characterization of copper(II)-chitosan complexes as antibiotic-free antibacterial biomaterial. *Carbohydrate Polymers*, 179: 370-378.

Gu, R., Sun, W., Zhou, H., Wu, Z., Meng, Z., Zhu, X., Tang, Q., Dong, J., & Dou, G. (2010). The performance of a fly-larva shell-derived chitosan sponge as an absorbable surgical hemostatic agent. *Biomaterials*, 31(6): 1270–1277.

Günbeyaz, M., Faraji, A., Özkul, A., Purali, N., & Şenel, S. (2010). Chitosan based delivery systems for mucosal immunization against bovine herpesvirus 1 (BHV-1). *European Journal of Pharmaceutical Sciences*, 41(3-4): 531–545.

Guo, X. F., Kikuchi, K., Matahira, Y., Sakai, K., & Ogawa, K. (2002). Water-soluble chitin of low degree of deacetylation. *Journal of Carbohydrate Chemistry*, 21: 149-161.

Habibie, S., Hamzah, M., Anggaravidya, M., & Kalembang, E. (2016). The effect of chitosan on physical and mechanical properties of paper. *Journal of Chemical Engineering and Materials Science*, 7(1): 1-10.

Halliwell, B., Aeschbach, R., Loliger, J., & Aruoma, O. I. (1995). The characterization of antioxidants. *Food and Chemical Toxicology*, 33(7): 601-617.

Han, H. D., Mangala, L. S., Lee, J. W., Shahzad, M. M., Kim, H. S., Shen, D., Nam, E. J., Mora, E. M., Stone, R. L., Lu, C., Lee, S. J., Roh, J. W., Nick, A. M., Lopez-Berestein, G., & Sood, A. K. (2010). Targeted gene silencing using RGD– labeled chitosan nanoparticles. *Clinical Cancer Research*, 16(15): 3910– 3922.

Han, L-K., Kimura, Y., & Okuda, H. (1999). Reduction in fat storage during chitin-chitosan treatment in mice fed a high-fat diet. *International Journal of Obesity and Related Metabolic Disorders*, 23: 174-179.

Hanahan, D., & Weinberg, R. A. (2011). Hallmarks of cancer: the next generation. *Cell*, 144: 646-674.

Hannon, G. J., & Beach, D. (1994). p15INK4B is a potential effector of TGF-beta-induced cell cycle arrest. *Nature*, 371(6494): 257-261.

Hannon., M. J. (2007). Metal-based anticancer drugs: From a past anchored in platinum chemistry to a post-genomic future of diverse chemistry and biology. *Pure and Applied Chemistry*, 79(12): 2243-2261.

Hanumantharao, R., Kalainathan, S., & Bhagavannarayana, G. (2012). Growth, spectral, optical, thermal, crystallization perfection and nonlinear optical studies of novel nonlinear optical crystal—Urea thiosemicarbazone monohydrate. *Spectrochimica Acta Part A: Molecular and Biomolecular Spectroscopy*, 91: 345–351.

Harish Prashanth, K. V., & Tharanathan, R. N. (2005). Depolymerized products of chitosan as potent inhibitors of tumor-induced angiogenesis. *Biochimica et Biophysica Acta (BBA)-General Subjects*, 1722(1): 22-29.

Harish Prashanth, K. V., & Tharanathan, R. N. (2007). Chitin/chitosan: modifications and their unlimited application potential—an overview. *Trends in Food Science and Technology*, 18(3): 117-131.

Hasegawa, M., Yagi, K., Iwakawa, S., & Hirai, M. (2001). Chitosan Induces Apoptosis via Caspase-3 Activation in Bladder Tumor Cells. *Japanese Journal of Cancer Research*, 92(4): 459-466.

Heux, L., Brugnerotto, J., Desbrières, J., Versali, M. F., & Rinaudo, M. (2000). Solid state NMR for determination of degree of acetylation of chitin and chitosan. *Biomacromolecules*, 1(4): 746-751.

Hidaka, Y., Ito, M., Mori, K., Yagasaki, H., & Kafrawy, A. H. (1999). Histopathological and immunohistochemical studies of membranes of deacetylated chitin derivatives implanted over rat calvaria. *Journal of Biomedical Material Research*, 46: 418-423.

Hosoda, J., Unezaki, S., Maruyama, K., Tsuchiya, S., & Iwatsuru, M. (1995). Antitumor activity of doxorubicin encapsulated in poly(ethylene glycol)-coated liposomes. *Biological and Pharmaceutical Bulletin*, 18(9): 1234-1237.

Hossain, Z., & Takahashi, K. (2008). Induction of Permeability and Apoptosis in Colon Cancer Cell Line with Chitosan. *Journal of Food and Drug Analysis*, 16(5): 1-8.

Hosseinzadeh, H., Atyabi, F., Dinarvand, R., & Ostad, S. N. (2012). Chitosan-Pluronic nanoparticles as oral delivery of anticancer gemcitabine: preparation and *in vitro* study. *International Journal of Nanomedicine*, 7: 1851-1863.

Huang, M., Khor, E., & Lim, L. Y. (2004). Uptake and Cytotoxicity of Chitosan Molecules and Nanoparticles: Effects of Molecular Weight and Degree of Deacetylation. *Pharmaceutical Research*, 21(2): 344-353.

Hur, G. M., Lewis, J., Yang, Q., Lin, Y., Nakano, H., Nedospasov, S., & Liu, Z. G. (2003). The death domain kinase RIP has an essential role in DNA damage-induced NF-kappa B activation. *Genes and Development*, 17(7): 873-882.

Hwang, S. M., Chen, C. Y., Chen, S. S., & Chen, J. C. (2000). Chitinous materials inhibit nitric oxide production by activated RAW 264.7 macrophages. *Biochemical and Biophysical Research Commun*ications, 271(1): 229-233.

Ihara, T., Uemura, A., Futamura, A., Shimizu, M., Baba, N., Nishizawa, S., Teramae, N., & Jyo, A. (2009). Cooperative DNA Probing Using a β-Cyclodextrin−DNA Conjugate and a Nucleobase-Specific Fluorescent Ligand. *Journal of American Chemical Society*, 131: 1386-1387.

Inukai, Y., Chinen, T., Matsuda, T., Kaida, Y., & Yasuda, S. (1998). Selective separation of germanium(IV) by 2,3- dihydroxypropyl chitosan resin. *Analytica Chimica Acta*, 371: 187–193.

Islam, Md. R., & Mohsin, M. (2007). Synthesis of isatin, 5-chloroisatin and their $\Delta^2$-1, 3, 4 oxadiazoline derivatives for comparative cytotoxicity study on brine shrimp. *Bangladesh Journal of Pharmacol*ogy, 2: 7-12.

Ismail, E. H., Sabry, D. Y., Mahdy, H., & Khalil, M. M. H. (2014). Synthesis and Characterization of some Ternary Metal Complexes of Curcumin with 1,10-phenanthroline and their Anticancer Applications. *Journal of Scientific Research*, 6(3): 509-519.

Ivan Segura Duran, University of Guadalajara (2017). Chitosan Scaffold for Sellar Floor Repair in Endoscopic Endonasal Transsphenoidal Surgery. Retrieved November 21, 2018 from https://ClinicalTrials.gov/ct2/show/NCT03280849.

Jayakumar, R., & Tamura, H. (2008). Synthesis, characterization and thermal properties of chitin-*g*-poly(*ε*-caprolactone) copolymers by using chitin gel. *International Journal of Biological Macromolecules*, 43(1): 32-36.

Jayakumar, R., Chennazhi, K. P., Muzzarelli, R. A., Tamura, H., Nair, S. V., & Selvamurugan, S. (2010). Chitosan conjugated DNA nanoparticles in gene therapy. *Carbohydrate Polymers*, 79(1): 1-8.

Jayakumar, R., Nagahama, H., Furuike, T., & Tamura, H. (2008). Synthesis of phosphorylated chitosan by novel method and its characterization. *International Journal of Biological Macromolecules*, 42(4): 335-339.

Jayakumar, R., Nwe, N., Tokura, S., & Tamura, H. (2007). Sulfated chitin and chitosan as novel biomaterials. *International Journal of Biological Macromolecules*, 40(3): 175-181.

Jayakumar, R., Prabaharan, M., Kumar, P. T. S., Nair, S. V., & Tamura, H. (2011). Biomaterials based on chitin and chitosan in wound dressing applications. *Biotechnology Advances*, 29(3): 322-337.

Jayakumar, R., Prabaharan, M., Nair, S. V., & Tamura, H. (2010). Novel chitin and chitosan nanofibers in biomedical applications. *Biotechnology Advances*, 28(1): 142-150.

Jayakumar, R., Prabaharan, M., Reis, R. L., & Mano, J. F. (2005). Graft copolymerized chitosan - present status and applications. *Carbohydrate Polymers*, 62(2): 142-158.

Jhaveri, J., Raichura, Z., Khan, T., Momin, M., & Omri, A. (2021). Chitosan Nanoparticles-Insight into Properties, Functionalization and Applications in Drug Delivery and Theranostics. *Molecules*, 26: 272-301.

Ji, J., Wu, D., Liu, L., Chen, J., & Xu, Y. (2012). Preparation, evaluation, and *in vitro* release of folic acid conjugated O-carboxymethyl chitosan nanoparticles loaded with methotrexate. *Journal of Applied Polymer Science*, 125(S2): E208-E215.

Ji, X., Zhong, Z. M., Chen, X. L., Xing, R., Liu, S., Wang, L., & Li, P. C. (2007). Preparation of 1,3,5-thiadiazine-2-thione derivatives of chitosan and their potential antioxidant activity *in vitro*. *Bioorganic and Medicinal Chemistry Letters*, 17(15): 4275–4279.

Jiang, M., Ouyang, H., Ruan, P., Zhao, H., Pi, Z., Huang, S., Yi, P., & Crepin, M. (2011). Chitosan derivatives inhibit cell proliferation and induce apoptosis in breast cancer cells. *Anticancer Research*, 31(4): 1321-1328.

Jiang, T. D. (2001). Chitosan. *Chemical Industry Press: Beijing, China*, p.91, p.100, p.108.

Jiang, Z., Han, B., Li, H., Yang, Y., & Liu, W. (2015). Carboxymethyl chitosan represses tumor angiogenesis *in vitro* and *in vivo*. *Carbohydrate polymers*, 129: 1-8.

Jiao, T. F., Zhou, J., Zhou, J-X., Gao, L-H., Xing, Y. Y., & Li, X-H. (2011). Synthesis and Characterization of Chitosan-based Schiff Base Compounds with Aromatic Substituent Groups. *Iranian Polymer Journal*, 20(2): 123-136.

Jin, Y. H., Hu, H. Y., Qiao, M. X., Zhu, J., Qi, J. W., Hu, C. J., Zhang, Q., & Chen, D. W. (2012). pH-Sensitive chitosan-derived nanoparticles as doxorubicin carriers for effective anti-tumor activity: Preparation and *in vitro* evaluation. *Colloids and Surfaces B: Biointerfaces*, 94: 184-191.

Joseph, M., Kuriakose, M., Kurup, M. R. P., Suresh, E., Kishore, A., & Bhat, S. G. (2006). Structural, antimicrobial and spectral studies of copper(II) complexes of 2-benzoylpyridine N(4)-phenyl thiosemicarbazone. *Polyhedron*, 25(1): 61–70.

Joseph, M., Suni, V., Prathapachandra Kurup, M. R., Nethaji, M., Kishore, A., & Bhat, S. G. (2004). Structural, spectral and antimicrobial studies of copper(II) complexes of 2-benzoylpyridine N(4)-cyclohexyl thiosemicarbazone. *Polyhedron*, 23(18): 3069–3080.

Kalinowska-Lis, U., Ochocki, J., & Matlawska-Wasowska., K. (2008). Trans geometry in platinum antitumor complexes. *Coordination Chemistry Reviews*, 252 (12-14): 1328-1345.

Kamath, P. R., & Sunil, D. (2017). Nano-Chitosan Particles in Anticancer Drug Delivery: An Up-to-Date Review. *Mini Reviews in Medicinal Chemistry*, 17(15): 1457-1487.

Kamiyama, K., Onishi, H., & Machida, Y. (1999). Biodisposition characteristics of N-succinyl-chitosan and glycol-chitosan in normal and tumor-bearing mice. *Biological and Pharmaceutical Bulletin*, 22(2): 179-186.

Karnofsky, D. A. (1968). Mechanism of Action of Anticancer Drugs at a Cellular Level. *A cancer journal for clinicians*, 18(4): 232-234.

Kasaai, M. R. (2011). The Use of Various Types of NMR and IR Spectroscopy for Structural Characterization of Chitin and Chitosan. *Chitin, Chitosan, Oligosaccharides and their Derivatives: Biological Activities and Applications, S. K. Kim, Ed.; CRC: Boca Raton,* pp. 149-170.

Kato, Y., Onishi, H., & Machida, Y. (2000). Evaluation of N-succinyl-chitosan as a systemic long-circulating polymer. *Biomaterials*, 21(15): 1579-1585.

Kato, Y., Onishi, H., & Machida, Y. (2005). Contribution of Chitosan and its Derivatives to Cancer Chemotherapy. *In Vivo*, 19(1): 301-310.

Katsetos, C. D., & Dráber, P. (2012). Tubulins as therapeutic targets in cancer: From bench to bedside. *Current Pharmaceutical Design*, 18: 2778-2792.

Kean, T., & Thanou, M. (2010). Biodegradation, biodistribution and toxicity of chitosan. *Advanced Drug Delivery Reviews*, 62(1): 3–11.

Khalid, M. N., Agnely, F., Yagoubi, N., Grossiord J. L., & Couarraze, G. (2002). Water State Characterization, Swelling Behavior, Thermal and Mechanical Properties of Chitosan Based Networks. *European Journal of Pharmaceutical Sciences*. 15(5): 425–432.

Khan, T. A., Peh, K. K., & Ch'ng, H. S. (2002). Reporting degree of deacetylation values of chitosan: The influence of analytical methods. *Journal of Pharmacy and Pharmaceutical Sciences*, 5: 205-212.

Khanmohammadi, M., Elmizadeh, H., & Ghasemi, K. (2015). Investigation of Size and Morphology of Chitosan Nanoparticles Used in Drug Delivery System Employing Chemometric Technique. *Iranian Journal of Pharmaceutical Research*, 14(3): 665–675.

Khor, E., & Lim, L. Y. (2003). Implantable applications of chitin and chitosan. *Biomaterials*, 24(13): 2339-2349.

Khoushab, F. & Yamabhai, M. (2010). Chitin Research Revisited. *Marine Drugs*, 8(7): 1988–2012.

Kim, J. K., Han, K-H., Lee, J. T., Paik, Y. H., Ahn, S. H., Lee, J. D., Lee, K. S., Chon, C. Y., & Moon, Y. M. (2006). Long-term Clinical Outcome of Phase IIb Clinical Trial of Percutaneous

Injection with Holmium-166/Chitosan Complex (Milican) for the Treatment of Small Hepatocellular Carcinoma. *Clinical Cancer Research*, 12(2): 543-548.

Kim, J-H., Kim, Y-S., Kim, S., Park, J. H., Kim, K., Choi, K., Chung, H., Jeong, S. Y., Park, R-W., Kim, I-S., & Kwon, I. C. (2006). Hydrophobically modified glycol chitosan nanoparticles as carriers for paclitaxel. *Journal of Controlled Release*, 111(1-2): 228–234.

Kinsella, J. E., Frankel, E., German, B., & Kanner, J. (1993). Possible mechanisms for the protective role of antioxidants in wine and plant foods. *Journal of Food Technology*, 47(4): 85–89.

Kittur, F. S., Prashanth, K. V. H., Sankar, K. U., & Tharanathan, R. N. (2002). Characterization of chitin, chitosan and their carboxymethyl derivatives by differential scanning calorimetry. *Carbohydrate Polymers*, 49: 185–193.

Klayman, D. L., Bartosevich, J. F., Griffin, T. S., Mason, C. J., & Scovill, J. P. (1979). 2-Acetylpyridine thiosemicarbazones. 1. A new class of potential antimalarial agents", *Journal of Medicinal Chemistry*, 22(7): 855-862.

Koopaei, M. N., Khoshayand, M. R., Mostafavi, S. H., Amini, M., Khorramizadeh, M. R., Tehrani, J. T., Atyabi, F., & Dinarvand, R. (2014). Docetaxel loaded PEG-PLGA nanoparticles: optimized drug loading, *in vitro* cytotoxicity and *in vivo* antitumor effect. *Iranian Journal of Pharmaceutical Research*, 13(3): 819–833.

Kraatz, H. B. (2005). Ferrocene-Conjugates of Amino Acids, Peptides and Nucleic Acids. *Journal of Inorganic and Organometallic Polymers and Materials*, 15: 83–106.

Kuan-Han, L., Huang, B.-R., & Tzeng, C. C. (1999). Synthesis and anticancer evaluation of certain alpha-methylene-gamma-(4-substituted phenyl)-gamma-butyrolactone bearing thymine, uracil, and 5-bromouracil. *Bioorganic & Medicinal Chemistry Letters*, 9(2): 241-244.

Kubo, T., Rumiana, B., Ohba, H., & Fujii, M. (2003). Antisense effects of DNA– peptide conjugates. *Nucleic Acids Research*, 3: 179-180.

Kucukgulmez, A., Celik, M., Yanar, Y., Sen, D., Polat, H., & Kadak, A. E. (2011). Physicochemical Characterization of Chitosan Extracted from *Metapenaeous stebbingi* Shells. *Food Chemistry*, 126: 1144–1148.

Kumar, P., Nagarajan, A., & Uchil, P. D. (2018). Analysis of Cell Viability by the MTT Assay. *Cold Spring Harbor Protocols,* 2018(6): pdb.prot095505. doi:10.1101/pdb. prot095505.

Kumar, S., Dutta, J., & Dutta, P. K. (2009). Preparation and characterization of N-heterocyclic chitosan derivatives-based gels for biomedical applications. *International Journal of Biological Macromolecules*, 45(4): 330-337.

Kumar, S., Dutta, P. K., & Sen, P. (2010). Preparation and characterization of optical property of crosslinkable film of chitosan with 2-thiophenecarboxaldehyde. *Carbohydrate Polymers*, 80(2): 564-570.

Kumar, S., Koh, J., Kim, H., Gupta, M. K., & Dutta, P. K. (2012). A new chitosan-thymine conjugate: Synthesis, characterization and biological activity. *International Journal of Biological Macromolecules*, 50(3): 493-502.

Kumar, S., Koh, J., Tiwari, D. K., & Dutta, P. K. (2011). Optical Study of Chitosan-Ofloxacin Complex for Biomedical Applications. *Journal of Macromolecular Science Part A*, 48(10): 789-795.

Kumar, S., Nigam, N., Ghosh, T., Dutta, P. K., Singh, S. P., Datta, P. K., An, L., & Shi, T. F. (2010). Preparation, characterization and optical properties of a novel azo based chitosan biopolymer. *Materials Chemistry and Physics*, 120(2-3): 361-370.

Kumari, S., Annamareddy, S. H. K., Abanti, S., & Rath, P. K. (2017). Physicochemical properties and characterization of chitosan synthesized from fish scales, crab and shrimp shells. *International Journal of Biological Macromolecules*, 104: 1697–1705.

Kumari, S., Rath, P., & Sri Hari Kumar, A. (2016). Chitosan from shrimp shell (Crangon crangon) and fish scales (Labeo rohita): Extraction and characterization. *African Journal of Biotechnology*, 15(24): 1258-1268.

Kumirska, J., Czerwicka, M., Kaczynski, Z., Bychowska, A., & Brzozowski, K., Thöming, J., Stepnowski, P. (2010). Application of spectroscopic Methods for Structural Analysis of Chitin and Chitosan. *Marine Drugs,* 8: 1567-1636.

Kuppusamy, S., & Karuppaiah, J. (2013). Screening of Antiproliferative Effect of Chitosan on Tumor Growth and Metastasis in T24 Urinary Bladder Cancer Cell Line. *Austral-Asian journal of cancer*, 12(3): 145-149.

Kurita, K., Ishii, S., Tomita, K., Nishimura, S. I., & Shimoda, K. (1994). Reactivity characteristics of squid beta-chitin as compared with those of shrimp chitin-high potentials of squid chitin as a starting material for facile chemical modifications. *Journal of Polymer Science Part A-Polymer Chemistry*, 32(6): 1027–1032.

Kurita, K., Tomita, K., Tada, T., Ishii, S., Nishimura, S. I., & Shimoda, K. (1993). Squid chitin as a potential alternative chitin source-deacetylation behavior and characteristic properties. *Journal of Polymer Science Part A-Polymer Chemistry*, 31(2): 485–491.

Kurniasih Purwati, M., Hermawan, D., & Zaki, M. (2014). Optimum Conditions for the Synthesis of High Solubility Carboxymethyl Chitosan. *Malaysian Journal of Fundamental and Applied Sciences*, 10(4): 189-194.

Lagares-Garcia, J. A., Moore, R. A., Collier, B., Heggere, M., Diaz, F., & Qian, F. (2001). Nitric oxide synthase as a marker in colorectal carcinoma. *The American Surgeon*, 67(7): 709-713.

Layek, B., & Singh, J. (2017). Chapter 8 - Chitosan for DNA and gene therapy. *Chitosan based biomaterials*, 2: 209-244.

Lee, E., Lee, J., Lee, I.-H., Yu, M., Kim, H., Chae, S. Y., & Jon, S. (2008). Conjugated chitosan as a novel platform for oral delivery of paclitaxel. *Journal of Medicinal Chemistry*, 51(20): 6442–6449.

Lee, H. Y., Kim, S. M., Kim, J. Y., Youn, S. K., Choi, J. S., Park, S. M., & Ahn, D. H. (2002). Effect of addition of chitosan on improvement for shelf-life of bread. *Journal of the Korean Society of the Food and Nutrition*, 31: 445-450.

Lee, J. H., Seo, Y. B., Yoon, M. Y., Choi, J. D., & Kim, Y. T. (2005). Isolation and Sequence Analysis of Two Ornithine Decarboxylase Antizyme Genes from Flounder (Paralichthys olivaceus). *Journal of Microbiology and Biotechnology*, 15(2): 321-329.

Lee, K. Y., Ha, W. S., & Park, W. H. (1995). Blood compatibility and biodegradability of partially N-acylated chitosan derivatives. *Biomaterials*, 16(16): 1211-1216.

Li, J., Ying, S., Ren, H., Dai, J., Zhang, L., Liang, L., Wang, Q., Shen, Q., & Shen, J-W. (2020). Molecular dynamics study on the encapsulation and release of anti-cancer drug doxorubicin by chitosan. *International Journal of Pharmaceutics, 580*: Article 119241.

Li, Q., Dunn, T., Grandmaison, E. W., & Goosen, M. F. A. (1992). Applications and properties of chitosan. *Bioactive and Compatible Polymers*, 7: 370-397.

Li, Q., Ren, J., Dong, F., Feng, Y., Gu, G., & Guo, Z. (2013). Synthesis and antifungal activity of thiadiazole functionalized chitosan derivatives. *Carbohydrate Research*, 373: 103-107.

Li, X., Min, M., Du, N., Gu, Y., Hode, T., Naylor, M., Chen, D., Nordquist, R. E., & Chen, W. R. (2013). Chitin, chitosan, and glycated chitosan regulate immune responses: the novel adjuvants for cancer vaccine. *Clinical and Developmental Immunology*, 2013: 1-8, Article no. 387023.

Li, Y., Neoh, K. G., & Kang, E. T. (2005). Controlled release of heparin from polypyrrole-poly(vinyl alcohol) assembly by electrical stimulation. *Journal of Biomedical Materials Research Part A*, 73A(2): 171-181.

Lifeng, Q., Zirong, X., & Minli, C. (2007). In vitro and in vivo suppression of hepatocellular carcinoma growth by chitosan nanoparticles. *European Journal of Cancer*, 43(1): 184-193.

Liotta, L. A., Tryggvason, K., Garbisa, S., Hart, I., Foltz, C. M., & Shafie, S. (1980). Metastatic potential correlates with enzymatic degradation of basement membrane collagen. *Nature*, 284(5751): 67-68.

Liu, H-T., Huang, P., Ma, P., Liu, Q-S., Yu, C., & Du, Y-G. (2011). Chitosan oligosaccharides suppress LPS-induced IL-8 expression in human umbilical vein endothelial cells through blockade of p38 and Akt protein kinases. *Acta Pharmacologica Sinica*, 32(4): 478-486.

Liu, J. M., Bignon, J., Haroun-Bouhedja, F., Bittoun, P., Vassy, J., Fermandjian, S., Wdzieczak-Bakala, J., & Boisson-Vidal, C. (2005). Inhibitory Effect of Fucoidan on the Adhesion of Adenocarcinoma Cells to Fibronectin. *Anticancer Research*, 25(3B): 2129-2133.

Liu, J., Bagheri-Yarmand, R., Xia, Y., & Crepin, M. (1997). Modulations of breast fibroblast and carcinoma cell interactions by a dextran derivative (CMDB7). *Anticancer Research*, 17(1A): 253-258.

Liu, X.-J., & Chen, R.-Y. (2001). Synthesis of Novel Phosphonotripeptides Containing Uracil or Thymine Group. *Phosphorus, Sulfur, and Silicon and the Related Elements*, 176: 19-28.

Logeart-Avramoglou, D., & Jozefonvicz, J. (1999). Carboxymethyl benzylamide sulfonate dextrans (CMDBS), a family of biospecific polymers endowed with numerous biological properties: a review. *Journal of Biomedical Materials Research*, 48(4): 578-590.

Lomadze, N., & Schneider, H. J. A. (2005). Chitosan-based chemo mechanical polymer triggered by stacking effects with aromatic effectors including amino acid derivatives. *Tetrahedron*, 61: 8694–8698.

Lopez-Moya, F., Colom-Valiente, M. F., Martinez-Peinado, P., Martinez-Lopez, J. E., Puelles, E., Sempere-Ortells, J. M., & Lopez-Llorca, L. V. (2015). Carbon and nitrogen limitation increase chitosan antifungal activity in *Neurospora crassa* and fungal human pathogens. *Fungal Biology*, 119(2-3): 154-169.

Madanagopal, A., Periandy, S., Gayathri, P., Ramalingam, S., Xavier, S., & Ivanov, V. K. (2017). Spectroscopic and computational investigation of the structure and pharmacological activity of 1-benzylimidazole. *Journal of Taibah University for Science*, 11: 975–996.

Maeda, H. (2001). The enhanced permeability and retention (EPR) effect in tumor vasculature: the key role of tumor-selective macromolecular drug targeting. *Advances in Enzyme Regulation*, 41: 189–207.

Maeda, Y., & Kimura, Y. (2004). Antitumor Effects of Various Low-Molecular-Weight Chitosans are due to Increased Natural Killer Activity of Intestinal Intraepithelial Lymphocytes in Sarcoma 180–Bearing Mice. *Journal of nutrition*, 134(4): 945-950.

Majtán, J., Bíliková, K., Markovič, O., Gróf, J., Kogan, G., & Šimúth, J. (2007). Isolation and characterization of chitin from bumblebee (*Bombus terrestris*). *International Journal of Biological Macromolecules*, 40(3): 237-241.

Malatesta, M., Grecchi, S., Chiesa, E., Cisterna, B., Costanzo, M., & Zancanaro, C. (2015). Internalized chitosan nanoparticles persist for long time in cultured cells. *European Journal of Histochemistry*, 59(1): 61-65.

Malherbe, S., Crepin, M., Legrand, C., & Wei, M. X. (2004). Cytostatic and pro-apoptotic effects of a novel phenylacetate-dextran derivative (NaPaC) on breast cancer cells in interactions with endothelial cells. *Anticancer Drugs*, 15(10): 975-981.

Manna, U., Bharani, S., & Patil, S. (2009). Layer-by-layer self-assembly of modified hyaluronic acid/chitosan based on hydrogen bonding. *Biomacromolecules*, 10(9): 2632-2639.

Marletta, M. A. (1993). Nitric oxide synthase structure and mechanism. *The Journal of Biological Chemistry*, 268(17): 12231-12234.

Marshall, J. L., Wellstein, A., Rae, J., DeLap, R. J., Phipps, K., Hanfelt, J., Yunmbam, M. K., Sun, J. X., Duchin, K. L., & Hawkins, M. J. (1997). Phase I trial of orally administered

pentosan polysulfate in patients with advanced cancer. *Clinical Cancer Research*, 3(12 Pt 1): 2347-2354.

Martinez, F., Voelkel, R., Naegele, D., & Naarmann, H. (1989). Thiophene Oligomers: Synthesis and Characterization. *Molecular crystals and liquid crystals incorporating nonlinear optics*, 167(1): 227–232.

Martins, A. F., Facchi, S. P., Follmann, H. D., Pereira, A. G., Rubira, A. F., Muniz, E. C. (2014). Antimicrobial activity of chitosan derivatives containing *N*-quaternized moieties in its backbone: a review. *International Journal of Molecular Science*, 15(11): 20800-20832.

Mary Lazer, L., Sadhasivam, B., Palaniyandi, K., Muthuswamy, T., Ramachandran, I., Balakrishnan, A., Pathak, S., Narayan, S., & Ramalingam, S. (2018). Chitosan-based nano-formulation enhances the anticancer efficacy of hesperetin. *International Journal of Biological Macromolecules*, 107(Pt B): 1988-1998.

Mathew, B., Suresh, J., Elizabeth Mathew, G., Haridas, A., Suresh, G., & Sabreena, P. (2016). Synthesis, ADME studies, toxicity estimation, and exploration of molecular recognition of thiophene based chalcones towards monoamine oxidase-A and B. *Beni-Suef University Journal of Basic and Applied Sciences (BJBAS)*, 5(4): 396–401.

Mathiyalagan, R., Subramaniyam, S., Kim, Y. J., Kim, Y. C., & Yang, D. C. (2014). Ginsenoside compound k-bearing glycol chitosan conjugates: Synthesis, physicochemical characterization, and *in vitro* biological studies. *Carbohydrate polymers*, 112: 359-366.

Mathur, N. K., & Narang, C. K. (1990). Chitin and Chitosan, Versatile Polysaccharides from Marine Animals. *Journal of Chemical Education*, 67(11): 938-942.

Mc Cord, J. M. (2000). The evolution of free radicals and oxidative stress. *American Journal of Medicine*, 108: 652–629.

McLeskey, S. W., Zhang, L., Trock, B. J., Kharbanda, S., Liu, Y., Gottardis, M. M., Lippman, M. E., & Kern, F. G. (1996). Effects of AGM-1470 and pentosan polysulphate on tumorigenicity and metastasis of GF-transfected MCF-7 cells. *British Journal of Cancer*, 73(9): 1053-1062.

Medical University of South Carolina (2018). Study of Chitosan for Pharmacologic Manipulation of AGE (Advanced Glycation End products) Levels in Prostate Cancer Patients. Retrieved November 21, 2018 from https://ClinicalTrials.gov/ct2/show /NCT03712371, ClinicalTrials.gov identifier: NCT03712371.

Mekahlia, S., & Bouzid, B. (2009). Chitosan-Copper (II) complex as antibacterial agent: synthesis, characterization and coordinating bond- activity correlation study. *Physics Procedia*, 2: 1045-1053.

Melo, M. R. S., Feitosa, J. P. A., Freitas, A. L. P., & de Paula, R. C. M. (2002). Isolation and characterization of soluble sulfated polysaccharide from the red seaweed Gracilaria cornea. *Carbohydrate Polymers*, 49(4): 491–498.

Mills, R. D., Cain, K. J., & Woods, G. L. (1989). Detection of influenza virus by centrifugal inoculation of MDCK cells and staining with monoclonal antibodies. *Journal of Clinical Microbiology*, 27: 2505-2508.

Minato, N., Reid, L., Cantor, H., Lengyel, P., & Bloom, B. R. (1980). Mode of regulation of natural killer cell activity by interferon. *The Journal of Experimental Medicine*, 152(1): 124-137.

Miura, S., Mitsuli, K., Heishi, T., Shukunami, C., Sekuguchi, K., Kondo, J., Sato, Y., & Hiraki, Y. (2010). Impairment of VEGF-A-stimulated lamellipodial extensions and motility of vascular endothelial cells by chondromodulin-I, a cartilage-derived angiogenesis inhibitor. *Experimental Cell Research*, 316(5): 775-788.

Mohamed, N. A., Mohamed, R. R., & Seoudi, R. S. (2014). Synthesis and characterization of some novel antimicrobial thiosemicarbazone O-carboxymethyl chitosan derivatives. *International Journal of Biological Macromolecules*, 63: 163-169.

Moore, E. C., & Sartorelli, A. C. (1989). The inhibition of ribonucleotide reductase by a-(N)-heterocyclic carboxaldehyde thiosemicarbazones. *Inhibitors of Ribonucleoside Diphosphate Reductase Activity, (J. G. Cory, A. H. Cory eds.), Pergamon Press; Oxford*, 12: 203-215.

Morere, J. F., Letourneur, D., Planchon, P., Avramoglou, T., Jozefonvicz, J., Israel, L., & Crepin, M. (1992). Inhibitory effect of substituted dextrans on MCF7 human breast cancer cell growth in vitro. *Anticancer Drugs*, 3(6): 629-634.

Morgan, D. O. (1995). Principles of CDK regulation. *Nature*, 374: 131-134.

Mourya, V. K., & Inamdar, N. N. (2008). Chitosan-modifications and applications: opportunities galore. *Reactive and Functional Polym*ers, 68(6): 1013-1051.

Munde, A. S., Jagdale, A. N., Jadhav, S. M., & Chondhekar, T. K. (2009). Synthesis and characterization of some transition metal complexes of unsymmetrical tetradentate Schiff base ligand. *Journal of the Korean Chemical Society*, 53(4): 407-414.

Mundhenke, C., Meyer, K., Drew, S., & Friedl, A. (2002). Heparan sulfate proteoglycans as regulators of fibroblast growth factor-2 receptor binding in breast carcinomas. *The American Journal of Pathology*, 160(1): 185-194.

Murphy, M. P. (2009). How mitochondria produce reactive oxygen species. *Biochemical Journal*, 417(1): 1-13.

Muslim, T., Morimoto, M., Saimoto, H., Okamoto, Y., Minami, S., & Shigemasa, Y. (2001). Synthesis and bioactivities of poly (ethylene glycol)-chitosan hybrids. *Carbohydrate Polymers*, 46(4): 323-330.

Muzzarelli, R. A. (1997). Human enzymatic activities related to the therapeutic administration of chitin derivatives. *Cellular and Molecular Life Sciences*, 53(2): 131–140.

Muzzarelli, R. A. A. (1996). Chitosan based dietary foods. *Carbohydrate polymers*, 29(4): 309-316.

Muzzarelli, R. A. A., Tanfani, F., Mariotti, S., & Emanuelli, M. (1982). Preparation and characteristic properties of dithiocarbamate chitosan, a chelating polymer. *Carbohydrate Research*, 104: 235–243.

Nagaset, H., & Woessner Jr., J. F. (1999). Matrix metalloproteinases. *The Journal of Biological Chemistry*, 274(31): 21491-21494.

Nakanishi, T., Fukushima, S., Okamoto, K., Suzuki, M., Matsumura, Y., Yokoyama, M., Okano, T., Sakurai, Y., & Kataoka, K. (2001). Development of the polymer micelle carrier system for doxorubicin. *Journal of Controlled Release*, 74(1-3): 295-302.

Nam, K. S., & Shon, Y. H. (2009). Suppression of Metastasis of Human Breast Cancer Cells by Chitosan Oligosaccharides. *Journal of Microbiology and Biotechnol*ogy, 19(6): 629-633.

Nam, K. S., Kim, M.-K., & Shon, Y.-H. (2007a). Chemopreventive Effect of Chitosan Oligosaccharide Against Colon Carcinogenesis. *Journal of Microbiology and Biotechnology*, 17(9): 1546-1549.

Nam, K. S., Kim, M.- K., & Shon, Y.-H. (2007b). Inhibition of proinflammatory cytokines-induced invasiveness of HT-29 cells by chitosan oligosaccharide. *Journal of Microbiology and Biotechnology*, 17(12): 2042-2045.

Nanbu, K., Kitamura, F., Ohsaka, T., and Tokuda, K. (1999). Adsorption of pyridine on a polycrystalline gold electrode surface studied by infrared reflection absorption spectroscopy. *Journal of Electroanalytical Chemistry*, 470(2): 136–143.

Nathan, C. F., Brukner, L. H., Silverstein, S. J. C., & Chon, Z. A. (1979). Extracellular cytolysis by activated macrophages and granulocytes. I. Pharmacologic triggering of effector cells and the release of hydrogen peroxide. *The Journal of Experimental Medicine*, 149(1): 84-99.

Nelson, D. L., & Cox, M. M. (2005). DNA replication. *Lehninger Principles of Biochemistry*, 4th ed., 950-966.

Nemtsev, S. V., Gamzazade, A. I., Rogozhin, S. V., Bykova, V. M., & Bykov, V. P. (2002). Deacetylation of chitin under homogeneous conditions. *Applied Biochemistry and Microbiology*, 38: 521–526.

Niazi, J. H., & Gu, M. B. (2009). Toxicity of metallic nanoparticles in microorganisms- A review. *Atmospheric and Biological Environmental Monitoring* Y. J.; Platt, U.; Gu, M. B.; 455 Iwahashi, H., Eds. Springer: Netherlands, pp 193-206.

Nishat, N., Ahamad, T., Zulfequar, M., & Hasnain, S. (2008). New Antimicrobial Polyurea: Synthesis, Characterization, and Antibacterial Activities of Polyurea-Containing Thiosemicarbazide–Metal Complexes. *Journal of Applied Polymer Science*, 110(6): 3305-3312.

Nishida, N., Yano, H., Nishida, T., Kamura, T., & Kajiro, M. (2006). Angiogenesis in Cancer. *Vascular Health and Risk Management*, 2(3): 213-219.

No, H, K., & Meyers, S. P. (2000). Application of chitosan for treatment of waste waters. In: Ware G. W. (eds.) Reviews of Environmental Contamination and Toxicology. Reviews of Environmental Contamination and Toxicology, Springer, New York, 163: 1-28.

No, H. K., & Lee, M. Y. (1995). Isolation of chitin from crab shell waste. *Journal of the Korean Society of the Food and Nutrition*, 24: 105–113.

No, H. K., Lee, S. H., Park, N. Y., & Meyers, S. P. J. (2003). Comparison of physicochemical, binding, and antibacterial properties of chitosans prepared without and with deproteinization process. *Journal of Agricultural and Food Chemistry*, 51(26): 7659-7663.

No, H. K., Meyers, S. P., Prinyawiwatkul, W., & Xu, Z. (2007). Applications of chitosan for improvement of quality and shelf life of foods: a review. *Journal of Food Science*, 72(5): R87-100.

Nurse, P. (2000). A long twentieth century of the cell cycle and beyond. *Cell*, 100(1): 71-78.

Oh., H., Kim, Y. J., Chang, E. J., & Kim, J. Y. (2001). Antimicrobial characteristics of chitosan against food spoilage microorganisms in liquid media and mayonnaise. *Bioscience, Biotechnology and Biochemistry*, 65: 2378–2383.

Okuyama, K., Noguchi, K., Miyazawa, T., Yui, T., & Ogawa, K. (1997). Molecular and Crystal Structure of Hydrated Chitosan. *Macromolecules*, 30: 5849–5855.

Omeir, R. L., Teferedegne, B., Foseh, G. S., Beren, J. J., Snoy, P. J., Brinster, L. R., Cook, J. L., Peden, K., & Lewis Jr, A. M. (2011). Heterogeneity of the Tumorigenic Phenotype Expressed by Madin–Darby Canine Kidney Cells. *Comparative Medicine*, 61(3): 243–250.

Omeir, R., Thomas, R., Teferedegne, B., Williams, C., Foseh, G., Macauley, J., Brinster, L., Beren, J., Peden, K., Breen, M., & Lewis Jr, A. M. (2015). A novel canine kidney cell line model for the evaluation of neoplastic development: karyotype evolution associated with spontaneous immortalization and tumorigenicity. *Chromosome Research*, 23(4): 663–680.

Onsosyen, E., & Skaugrud, O. (1990). Metal recovery using chitosan. *Journal of Chemical Technology and Biotechnology*, 49(4): 395–404.

Park, H. J., Kim, M. N., Kim, J. G., Bae, Y. H., Bae, M. K., Wee, H. J., Kim, T. W., Kim, B. S., Kim, J. B., Bae, S. K., & Yoon, S. (2007). Up-regulation of VEGF expression by NGF that enhances reparative angiogenesis during thymic regeneration in adult rat. *Biochimica et Biophysica Acta*, 1773(9): 1462-1472.

Park, J. H., Saravanakumar, G., Kim, K., & Kwon, I. C. (2010). Targeted delivery of low molecular drugs using chitosan and its derivatives. Advanced *Drug Delivery Reviews*, 62 (1): 28–41.

Park, J. K., Chung, M. J., Choi, H. N., & Park, Y.II (2011). Effects of the Molecular Weight and the Degree of Deacetylation of Chitosan Oligosaccharides on Antitumor Activity. *International Journal of Molecular Science*, 12(1): 266-277.

Park, P-J., Je, J. Y., & Kim, S. K. (2003). Free radical scavenging activity of chito oligosaccharides by electron spin resonance spectrometry. *Journal of Agriculture and Food Chemistry*. 51(16): 4624-4627.

Patel, A., & Sadasivan, R. (2017). Microwave assisted one pot synthesis and characterization of Cesium salt of di-copper substituted phosphotungstate and its application in the selective epoxidation of cis-cyclooctene with tert-butyl hydroperoxide. *Inorganica Chimica Acta*, 458: 101–108.

Pawlak, A., & Mucha, M. (2003). Thermogravimetric and FTIR studies of chitosan blends. *Thermochimica Acta*, 396: 153–166.

Pearson, F. G., Marchessault, R. H., & Liang, C. Y. (1960). Infrared spectra of crystalline polysaccharides. V. Chitin. *Journal of Polymer Science Banner*, 43(141): 101-116.

Peniche, C., Argüelles-Monal, W., & Goycoole, F. M. (2008). Chitin and Chitosan: Major Sources, Properties and Applications. *Monomers, Polymers and Composites from Renewable Resources; M. N. Belgacem, A. Gandini, Eds.; Elsevier: Oxford,* pp. 517-542.

Percot, A., Viton, C., & Domard, A. (2003). Optimization of chitin extraction from shrimp shells. *Biomacromolecules*, 4(1): 12-18.

Pestov, A., & Bratskaya, S. (2016). Chitosan and Its Derivatives as Highly Efficient Polymer Ligands. *Molecules*, 21(3): 330-364.

Pighinelli, L., Guimarães, M. F., Becker, C. M., Zehetmeyer, G., Rasia, M. G., Corrêa, D. S., Paz, R. L., Zannin, B. G., Kmiec, M., Tedesco, M. F., Reis, V., Silva, M. M., & Feijó, C.T., C. C. Feistel, C. C. (2016). Structure and Properties of Nanocrystalline Chitosan. *Journal of Applied Biotechnology and Bioengineering*, 1(1): 23-30.

Pike, A. R., Ryder, L. C., Horrocks, B. R., Clegg, W., Elsegood, M. R. J., Connolly, B. A., & Houlton, A. (2002). Metallocene-DNA: synthesis, molecular and electronic structure and DNA incorporation of C5-ferrocenylthymidine derivatives. *Chemistry- A European Journal*, 8(13): 2891-2899.

Pillai, C. K. S., Paul, W., & Sharma, C. P. (2009). Chitin and chitosan polymers: Chemistry, solubility and fiber formation, *Progress in Polymer Science, 34* (7), 641-678.

Pires, N. R., Cunha, P. L. R., Maciel, J. S., Angelim, A. L., Melo, V. M. M., de Paula, R. C. M., & Feitosa, J. P. A. (2013). Sulfated chitosan as tear substitute with no antimicrobial activity. *Carbohydrate Polymers*, 91(1): 92-99.

Qi, L. F., Xu, Z. R., Li, Y., Jiang, X., & Han, X. Y. (2005). In vitro effects of chitosan nanoparticles on proliferation of human gastric carcinoma cell line MGC803 cells. *World Journal of Gastroenterology*, 11: 5136-5141.

Qi, L., Xu, Z., & Chen, M. (2007). In vitro and in vivo suppression of hepatocellular carcinoma growth by chitosan nanoparticles. *European Journal of Cancer*, 43: 184-93.

Qi, L., Xu, Z., Jiang, X., Hu, C., & Zou, X. (2004). Preparation and antibacterial activity of chitosan nanoparticles. *Carbohydrate Research*, 339(16): 2693-700.

Qiao, D., Meyer, K., Mundhenke, C., Drew, S, A., & Friedl, A. (2003). Heparan sulfate proteoglycans as regulators of fibroblast growth factor-2 signaling in brain endothelial cells. Specific role for glypican-1 in glioma angiogenesis. *Journal of Biological Chemistry*, 278(18): 16045-16053.

Qin, C. Q., Du, Y. M., & Xiao, L. (2002). Effect of hydrogen peroxide treatment on the molecular weight and structure of chitosan. *Polymer Degradation and Stability*, 76(2): 211-218.

Qin, C. Q., Zhou, B., Zeng, L. T., Zhang, Z. H., Liu, Y., Du, Y. M., & Xiao, L. (2004). The physicochemical properties and antitumor activity of cellulase-treated chitosan, *Food Chemistry*, 84(1): 107-115.

Qin, C., Du, Y., Xiao, L., Li, Z., & Gao, X. (2002). Enzymic preparation of water- soluble chitosan and their antitumor activity. *International Journal of Biological Macromolecules*. 31(1-3): 111-117.

Qin, Y., Xing, R., Liu, S., Li, K., Meng, X., Li, R., Cui, J., Li, B., & Li, P. (2012). Novel thiosemicarbazone chitosan derivatives: Preparation, characterization, and antifungal activity. *Carbohydrate Polymers*, 87: 2664-2670.

Qu, X., Wirsen, A., & Albertsson, A. (2000). Effect of lactic/glycolic acid side chains on the thermal degradation kinetics of chitosan derivatives. *Polymer*, 41: 4841-4847.

Quan, H., Zhu, F., Han, X., Xu, Z., Zhao, Y., & Miao, Z. (2009). Mechanism of anti-angiogenic activities of chitooligosaccharides may be through inhibiting heparanase activity. *Medical Hypotheses*, 73(2): 205-206.

Ramasamy, T., Ruttala, H. B., Chitrapriya, N., Poudal, B. K., Choi, J. Y., Kim, S. T., Youn, Y. S., Ku, S. K., Choi, H. G., Yong, C. S., & Kim, J. O. (2017). Engineering of cell micro environment-responsive polypeptide nanovehicle co-encapsulating a synergistic combination of small molecules for effective chemotherapy in solid tumors. *Acta Biomaterialia*, 48: 131-143.

Rampino, A., Borgogna, M., Blasi, P., Bellich, B., & Cesàro, A. (2013). Chitosan nanoparticles: preparation, size evolution and stability. *International Journal of Pharmaceutics*, 455(1-2): 219–228.

Ramya, R., Sudha, P. N., & Mahalakshmi, J. (2012). Preparation and Characterization of Chitosan Binary Blend. *International journal of scientific and research publications*, 2:1-9.

Rao, A. L., Bharani, M., & Pallavi, V. (2006). Role of antioxidants and free radicals in health and disease. *Advances in Pharmacology and Toxicology*, 7: 29–38.

Rapheal, P. F., Manoj, E., & Prathapachandra Kurup, M. R. (2007). Copper(II) complexes of N(4)-substituted thiosemicarbazones derived from pyridine-2-carbaldehyde: Crystal structure of a binuclear complex. *Polyhedron*, 26: 818–828.

Ravi Kumar, M. N. V. (2000). A review of chitin and chitosan application. *Reactive Functional Polymers*, 46(1): 1-27.

Ray, S. D. (2011). Potential aspects of chitosan as pharmaceutical excipient. *Acta Poloniae Pharmaceutica*, 68(5): 619–622.

Rejinold, N. S., Chennazhi, K. P., Nair, S. V., Tamura, H., & Jayakumar, R. (2011). Biodegradable and thermo-sensitive chitosan-*g*-poly(*N*-vinylcaprolactam) nanoparticles as a 5-fluorouracil carrier. *Carbohydrate Polymers*, 83(2): 776-786.

Remesh, A. (2012). Toxicities of anticancer drugs and its management. *International Journal of Basic and Clinical Pharmacology*, 1(1): 2-12.

Reynisdottir, I., Polyak, K., Iavarone, A., & Massague, J. (1995). Kip/Cip and Ink4 Cdk inhibitors cooperate to induce cell cycle arrest in response to TGF-beta. *Genes and Development*, 9(15): 1831-1845.

Rinaudo, M. (2006). Chitin and Chitosan: Properties and Applications. *Progress in Polymer Science*, 31(7): 603-632.

Ringsdorf, H. (1975). Structure and properties of pharmacologically active polymers. *Journal of Polymer Science: Polymer Symposia*, 51: 135-153.

Rizkita, L. D., Ysrafil, Martien, R., & Astuti, I. (2021). Chitosan Nanoparticles Mediated Delivery of MIR-106B-5P to Breast Cancer Cell Lines MCF-7 and T47D. *International Journal of Applied Pharmaceutics*, 13(1): 129-134.

Rodde, R., Einbu, A., & Varum, K. M. (2008). A seasonal study of the chemical composition and chitin quality of shrimp shells obtained from northern shrimp (*Pandalus borealis*). *Carbohydrate Polymers*, 71(3): 388–393.

Roskoski, R. Jr. (2007). Vascular endothelial growth factor (VEGF) signaling in tumor progression. *Critical Reviews in Oncology/Hematology*, 62(3): 179-213.

Roviello, G. N., Benedetti, E., Pedone, C., & Bucci, E. M. (2010). Nucleobase-containing peptides: an overview of their characteristic features and applications. *Amino Acids*, 39: 45-57.

Rozhin, J., Wilson, P. S., Bull, A. W., & Nigro, N. D. (1984). Ornithine Decarboxylase Activity in the Rat and Human Colon. *Cancer Research*, 44(8): 3226-3230.

Sabouraud, A., Chappey, O., Dupin, T., & Scherrmann, J. M. (1994). Binding of colchicine and thiocolchicoside to human serum proteins and blood cells. *International Journal of Clinical Pharmacology and Therapeutics*, 32(8): 429-432.

Sadeghi, A. M. M., Dorkoosh, F. A., Avadi, M. R., Weinhold, M., Bayat, A., Delie, F., Gumy, R., Larijani, B., Rafiee-Tehrani, M., & Junginger, H. E. (2008). Permeation enhancer effect of chitosan and chitosan derivatives: Comparison of formulations as soluble polymers and nanoparticulate systems on insulin absorption in Caco-2 cells. *European Journal of Pharmaceutics and Biopharmaceutics*, 70(1): 270–278.

Sagheer, F. A. A., Al-Sughayer, M. A., Muslim, S., Elsabee, M. Z. (2009). Extraction and characterization of chitin and chitosan from marine sources in Arabian Gulf. Carbohydrate Polymers, 77: 410-419.

Salahuddin, N., Elbarbary, A. A., & Alkabes, H. A. (2017a). Quinazolinone Derivatives Loaded Polypyrrole/ Chitosan Core–Shell Nanoparticles with Different Morphologies: Antibacterial and Anticancer Activities. *Nano*, 12(1): 1-17, Article ID 1750002.

Salahuddin, N., Elbarbary, A. A., & Alkabes, H. A. (2017b). Antibacterial and antitumor activities of 3-amino-phenyl-4(3*H*)-quinazolinone/polypyrrole chitosan core shell nanoparticles. *Polymer Bulletin*, 74(5): 1775-1790.

Salahuddin, N., Elbarbary, A. A., Salem, M. L., & Elksass, S. (2017). Antimicrobial and antitumor activities of 1,2,4-triazoles/polypyrrole chitosan core shell nanoparticles. *Journal of Physical Organic Chemistry*, 30(12): e3702. https://doi.org/10.1002/poc.3702.

Santhakumari, R., Ramamurthi, K., Vasuki, G., Yamin, B. M., & Bhagavannarayana, G. (2010). Synthesis and spectral characterization of acetophenone thiosemicarbazone—A nonlinear optical material. *Spectrochimica Acta Part A: Molecular and Biomolecular Spectroscopy*, 76: 369–375.

Sarker, D., Karim, M. R., Haque, M. M., Zamir, R., & Asraf, M. A. (2019). Copper (II) Complex of Salicylaldehyde Semicarbazone: Synthesis, Characterization and Antibacterial Activity. *Asian Journal of Chemical Sciences*, 6(4): 1-8.

Saruc, M., Standop, S., Standop, J., Nozawa, F., Itami, A., Pandey, K. K., Batra, S. K., Gonzalez, N. J., Guesry, P., & Pour, P. M. (2004). Pancreatic enzyme extract improves survival in murine pancreatic cancer. *Pancreas*, 28(4), 401-412.

Sashikala, S., & Shafi, S. S. (2014). Synthesis and Characterization of Chitosan Schiff Base Derivatives. *Der Pharmacia Lettre*, 6(2): 90–97.

Saud, R., Pokhrel, S., & Yadav, P. N. (2019). Synthesis, Characterization and Antimicrobial Activity of Maltol Functionalized Chitosan Derivatives. *Journal of Macromolecular Science, Part* A, 56: 375–383.

Segal, B. G., Kaplan, M., & Fraenkel, G. K. (1965). Measurement of g Values in the Electron Spin Resonance Spectra of Free Radicals. *The Journal of Chemical Physics*, 43(12): 4191–4200.

Seligmann, J., & Twelves, C. (2013). Tubulin: an example of targeted chemotherapy. *Future Medicinal Chemistry*, 5: 339-352.

Senturk, S., Mumcuoglu, M., Gursoy-Yuzugullu, O., Cingoz, B., Akcali, K. C., & Ozturk, M. (2010). Transforming Growth Factor-Beta Induces Senescence in Hepatocellular Carcinoma Cells and Inhibits Tumor Growth. *Hepatology*, 52(3): 966-974.

Seo, W. G., Pae, H. O., Kim, N. Y., Oh, G. S., Park, I. S., Kim, Y. H., Kim, Y. M., Lee, Y., Jun, C. D., & Chung, H. T. (2000). Synergistic cooperation between water-soluble chitosan oligomers and interferon-gamma for induction of nitric oxide synthesis and tumoricidal activity in murine peritoneal macrophages. *Cancer Letters*, 159(2): 189-195.

Seok Won Kim, Samsung Medical Center (2016). Anti-adhesive Effect and Safety of a Mixed Solid of Poloxamer, Gelatin and Chitosan (Medichlore®) After Axillary Dissection for Breast Cancer. Retrieved November 21, 2018 from https://ClinicalTrials.gov/ct2/show/NCT02967146, ClinicalTrials.gov Identifier: NCT02967146.

Shahneh, F. Z., Valiyari, S., Azadmehr, A., Hajiaghaee, R., Yaripour, S., Bandehagh, A., Baradaran, B. (2013). Inhibition of Growth and Induction of Apoptosis in Fibrosarcoma cell Lines by Echinophora platyloba DC: In Vitro Analysis. *Advances in Pharmacological and Pharmaceutical Sciences*, 2013: 1-7, Article ID 51293.

Sharma, S., Athar, F., Maurya, M. R., & Azam, A. (2005). Copper(II) complexes with substituted thiosemicarbazones of thiophene-2-carboxaldehyde: synthesis, characterization and antiamoebic activity against *E. histolytica*. *European Journal of Medicinal Chemistry*, 40(12): 1414–1419.

Shen, K. T., Chen, M. H., Chan, H. Y., Jeng, J. H., & Wang, Y. J. (2009). Inhibitory effects of chitooligosaccharides on tumor growth and metastasis. *Food and Chemical Toxicology*, 47(8): 1864-1871.

Sheweita, S. A., & Tilmisany, A. K. (2003). Cancer and phase II drug-metabolizing enzymes. *Current Drug Metabolism*, 4(1): 45-58.

Shibuya, M., & Claesson-Welsh, L. (2006). Signal transduction by VEGF receptors in regulation of angiogenesis and lymphangiogenesis. *Experimental Cell Research*, 312(5): 549-560.

Shields, K. M., Smock, N., McQueen, C. E., & Bryant, P. J. (2003). Chitosan for weight loss and cholesterol management. *American Journal of Health-system Pharmacy*, 60(13): 1315-1316.

Shivashankar, M., Mandal, B. K., & Uma, K. (2013). Chitosan-acryl amide grafted polyethylene glycol interpenetrating polymeric network for controlled release studies of Cefotaxime. *Journal of Chemical and Pharmaceutical Research*, 5(5): 140-146.

Shweiki, D., Itin, A., Soffer, D., & Keshet, E. (1992). Vascular endothelial growth factor induced by hypoxia may mediate hypoxia-initiated angiogenesis. *Nature*, 359 (6398): 843-845.

Silano, M., Vincentini, O., Muzzarelli, R. A. A., Muzzarelli, C., & De Vincenzi, M. (2004). MP-Chitosan protects Caco-2 cells from toxic gliadin peptides. *Carbohydrate Polymers*, 58(2): 215-219.

Silva, D. J. B., Zuluaga, F., & Carlos, H. (2015). Evaluation of Biocompatibility of Chitosan Films from the Mycelium of Aspergillus niger in Connective Tissue of Rattus norvegicus. *Journal of Molecular and Genetic Medicine*, 9(3): 1–8.

Singh, B., & Mishra, H. (1986). Complexes of cobalt(II), nickel(II), copper(II), zinc(II) cadmium(II) and dioxouranium(VI) with thiophene-2-aldehydethiosemicarbazones. *Journal of the Indian Chemical Society*, 63(7): 692-694.

Singla, A. K., & Chawla, M. (2001). Chitosan: some pharmaceutical and biological aspects--an update, *Journal of Pharmacy and Pharmacology*, 53(8): 1047-1067.

Skiba, J., Karpowicz, R., Szabó, I., Therrien, B., & Kowalski, K. (2015). Synthesis and anticancer activity studies of ferrocenyl-thymine-3,6-dihydro-2*H*-thiopyranes – A new class of metallocene-nucleobase derivatives. *Journal of Organometallic Chemistry*, 794: 216-222.

Song, Y., Onishi, H., & Nagai, T. (1992). Synthesis and drug-release characteristics of the conjugates of mitomycin C with N-succinyl-chitosan and carboxymethyl-chitin, *Chemical and Pharmaceutical Bulletin*, 40(10): 2822-2825.

Song, Y., Onishi, H., & Nagai, T. (1993a). Conjugate of mitomycin C with N-succinyl-chitosan: *in vitro* drug release properties, toxicity and antitumor activity. *International Journal of Pharmaceutics*. 98(1-3): 121-130.

Song, Y., Onishi, H., & Nagai, T. (1993b). Toxicity and antitumor activity of the conjugate of mitomycin C with carboxymethyl-chitin. *Yakuzaigaku*, 53: 141-147.

Song, Y., Onishi, H., & Nagai, T. (1993c). Pharmacokinetic characteristics and antitumor activity of the N-succinyl-chitosan-mitomycin C conjugate and the carboxymethyl-chitin-mitomycin C conjugate. *Biological and Pharmaceutical Bulletin*, 16(1): 48-54.

Song, Y., Onishi, H., Machida, Y., & Nagai, T. (1996). Drug release and antitumor characteristics of N-succinyl chitosan-mitomycin C as an implant. *Journal of Controlled Release*, 42: 93-100.

Soni, P., Kaur, J., & Tikoo, K. (2015). Dual drug–loaded paclitaxel–thymoquinone nanoparticles for effective breast cancer therapy. *Journal of Nanoparticle Research*, 17(1): 18.

Soule, H. D., Vazquez, J., Long, A., Albert, S., & Brennan, M. (1973). A human cell line from a pleural effusion derived from a breast carcinoma. *Journal of the National Cancer Institute*, 51(5): 1409–1416. doi*:*10.1093/jnci/51.5.1409.

Stec-Martyna, E., Ponassi, M., Miele, M., Parodi, S., Felli, L., & Rosano, C. (2012). Structural Comparison of the Interaction of 406 Tubulin with Various Ligands Affecting Microtubule Dynamics. *Current Cancer Drug Targets*, 12: 658-666.

Steinborn, D., & Junicke., H. (2000). Carbohydrate Complexes of Platinum-Group Metals. *Chemical Reviews*, 100(12): 4283-4318.

Stetler-Stevenson, W. G., Aznavoorian, S., & Liotta, L. (1993). Tumor cell interactions with the extracellular matrix during invasion and metastasis. *Annual Review of Cell and Developmental Biology*, 9: 541-573.

Stoscheck, C. M. (1990). Quantitation of protein, in: *P.D. Murray (Ed.)*, *Methods in Enzymology*, *Academic Press*, pp. 50–68.

Struszczyk, H. (1987). Microcrystalline chitosan. I. Preparation and properties of microcrystalline chitosan. *International Journal of Applied Polymer Science*, 33: 177-189.

Sugano, M., Fujikawa, T., Hiratsuji, Y., Nakashima, K., Fukuda, N., & Hasegawa, Y. (1980). A novel use of chitosan as a hypocholesterolemic agent in rats. *The American Journal of Clinical Nutrition*, 33(4): 787-793.

Suresh, E., Bhadbhade, M. M., & Srinivas, D. (1996). Molecular association, chelate conformation and reactivity correlations in substituted *o*-phenylenebis(salicylidenato) copper(*II*) complexes: UV-visible, EPR and X-ray structural investigations. *Polyhedron*, 15(23): 4133-4144.

Suzuki, K., Mikami, T., Okawa, Y., Tokoro, A., Suzuki, S., & Suzuki, M. (1986). Antitumor effect of hexa-N-acetylchitohexaose and chitohexaose. *Carbohydrate Research*, 151: 403-408.

Svirshchevskaya, E. V., Graxcheva, I. A., Kuznetsov, A. G., Myrsikova, E. V., Grechikhina, M. V., Zubareva, A. A., & Fedorov, A. Y. (2016). Antitumor Activity of Furanoallocolchicinoid-Chitosan Conjugate. *Medicinal Chemistry*, 6(9): 571-577.

Syamal, A., & Kale, K. S. (1975). Magnetic Properties of Copper(II) Complexes of Schiff Bases Derived from Pyrrole-2-aldehyde and Isopropanolamine /2-amino-2-methylpropanol. *Current Science*, 44(8): 256-258.

Takimoto, H., Hasegawa, M., Yagi, K., Nakamura, T., Sakaeda, T., Hirai, M. (2004). Proapoptotic Effect of a Dietary Supplement: Water Soluble Chitosan Activates Caspase-8 and Modulating Death Receptor Expression. *Drug Metabolism and Pharmacokinetics*, 19(1): 76-82.

Talalay, P., Fahey, J. W., Holtzclaw, W. D., Prestera, T., & Zhang, Y. (1995). Chemoprotection against cancer by phase 2 enzyme induction. *Toxicology Letters*, 82/83: 173-179.

Tao, F., Ma, S., Tao, H., Jin, L., Luo, Y., Zheng, J., Xiang, W., & Deng, H. (2021). Chitosan-based drug delivery systems: From synthesis strategy to osteomyelitis treatment – A review. *Carbohydrate Polymers*, 251: 1-15, Article no. 117063.

Terbojevidh, M., & Cosani, A. (1997). Molecular weight determination of chitin and chitosan. *Chitin Handbook (R. A. A. Muzzarelli, M. G. Peter, eds) European Chitin Society*, pp. 87–101.

Thelander, L., & Reichard, P. (1979). Reduction of ribonucleotides. *Annual Review of Biochemistry*, 48: 133-158.

Thonou, M., Verhoef, J. C., & Juginger, H. E. (2001). Chitosan and its derivatives as intestinal absorption enhancers. *Advanced Drug Delivery Reviews*, 50(1): S91-S101.

Tiwari, D., Basnet, K., Lamichhane, J., Niraula, P., Bhandari, S., & Yadav, P. N. (2016). Copper Complexes of Imidazole-2-carbaldehyde N(4)-Substituted Thiosemicarbazones: Synthesis, Characterization and Antimicrobial Activity. *Asian Journal of Chemistry*, 28(12): 2793-2797.

Tokoro, A., Kobayashi, M., Tatewaki, N., Suzuki, K., Okawa, Y., Mikami, T., Suzuki, S., & Suzuki, M. (1989). Protective Effect of N-Acetyl Chitohexaose on Listeria monocytogenes Infection in Mice. *Microbiology and Immunology*, 33(4): 357-367.

Tokoro, A., Suzuki, K., Matsumoto, T., Mikami, T., Suzuki, S., & Suzuki, M. (1988). Chemotactic response of human neutrophils to N-acetyl chitohexaose *in vitro*. *Microbiology and Immunology*, 32(4): 387-395.

Tolimate, A., Desbrieres, J., Rhazi, M., Alagui, A., Vincendon, M., & Vottero, P. (2000). On the influence of deacetylation process on the physicochemical characteristics of chitosan from squid chitin. *Polymer*, 41: 2463-2469.

Triana-Guzmán, V. L., Ruiz-Cruz, Y., Romero-Peñaloza, E. L., Zuluaga-Corrales, H. F., & Chaur-Valencia, M. N. (2018). New chitosan-imine derivatives: from green chemistry to removal of heavy metals from water. *Revista Facultad de Ingeniería, Universidad de Antioquia*, 89: 34-43.

Trubiani, O., Bosco, D., & Di Primio, R. (1994). Interferon-gamma (IFN-gamma) induces programmed cell death in differentiated human leukemic B cell lines. *Experimental Cell Research*, 215(1): 23-27.

Truitt, G. A., Dennison, D. K., Rich, R. R., & Rich, S. S. (1979). Interaction between T cells and non-T cells in suppression of cytotoxic lymphocyte responses. *The Journal of Immunology*, 123(2): 745-750.

Tsukada, K., Matsumoto, T., Aizawa, K., Tokoro, A., Naruse, R., Suzuki, S., & Suzuki, M. (1990). Antimetastatic and growth-inhibitory effects of N-acetylchitohexaose in mice bearing Lewis lung carcinoma. *Japanese Journal of Cancer Research*, 81(3): 259-265.

Tuangpholkrung, P., Muanprasat, C., & Chatsudthipong, V. (2018). Chitooligosaccharide inhibits cyst formation and enlargement through calcium restoration and AMPK activation. *The Federation of American Societies for Experimental Biology (FASEB) Journal*, 31 (S1): 1032.6-1032.6. doi: 10.1096/fasebj.31.1_supplement.1032.6

Tumir, L-M., Grabar, M., Tomic, S., & Piantanida, I. (2010). The interactions of bis-phenanthridinium–nucleobase conjugates with nucleotides: adenine-conjugate recognizes UMP in aqueous medium. *Tetrahedron*, 66: 2501-2513.

University Hospital, Basel, Switzerland (2015). Comparison of Oral Morphine Versus Nasal Ketamine Spray with Chitosan in Cancer Pain Outpatients. Retrieved November 21, 2018 from https://ClinicalTrials.gov/ct2/show/NCT02591017, ClinicalTrials.gov Identifier: NCT02591017.

Vane, J. R., & Botting, R. M. (1998). Mechanism of action of nonsteroidal anti-inflammatory drugs. *The American Journal of Medicine*, 104(3A): 2S-8S.

Varma, A. J., Deshpandea, S. V., & Kennedy, J. F. (2004). Metal complexation by chitosan and its derivatives: A review. *Carbohydrate Polymers*, 55(1): 77-93.

Vermeulen, K., Van-Bockstaele, D. R., & Berneman, Z. N. (2003). The cell cycle: a review of regulation, deregulation and therapeutic targets in cancer. *Cell prolif*eration, 36(3): 131-149.

Vishu Kumar, B. A., Varadaraj, M. C., & Tharanathan, R. N. (2007). Low molecular weight chitosan--preparation with the aid of pepsin, characterization, and its bactericidal activity. *Biomacromolecules*, 8(2): 566-572.

Voitovich, Y. V., Shegravina, E. S., Sitnikov, N. S., Faerman, V. I., Fokin, V. V., Schmalz, H-G., Combes, S., Allegro, D., Barbier, P., Beletskaya, I. P., Svirshchevskaya, E. V., &

Fedorov, A. Y. (2015). Synthesis and Biological Evaluation of Furanoallocolchicinoids. *Journal of Medicinal Chemistry*, 58(2): 692-704.

Wang, F. Y., & He, Y. S. (2001). Study on antitumor effect of water-soluble chitosan. *Journal of Clinical Biochemistry Drug*, 22: 21-22.

Wang, J. C., & Kinsella, J. E. J. (1976). Functional properties of novel proteins: Alfalfa leaf protein. *Journal of Food Science*, 41(2): 286-292.

Wang, J., Jiang, J-Z., Chen, W., & Bai, Z-W. (2016). Data of $^{1}H/^{13}C$ NMR spectra and degree of substitution for chitosan alkyl urea. *Data in Brief*, 7: 1228–1236.

Wang, R-M., He, N-P., Song, P-F., He, Y-F., Ding, L., & Lei, Z. (2009). Preparation of low-molecular-weight chitosan derivative zinc complexes and their effect on the growth of liver cancer cells *in vitro*. *Pure and Applied Chemistry*, 81(12): 2397-2405.

Wang, S.-L., Lin, H.-T., Liang, T.-W., Chen, Y.-J., Yen, Y.-H., & Guo, S.-P. (2008). Reclamation of chitinous materials by bromelain for the preparation of antitumor and antifungal materials. *Bioresource Technology*, 99(10): 4386-4393.

Wang, X., Du, Y., Fan, L., Liu, H., & Hu, Y. (2005). Chitosan- metal complexes as antimicrobial agent: Synthesis, characterization and Structure-activity study. *Polymer Bulletin*, 55: 105–113.

Wang, Y., Shen, X., Liao, W., Fang, J., Chen, X., Dong, Q., & Ding, K. (2014). A heteropolysaccharide, L-fuco-D-manno-1,6-α-D-galactan extracted from *Grifola frondosa*and antiangiogenic activity of its sulfated derivative. *Carbohydrate Polymers*, 101: 631-641.

Wang, Y., Yang, X., Yang, J., Wang, Y., Chen, R., Wu, J., Liu, Y., & Zhang, N. (2011). Self-assembled nanoparticles of methotrexate conjugated *O*-carboxymethyl chitosan: Preparation, characterization and drug release behavior *in vitro*. *Carbohydrate Polymers*, 86(4): 1665-1670.

West, D. X., & Liberta, A. E. (1993). Thiosemicarbazone complexes of copper(II): structural and biological studies. *Coordination Chemistry Reviews*, 123(1-2): 49–71.

Wiegand, C., Winter, D., & Hipler, U. C. (2010). Molecular-weight dependent toxic effects of chitosans on the human keratinocyte cell line HaCaT. *Skin Pharmacology and Physiology*, 23: 164-70.

Wiles, D. M., Gingras, B. A., & Suprunchuk, T. (1967). The C=S stretching vibration in the infrared spectra of some thiosemicarbazones. *Canadian Journal of Chemistry*, 45: 470-473.

Wilhelm, S. M., Adnane, L., Newell, P., Villanueva, A., Llovet, J. M., & Lynch, M. (2008). Preclinical overview of sorafenib, a multikinase inhibitor that targets both Raf and VEGF and PDGF receptor tyrosine kinase signalling. *Molecular Cancer Therapeutics*, 7(10): 3129-3140.

Wimardhani, Y. S., Suniarti, D. F., Freisleben, H. J., Wanandi, S. I., Siregar, N. C., Ikeda, M. -A. (2014). Chitosan exerts anticancer activity through induction of apoptosis and cell cycle arrest in oral cancer cells. *Journal of oral science*, 56(2): 119-126.

Wimardhani, Y., Suniarti, D. F., Freisleben, H-J., Wanandi, S. I., & Ikeda, M-A. (2012). Cytotoxic effects of chitosan against oral cancer cell lines are molecular-weight-dependent and cell-type-specific. *International Journal of Oral Research*, 3(e1): 1-10.

Witte, L., Hicklin, D. J., Zhu, Z., Pytowski, B., Kotanides, H., Rockwell, P., & Bohlen, P. (1998). Monoclonal antibodies targeting the VEGF receptor-2 (Flk1/KDR) as an anti-angiogenic therapeutic strategy. *Cancer and Metastasis Reviews*, 17(2): 155-161.

Wlassoff, W. A., & King, G. C. (2002). Ferrocene conjugates of dUTP for enzymatic redox labelling of DNA. *Nucleic Acids Research*, 30(12e58): 1-7.

Wojtasz-Pajak, A., Kolodziejska, I., Debogorska, A., & Malesa-Ciecwierz, M. (1998). Enzymatic, physical and chemical modification of krill chitin. *Bulletin of the Sea Fisheries Institute, Gdynia -Bull Sea Fish Inst*, 143: 29-39.

Wong, J. Y., Langer, R., & Ingber, D. E. (1994). Electrically conducting polymers can noninvasively control the shape and growth of mammalian cells. *Proceedings of the National Academy of Sciences of the United States of America*, 91(8): 3201-3204.

Xia, W., Liu, P., & Liu, J. (2008). Advance in chitosan hydrolysis by non-specific cellulases, *Bioresource Technology*, 99(15): 6751-6762.

Xie, W., Xu, P., & Liu, Q. (2001). Antioxidant activity of water-soluble chitosan derivatives. *Bioorganic and Medicinal Chemistry Letters*, 11(13): 1699–1702.

Xu, T., Xin, M., Li, M., Huang, H., & Zhou, S. (2010). Synthesis, characteristic and antibacterial activity of *N*, *N*, *N*-trimethyl chitosan and its carboxymethyl derivatives. *Carbohydrate Polymers*, 81: 931–936.

Xu, Y., Jin, H., Yang, Z., Zhang, L., & Zhang, L. (2009). Synthesis and biological evaluation of novel neamine–nucleoside conjugates potentially targeting to RNAs. *Tetrahedron*, 65: 5228-5239.

Xu, Y., Wen, Z., & Xu, Z. (2009). Chitosan Nanoparticles Inhibit the Growth of Human Hepatocellular Carcinoma Xenografts through an Antiangiogenic Mechanism. *Anticancer Research*, 29(12): 5103-5109.

Yadav, H. K. S., & Shivakumar, H. G. (2012). In Vitro and In Vivo Evaluation of pH-Sensitive Hydrogels of Carboxymethyl Chitosan for Intestinal delivery of Theophylline. *International Scholarly Research Network,* 2012: 9 pages. Article ID 763127, doi:10.5402/2012/763127.

Yadav, M. K., Pokhrel, S., & Yadav, P. N. (2020). Novel chitosan derivatives of 2-imidazolecarboxaldehyde and 2- thiophenecarboxaldehyde and their antibacterial activity. *Journal of Macromolecular Science, Part A*, 57(10): 703-710.

Yadav, P., Bandyopadhyay, A., Chakraborty, A., & Sarkar, K. (2018). Enhancement of anticancer activity and drug delivery of chitosan-curcumin nanoparticle via molecular docking and simulation analysis. *Carbohydrate Polymers,* 182: 188-198.

Yagihashi, N., Kasajima, H., Sugai, S., Matsumoto, K., Ebina, Y., Morita, T., Murakami, T., & Yagihashi, S. (2000). Increased in situ expression of nitric oxide synthase in human colorectal cancer. *Virchows Archiv*, 436(2): 109-114.

Yamada, K. M., & Clark, K. (2002). Cell biology: survival in three dimensions. N*ature*, 419(6909): 790-791.

Yamada, S., Ganno, T., Ohara, N. & Hayashi, Y. (2007). Chitosan monomer accelerates alkaline phosphatase activity on human osteoblastic cells under hypofunctional conditions. *Journal of Biomedical Materials Research Part A*, 83: 290-295.

Yamaguchi, A., Penland, R. B., Mizushima, S., Lane, T. J., Curran, C., & Quagliano, J. V. (1958). Infrared Absorption Spectra of Inorganic Coordination Complexes. XIV. Infrared Studies of Some Metal Thiourea Complexes. *Journal of American Chemical Society*, 80: 527.

Yan, C., Chen, D., Gu, J., Hu, H., Zhao, X., & Qiao, M. (2006). Preparation of *N*-Succinyl-chitosan and Their Physical-Chemical Properties as a Novel Excipient. *Yakugaku Zasshi*, 126(9): 789-793.

Yen, M-T., Yang, J-H., & Mau, J-L. (2009). Physicochemical characterization of chitin and chitosan from crab shells. *Carbohydrate Polymers*, 75: 15-21.

Yilmaz, M., Christofori, G., & Lehembre, F. (2007). Distinct mechanisms of tumor invasion and metastasis. *Trends in Molecular Medicine*, 13(2): 535-541.

Yin, X., Xiaoli, Zhang, X., Lin, Q., Feng, Y., Yu, W. & Zhang, Q. (2004). Metal-coordinating controlled oxidative degradation of chitosan and antioxidant activity of chitosan-metal complex. *Arkivoc*, IX: 66-78.

Yu, A. E., Hewitt, R. E., Kleiner, D. E., & Stetler-Stevenson, W. G. (1996). Molecular regulation of cellular invasion-role of gelatinase A and TIMP-2. *Biochemistry and Cell Biology*, 74: 823-831.

Yuan, Y., Chesnutt, B. M., Haggard, W. O., & Bumgardner, J. D. (2011). Deacetylation of Chitosan: Material Characterization and *in vitro* Evaluation via Albumin Adsorption and Pre-Osteoblastic Cell Cultures. *Materials*, 4(8): 1399-1416.

Yunmbam, M. K., & Wellstein, A. (2001). The bacterial polysaccharide tecogalan blocks growth of breast cancer cells in vivo. *Oncology Reports*, 8(1): 161-164.

Zaslau, S., Riggs, D. R., Jackson, B. J., Adkins, F. C., John, C. C., Kandzari, S. J., & McFadden, D. W. (2004). In vitro effects of pentosan polysulfate against malignant breast cancer cells. *The American Journal of Surgery*, 188(5): 589-592.

Zhang, H. T., Craft, P., Scott, P. A., Marina, Z., Weich, H. A., Harris, A. L., & Bicknell, R. (1995). Enhancement of tumor growth and vascular density by transfection of vascular endothelial cell growth factor into MCF-7 human breast carcinoma cells. *Journal of National Cancer Institute*, 87(3): 213-219.

Zhang, H., Wu, F., Li, Y., Yang, X., Huang, J., Lv, T., Zhang, Y., Chen, J., Chen, H., Gao, Y., Liu, G., & Jia, L. (2016). Chitosan-based nanoparticles for improved anticancer efficacy and bioavailability of mifepristone. *Beilstein Journal of Nanotechnology*, 7: 1861-1870.

Zhang, J., Xia, W., Liu, P., Cheng, Q., Tahirou, T., Gu, W., & Li, B. (2010). Chitosan modification and pharmaceutical/biomedical applications. *Marine Drugs*, 8(7): 1962-1987.

Zhang, L., & Webster, T. J. (2009). Nanotechnology and Nanomaterials Promises for Improved Tissue Regeneration. *Nano Today*, 4(1): 66-80.

Zhang, S., Li, J., Li, J., Du, N., Li, D., Li, F., & Man, J. (2020). Application status and technical analysis of chitosan-based medical dressings: a review, *RSC Advances*, 10(56)**:** 34308-34322.

Zhang, Y. Q., Xue, C. H., Xue, Y., Gao, R. C., & Zhang, X. L. (2005). Determination of the degree of deacetylation of chitin and chitosan by X-ray powder diffraction. *Carbohydrate Research*, 340: 1914-1917.

Zhang, Y., & Zhang, M. (2002). Three-dimensional macroporous calcium phosphate bioceramics with nested chitosan sponges for load-bearing bone implants. *Journal of Biomedical Materials Research*, 61(1): 1-8.

Zhang, Y., Huo, M., Zhou, J., Yu, D., & Wu, Y. (2009). Potential of amphiphilically modified low molecular weight chitosan as a novel carrier for hydrophobic anticancer drug: Synthesis, characterization, micellization and cytotoxicity evaluation. *Carbohydrate Polymers*, 77(2): 231–238.

Zhang, Z-T., Chen, D-H., & Chen, L. (2002). Preparation of two different serials of chitosan. *The Journal of Dong Hua University, (Eng. Ed.)*, 19(3): 36-39.

Zheng, M., Han, B., Yang, Y., & Liu, W. (2011). Synthesis, characterization and biological safety of O-carboxymethyl chitosan used to treat Sarcoma 180 tumor. *Carbohydrate Polymers*, 86(1): 231-238.

Zheng, Y., Yi, Y., Qi, Y., Wang, Y., Zhang, W., & Du, M. (2006). Preparation of chitosan–copper complexes and their antitumor activity. *Bioorganic and Medicinal Chemistry Letters*, 16(15): 4127-4129.

Zhong, Z., Aotegen, B., & Xu, H. (2011). The influence of the different inductivity of acetyl phenyl–thiosemicarbazone–chitosan on antimicrobial activities. *International Journal of Biological Macromolecules*, 48(5): 713-719.

Zhong, Z., Zhong, Z., Xing, R., Li, P., & Mo, G-L. (2010). The preparation and antioxidant activity of 2- [phenylhydrazine (or hydrazine)- thiosemicarbazone]-chitosan. *International journal of biological macromolecules*, 47(2): 93-97.

Zhou, Y., Wong, C-O., Cho, K-j., van der Hoeven, D., Liang, H., Thakur, D. P., Luo, J., Babic, M., Zinsmaier, K. E., Zhu, M. X., Hu, H., Venkatachalam, K., & Hancock, J. F. (2015). Signal transduction. Membrane potential modulates plasma membrane phospholipid dynamics and K-Ras signaling. *Science*, 349: 873–876.

Zong, A., Zhao, T., Zhang, Y., Song, X., Shi, Y., Cao, H., Liu, C., Cheng, Y., Qu, X., Cao, J., & Wang, F. (2013). Anti-metastatic and anti-angiogenic activities of sulfated polysaccharide of *Sepiella maindroni* ink. *Carbohydrate Polymers*, 91(1): 403-409.

# APPENDIX

## List of Publications

Adhikari, H. S., & Yadav, P. N. (2018). Anticancer Activity of Chitosan, Chitosan Derivatives, and Their Mechanism of Action. *International Journal of Biomaterials*, 2018: 1-29, Article no. 2952085.

Adhikari, H. S., Garai, A., Marasini, B. P., Adhikari, R., & Yadav, P. N. (2021). Synthesis and Characterization of High Molecular Weight Chitosan, and Antioxidant Activity of Its Chitosan Oligosaccharide Encapsulation. *Journal of Nepal Chemical Society (JNCS)*, 42(1): 29-38.

Adhikari, H. S., Garai, A., Khanal, C., Adhikari, R., & Yadav, P. N. (2021). Imidazole-2-carboxaldehyde Chitosan Thiosemicarbazones, and Their Copper(II) Complexes: Synthesis, Characterization, and Antitumorigenic Activity against Madin-Darby Canine Kidney Cell Line. *Asian Journal of Chemistry*, 33(5): 969-976.

Adhikari, H. S., Garai, A., Thapa, M., Adhikari, R., & Yadav, P. N. (2022). Chitosan functionalized thiophene-2-thiosemicarbazones, and their copper(II) complexes: synthesis, characterization, and anticancer activity. *Journal of Macromolecular Science, Paryt A: Pure and Applied Chemistry*, 59(3), 211-227. DOI: 10.1080/10601325.2021.2022982. Published on 5 Jan., 2022.

Adhikari, H. S., Garai, A., Khanal, C., Adhikari, R., & Yadav, P. N. (2022). Low and High Molecular Weight Chitosan Analogues of Imidazole-2-Thiosemicarbazones and Their Copper(II) Complexes: Synthesis, Characterization, and Antitumorigenic Activity *in vitro*. In chapter 12: *Challenges and Advances in Chemical Science*: *B. P. International*, vol. 8, 121-137. DOI: 10.9734/bpi/cacs/v8/15406D.

## List of Presentations

Poster presentation: Chitosan Tailoring on the Pathways of Antitumor Drug development Strategy (Best Poster Award). Nepal Polymer Institute (NPI), Fifth Micro Symposium on Applied Sciences [Nano/Bio], Apr. 29, 2017, Kathmandu, Nepal.

Oral presentation: Characterization of Chitosan Thiosemicarbazones and their Copper(II) Complexes. Departmental Seminar of Department of Inorganic and Physical Chemistry, Indian Institute of Science (IISc), Sept. 13, 2017, Bangalore, India.

Oral lecture: Functionalization of Chitosan as Chitosan Thiosemicarbazones. Regional Chemical Congress- 2017, Nepal Chemical Society, Prithwi Narayan Campus, Tribhuvan University, Oct. 14, 2017, Pokhara, Nepal.

Invited lecture: Correlative Characterization of Imidazole 2-Carboxaldehyde Thiosemicarbazone Chitosan, Thiophene 2-Carboxaldehyde Thiosemicarbazone Chitosan and their Copper(II) Complexes. Fourth International Symposium on Advances in Sustainable Polymers2017 (ASP 2017), Jan. 08-11, 2018, Guwahati, India.

Oral presentation: Semi Synthetic Natural Product Chitosan, Its Characterization and Coordination Behavior with Copper(II) ion. International Conference on Emerging Trends in Chemical Sciences (ICETCS), DDU Gorakhpur University, Feb. 24-25, 2018, Gorakhpur, India.

Oral presentation: Chitosan from Crab Shells: Preparation, Characterization, and Investigation of Physicochemical Properties. Fourth International Conference, Kathmandu Symposia on Advanced Materials- 2018 (KaSAM-2018), Kathmandu, Oct. 26-29, 2018.

Oral presentation: Imidazole-2-carboxaldehyde Chitosan Thiosemicarbazones: Synthesis, Characterization and Antioxidant Activity. Fifth International Symposium on Advances in Sustainable Polymers (ASP-2019), KIT, Kyoto, Japan, Oct 14-18, 2019.